



Ministério de Ciência e Tecnologia
Observatório Nacional
Divisão de Programas de Pós-Graduação
Astronomia e Astrofísica

Metalicidades e Abundâncias de Lítio em Estrelas com Planetas como Vínculos para os Modelos de Formação Planetária

Tese de Doutorado

Luan Ghezzi

Orientadora: Dra. Katia Cunha (ON/MCT)

Tese apresentada como requisito
para a obtenção do título de doutor em Astronomia

Rio de Janeiro - Julho de 2010

Livros Grátis

<http://www.livrosgratis.com.br>

Milhares de livros grátis para download.

*"I had a dream of Unity
Where we would work side by side
But today I see that it's only me
Just trying to get by*

*Sometimes we strive, undeterred
To walk as one toward our goal
But as people stray toward more selfish ways
We see we have no control*

*I had a dream of Unity
Where we would work side by side
But today I see that it's only me
Just trying to get by, just trying to get by"*

Dream of Unity - Bad Religion

*Dedico esta tese à memória do Prof. Dr. Francisco Xavier de Araújo,
que era nosso amigo, orientador e colaborador.*

*Sem o seu incentivo e a sua participação,
este trabalho não teria acontecido.*

Agradecimentos

A minha família, pelo amor e apoio incondicionais e por toda a paciência e compreensão nos últimos meses do Doutorado. Em especial, agradeço aos meus pais, por tudo e sempre; à Rafa, pela maravilhosa vida que temos construído juntos ao longo dos últimos dez anos; ao Edie e à Eva, pela companhia nas longas jornadas em frente ao computador.

A minha orientadora Dra. Katia Cunha, que sempre se fez presente mesmo estando fisicamente distante e foi a principal responsável pelo meu crescimento profissional; ao Dr. Verne Smith, pela participação constante nesta tese apesar do pouquíssimo tempo disponível; ao Dr. Simon Schuler, que hoje, além de colaborador, é um grande amigo; ao Dr. Ramiro de la Reza, por ter assumido a função do saudoso Dr. Francisco Xavier de Araújo; ao Dr. Steven Margheim, pela ajuda na obtenção e redução dos espectros bHROS.

Aos meus amigos Bruna, Cristiane, Guto, Letícia, Marcelo, Maurício, Pedro Newlands, Pedro Pan e Thatiana, pelo incentivo nos (poucos) momentos sérios e por todas as risadas nos (muitos) momentos divertidos.

Aos professores do Observatório Nacional, Observatório do Valongo e da UFRJ, por contribuírem para a minha formação; ao Dr. Cláudio Bastos, por toda a ajuda e pelas discussões futebolísticas; aos Drs. Gustavo Porto de Mello, Simone Daflon e Vladimir Ortega, pelo constante incentivo.

Aos meus colegas de sala Carol, Daniel, Guga, Maria Aldinêz, Maria Isela e Nobar, por tornarem mais agradáveis os longos dias de trabalho.

Ao CNPq, pela concessão da bolsa de Doutorado.

Valeu, Digão!!!

Resumo

Este trabalho apresenta uma determinação homogênea de parâmetros atmosféricos e evolutivos, metalicidades, abundâncias de lítio e velocidades de rotação projetadas para uma amostra de 148 estrelas com planetas e 160 estrelas de comparação do disco fino da Galáxia (sem planetas detectados). Os resultados indicam que a distribuição de metalicidades das estrelas com planetas é ~ 0.15 dex mais rica do que a da amostra de controle. A separação da amostra de acordo com a massa planetária revela que a distribuição de metalicidades das estrelas apenas com planetas netunianos é mais pobre em metais, quando comparada a das estrelas com planetas gigantes próximos. Este resultado pode sugerir a existência de uma conexão entre a metalicidade da estrela e a massa dos seus planetas, com a primeira determinando o valor máximo da última. Uma comparação das distribuições de [Fe/H] em estrelas de seqüência principal, subgigantes e gigantes com planetas mostra que a metalicidade média dos dois primeiros grupos é 0,17 dex maior do que a do último. Este resultado indica que não houve acresção significativa de material sólido rico em metais às estrelas com planetas, visto que este seria diluído na evolução da seqüência principal para a fase de subgigante. A interpretação das metalicidades mais baixas das gigantes com planetas está relacionada com as suas maiores massas. Em média, os seus discos protoplanetários também terão maiores massas, podendo conter a quantidade crítica de metais necessária à formação de planetas gigantes mesmo para metalicidades mais baixas. Uma comparação global das abundâncias de lítio não mostra nenhuma diferença significativa entre as estrelas com e sem planetas. No entanto, o comportamento destas abundâncias em um pequeno intervalo de temperaturas efetivas ($5700 \text{ K} \leq T_{\text{ef}} \leq 5850 \text{ K}$) revela diferenças sutis entre as duas amostras. As estrelas com planetas possuem abundâncias de Li menores ($\sim 0,26$ dex) do que as estrelas de comparação. Esta diferença é refletida nos níveis de atividade cromosférica. As estrelas com planetas também exibem índices de atividade um pouco mais baixos, fato que é interpretado como uma manifestação das velocidades de rotação levemente menores destes objetos. Diferenças na evolução destas velocidades podem ocasionar comportamentos distintos das abundâncias de Li ao longo do tempo. Uma procura por ${}^6\text{Li}$ em 5 estrelas com planetas não revela quantidades detectáveis deste isótopo. Os limites típicos derivados para as razões isotópicas são ${}^6\text{Li}/{}^7\text{Li} \leq 0,00\text{--}0,02$. Estes limites superiores restringem a quantidade de material acrescido a menos de $\sim 0,02\text{--}0,50$ massas de Júpiter.

Abstract

This work presents a homogeneous determination of atmospheric and evolutionary parameters, metallicities, lithium abundances and projected rotational velocities for a sample of 148 stars with planets and 160 comparison stars from the Galactic thin disk (without detected planets). The results indicate that the metallicity distribution of planet hosting stars is more metal-rich by ~ 0.15 dex when compared to the control sample stars. A segregation of the sample according to planet mass reveals that the metallicity distribution of stars hosting only Neptunian-mass planets tends to be more metal-poor in comparison with that obtained for stars hosting closely orbiting Jovian planets. This result would suggest that there is a link between planet mass and metallicity such that metallicity plays a role in setting the mass of the most massive planet. A comparison between the distributions of [Fe/H] in planet-hosting main-sequence stars, subgiants, and giants finds that the main-sequence stars and subgiants have both a mean metallicity that is higher by 0.17 dex than that of the giant sample indicating that significant accretion of solid metal-rich material onto the planet-hosting stars has not taken place, as such material would be diluted in the evolution from dwarf to subgiant. The lower metallicity found for the planet-hosting giant stars is interpreted as being related to the underlying stellar mass, with giants having larger masses and thus, on average larger-mass protoplanetary disks, which can contain the critical amount of metals necessary to form giant planets even at lower metallicities. An overall broad comparison of the lithium abundances shows no large differences between stars with and without planets. The behavior of the Li abundances over a narrow range of effective temperatures ($5700 \text{ K} \leq T_{\text{eff}} \leq 5850 \text{ K}$), however, reveals subtle differences between the two stellar samples. Planet hosting stars have lower Li abundances (by ~ 0.26 dex) than the comparison stars. This difference is mirrored in the chromospheric activity levels, with the planet hosting stars also exhibiting somewhat lower levels of activity, which is interpreted as a manifestation of slightly lower rotational velocities among the planet hosting stars. Different rotational velocity histories would lead to different behaviors of the Li abundances over time. A search for ${}^6\text{Li}$ in 5 stars which host extrasolar planets reveals no detectable amounts of this isotope. The typical limits in the derived isotopic fraction are ${}^6\text{Li}/{}^7\text{Li} \leq 0.00\text{--}0.02$. These upper limits constrain the amount of accreted material to less than $\sim 0.02\text{--}0.50$ Jovian masses.

Sumário

1	Introdução	1
1.1	Metalicidades das Estrelas com Planetas	5
1.2	Abundâncias de Lítio em Estrelas com Planetas	6
1.3	Razões Isotópicas de ${}^6\text{Li}/{}^7\text{Li}$ em Estrelas com Planetas	8
1.4	Abundâncias de Outros Elementos	9
1.5	Este Trabalho	11
2	Metalicidades em Estrelas com Planetas Gigantes e Netunianos	13
3	Metalicidades de Estrelas Evoluídas com Planetas	57
4	Abundâncias de Lítio em Estrelas com Planetas	97
5	Razões Isotópicas de ${}^6\text{Li}/{}^7\text{Li}$ em Estrelas com Planetas	129
6	Conclusões e Perspectivas Futuras	141
Apêndice		147
A	Espectros FEROS	147
B	Medidas de Larguras Equivalentes	159
C	Tabelas Eletrônicas	223
D	Espectros Sintéticos para a Região do Li	263
	Referências Bibliográficas	269

Capítulo 1

Introdução

O primeiro indício da existência de planetas extra-solares foi apresentado por Campbell et al. (1988), que realizaram o monitoramento das velocidades radiais de estrelas de tipo solar próximas. Os resultados revelaram que os objetos γ Cephei e χ^1 Orionis exibiam variações significativas em suas velocidades radiais, provavelmente causadas pela presença de companheiras estelares. Após a subtração deste efeito, a velocidade radial de γ Cephei ainda apresentava pequenas variações, consistentes com uma semi-amplitude $K = 25 \text{ m s}^{-1}$ e um período de 2,7 anos. Com base neste resultado, os autores concluem que este sistema provavelmente tem um terceiro objeto cuja massa é $M_P \sin i = 1,7 M_J$ (onde M_J é a massa de Júpiter e i é o ângulo de inclinação do plano orbital em relação à linha de visada). No entanto, a existência deste planeta só foi confirmada 15 anos depois (Hatzes et al. 2003).

Latham et al. (1989) analisaram a estrela HD 114762 e encontraram variações periódicas de pequena amplitude em sua velocidade radial. Este efeito foi atribuído à existência de um companheiro de massa $M_P \sin i > 11 M_J$, em uma órbita com período $P = 84$ dias e excentricidade $e = 0,25$. Baseados neste valor mínimo da massa, os autores afirmaram que este objeto provavelmente seria uma anã marrom e, talvez, até mesmo um planeta. Estudos posteriores (Cochran et al. 1991; Hale 1995) sugeriram que a massa deste objeto poderia ser bem maior, situada inclusive no regime estelar. Análises subsequentes (por exemplo, Mazeh et al. 1996, Marcy et al. 1999 e Butler et al. 2006), entretanto, confirmaram que a estrela HD 114762 possui um companheiro com massa entre 9,0 e 11,0 M_J . Como acredita-se, atualmente, que as reações termonucleares envolvendo a fusão do deutério (que caracterizam as anãs marrons) começam a ocorrer no limite $M \gtrsim 13 M_J$, este objeto parece

ser um planeta extra-solar.

Em 1992, Wolszczan & Frail (1992) observaram variações periódicas nos pulsos de rádio emitidos pelo pulsar PSR 1257+12 e demonstraram que elas eram causadas por dois planetas¹ com massas mínimas iguais a 3,4 e 2,8 M_{\oplus} (estes valores foram posteriormente revisados para 4,3 e 3,9 M_{\oplus} por Konacki & Wolszczan 2003), onde M_{\oplus} é a massa da Terra. A confirmação deste resultado, assim como a descoberta de mais um planeta no mesmo sistema (com massa 0,02 M_{\oplus} , ou seja, similar a da Lua), veio dois anos depois (Wolszczan 1994). Neste mesmo ano, Rasio (1994) concluiu que poderia haver um planeta com uma massa da ordem de 1,0 M_J ao redor do pulsar PSR B1620-26, fato que foi confirmado 9 anos depois (Sigurdsson et al. 2003).

A primeira confirmação da existência de um planeta extra-solar ao redor de uma estrela de tipo solar foi feita por Mayor & Queloz (1995). Através da medida das variações da velocidade radial da estrela 51 Peg, os autores concluíram que, ao seu redor, girava um planeta de massa $M_P \sin i \simeq 0,5 M_J$, semi-eixo maior $a \simeq 0,05$ UA, período $P \simeq 4$ dias e excentricidade $e = 0,00$. Esta descoberta foi logo seguida pela confirmação da presença de outros planetas ao redor das estrelas 70 Vir (Marcy & Butler 1996) e 47 UMa (Butler & Marcy 1996). As seguintes propriedades foram estimadas para o objeto ao redor de 70 Vir: $M_P \sin i \simeq 6,6 M_J$, $a \simeq 0,43$ UA, $P \simeq 116,6$ dias e $e = 0,40$. O planeta em torno de 47 UMa, por sua vez, tinha as seguintes propriedades: $M_P \sin i \simeq 2,39 M_J$, $a \simeq 2,1$ UA, $P \simeq 1090$ dias ($\simeq 3$ anos) e $e = 0,03$.

Nos anos que se seguiram a estes notáveis avanços, o desenvolvimento de inúmeros projetos voltados para a busca de planetas extra-solares, o aumento da precisão nas medidas de velocidades radiais e a utilização de novos métodos de detecção permitiram um aumento constante na taxa anual de descobertas de novos objetos. No dia 29 de junho de 2010, a Enciclopédia dos Planetas Extra-solares² (mantida por Jean Schneider, *CNRS/LUTH - Paris Observatory*) listava 464 planetas ao redor de 396 estrelas. A medida de variações nas velocidades radiais das estrelas ainda constitui o principal método de detecção, sendo responsável pela descoberta de 346 planetas (equivalente a 75% do número total). Além disso, o aumento significativo da precisão neste tipo de análise (atualmente, já é possível

¹Alguns autores referem-se a estes objetos como planetas de “segunda geração”, uma vez que eles possivelmente foram formados a partir dos restos (*debris*) deixados pela explosão da supernova que deu origem ao pulsar.

²Disponível no website <http://exoplanet.eu>

medir variações $\sim 1 \text{ m s}^{-1}$) permitiu a descoberta do menor planeta já encontrado ao redor de uma estrela de seqüência principal ($M_P \sin i = 1,94 M_{\oplus}$; Mayor et al. 2009). A técnica do trânsito planetário, por sua vez, permitiu a identificação de 87 planetas (19% do número total). Os 31 planetas restantes foram descobertos através das técnicas de imageamento direto (13 objetos ou 3%), microlentes gravitacionais (10 objetos ou 2%) e cronometragem dos pulsos de rádio emitidos por pulsares (4 objetos ou 1%).

Uma grande parte dos planetas encontrados até hoje possui altas massas ($\gtrsim 1,0 M_J$) e está localizada a pequenas distâncias das estrelas hospedeiras ($a \lesssim 1 \text{ UA}$). Apesar de este fato basicamente refletir uma limitação do método das velocidades radiais (que detecta, preferencialmente, objetos de maior massa e mais próximos das estrelas, pois são eles que causam as maiores variações nas velocidades radiais das últimas), estas características desafiaram o conhecimento que se tinha a respeito da formação e evolução planetária com base no exemplo do Sistema Solar. Neste sentido, inúmeros estudos (teóricos e observacionais) a respeito das propriedades dos planetas e de suas estrelas hospedeiras foram realizados ao longo dos últimos 15 anos. Apesar deste esforço, apenas uma conclusão foi obtida: as estrelas de seqüência principal com planetas extra-solares gigantes ($M_P \sin i \gtrsim 1,0 M_J$) apresentam, em média, uma metalicidade³ mais alta (cerca de $\sim 0,2 \text{ dex}$) quando comparadas às estrelas de campo de tipos espectrais F, G e K (ver, por exemplo, Santos et al. 2005; Fischer & Valenti 2005).

Duas hipóteses foram sugeridas para explicar esta diferença sistemática: *enriquecimento primordial* e *poluição*. A primeira sustenta que a probabilidade de formação de um planeta gigante cresce fortemente com o aumento da metalicidade da nuvem de gás e poeira que deu origem ao sistema. O cenário da poluição, por sua vez, diz que a metalicidade da estrela pode ser modificada pela presença de planetas ao seu redor. Durante o processo de migração destes últimos objetos, material sólido do disco protoplanetário (ou, até mesmo, planetesimais e planetas) podem ser acrescidos à zona convectiva da estrela. Como este material é desprovido de H e He, a metalicidade da estrela seria aumentada (Lin et al. 1996).

A confirmação destas hipóteses é de fundamental importância para a distinção entre os dois principais modelos propostos para explicar a formação planetária: *acresção do*

³Ao longo deste trabalho, a metalicidade será representada pela grandeza $[\text{Fe}/\text{H}] = \log(N_{\text{Fe}}/N_{\text{H}})_{\star} - \log(N_{\text{Fe}}/N_{\text{H}})_{\odot}$.

núcleo (Pollack et al. 1996) e *instabilidade gravitacional* (Boss 1997). De acordo com o primeiro modelo, um núcleo sólido seria inicialmente aglutinado por colisões sucessivas de planetesimais. À medida que a massa deste núcleo aumentasse, ele passaria a ser capaz de reter materiais gasosos de forma mais eficiente. Ao atingir uma determinada massa crítica, uma rápida acresção de gases começaria a ocorrer e um planeta seria formado. No segundo modelo, por outro lado, instabilidades gravitacionais dariam origem a regiões mais densas no disco protoplanetário. Os planetas seriam o resultado do colapso gravitacional destas regiões. Vemos, então, que o modelo de acresção do núcleo é consistente com a hipótese do enriquecimento primordial. A maior quantidade de metais disponíveis aumentaria a densidade superficial de material sólido do disco, provocando uma aglutinação mais eficiente dos núcleos rochosos. Para mais detalhes a respeito dos modelos de formação planetária, sugerimos as revisões recentes de Matsuo et al. (2007), Boss (2010) e Valenti (2010).

Santos et al. (2003) e Santos et al. (2004) mostraram que a probabilidade de formação de um planeta gigante cresce com a metalicidade da estrela (Seção 1.1). Fischer & Valenti (2005) quantificaram esta relação e obtiveram a expressão $P(\text{planeta}) = 0,03 \times 10^{2,0[\text{Fe}/\text{H}]}$, válida no intervalo $-0,5 \lesssim [\text{Fe}/\text{H}] \lesssim +0,5$ e para planetas com $P < 4$ anos e $K > 30 \text{ m s}^{-1}$. Lembrando da definição de $[\text{Fe}/\text{H}]$, vemos que a probabilidade de formação de um planeta gigante gasoso é aproximadamente proporcional ao quadrado do número de átomos de Fe disponíveis. Portanto, este resultado favorece o cenário do enriquecimento primordial e, consequentemente, o modelo de acresção do núcleo. Análises recentes de estrelas subgigantes com planetas gigantes ou de estrelas de seqüência principal com planetas netunianos ($M_P \sin i \lesssim 25 M_{\oplus}$) fornecem um suporte adicional para estas hipóteses. Por outro lado, as evidências em favor da poluição ou, de forma mais geral, da alteração da composição química superficial das estrelas devido à presença de planetas ainda são ambíguas. Resultados discrepantes são obtidos por diversos estudos na literatura (Gonzalez 2006a).

A seguir, faremos um breve resumo dos estudos das abundâncias químicas em estrelas com planetas cujo objetivo era ajudar na melhor compreensão destes possíveis cenários de formação planetária. Devemos ressaltar que esta revisão não tem a pretensão de ser completa, uma vez que a literatura na área de Planetas Extra-solares é extremamente vasta. O propósito principal é fazer uma breve introdução às questões fundamentais que serão abordadas ao longo desta tese. Para revisões mais detalhadas sobre o tema, sugerimos os artigos de Gonzalez (2006a) e Udry & Santos (2007), por exemplo.

1.1 Metalicidades das Estrelas com Planetas

Como mencionado anteriormente, a metalicidade das estrelas de seqüência principal com planetas gigantes é, em média, cerca de 0,2 dex maior quando comparada com às estrelas de campo de tipo F, G e K (sem planetas detectados ainda). Este resultado foi inicialmente obtido por Gonzalez (1997) e amplamente confirmado por diversos estudos subseqüentes (ver, por exemplo, Santos et al. 2001; Laws et al. 2003; Santos et al. 2005; Fischer & Valenti 2005; Bond et al. 2006; Luck & Heiter 2006; Sousa et al. 2008). Inicialmente, acreditava-se que esta era uma característica global das estrelas com planetas. Entretanto, estudos recentes começam a sugerir que esta propriedade restringe-se apenas às anãs e subgigantes que possuem planetas gigantes ao seu redor.

O aumento na precisão dos métodos de detecção de planetas têm permitido a identificação de objetos com massas cada vez menores. Nos últimos 4 anos, aproximadamente 50 planetas com $M_P \sin i < 25 M_{\oplus}$ (chamados de “netunianos” ou “super-Terras”) foram descobertos ao redor de cerca de 30 estrelas. Análises das propriedades destes últimos objetos têm sugerido que eles talvez não sigam o padrão de altas metalicidades das estrelas com planetas gigantes (Udry et al. 2006; Sousa et al. 2008). No entanto, estes resultados ainda são baseados em amostras muito pequenas.

Os últimos anos também revelaram a existência de planetas ao redor de estrelas mais evoluídas, particularmente no ramo das gigantes vermelhas. Schuler et al. (2005) observaram que as metalicidades de 7 estrelas gigantes com planetas eram mais baixas quando comparadas à conhecida distribuição de metalicidades para as anãs com planetas (cujo pico ocorre em $[Fe/H] \sim 0,2$ dex). Este resultado foi confirmado por Pasquini et al. (2007), que analisaram uma amostra de 14 gigantes com planetas. Os autores interpretaram este resultado como uma evidência de poluição, uma vez que o excesso de elementos pesados adquirido durante a seqüência principal teria sido diluído com o aprofundamento da zona convectiva da estrela à medida em que ela evolui em direção ao ramo das gigantes vermelhas. Este cenário já havia sido discutido e descartado por Schuler et al. (2005), visto que Fischer & Valenti (2005) mostraram que as metalicidades das subgigantes com planetas seguem a mesma tendência observada para as anãs. Alternativamente, os autores propõem que a formação planetária também depende da massa da estrela hospedeira.

Hekker & Meléndez (2007) determinaram as metalicidades de 380 gigantes de tipo G

e K, das quais 5 apresentavam planetas. Compilando resultados da literatura para outras 15 gigantes, os autores encontraram uma diferença de 0,13 dex entre as metalicidades médias das gigantes com e sem planetas (com as últimas sendo mais pobres em metais). Esta diferença, que é consistente com os resultados robustos obtidos para as anãs, não foi corroborada pelo trabalho de Takeda et al. (2008). A análise de uma amostra de 322 gigantes de tipo G tardio e massas intermediárias (das quais 10 têm planetas) não revelou nenhuma diferença significativa entre as distribuições de metalicidades das estrelas com e sem planetas. Os autores atribuem a diferença encontrada por Hekker & Meléndez (2007) a uma possível inclusão de subgigantes (tão ricas em metais quanto às anãs, de acordo com Fischer & Valenti 2005) na amostra de gigantes. Além disso, eles afirmam que o uso de metalicidades de diversas referências da literatura pode ter inserido diferenças sistemáticas nos resultados.

1.2 Abundâncias de Lítio em Estrelas com Planetas

As confirmações iniciais de que as metalicidades das estrelas com planetas eram mais elevadas geraram uma intensa busca por outras peculiaridades nas abundâncias químicas destes objetos. Um dos elementos que recebeu mais atenção foi o lítio (Li), cujas abundâncias $A(\text{Li})$ ⁴ nas atmosferas das estrelas podem conter pistas importantes para a melhor compreensão de diversos processos, que vão desde a Nucleossíntese no Big Bang até a formação e evolução de sistemas planetários (ver, por exemplo, Meléndez et al. 2010; Santos et al. 2010). Entretanto, a determinação destas abundâncias é bastante difícil, pois são necessários espectros de alta resolução e relação sinal-ruído (S/R). Além disso, a própria interpretação dos resultados é complexa porque sabe-se que as abundâncias de Li dependem de diversos parâmetros, tais como: temperatura efetiva (T_{ef}), metalicidade, massa, idade, velocidade de rotação projetada (representada aqui por $v \sin i$) e nível de atividade cromosférica medido a partir das linhas H e K do Ca II (representado aqui por $\log R'_{HK}$).

Estas dificuldades fizeram com que diversos autores chegassem a conclusões conflitantes após analisarem uma possível diferença entre as abundâncias de Li em estrelas com e sem planetas. Em um dos primeiros estudos sobre este tema, Gonzalez & Laws (2000) compararam as abundâncias de Li de 8 estrelas com planetas e de uma amostra de estrelas

⁴Ao longo desta tese, usaremos a notação $A(\text{Li}) = \log[\text{N}(\text{Li})/\text{N}(\text{H})] + 12$

de campo da literatura. Após corrigirem estas grandezas para diferenças sistemáticas em T_{ef} , $[\text{Fe}/\text{H}]$ e $\log R'_{HK}$, os autores concluíram que as estrelas com planetas possuem valores menores de $A(\text{Li})$. Este resultado não foi confirmado por Ryan (2000), que comparou as abundâncias de Li (todas retiradas da literatura) das estrelas com planetas e de uma amostra de estrelas de campo e de aglomerados abertos. Estes objetos de comparação foram cuidadosamente selecionados com o objetivo de cobrir o espaço de parâmetros (temperatura efetiva, idade e composição química) ocupado pelas estrelas com planetas.

Aproveitando o número crescente de sistemas planetários descobertos, Israeli et al. (2004) determinou abundâncias de Li para 79 e 38 estrelas com e sem planetas, respectivamente. Nenhuma diferença foi encontrada, mas os autores afirmaram que a amostra de comparação tinha muitos objetos para os quais só foi possível derivar limites superiores para $A(\text{Li})$. Desta forma, uma nova comparação foi feita com uma amostra de 157 estrelas sem planetas retiradas de Chen et al. (2001) e a seguinte conclusão foi obtida: as estrelas com planetas e temperaturas efetivas entre 5600 e 5850 K possuem uma depleção mais acentuada do Li.

Este resultado foi confirmado pelo trabalho de Takeda & Kawanomoto (2005), no qual 160 anãs e subgigantes do disco Galáctico (entre as quais havia 27 objetos com planetas) tiveram suas abundâncias de Li determinadas. A diferença, porém, foi encontrada no pequeno intervalo $5800 \text{ K} \lesssim T_{\text{ef}} \lesssim 5900 \text{ K}$. Vale ressaltar que esta conclusão só foi obtida quando a amostra de estrelas com planetas de Israeli et al. (2004) foi usada. Na comparação feita apenas com os valores de $A(\text{Li})$ de Takeda & Kawanomoto (2005), nenhuma diferença foi encontrada, mas os autores argumentam que o número de estrelas com planetas não é grande o suficiente para a realização de análises estatísticas relevantes. Baseados em amostras de estrelas com e sem planetas menores (16 e 20 objetos, respectivamente), Chen & Zhao (2006) forneceram uma nova confirmação da depleção mais acentuada do Li em estrelas com planetas no intervalo $5600 \text{ K} \lesssim T_{\text{ef}} \lesssim 5900 \text{ K}$.

A controvérsia ganhou um novo capítulo com o trabalho de Luck & Heiter (2006). Após realizarem uma determinação homogênea das abundâncias de Li em uma amostra de 216 anãs próximas, os autores não encontraram diferenças entre as estrelas com (55 objetos) e sem planetas. Além disso, eles afirmaram que o resultado de Israeli et al. (2004) era apenas uma consequência das diferentes escalas de temperaturas efetivas adotadas naquele trabalho e no estudo de Chen et al. (2001). Com o objetivo de tentar esclarecer a contro-

vérsia em torno do Li, Gonzalez (2008) compilou uma amostra de 37 e 147 estrelas com e sem planetas, respectivamente. Apesar de os dados serem da literatura, os autores fizeram correções com o objetivo de suprimir diferenças sistemáticas nos valores de T_{ef} , $\log g$, $[\text{Fe}/\text{H}]$ e $A(\text{Li})$ das diversas referências utilizadas. Foi observado que as estrelas com planetas apresentavam abundâncias de Li menores para $T_{\text{ef}} \lesssim 5800$ K e maiores para $T_{\text{ef}} \gtrsim 6100$ K, com a transição ocorrendo em $T_{\text{ef}} \simeq 5950$ K.

Mais recentemente, Meléndez et al. (2010) analisaram uma pequena amostra de 4 e 6 estrelas com e sem planetas, respectivamente, e não encontraram nenhum distinção entre as suas abundâncias de Li. Vale ressaltar que os 10 objetos possuíam $T_{\text{ef}} \sim 5800$ K, ou seja, estavam no regime de temperaturas efetivas no qual Gonzalez (2008) observou a diferença. Israelian et al. (2009), por outro lado, determinou abundâncias de Li, de forma homogênea, para uma amostra consideravelmente maior, composta por 451 estrelas (sendo 70 com planetas) do projeto HARPS GTO (Sousa et al. 2008). Além disso, foram incluídas mais 29 estrelas (16 com e 13 sem planetas) com $5600 \text{ K} \lesssim T_{\text{ef}} \lesssim 5900$ K. Os resultados confirmaram as abundâncias de Li mais baixas para as estrelas com planetas neste intervalo de temperaturas, assim como para o regime das análogas solares ($T_{\text{ef},\odot} = 5777 \pm 80$ K, como definido pelos autores). Complementando este estudo, Sousa et al. (2010) mostraram que esta diferença não era causada por efeitos relacionados às massas e idades das estrelas e propuseram que ela estava diretamente ligada à presença de planetas. Finalmente, Gonzalez et al. (2010a) derivaram abundâncias de Li para uma grande amostra de estrelas com e sem planetas (90 e 60, respectivamente). Os resultados basicamente confirmam as conclusões de Gonzalez (2008), mas encontram uma temperatura menor ($T_{\text{ef}} = 5850$ K) para a transição entre os regimes de baixas e altas abundâncias de Li nas estrelas com planetas.

1.3 Razões Isotópicas de ${}^6\text{Li}/{}^7\text{Li}$ em Estrelas com Planetas

As possíveis contribuições do Li para um melhor entendimento da formação e evolução dos sistemas planetários não se limitam apenas as suas abundâncias. A medida das razões isotópicas ${}^6\text{Li}/{}^7\text{Li}$ constitui um teste bastante sensível para verificar a ocorrência da acresção de pequenas quantidades material sólido às atmosferas das estrelas (Sandquist et al. 2002).

Durante a fase anterior à seqüência principal das estrelas de tipo solar, os dois isótopos do Li (${}^6\text{Li}$ e ${}^7\text{Li}$) são destruídos através de reações nucleares em temperaturas relativamente baixas ($T = 2,0 \times 10^6$ K para o ${}^6\text{Li}$ e $T = 2,5 \times 10^6$ para o ${}^7\text{Li}$). A fração de Li que é destruída é uma função muito forte da massa estelar. Existe, porém, um intervalo no qual o ${}^6\text{Li}$ é completamente destruído e uma quantidade apreciável de ${}^7\text{Li}$ sobrevive. O limite inferior deste intervalo de massas está logo acima da massa solar (correspondendo a estrelas de seqüência principal do tipo F tardio) para metalicidades solares. Desta forma, espera-se que não haja ${}^6\text{Li}$ nas atmosferas de estrelas de tipo solar. A detecção de uma razão isotópica ${}^6\text{Li}/{}^7\text{Li}$ positiva seria um indício da ocorrência do processo de poluição da zona convectiva da estrela.

Israelian et al. (2001) mediram a razão isotópica na estrela HD 82943 (que possui dois planetas gigantes próximos e uma massa $\simeq 1,1 M_\odot$) e encontraram o valor ${}^6\text{Li}/{}^7\text{Li} = 0,126 \pm 0,014$. Este resultado foi contestado por Reddy et al. (2002), que determinou a razão isotópica ${}^6\text{Li}/{}^7\text{Li} = 0,00 \pm 0,03$ para HD 82943. Além disso, um limite de ${}^6\text{Li}/{}^7\text{Li} < 0,03 \pm 0,03$ foi obtido para outras 7 estrelas com planetas. A diferença em relação ao resultado de Israelian et al. (2001) foi atribuída ao uso de uma lista de linhas mais completa. Israelian et al. (2003) analisaram os espectros de estrelas com diferentes temperaturas efetivas e concluíram que a linha não identificada em 6708,025 Å deveria ser atribuída ao Si I (e não ao Ti I, como foi proposto por Reddy et al. 2002). Com base nesta nova lista de linhas e em espectros de maior qualidade, os autores revisaram a razão isotópica de HD 82943 para ${}^6\text{Li}/{}^7\text{Li} = 0,05 \pm 0,02$. Apesar de ser significativamente menor do que o valor anterior, este resultado ainda sustentava a ocorrência de um processo de poluição.

Por fim, Mandell et al. (2004) compilaram uma lista de linhas consideravelmente mais detalhada do que as anteriores (principalmente, para as contribuições do CN) e testaram três possibilidades para a estrutura desconhecida em 6708,025 Å: Si I, Ti I e Ti II. Para os três casos, os autores não detectaram ${}^6\text{Li}$ em nenhuma das três estrelas com planetas analisadas. Infelizmente, a estrela HD 82943 não foi analisada neste último trabalho.

1.4 Abundâncias de Outros Elementos

Além do Fe e do Li, cerca de 20 outros elementos químicos (Be, C, N, O, Na, Mg, Al, Si, S, Ca, Sc, Ti, V, Cr, Ni, Co, Zn, Cu, Ba e Eu) tiveram suas abundâncias estudadas no

contexto das estrelas com planetas. Devido ao grande número de trabalhos na literatura que tratam deste tema, sugerimos as revisões de Gonzalez (2006a) e Udry & Santos (2007) para o direcionamento a referências mais detalhadas. Alguns trabalhos apresentam indícios de anomalias nas abundâncias químicas das estrelas com planetas (ver, por exemplo, Robinson et al. 2006 e Gonzalez & Laws 2007). De uma maneira geral, no entanto, os estudos mostram que não há diferenças nos padrões de evolução química (representados por gráficos do tipo $[X/\text{Fe}]$ *versus* $[\text{Fe}/\text{H}]$, onde X é um elemento químico qualquer) das estrelas com e sem planetas. Aparentemente, as estrelas com planetas gigantes apenas estão localizadas no extremo mais rico das distribuições de abundâncias químicas do disco fino da Galáxia. Este resultado é amplamente confirmado pelo estudo recente de Neves et al. (2009).

Se a análise individual de diversos elementos químicos não fornece vínculos fortes para os modelos de formação planetária, a situação parece mudar quando eles são estudados em conjunto. Em teoria, o fenômeno da poluição deixaria uma importante assinatura química nas estrelas: a correlação entre as abundâncias $[X/\text{H}]$ dos elementos e suas temperaturas de condensação T_C (ver Gonzalez 1997). Os elementos com as maiores T_C (chamados de *refratários*) apresentarão as menores abundâncias na fase gasosa. O oposto correrá para os elementos com as menores T_C (chamados de *voláteis*). Como o fenômeno da poluição ocorre em um ambiente relativamente quente (próximo à estrela), esperamos que os elementos refratários sejam acrescidos à atmosfera da estrela em maior quantidade. Portanto, uma inclinação positiva em um gráfico do tipo $[X/\text{H}]$ *versus* T_C (onde X representa os diversos elementos químicos considerados) seria uma evidência de poluição.

Smith et al. (2001) conduziram a primeira investigação desta possível correlação em uma amostra contendo HD 19994 e diversas outras estrelas com e sem planetas da literatura. Os resultados revelaram que 6 estrelas com planetas poderiam ter passado pelo processo de acreção. Vale notar que estas estrelas eram as de maior massa da amostra (ou seja, possuem as menores zonas convectivas) e seus planetas possuem pequenas separações orbitais. Estes dois fatores facilitariam o encontro de assinaturas da poluição. Estudos homogêneos feitos posteriormente (por exemplo, Ecuillon et al. 2006 e Gonzalez 2006b), por outro lado, não observaram diferenças significativas entre as estrelas com e sem planetas.

Mais recentemente, Meléndez et al. (2009) encontraram uma correlação significativa entre as abundâncias dos elementos químicos (representadas, agora, por $[X/\text{Fe}]$) e suas temperaturas de condensação. A análise de uma amostra de gêmeas e análogas solares

revelou que elas apresentavam maiores quantidades de elementos refratários em relação ao Sol. Este resultado, que é oposto ao esperado no caso de ocorrência da poluição, foi logo confirmado por Ramírez et al. (2009). Os autores sugerem que esta diferença poderia estar relacionada com a formação de sistemas planetários parecidos com o nosso e, em particular, com a existência de planetas terrestres. A formação destes últimos objetos faria com que os elementos refratários ficassem retidos, gerando a depleção observada no Sol. Esta conclusão é corroborada pelo trabalho de Gonzalez et al. (2010b), que mostra que as estrelas com planetas apresentam inclinações mais negativas (ou seja, os elementos refratários aparecem em menor quantidade) do que as estrelas sem planetas em um gráfico do tipo $[X/H]$ *versus* T_C .

1.5 Este Trabalho

As seções anteriores deixaram claro que o completo entendimento dos processos de formação e evolução planetária ainda está longe de ser alcançado. Esta tese tem como principal objetivo fornecer contribuições observacionais que ajudem a esclarecer algumas das principais questões em aberto. O nosso estudo é baseado em uma análise espectroscópica detalhada de uma amostra contendo 148 estrelas com planetas extra-solares e 160 objetos de comparação (sem planetas detectados ainda). Esta é a maior amostra de estrelas com planetas analisada de forma homogênea até o presente momento.

Os resultados serão apresentados na forma de uma compilação de 4 artigos, cada um deles exposto em um capítulo e precedido por uma breve introdução. A organização não segue a ordem cronológica de publicação dos artigos. O artigo (aceito para publicação no *Astrophysical Journal*) que discute as diferenças nas metalicidades de estrelas com planetas gigantes e netunianos é mostrado no Capítulo 2. O Capítulo 3, por sua vez, apresenta o artigo (submetido ao *Astrophysical Journal*) que analisa as metalicidades das estrelas com planetas em diferentes estágios evolutivos (anãs, subgigantes e gigantes). O artigo (submetido ao *Astrophysical Journal*) que aborda a questão das abundâncias de Li nas estrelas de seqüência principal com planetas é mostrado no Capítulo 4. No Capítulo 5, apresentaremos o artigo (publicado no *Astrophysical Journal*) que trata das razões isotópicas ${}^6\text{Li}/{}^7\text{Li}$. Finalmente, o Capítulo 6 traz as conclusões do nosso estudo e indica as perspectivas futuras deste trabalho.

Capítulo 2

Metalicidades em Estrelas com Planetas Gigantes e Netunianos

Os espectros utilizados nos Artigos I (apresentado neste capítulo), II e III (discutidos nos Capítulos 3 e 4) foram todos obtidos dentro do acordo entre o Observatório Nacional e o ESO (*European South Observatory*). Durante os anos de 2007 e 2008, realizamos seis missões observacionais em La Silla (Chile): abril, agosto e outubro de 2007; fevereiro, abril e agosto de 2008. As missões de outubro de 2007 e fevereiro de 2008 foram conduzidas, respectivamente, pelos Drs. Simon Schuler e Cláudio Bastos. Eu fui o responsável pela realização das outras 4 missões. Ao longo das 12,5 noites concedidas ao nosso projeto, observamos 148 estrelas com planetas extra-solares e 160 objetos de comparação. Os dados foram obtidos com o espectrógrafo FEROS (*Fiber-fed Extended Range Optical Spectrograph*) acoplado ao telescópio Max Planck Gesellschaft (MPG/ESO) de 2,2 m. Os espectros têm uma resolução $R \simeq 48.000$ e possuem, em geral, $S/R \gtrsim 200$ na região $\sim 6700 \text{ \AA}$. A redução foi feita com o auxílio do pacote FEROS *Data Reduction System* (DRS). Como um exemplo, mostramos o espectro da estrela HD 2039 no apêndice A.

A determinação dos parâmetros atmosféricos (temperatura efetiva, gravidade superficial e velocidade de microturbulência) e das metalicidades das estrelas foi feita através do método espectroscópico clássico, baseado nos equilíbrios de excitação e ionização das linhas do Fe I e Fe II (o apêndice B contém as larguras equivalentes destas linhas para todas as estrelas da amostra). Com o objetivo de otimizar esta etapa, foi desenvolvido um conjunto de códigos (escritos nas linguagens BASH e FORTRAN) que realizam a iteração automática

dos parâmetros atmosféricos. Os resultados para a nossa amostra de 308 estrelas foram obtidos em 2 dias aproximadamente. Neste capítulo, apresentaremos o artigo (aceito para publicação no *Astrophysical Journal*) que discute as metalicidades de uma subamostra de 262 estrelas de seqüência principal (as tabelas 1, 3 e 4 deste artigo são reproduzidas por completo no apêndice C). Este trabalho contém a mais abrangente comparação homogênea entre estrelas com planetas gigantes e netunianos (108 e 9 objetos, respectivamente) até o presente momento. A análise das distribuições de metalicidades destes dois grupos forneceu possíveis evidências a respeito da influência deste parâmetro na formação planetária.

Stellar Parameters and Metallicities of Stars Hosting Jovian and Neptunian mass Planets: A Possible Dependence of Planetary Mass on Metallicity¹

L. Ghezzi¹, K. Cunha^{1,2,3}, V. V. Smith², F. X. de Araújo^{1,4}, S. C. Schuler² & R. de la Reza¹

ABSTRACT

The metal content of planet hosting stars is an important ingredient which may affect the formation and evolution of planetary systems. Accurate stellar abundances require the determinations of reliable physical parameters, namely the effective temperature, surface gravity, microturbulent velocity, and metallicity. This work presents the homogeneous derivation of such parameters for a large sample of stars hosting planets ($N=117$), as well as a control sample of disk stars not known to harbor giant, closely orbiting planets ($N=145$). Stellar parameters and iron abundances are derived from an automated analysis technique developed for this work. As previously found in the literature, the results in this study indicate that the metallicity distribution of planet hosting stars is more metal-rich by ~ 0.15 dex when compared to the control sample stars. A segregation of the sample according to planet mass indicates that the metallicity distribution of stars hosting only Neptunian-mass planets (with no Jovian-mass planets) tends to be more metal-poor in comparison with that obtained for stars hosting a closely orbiting Jovian planet. The significance of this difference in metallicity arises from a homogeneous analysis of samples of FGK dwarfs which do not include the cooler and more problematic M dwarfs. This result would indicate that there is a possible link between planet mass and metallicity such that metallicity plays a role in setting the mass of the most massive planet. Further confirmation, however, must await larger samples.

Subject headings: Planets and satellites: formation – Stars: abundances – Stars: atmospheres – Stars: fundamental parameters – (Stars): planetary systems

¹Observatório Nacional, Rua General José Cristino, 77, 20921-400, São Cristóvão, Rio de Janeiro, RJ, Brazil; luan@on.br

²National Optical Astronomy Observatory, 950 North Cherry Avenue, Tucson, AZ 85719, USA

³Steward Observatory, University of Arizona, Tucson, AZ 85121, USA

⁴Deceased in July 2009

1. Introduction

More than 380 stars with planets have been discovered to date, half of which were detected in the past three years. Most of the extrasolar planets have been discovered via radial-velocity measurements of the reflex motions of the planet-hosting star and such surveys are biased to detect preferentially the largest and most closely orbiting planets. Within an ever increasing sample size, one statistically significant property has been confirmed for these objects: the average metallicity of the solar-like stars known to have giant planets (i.e. those planets close to the mass of Jupiter or larger) is higher when compared to field F, G and K dwarfs not known to host giant planets (see, e.g., Gonzalez 1997; Santos et al. 2001; Laws et al. 2003; Santos et al. 2005; Fischer & Valenti 2005; Bond et al. 2006; Sousa et al. 2008). This difference is attributed to two possible scenarios: primordial enrichment and pollution. At present, the former seems to best account for the metal-rich nature of the planet hosting stars, since the probability of finding a planet is a steeply rising function of the stellar metallicity (e.g., Santos et al. 2004; Fischer & Valenti 2005). However, the pollution hypothesis cannot be discarded, as contradictory conclusions have been found by several studies which attempted to unveil other chemical peculiarities in planet hosting stars (for a comprehensive review, see Gonzalez 2006; Udry & Santos 2007).

In addition to the population of rather metal rich stars hosting Jovian-mass planets, there is a growing number of known systems with considerably lower-mass planetary companions. The range of planetary masses now includes objects with minimum masses of only about $M_p \sin i \sim 4M_{\oplus}$, with many systems containing “Neptunian-mass” planets, with $M_p \sin i < 25M_{\oplus}$. It is of interest to investigate whether the trend for Jovian-mass planets to have a metal-rich stellar parent continues towards systems with lower-mass planets that do not contain the large Jovian-mass planets. Udry et al. (2006), Sousa et al. (2008), and Mayor et al. (2009) suggest that stars which have as their most massive planets Neptunian-mass objects may not be metal rich; however, the number of such systems which have been studied is just a few. The list of stars with Neptunian-mass planets continues to grow and these objects will help to probe the possibility of a stellar-metallicity planet-mass connection.

The observed variety of exo-planetary masses and orbital separations, along with evidence of planetary migration and its possible influence on proto-planetary disk – stellar interactions suggests that it is of importance to determine chemical abundance distributions in different populations of exo-planet host stars. The search for subtle patterns in the abundances of stars with and without planets that may reveal details of planetary formation or

¹Based on observations made with the 2.2 m telescope at the European Southern Observatory (La Silla, Chile), under the agreement ESO-Observatório Nacional/MCT.

planetary system architecture is based ideally on a homogeneous and self-consistent analysis. If all samples are observed with the same instrumental setup and analyzed with a consistent methodology, systematic effects are more likely to be avoided. This study sets forth a homogeneous determination of stellar parameters and metallicities for a large sample of stars with planets, including a few stars hosting only Neptunian mass planets, as well as a control sample comprised of field stars not known to host giant planets. §2 describes the observational data, sample selection criteria, and data reduction. The determination of stellar parameters, effective temperatures, surface gravities and metallicities, including the adopted iron line list, are presented in §3. In §4, results from this work are compared with those from the literature and discussed in light of various planet-metallicity correlations. Included in this discussion is an investigation into whether metallicity plays a role in determining the mass of the most massive planet in an exo-planetary system. Finally, concluding remarks are presented in §5. The derivation of the elemental abundances other than Fe will be treated in subsequent papers.

2. Observations and Data Reduction

2.1. Sample Selection

Planet Hosting Stars: The sample of main-sequence stars with planets analyzed in this study contains 117 targets. The target list was compiled using the Extrasolar Planet Encyclopaedia² and updated with newly discovered systems until August 2008. We selected all planet hosting stars having $\delta < +26^\circ$ and $V < 12$. The declination limit was imposed by object observability at La Silla Observatory in Chile, and the limiting magnitude was set in order to keep exposure times needed to achieve the desired S/N relatively short. Several stars in this sample have been previously analyzed in recent studies of planet hosting stars (Laws et al. 2003; Santos et al. 2004, 2005; Takeda et al. 2005; Valenti & Fischer 2005; Luck & Heiter 2006; Bond et al. 2006; Sousa et al. 2008). We note that 16 planet hosting stars in this sample are not included in these previous abundance studies.

Control Sample: A control sample of main-sequence disk stars which are not known to host giant planets was selected from the list of nearby F, G and K stars in Fischer & Valenti (2005) which has been targeted in the planet search programs conducted at the Keck Observatory, Lick Observatory and the Anglo-Australian Telescope. That study identified 850 stars for which there are enough observations to securely detect the presence of compan-

²Available at <http://exoplanet.eu>

ions with velocity amplitudes $K > 30 \text{ m s}^{-1}$ and orbital periods shorter than 4 yr. From the subsample of stars with non-detections of giant planets, we eliminated stars with $[\text{M}/\text{H}] < -1.0$; $v \sin i > 10 \text{ km s}^{-1}$ (typical rotational velocities are much lower for solar-type stars) and $\delta > +26^\circ$. In addition, any stars which were found subsequently to host giant planets (the only case being HD 16417) were obviously removed from the list. Binaries, as well as targets having one single spectrum analyzed were also excluded (according to Table 8 in Valenti & Fischer 2005). HD 36435 was added to the list as it was previously analyzed for ${}^6\text{Li}$ (Ghezzi et al. 2009). The final sample of comparison stars in this study has 145 targets. A list with all targets analyzed, planet hosting stars as well as control sample stars, is presented in Table 1.

2.2. Observations and Data Reduction

High-resolution spectra were obtained with the Fiber-fed Extended Range Optical Spectrograph (FEROS; Kaufer et al. 1999) attached to the MPG/ESO-2.20m telescope (La Silla, Chile). The detector was a 2k X 4k EEV CCD with $15 \mu\text{m}$ pixels. This instrumental setup produces spectra with almost complete spectral coverage from 3,560 to 9,200 Å (over 39 échelle orders) and at a nominal resolution $R = \lambda/\Delta\lambda \sim 48,000$. The observations were conducted during 6 observing runs between April 2007 and August 2008³. A solar spectrum of the afternoon sky ($T_{exp} = 2 \times 120\text{s}$) was taken before each observing night. A detailed log of the observations, including V magnitudes, observation dates, total integration times and the resulting S/N per resolution element, is found in Table 1.

The spectra were reduced with the FEROS Data Reduction System (DRS)⁴. The data reduction followed standard procedures. An average flat-field image was used in order to define the positions of the échelle orders. The background (bias level and scattered light) was subtracted from the images. The bias level was determined from the overscan region of the CCD and the scattered light was measured in the interorder space and in the region between the two fibers. The extraction of the échelle orders was done with a standard algorithm that also finds and removes cosmic rays. All extracted images were divided by the average flat-field in order to remove pixel-to-pixel variations and they were corrected for the blaze function. The flat-fielded spectra were wavelength calibrated using ThArNe and/or ThAr+Ne calibration frames. The calibrated spectra were rebinned in constant steps of wavelength and a barycentric correction was applied. Finally, the reduced spectra were

³Under the agreement ESO-Observatório Nacional/MCT

⁴Available at <http://www.eso.org/sci/facilities/lasilla/instruments/feros/tools/DRS/index.html>

corrected for radial velocity shifts by comparing the observed wavelengths of some isolated and moderately strong iron lines with their rest wavelenghts taken from Vienna Atomic Line Database⁵ (VALD; Kupka et al. 1999).

3. Analysis

3.1. The Fe Line List

The line lists for Fe I and Fe II were compiled from the line sample in Sousa et al. (2008) and Meléndez & Barbuy (2009). The initial line list contained over 100 iron lines but using both the Solar Flux Atlas (Kurucz et al. 1984) as well as the solar spectrum taken with FEROS on 20 August 2008, and from results of test calculations with a variety of *gf*-values from the literature, we selected 27 Fe I and 12 Fe II suitable lines which were unblended and of intermediate strength (equivalent widths less than 90 mÅ, in order to limit the effects of damping on the abundance determination). The final line list adopted in this Fe abundance analysis is presented in Table 2. The wavelengths and lower excitation potentials (LEP) of the Fe transitions were taken from VALD. The *gf*-values for Fe I transitions were taken from: Blackwell et al. (1982a,b, 1984, 1986, 1995), Bard, Kock & Kock (1991) and Bard & Kock (1994), and O'Brian et al. (1991). The *gf*-values from these studies were carefully compared in Lambert et al. (1996) and found to be in excellent agreement. Fulbright et al. (2006) also argue that differences between the *gf*-values of these three groups are comparable to random uncertainties in the measurements. Corrections to the log *gf* scales from these different sources were therefore deemed not necessary in this study; whenever a transition had more than one *gf*-value available, an average value was adopted. The *gf*-values for the Fe II lines in this study were taken from the critical analysis of Lambert et al. (1996).

3.2. Equivalent Width Measurements

The code ARES⁶ (Sousa et al. 2007) was used in order to measure equivalent widths (EWs) of sample Fe lines automatically. Briefly, this program first fits a polynomial to the local continuum in a spectral region defined by the user. It then determines which lines inside the given interval can be fit by a Gaussian profile. Finally, it computes the equivalent width(s) for the line(s) of interest assuming a Gaussian profile. More details about the ARES

⁵Available at <http://ams.astro.univie.ac.at/~vald/>

⁶<http://www.astro.up.pt/~sousasag/ares/>

code can be found in Sousa et al. (2007) and Sousa et al. (2008). The equivalent widths measured for all program stars can be found in Ghezzi (2010).

Possible systematic effects in the automatic ARES equivalent width measurements were investigated here. We measured (using the `splot` task of IRAF) equivalent widths of 75 Fe I lines and 22 Fe II lines in 6 stars which were selected to bracket the range in effective temperature, metallicity and spectrum quality (signal-to-noise ratio) of our sample as well as the Sun. A comparison between manual and automatic equivalent width measurements for 638 lines is shown in Figure 1. The mean difference between the two sets of equivalent widths is $\langle \text{EW}_{\text{ARES}} - \text{EW}_{\text{Manual}} \rangle = -0.53 \pm 2.10 \text{ m}\text{\AA}$. Also, the following linear fit is obtained: $\text{EW}_{\text{ARES}} = (1.005 \pm 0.002)\text{EW}_{\text{Manual}} + (-0.77 \pm 0.16)$. The correlation coefficient and the standard deviation are $R = 0.99627$ and $\sigma = 2.09 \text{ m}\text{\AA}$, respectively.

The exercise above indicates that the equivalent widths which were measured automatically using the ARES code are consistent with our measurements, although there is a slight trend of ARES equivalent widths being marginally smaller than the ones measured manually in this study. This result is in line with what was found in Sousa et al. (2007). Although we find an overall good agreement between manual and automatic equivalent widths, it is important to carefully check the results because ARES does not make quality assessments of the measurements it outputs. For instance, in the tests described above we note that there were 10 lines with obviously erroneous equivalent width measurements, which were discarded. In this study we estimate an uncertainty of $\sim 2 \text{ m}\text{\AA}$ as the typical uncertainty in the equivalent width measurements. Differences in equivalent widths of $\pm 2 \text{ m}\text{\AA}$ are about what is expected given the resolution, sampling, and S/N of the spectra and no significant systematic effects are found between ARES and manual measurements.

3.3. Derivation of Stellar Parameters and Iron Abundances

Stellar parameters (T_{eff} , $\log g$ and ξ) and metallicities ([Fe/H]) were derived homogeneously and following standard spectroscopic methods which are based on requirements of excitation and ionization equilibria. This abundance analysis was done in Local Thermodynamic Equilibrium (LTE) using the 2002 version of MOOG⁷ (Sneden 1973). In all calculations van der Waals constants were multiplied by an enhancement factor of 2.0 (Holweger et al. 1991). The model atmospheres in this study were interpolated from the ODFNEW grid

⁷Available at <http://verdi.as.utexas.edu/moog.html>.

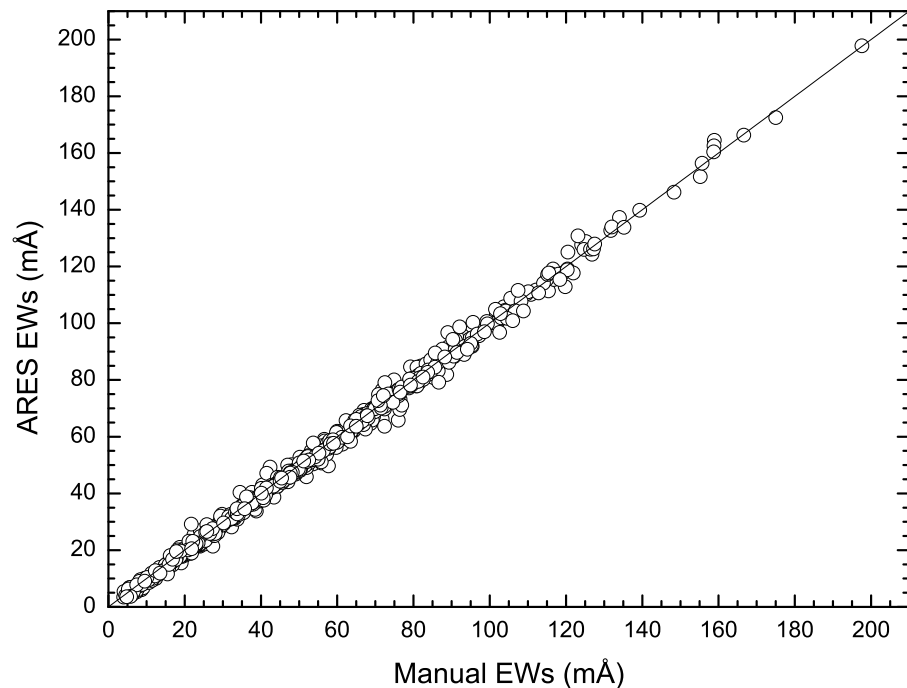


Fig. 1.— A comparison between manual (using IRAF `splot`) and automatic measurements of equivalent widths (using ARES code) for a sample of Fe I and Fe II lines in six target stars and the Sun. The solid line represents perfect agreement.

of ATLAS9 models⁸ (Castelli & Kurucz 2004).

Effective temperatures and microturbulent velocities were iterated until the slopes of $A(\text{Fe I})^9$ *versus* excitation potential, χ , and $A(\text{Fe I})$ *versus* reduced equivalent width, $\log(EW/\lambda)$, were respectively zero (excitation equilibrium). Only lines with $\log(EW/\lambda) < -5.00$ (this limit was changed to larger values for cooler stars) were used in the first iteration, in order to decouple the T_{eff} and ξ determinations. Surface gravities were iterated until Fe I and Fe II returned the same mean abundances (ionization equilibrium). At the end of the iterative process, a consistent set of values of T_{eff} , $\log g$ and microturbulent velocity as well as the mean Fe I (= Fe II) abundance is obtained for the star. This procedure was adopted for all stars in our sample except for seven targets which had lower metallicities and solar temperatures (namely HD 6434, HD 51929, HD 80913, HD 114762, HD 153075, HD 155918 and HD 199288). In these cases, the microturbulent velocities were kept at a fixed value because there were no lines strong enough in order to anchor the iteration of this parameter. As an example, Figure 2 shows the final iterated plots of $A(\text{Fe I})$ *versus* χ (top panel) and $A(\text{Fe I})$ *versus* $\log(EW/\lambda)$ (bottom panel) for target HD 2039.

An Automated Analysis: Due to the large number of stars in our sample and Fe lines included in the analysis, BASH and FORTRAN codes were built in order to automate the whole iterative process described above. In summary, the code starts with automatic equivalent width measurements using ARES (Section 3.2) and iterates to a final set of consistent values of effective temperature, surface gravity, microturbulence and Fe abundance (both from Fe I and Fe II). With the development of an automatic procedure it is now possible to analyze the entire sample of over 300 stars studied here in a few days without interventions.

In order to further test our line list (Table 2) and analysis method, the solar spectrum (observed with FEROS spectrograph on August 20, 2008) was analyzed in a similar manner, with automatic measurements of equivalent widths (the measured solar equivalent widths are found in the last column of Table 2). Solar abundances $A(\text{Fe I}) = 7.43 \pm 0.07$ and $A(\text{Fe II}) = 7.44 \pm 0.05$ as well as a microturbulence $\xi = 1.00 \text{ km s}^{-1}$ were derived using a Kurucz ODFNEW model atmosphere with $T_{\text{eff}} = 5777 \text{ K}$, $\log g = 4.44$, a model turbulence of $\xi = 2.0 \text{ km s}^{-1}$, and $l/H_p = 1.25$. This solar Fe abundance is in excellent agreement with the results of Reddy et al. (2003) and Fulbright et al. (2006) ($A(\text{Fe})=7.45$), which use gf -values from the same sources as here. The derived solar iron abundance also compares well (within the uncertainties) with recent solar abundance determinations for 3D hydrodynamical models from Asplund et al. (2009, $A(\text{Fe})= 7.50 \pm 0.04$) and Caffau et al. (2010, $A(\text{Fe})=7.52 \pm 0.06$).

⁸Available at <http://kurucz.harvard.edu/>

⁹ $A(\text{Fe I}) = \log [\text{N(Fe I)}/\text{N(H)}] + 12$

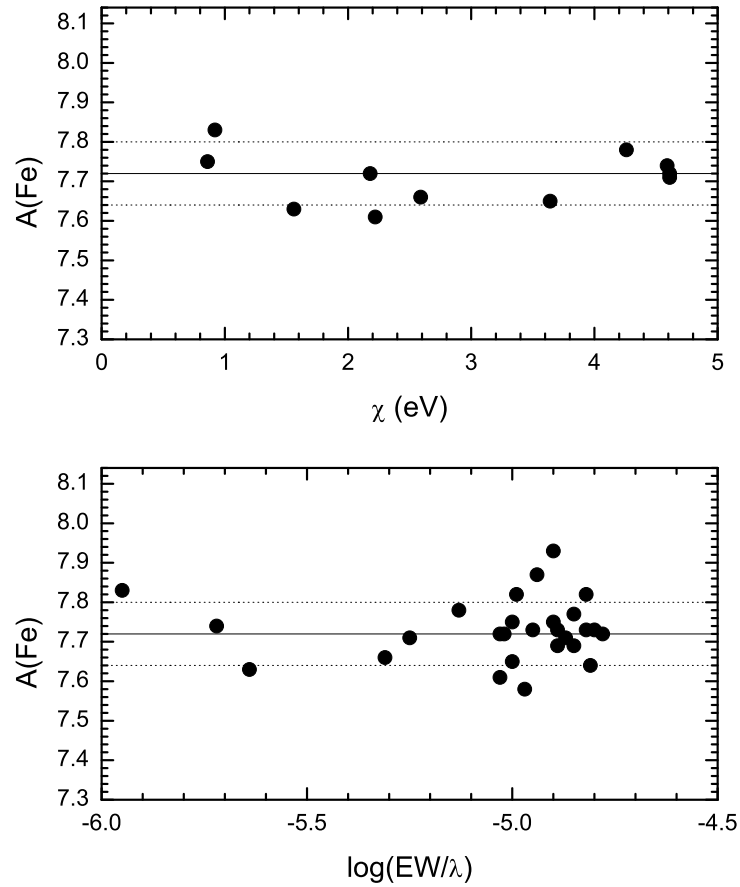


Fig. 2.— The spectroscopic determination of effective temperature and microturbulent velocity for HD 2039 obtained from zero slopes in the runs of Fe I abundances with excitation potential of the transitions (top panel) and reduced equivalent widths (bottom panel). The solid line represents the mean iron abundance and the dashed lines represent the $1-\sigma$ of the distribution. The top panel shows only those lines with $\log(EW/\lambda) < -5.00$ which were used in the T_{eff} iteration. Fe I and Fe II abundances are consistent and the slopes are zero for $A(\text{Fe}) = 7.73$.

Final values of effective temperatures, surface gravities and microturbuleny velocities for all stars are presented in Table 3. The metallicities [Fe/H] (listed in the last column in Table 3) were calculated for a solar abundance $A(\text{Fe})_{\odot} = 7.43$ (as derived here). The σ -values listed in columns 6 and 8 correspond to the standard deviations of the final mean abundances of Fe I and Fe II. The number of Fe I and Fe II lines considered for each star are listed in columns 7 and 9, respectively.

As a comparison, photometric effective temperatures were also derived using the T_{eff} versus $V - K$ calibration recently published by Casagrande et al. (2010). The V and K_s magnitudes for the target stars were taken, respectively, from *The Hipparcos and Tycho Catalogues* (ESA 1997) and the *2MASS* All-Sky Catalog of Point Sources (Cutri et al. 2003). A comparison between the spectroscopic and photometric temperatures shows that the latter are systematically higher (Figure 3). The mean difference for all studied stars is $\Delta T_{\text{eff}}(\text{spec} - \text{phot}) = -63 \pm 113$ K, indicating reasonable agreement.

Uncertainties in the parameters T_{eff} , $\log g$, ξ and [Fe/H] were estimated as in Gonzalez & Vanture (1998) and can be seen in Table 3. We note that these are internal errors and that the real uncertainties might be somewhat larger. Departures from LTE were not considered in this study and these can affect the derived LTE abundances. Non-LTE effects are expected to be smaller for Fe II lines as Fe II (and not Fe I) is the dominant ionization stage in solar type stars. For Fe I, departures from LTE are larger and may be at the level of ~ 0.1 dex (Gehren et al. 2001a,b).

3.4. Evolutionary Parameters

Stellar luminosities, masses, radii and ages define the evolutionary stages of stars and for this sample these were calculated in the following way. Absolute magnitudes M_V were determined using the classical formula:

$$M_V = V + 5 + 5 \log \pi - A_V. \quad (1)$$

As already mentioned, the apparent V magnitudes (Table 1) were taken from *The Hipparcos and Tycho Catalogues* (ESA 1997). As the uncertainties in this magnitude are not listed, we adopted the errors in V_T , given the similarities between the two passbands (van Leeuwen et al. 1997). The parallaxes π and their uncertainties (Table 4; columns 2 and 3) were taken from van Leeuwen (2007). Three stars (namely HD 70573, BD-10 3166 and WASP 2) were not present in the sources above, thus their V magnitudes and parallaxes come from

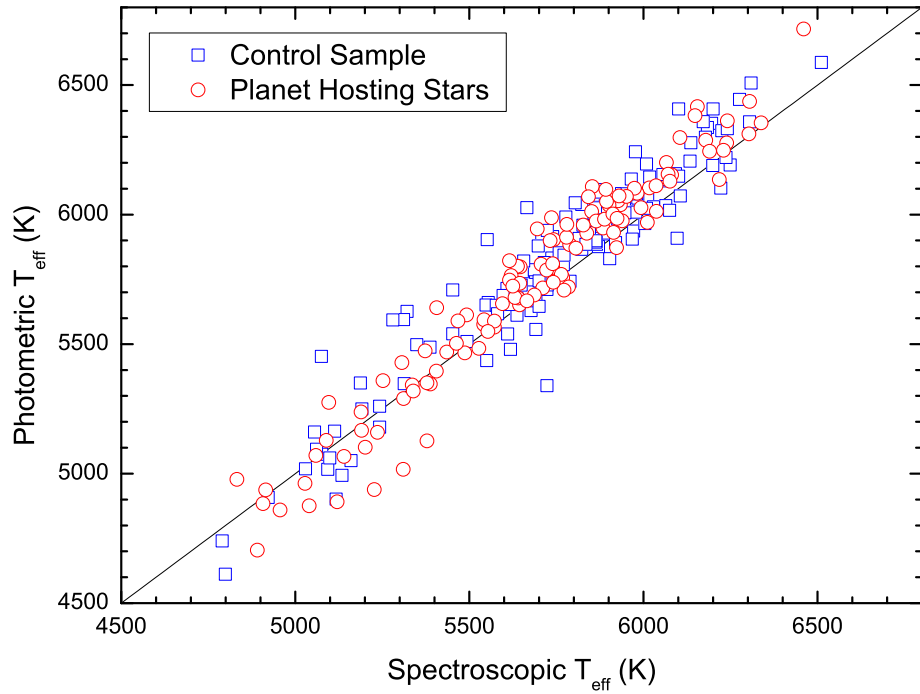


Fig. 3.— A comparison between photometric temperatures derived with the $V - K$ calibration in Casagrande et al. (2010) and spectroscopic temperatures derived in this study for planet hosting stars (red open circles) and control sample (blue open squares). The solid line represents the bisector. The two effective temperature scales are in reasonable agreement, however, there is a tendency for the photometric T_{eff} s to be higher than the spectroscopic ones at the high T_{eff} end and lower at the low T_{eff} end.

the references in SIMBAD¹⁰ and The Extrasolar Planet Encyclopaedia. The interstellar monochromatic extinction at V magnitude, A_V (Table 4; column 4), as well as its error were calculated using the tables from Arenou et al. (1992) and the code EXTINCT.FOR from Hakkila et al. (1997). Note that the Arenou et al. (1992) model is accurate to distances within 1 kpc of the Sun.

Absolute magnitudes were converted to bolometric magnitudes M_{bol} by adding bolometric corrections in the V band, BC_V (Table 4; column 5), linearly interpolated from the grids of Girardi et al. (2002) for the atmospheric parameters given in Table 3. The luminosities were then calculated using the well known relation:

$$\log \frac{L}{L_\odot} = -0.4(M_{bol} - M_{bol,\odot}), \quad (2)$$

where $M_{bol,\odot} = 4.77$ (Girardi et al. 2002). The uncertainties in M_V , M_{bol} and $\log(L/L_\odot)$ were derived considering that $\sigma(BC_V)$ and $\sigma(M_{bol,\odot})$ are zero. The luminosities and uncertainties are listed in Table 4 (columns 6 and 7).

Effective temperatures and luminosities were used to place the stars on a grid of Y² isochrones from Demarque et al. (2004), thus allowing for an age determination. An interpolation code provided by the authors¹¹ was used in order to obtain a set of isochrones ranging from 1.0 to 13.0 Gyr in age and from −0.70 dex to +0.40 dex in metallicity (with steps of 1.0 Gyr and 0.1 dex, respectively). As an example, we show the grid of isochrones for [Fe/H] = +0.30 dex in Figure 4 (top panel). The locations of all targets stars are indicated. The age of the closest isochrone was attributed for each star. Given the uncertainties in T_{eff} , $\log(L/L_\odot)$ and [Fe/H] and the proximity of the isochrones, an age interval was also estimated for each star together with a single age (see Table 4). Also, some stars were located outside the grid and their ages were indicated as lower or upper limits.

Stellar radii and spectroscopic masses M_{spec} (as well as their uncertainties) were derived using standard relations (see e.g. eqs. 5–8 from Valenti & Fischer 2005). The masses were also calculated by placing the stars on a grid of evolutionary tracks from Yi et al. (2003). The mass of the closest track was attributed for each star. An interpolation code (provided by the authors¹²) was used in order to obtain a set of tracks ranging from 0.5 to 2.0 M_\odot in mass and from −0.70 dex to +0.40 dex in metallicity (with steps of 0.1 M_\odot and 0.1 dex, respectively). A typical uncertainty in mass of 0.1 M_\odot was estimated by considering the

¹⁰<http://simbad.u-strasbg.fr/simbad/>

¹¹Available at <http://www.astro.yale.edu/demarque/yyiso.html>

¹²Available at <http://www.astro.yale.edu/demarque/yystar.html>

errors in T_{eff} , $\log(L/L_\odot)$ and [Fe/H]. In some cases, however, this error was larger because of the location of the star on the grid or due to a larger uncertainty in the luminosity. Also, a few stars were located below the Zero Age Main Sequence (ZAMS) and their masses had to be estimated through an extrapolation. As an example, the grid of evolutionary tracks for [Fe/H] = +0.30 dex is shown in Figure 4 (bottom panel). The stellar radii and masses (spectroscopic, M_{spec} , and those derived with the evolutionary tracks, M_{track}) can be found in Table 4.

As the spectroscopic masses have greater errors, we adopt the masses obtained with the grid of evolutionary tracks. Using those masses, the Hipparcos surface gravities can be calculated with the relation:

$$\log g = \log g_\odot + \log \frac{M}{M_\odot} - \log \frac{L}{L_\odot} + 4 \log \frac{T_{eff}}{T_{eff,\odot}}, \quad (3)$$

where $T_{eff,\odot} = 5777$ K and $\log g_\odot = 4.44$. The uncertainty in these gravities was calculated considering $\sigma(T_{eff,\odot}) = 0$ and $\sigma(\log g_\odot) = 0$. The results are presented in Table 4 (columns 14 and 15). In Figure 5 we show a comparison between the derived spectroscopic log g's (listed in Table 3) with Hipparcos log g's (listed in Table 4; column 14). The line indicating perfect agreement is also shown as a solid line in the figure. The agreement between the two sets of log g's is good although we note that the Hipparcos gravities are typically found to be higher (by 0.06 dex on the average) than the spectroscopic values with a standard deviation of ± 0.15 dex, which is of the order of the estimated uncertainties in the derived log g from the iron line analysis.

In addition, masses, radii, ages and trigonometric gravities were also derived with Leo Girardi's web code PARAM¹³, which is based on a Bayesian parameter estimation method (da Silva et al. 2006). The mean differences between the results discussed above (This work - Girardi's code) are small and indicate good agreement: $\Delta M = 0.03 \pm 0.05 M_\odot$ (N=262), $\Delta R = 0.01 \pm 0.06 R_\odot$ (N=223), $\Delta t = 0.37 \pm 1.46$ Gyr (N=211) and $\Delta \log g = 0.03 \pm 0.05$ (N=262).

4. Discussion

4.1. Comparisons with Other Studies

Several recent studies in the literature have derived stellar parameters and metallicities for samples of planet hosting stars. In the following we briefly summarize some of these works

¹³Available at <http://stev.oapd.inaf.it/cgi-bin/param>

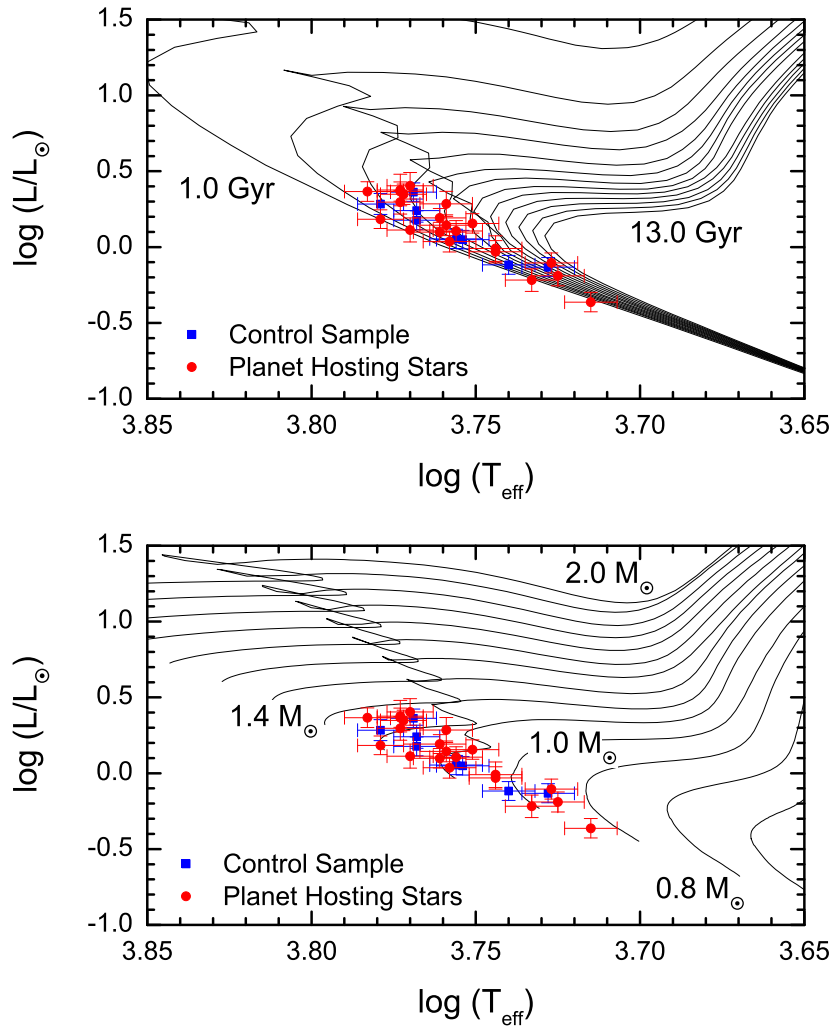


Fig. 4.— The location of sample planet hosting stars (red circles) and control disk sample stars (blue squares) in an HR diagram. The values of effective temperature and luminosity for the targets are from Tables 3 and 4, respectively. The top panel shows isochrones for ages varying between 1 and 13 Gyr and the bottom panel shows evolutionary tracks for mass tracks between $0.8 M_\odot$. The grids of isochrones and evolutionary tracks were calculated for $[\text{Fe}/\text{H}] = +0.30$ dex (Demarque et al. 2004; Yi et al. 2003)

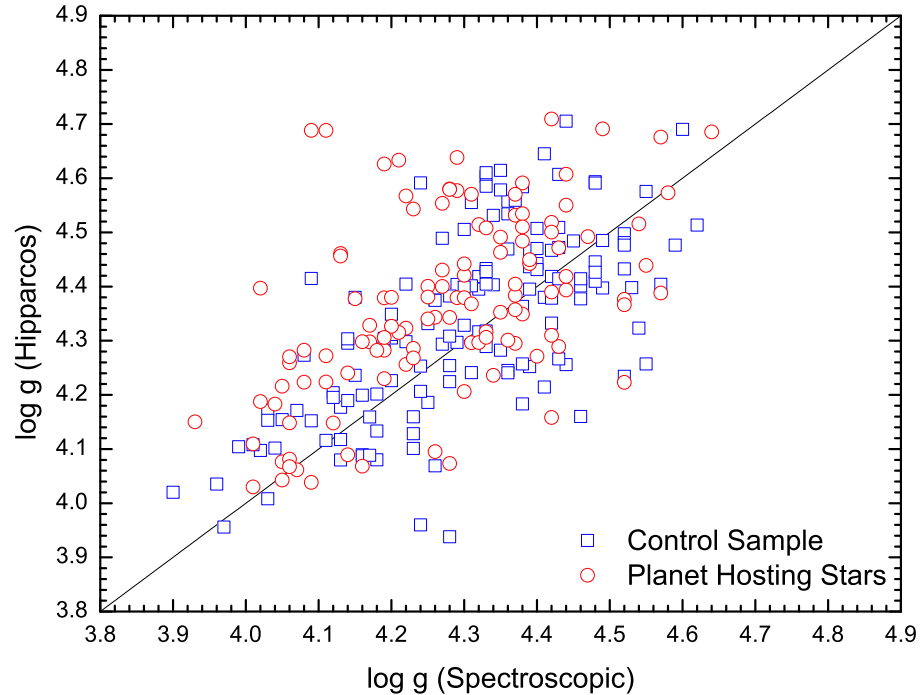


Fig. 5.— A comparison between Hipparcos and spectroscopic gravities for planet hosting stars and control sample. The agreement between the two sets of surface gravities is found to be good and systematic differences between the two independent scales are less than ~ 0.1 dex on average. The solid line is the bisector and represents the perfect agreement between the two determinations.

and then compare their results of effective temperatures, surface gravities and metallicities with the ones obtained in this study.

Laws et al. (2003) determined spectroscopic parameters for 30 stars with giant planets and/or brown dwarf companions. Their analysis method is similar to this study, the difference being the line list and *gf*-values which were obtained from an inverted solar analysis. **Santos et al. (2004, 2005)** did a spectroscopic analysis of a large sample of stars with and without planets (119 and 94 targets, respectively). Their method is very similar to the one used by Laws et al. (2003), with the difference being the list of iron lines (the *gf*-values are also solar). **Takeda et al. (2005)** obtained stellar parameters for a set of 160 mid-F through early-K dwarfs/subgiants. The difference with previous studies is the selected iron lines. **Valenti & Fischer (2005)** derived stellar properties for 1040 nearby F, G and K stars observed as part of the Keck Observatory, Lick Observatory and Anglo-Australian Telescope (AAT) planet search programs. Their method was different; stellar parameters and abundances were determined from a direct comparison of observed and synthetic spectra across certain spectral intervals using the spectral modelling program, SME. In addition, a fixed value of 0.85 km s^{-1} for the microturbulence was adopted for all stars. **Luck & Heiter (2006)** derived atmospheric parameters for a sample of 216 nearby dwarf stars. They used the standard spectroscopic method, but with differential abundances relative to the Sun. **Bond et al. (2006)** determined atmospheric parameters from 136 G-type stars from the AAT planet search program. In that study, photometric temperatures are obtained from $B-V$ colours listed in the *Hipparcos* catalog, with discrete values of microturbulence set at 1.00, 1.25 and 1.50 km s^{-1} . The metallicities and gravities are determined by iterating this parameters until the Fe I and Fe II abundances are the same. **Sousa et al. (2008)** derived spectroscopic parameters for all 451 solar-type stars from the HARPS Guaranteed Time Observations (GTO) “high-precision” sample. Their method closely resembles that from Santos et al. (2004, 2005), except for a larger line list and the usage of automatic measurements of equivalent widths.

A direct comparison of the stellar parameters and metallicities obtained for some studied stars in our sample with results from other studies discussed above is possible given that there are several targets in common. Table 5 shows the average differences (in the sense This study - Literature study) computed for the effective temperatures ($\langle \Delta T_{\text{eff}} \rangle$), surface gravities ($\langle \Delta \log g \rangle$) and metallicities ($\langle \Delta [\text{Fe}/\text{H}] \rangle$) obtained for all target stars we have in common with the studies of Laws et al. (2003); Santos et al. (2004, 2005); Takeda et al. (2005); Valenti & Fischer (2005); Luck & Heiter (2006); Bond et al. (2006); Sousa et al. (2008); Santos et al. (2004, 2005). The number of stars compared in each case is found in Table 5 (column 5). Results from this simple and direct comparison are briefly summarized below.

Effective Temperatures: In general, there is not a significant offset in the effective temperature scale in this study in comparison with the other studies in Table 5. In particular, for 5 studies we find $\langle \Delta T_{\text{eff}} \rangle$ to be less than 15 K, which is a quite small systematic offset; the Luck & Heiter (2006) study has a difference which is only slightly larger (~ 35 K). A comparison with the T_{eff} from results in Bond et al. (2006) indicates, however, a more significant systematic difference of ~ 75 K. The standard deviations around the mean values are all ~ 100 K or less, which is in general agreement with the estimated uncertainties for the derived effective temperatures in this study.

Surface Gravities: A direct comparison between the average surface gravity value derived for selected targets in this study with average results from Laws et al. (2003); Santos et al. (2004, 2005); Valenti & Fischer (2005); Luck & Heiter (2006) and Sousa et al. (2008) indicates that there is a small offset (~ 0.08 dex – 0.12 dex) in the $\log g$ scales. An agreement (at the level of 0.05 dex or better) is found between our results and Takeda et al. (2005) and Bond et al. (2006). The standard deviations of the distributions around the average differences in $\log g$ are in all cases less than 0.2 dex; in agreement with the estimated uncertainties in the derived surface gravities.

Metallicities: In terms of average metallicity values, the iron abundances derived in this study compare very well with results obtained in other studies in the literature for stars in common. There is a slight tendency, however, for the metallicities here to be just marginally lower (0.03 dex or less) than the other studies; but such differences are probably statistically insignificant. Note, however, that the iron abundance results in Bond et al. (2006) are on average 0.09 dex lower than ours.

4.2. Metallicity Trends with Effective Temperature and Stellar Mass

Given our sample of 262 stars which have been subjected to a homogeneous analysis it is possible to search for differences in the properties of stars with planets compared to those stars not known to harbor giant planets with periods less than about 4 years. Two key defining properties of stars are their effective temperatures and masses, which on the main-sequence are related to each other, such that increasing T_{eff} maps into increasing mass, at least over the relatively limited range of metallicities explored in this sample. In order to isolate possible differences between the two samples that might be related to T_{eff} or mass, stars having surface gravities with $\log g < 4.2$ were excluded from comparisons in this section. The resultant sample consists of 79 stars with planets and 109 stars without planets. Figure 6 compares the properties T_{eff} and derived evolutionary track mass for the two samples of stars, with mass plotted versus T_{eff} . The main-sequence nature of these stars is obvious from

the figure, with no significant differences in the distribution along the main sequence of stars with and without planets.

4.2.1. Effective Temperatures, Iron Abundances and Solid-Body Accretion

The defined set of target stars with $\log g \geq 4.2$ (or those very near to the main sequence) are now illustrated with their values of [Fe/H] plotted versus T_{eff} in Figure 7. The top panel contains stars without planets and the bottom panel shows stars with planets. Since these are main-sequence stars, the effective temperature follows the stellar mass. No strong trends between [Fe/H] and T_{eff} are apparent in either sample, with the lack of an increase of [Fe/H] with increasing effective temperature placing limits on the amount of solid-body accretion (material depleted in H and He, for example) that might have occurred in these stars, since the convective-zone mass of a main-sequence star is a strongly decreasing function of increasing T_{eff} .

This same accretion test was conducted by Pinsonneault et al. (2001) on an early small sample (~ 30) of stars with planets and they found no trend of increasing [Fe/H] with T_{eff} . Accretion of solid material could create a positive trend due to the significantly decreasing convective zone mass in main-sequence stars with increasing effective temperatures: e.g., the convective-zone mass decreases by about a factor of 50 in going from $T_{\text{eff}} = 5000$ K to 6400 K (Pinsonneault et al. 2001). Accretion of only a few Earth masses of solid material would increase the surface value of [Fe/H] by $\sim +0.3$ dex in a solar-metallicity star with $T_{\text{eff}} = 6400$ K (see Figure 2 in Pinsonneault et al. 2001). No such trend is seen in Figure 7, suggesting that accretion of more than a few Earth masses of solid material is either rare, or such accreted material sinks rapidly out of the outer convection zone.

4.2.2. Stellar Mass and Metallicity

In addition to the comparison carried out above between [Fe/H] and T_{eff} , it is also instructive to do a similar comparison with stellar mass (in this case using the evolutionary track masses); this comparison is shown in Figure 8, again, where stars without planets are plotted in the upper panel and stars with planets in the lower panel. The samples have been binned in mass intervals of $0.25 M_{\odot}$, as represented by the error bars in the abscissa. The values of [Fe/H] plotted represent the mean value within that mass interval, with the error bars showing the standard deviations of [Fe/H] at that mass. In both samples, the values of [Fe/H] increase with increasing stellar mass. Such an increase was noted in the review by

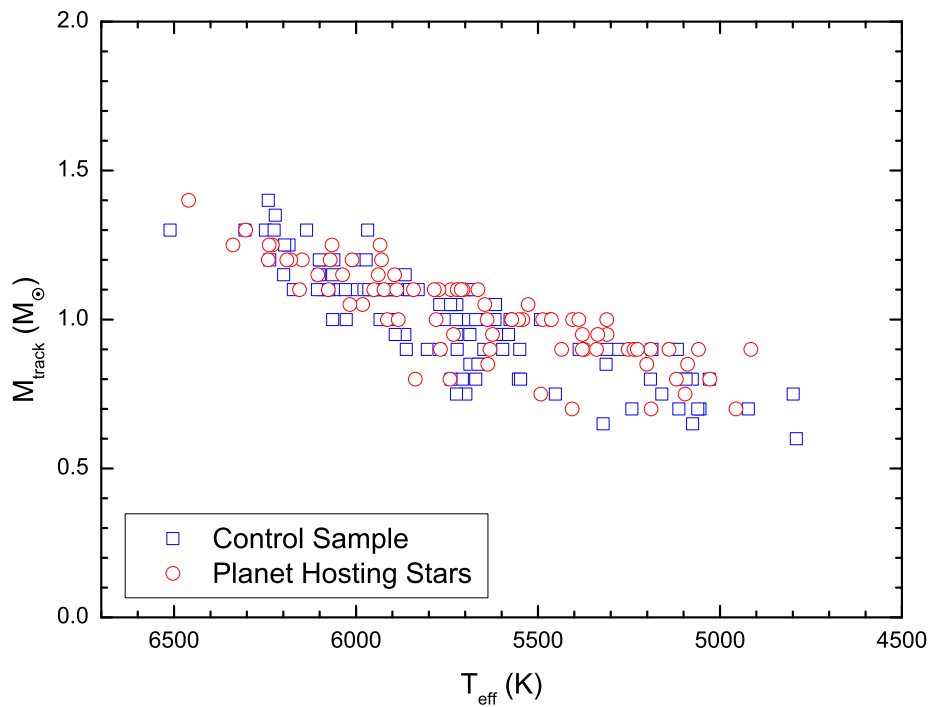


Fig. 6.— The relation between evolutionary track mass and effective temperatures for stars with (red open circles) and without (blue open squares) planets. Stars in both samples populate a well-defined “main-sequence”, with significant overlap in mass and T_{eff} between the stars with giant planets and those without.

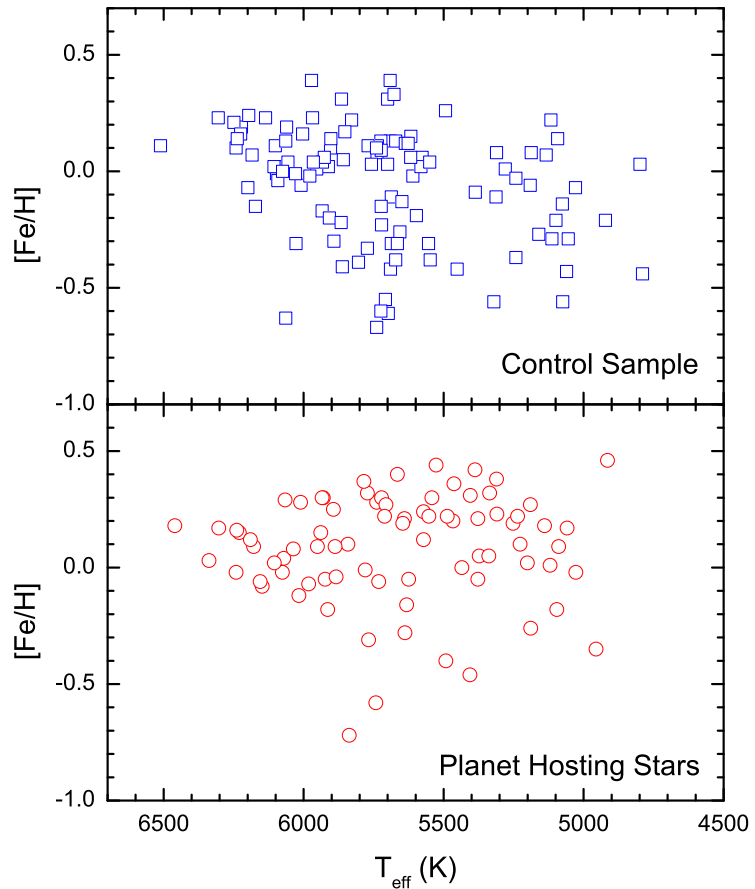


Fig. 7.— The trend between metallicities and effective temperatures for control sample stars (upper panel) and planet hosting stars (lower panel). There is a spread of metallicities at each T_{eff} , with no strong trends. Significant solid-body accretion would produce an upturn in the upper envelope of $[\text{Fe}/\text{H}]$ with increasing T_{eff} : such an effect is not observed in either sample.

Gonzalez (2006, his Figure 1) using the abundance results from Fischer & Valenti (2005).

A signature of solid-body accretion polluting the stellar convective envelopes would be an upturn in [Fe/H] with increasing stellar mass, since the convective envelope mass is a rapidly decreasing function of increasing stellar mass. At first glance, the increase in [Fe/H] with mass found here (and noted by Gonzalez 2006 based on the Fischer & Valenti 2005 results) might suggest that solid-body accretion has taken place. Two effects, however, indicate that this has not affected the overall metallicities. First, the slopes of $\Delta[\text{Fe}/\text{H}]/\Delta M$ are identical in both the stars with planets and stars without planets. This slope is very roughly $+0.7 \text{ dex}/M_{\odot}$ and is similar to the slope that would be deduced from Figure 1 in Gonzalez (2006). The fact that all of the various samples of stars, with and without giant planets, exhibit similar behavior in metallicity with mass argues that pollution has not selectively altered the values of [Fe/H] in a significant way for the stars with giant planets. The second point to note is that a positive slope of [Fe/H] with stellar mass would result from an age-metallicity relation. Since more massive stars have shorter main-sequence lifetimes, they would be biased towards higher values of [Fe/H], while lower-mass stars would be a mixture of old and young stars, which would shift the overall distribution to lower average values of [Fe/H].

In summary, comparisons among iron abundances with effective temperatures and stellar masses in both samples of stars (with and without large planets, respectively) reveal that accretion of solid-body material does not affect significantly ($\sim 0.1\text{-}0.2 \text{ dex}$) the overall bulk metallicity in either sample. This does not rule out smaller amounts of accretion, which might affect abundance ratios between certain types of elements (such as volatile versus refractory species, as suggested by Smith et al. 2001; see Meléndez et al. 2009 for an alternative interpretation). This question will be addressed in a later paper using the spectra from this dataset and analyzing a broad range of elements.

4.3. Metallicity Distributions of Sample Stars

As discussed in Section 4.1 the metallicities ([Fe/H]) derived here are generally consistent (within the expected errors) with metallicities found in other studies of planet hosting stars in the literature. As the present study relies on a homogeneous and self-consistent analysis of a sample of 262 stars, having comparable numbers of planet hosting and comparison disk stars, it is possible to quantify differences in the metallicity distributions in these two populations. Figure 9 shows the metallicity distributions for stars with planets (solid line histogram) and comparison stars (dashed line histogram). There is an offset in the peak metallicity of the two histograms in the figure. The peak of the distribution for stars with planets is located

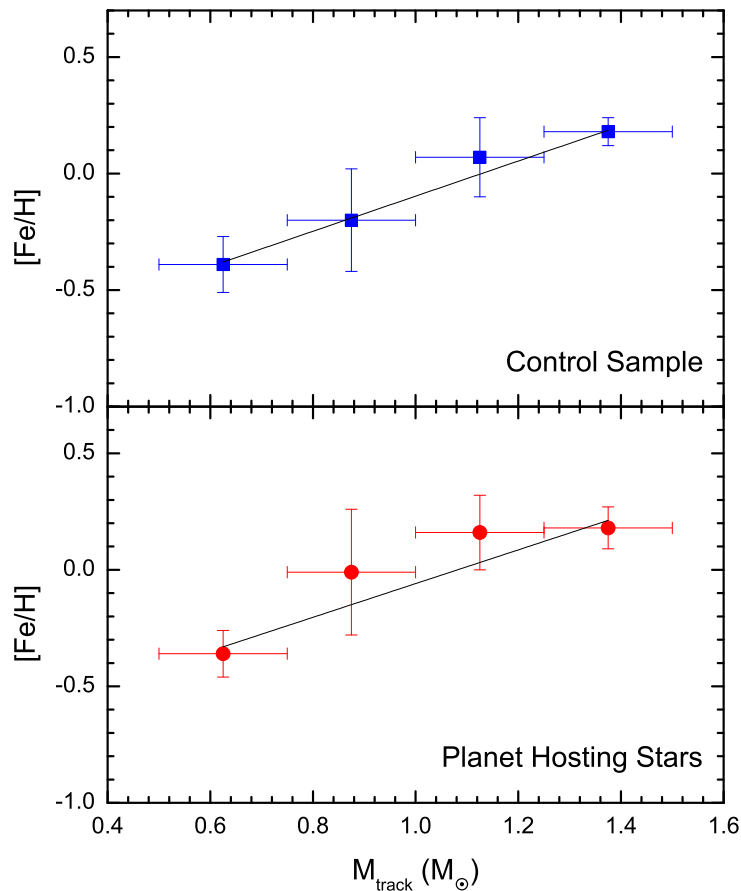


Fig. 8.— Average metallicities versus binned evolutionary track mass for control sample stars (upper panel) and planet hosting stars (lower panel). Masses are binned in $0.25 M_{\odot}$ intervals with each point showing the mean value and standard deviation of $[\text{Fe}/\text{H}]$ within that mass interval. The slopes of $\Delta[\text{Fe}/\text{H}]/\Delta M$ are the same within their uncertainties, in each sample and are likely the result of the age-metallicity relation. Selective accretion of solid-body material in stars with giant, closely orbiting planets would result in different slopes between the two samples and this is not observed.

in the bin centered at $[Fe/H] = +0.20$ dex and the average metallicity of this sample is $\langle [Fe/H] \rangle = +0.11$ dex. For the comparison stars, the peak is on the bin centered at $[Fe/H] = +0.10$ dex and the average metallicity in this case is lower: $\langle [Fe/H] \rangle = -0.04$ dex. Thus, there is an offset of 0.15 dex between the mean metallicities of the two samples.

When comparing properties, such as metallicity, between samples of planet hosting stars and those without giant planets, it is worth noting some selection biases inherent in these samples. As summarized by Gonzalez (2006), Doppler surveys avoid young, chromospherically active stars (which also typically are fast rotators) and contain only small numbers of metal poor stars (with $[Fe/H] < -0.5$ dex) because these objects are rare in the solar neighbourhood. In particular, our control sample of disk stars would also suffer from such biases since it was selected in order to search for the presence of planets.

As this offset between the peak values of the two histograms is of the order of, or just slightly higher than, the expected uncertainties in the derived iron abundances themselves, it is useful to perform a robust statistical test in order to further investigate whether the metallicity offset is meaningful. In this sense, we conducted a Two-Sample Kolmogorov-Smirnov test and found a probability $P = 6.17 \times 10^{-6}$ that the two samples are drawn from the same parent population. This low probability confirms the results previously found in the literature that the population of stars hosting giant planets is more metal-rich than the population of stars not known to harbour such planets.

If a volume limited sample with a radius of 18 pc is defined here for comparison, the mean metallicity for the control sample disk stars ($N=46$) is now -0.11 dex and the offset relative to planet-hosting stars becomes 0.22 dex, similar to the one found by Fischer & Valenti (2005) based on a much larger sample. The average metallicity found for the volume-limited sample in this study is also consistent with the results from Santos et al. (2004, 2005) and Sousa et al. (2008). The former study uses a comparison sample of 94 stars within 20 pc of the Sun and finds $\langle [Fe/H] \rangle = -0.11$ dex. The latter work extends the comparison sample to 385 stars and the enclosed radius to 56 pc and finds $\langle [Fe/H] \rangle = -0.12$ dex.

The results from Sections 4.2.1 and 4.2.2 indicate that solid body accretion has probably not altered surface values of $[Fe/H]$ at the level of the offset in metallicity; the difference in $[Fe/H]$ between the two samples suggests that intrinsic metallicity influences giant planet formation and migration.

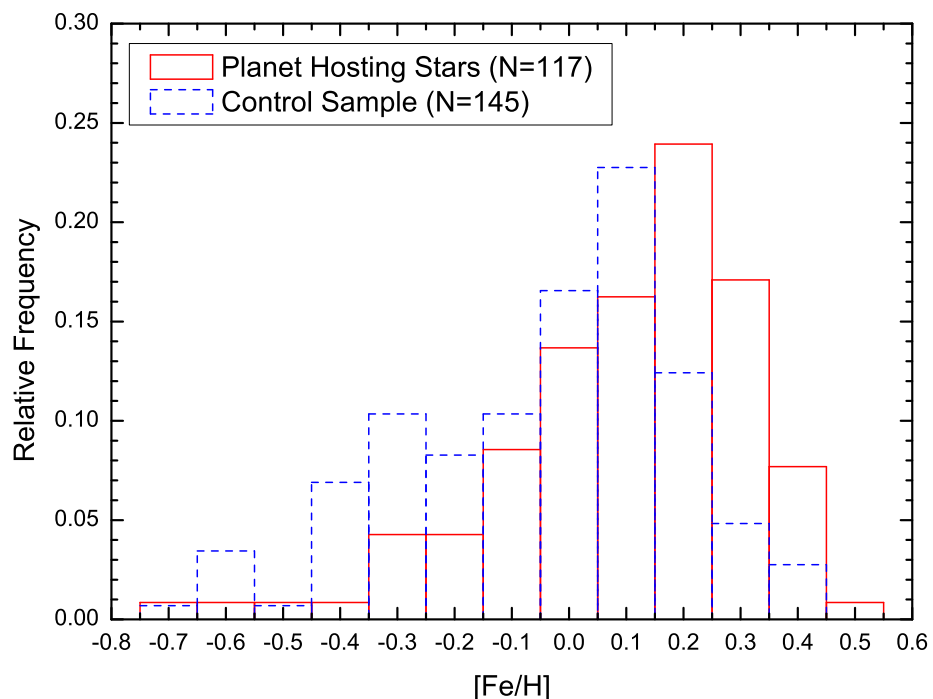


Fig. 9.— Metallicity distributions obtained for planet hosting stars (red solid line) and a control sample of disk stars not known to host giant planets (blue dashed line). The peaks of the metallicity distributions are offset by 0.15 dex indicating that the sample of stars which host planets is typically more metal rich.

4.3.1. *Metallicities of stars hosting Neptunian-mass planets*

The conclusions from the previous section favor the premise that metallicity plays a role in influencing the formation of giant planets, i.e., planets with roughly the mass of Jupiter. Within this model it is worthwhile exploring whether stellar metallicity also plays a role in the mass distribution of planetary systems. Such a comparison begins to probe how the underlying planetary system architecture might depend on metallicity. In this section, the metallicities of stars harboring only lower mass planets, i.e. those having Neptunian masses, are compared to systems containing the larger Jovian mass planets.

Sousa et al. (2008) presented preliminary results in which they found possible metallicity differences between stars hosting Jovian mass planets compared to those hosting Neptunian-mass planets ($M_p \sin i < 25M_{\oplus}$). The differences between the two metallicity distributions defined respectively by stars with Jovian-mass planets as opposed to Neptunian-mass planets indicated that these groups are not likely to belong to the same populations of stars. This conclusion, however, was based on a comparison of 63 Jovian hosting stars with a sample of 11 Neptunian hosting stars (those which contained at least one Neptune mass planet). Five of these 11 stars were M dwarfs and their metallicities were taken from the literature, while three were FG dwarfs analyzed by Sousa et al. (2008, HARPS GTO). The difference between the two metallicity distributions was a small mean offset of about 0.1 dex, with the Neptune hosting stars having a slightly lower mean metallicity.

Because M dwarfs are more difficult to analyze spectroscopically, due to considerable line blending and blanketing from molecules, it is necessary to consider abundance uncertainties and systematics when using results from these complex stellar spectra. Recent abundance analyses of M dwarfs include Bonfils et al. (2005); Woolf & Wallerstein (2006); Bean et al. (2006) and Johnson & Apps (2009). The studies by Bonfils et al. (2005) and Johnson & Apps (2009) point, for instance, to potentially large uncertainties in derived M dwarf abundances. For example, Johnson & Apps (2009) find an average offset of ~ 0.30 dex in [Fe/H] when their abundances are compared to the same M dwarfs from Bonfils et al. (2005, see Table 6). Such discrepancies suggest that, until results for the cooler M dwarfs are on firmer ground, it is prudent to investigate the effects of both including M dwarf metallicities in such comparisons, as well as excluding them.

The sample studied here contains 9 systems which host at least one Neptunian mass planet, none of which are M dwarfs. This is the largest sample of stars hosting Neptunian size planets analyzed homogeneously for metallicities to date and this subsample can be directly compared to the Jupiter-like planet hosting stellar sample. The strength of such a comparison rests upon the fact that all stars have been analyzed homogeneously and are within a similar range of stellar parameters, so that systematic errors are not likely to

produce spurious differences in the metallicity distributions. The weakness is that the sample of Neptune-mass hosts has only a small number of stars.

Figure 10 (top panel) shows histograms representing metallicity distributions of two samples: those stars hosting at least one Jupiter-mass planet ($N=112$; black solid line) and stars hosting only Neptune-mass planets ($N=5$; represented by the dashed red line). There is a hint that stars with only Neptunian planets tend to be more metal poor compared to Jovian-planet hosting stars. The average metallicity of the Neptunian hosts is -0.08 dex, while the Jupiter host metallicity distribution has an average of $+0.12$ dex. If a Two-Sample Kolmogorov-Smirnov test is performed, we find a probability of 8% that the stars in the two samples belong to the same metallicity population (which agrees with Sousa et al. 2008). This is a tantalizing result that suggests that metallicity may play a role not just in the formation of giant planets, but may also influence the distribution of planetary masses within exo-solar systems. This important question needs to be answered more definitively, but this will require larger samples.

In order to extend the sample of stars with Neptunian mass planets (shown in the top panel of Figure 10) in this discussion, a list of stars with at least one Neptunian planet was compiled from The Extrasolar Planet Encyclopaedia and is presented in Table 6 along with the metallicity results from the different studies in the literature. In a similar analysis as was done for the sample of stars studied here (discussed above), Two-Sample Kolmogorov-Smirnov tests were done now with the inclusion of the literature sample using different permutations. The results from these tests are discussed below.

- 1) Using the literature values of $[Fe/H]$ for only F, G, and K dwarfs (no M dwarfs) a difference in the mean $[Fe/H]$ of $+0.11$ dex (in the sense of Jovian-mass hosts minus Neptunian-mass hosts) is found, with a probability of $P=17\%$ that the two samples were drawn from the same $[Fe/H]$ populations (with $N(\text{Jovian-mass})=112$ and $N(\text{Neptunian-mass})=15$). The histogram showing the comparison of these two distributions is presented in the bottom panel of 10.
- 2) Using all literature values, with M dwarf abundances from Johnson & Apps (2009) included, we find $\Delta[Fe/H]=+0.10$ dex and $P=17\%$ ($N(\text{Jovian-mass})=112$ and $N(\text{Neptunian-mass})=19$).
- 3) When M-dwarf abundances from Bonfils et al. (2005, 2007) are used instead, $\Delta[Fe/H]=+0.14$ dex and $P=5\%$ ($N(\text{Jovian-mass})=112$ and $N(\text{Neptunian-mass})=18$).

In the above exercise the stars with planets were divided into systems with Jovian-mass planets and those with Neptunian-mass planets, respectively. The metallicity comparison can also be carried out by dividing the sample into stars with at least one Neptunian-mass

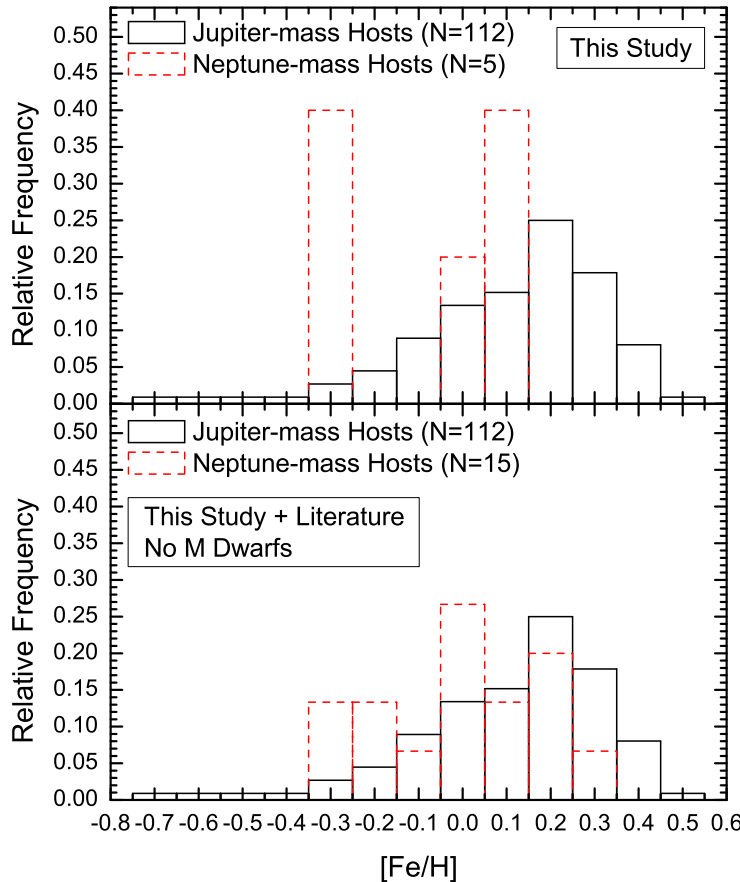


Fig. 10.— A comparison between the metallicity distributions for planet hosting stars. **Top panel:** The black solid line histogram represents the sample of planet hosting stars containing at least one Jupiter planet. The red dashed line represents the sample of stars hosting **only** planets with Neptune-like masses. The metallicities are from this study. **Bottom panel:** Results for metallicities in Neptunian-mass hosting stars from the literature are added (red dashed line histogram). Given the large uncretainties in the M dwarf metallicities these stars have not been added to the sample. There is a hint that there is offset between the two distributions represented both in the top and bottom panels.

planet, regardless of whether there is also a Jovian mass planet in the system, and those systems with Jovian mass planets but no Neptunian-mass planets. The average metallicity of the sample of stars which host at least one Neptunian planet ($N=9$) is +0.09 dex, close to the value derived for stars hosting at least one Jupiter-mass planet (+0.12 dex; $N=112$). A Two-Sample Kolmogorov-Smirnov test reveals that the probability that these two samples belong to the same parent population is 91%. This comparison strengthens the idea that metallicity played a role in setting the mass of the most massive planet in a system.

All of these various comparisons taken together suggest that lower values of [Fe/H] tend to produce lower-masses of the most massive planet within a planetary system. Such conclusions, however, should be viewed with caution since the number of stars harboring Neptune-size planets analyzed to date is still rather small, but in line with what would be expected from models of planet formation via core accretion (Ida & Lin 2004; Mordasini et al. 2009a,b; see also review by Boss 2010).

5. Conclusions

We have determined stellar parameters for 117 main-sequence stars with planets discovered via radial velocity surveys and 145 comparison stars which have been found to exhibit nearly constant radial velocities and are not likely to host large, closely orbiting planets. The stellar parameters were derived from a classical spectroscopic analysis, using accurate laboratory *gf*-values of Fe lines and automatically measured equivalent widths, after critical evaluations of their quality. The values of effective temperature, surface gravity (as $\log g$), microturbulent velocities, and iron abundances are in general good agreement with most of the values presented in a number of literature studies, but problems with a few individual stars may remain.

Correlations between [Fe/H] and T_{eff} in members of either sample are not found, which places stringent limits on the possible accretion of solid material (of less than a few Earth masses) onto the surfaces of these stars. A trend of increasing [Fe/H] with increasing stellar mass is found in both samples of stars, with the slope of $\Delta[\text{Fe}/\text{H}]/\Delta M$ being the same for stars with giant planets and control sample stars. The same value of $\Delta[\text{Fe}/\text{H}]/\Delta M$ for both samples rules out solid-body accretion, which leaves the underlying disk age-metallicity relation as the likely cause of the positive correlation of [Fe/H] with mass.

It should be noted that the samples analyzed here were not selected based on any rigorous criteria, other than being segregated based on the presence of giant planets in one sample and the probable absence of such planets in the other. The list of stars without

planets preferentially included metal-rich stars, while some stars with planets were discovered by surveys that were based on high-metallicity as a criterion.

A comparison of iron abundances between the stars with planets with the results from the control sample of disk stars confirms the results obtained by previous studies showing that planet-hosting stars exhibit larger metallicities than stars not harboring planets; the difference found in this sample is that stars with planets are shifted by +0.15 dex in [Fe/H] when compared to the stars without planets.

The sample of stars with planets discussed here contains 9 stars which host at least one Neptunian-mass planet; of these 9 systems, 4 also contain a Jovian-mass planet, while 5 contain only Neptunian-sized planets and no Jovian-mass closely orbiting planets. A statistical test of the iron abundances indicates that there is probably a real difference between the metallicity distributions of stars which contain *only* smaller Neptunian-sized planets in comparison with stars hosting the larger Jovian-mass planets (see also Sousa et al. 2008).

Although it should be recognized that the sample sizes are still small, there seems to be early indications that metallicity plays an important role in setting the mass of the most massive planet. It is also important to note that such a conclusion obtained here is based on stars which have all been analyzed homogeneously and which also have similar stellar parameters, therefore avoiding the large uncertainties still hampering the analyses and derived metallicities for the cooler M dwarfs. The same statistical test applied to metallicity results in the literature obtained for all FGK stars which host only Neptunian-sized planets allows for a larger sample and overall corroborates the results obtained with our sample.

We would like to dedicate this paper to the co-author Chico Araújo who was our friend, adviser and colleague and passed away in 2009. We acknowledge the financial support of CNPq. Research presented here was supported in-part by NASA grant NNH08AJ581. Luan Ghezzi thanks Oliver Schütz for his valuable help in using the FEROS DRS package, and Cláudio Bastos for conducting the observing run in February 2008. We thank the anonymous referee for useful comments that helped improving the paper.

REFERENCES

- Arenou, F., Grenon, M., & Gómez, A. 1992, A&A, 258, 204
Asplund, M., Grevesse, N., Sauval, A. J., & Scott, P. 2009, ARA&A, 47, 481

- Bakos, G. Á., et al. 2010, ApJ, 710, 1724
- Bard, A., Kock, A., & Kock, M. 1991, A&A, 248, 315
- Bard, A., & Kock, M. 1994, A&A, 282, 1014
- Bean, J. L., Benedict, G. F., Endl, M. 2006, ApJ, 653, L65
- Blackwell, D. E., Booth, A. J., Haddock, D. J., & Petford, A. D. 1986, MNRAS, 220, 549
- Blackwell, D. E., Booth, A. J., & Petford, A. D. 1984, A&A, 132, 236
- Blackwell, D. E., Lynas-Gray, A. E., & Smith, G. 1995, A&A, 296, 217
- Blackwell, D. E., Petford, A. D., Shallis, M. J., & Simmons, G. J. 1982a, MNRAS, 199, 43
- Blackwell, D. E., Petford, A. D., & Simmons, G. J. 1982b, MNRAS, 201, 595
- Bond, J. C., Tinney, C. G., Butler, R. P., Jones, H. R. A., Marcy, G. W., Penny, A. J., & Carter, B. D. 2006, MNRAS, 370, 163
- Bonfils, X., et al. 2007, A&A, 474, 293
- Bonfils, X., Delfosse, X., Udry, S., Santos, N. C., Forveille, T., Ségransan, D. 2005, A&A, 442, 635
- Borucki, W. J., et al. 2010, ApJ, 713, L126
- Boss, A. P. 2010, in IAU Symp. 265, Chemical Abundances in the Universe: Connecting First Stars to Planets, ed. K. Cunha, M. Spite & B. Barbuy (Cambridge:Cambridge University Press), 391
- Caffau, E., Ludwig, H.-G., Steffen, M., Freytag, B., Bonifacio, P. 2010 (arXiv:1003.1190)
- Casagrande, L., Ramírez, I., Meléndez, J., Bessel, M., & Asplund, M. 2010, arXiv:astro-ph/1001.3142v1
- Castelli, F., & Kurucz, R. L. 2004, in Proc. IAU Symp. 210, Modelling of Stellar Atmospheres ed. N. Piskunov, et al. (Dordrecht: Kluwer), poster A20 (arXiv:astro-ph/0405087)
- Cutri, R. M., et al. 2003, VizieR Online Data Catalog, II/246
- da Silva, L., et al. 2006, A&A, 458, 609
- Demarque, P., Woo, J.-H., Kim, Y.-C., & Yi, S. K. 2004, ApJS, 155, 667

- Endl, M., Cochran, W. D., Wittenmyer, R. A., & Boss, A. P. 2008, ApJ, 673, 1165
- ESA 1997, The Hipparcos and Tycho Catalogues, SP 1200 (ESA)
- Fischer, D. A., & Valenti, J. 2005, ApJ, 622, 1102
- Fuhr, J. R., Martin, G. A., & Wiese, W. L. 1988, J. Phys. Chem. Ref. Data 17, Suppl. 4
- Fulbright, J. P., McWilliam, A., & Rich, R. M. 2006, ApJ, 636, 821
- Gehren, T., Butler, K., Mashonkina, L., Reetz, J., & Shi, J. 2001, A&A, 366, 981
- Gehren, T., Korn, A.J., & Shi, J. 2001, A&A, 380, 645
- Ghezzi, L., Cunha, K., Smith, V.V., Margheim, S., Schuler, S., de Araújo, F.X., & de la Reza, R. 2009, ApJ, 698, 451
- Ghezzi, L. 2010, Ph.D. thesis, Observatório Nacional, Rio de Janeiro
- Girardi, L., Bertelli, G., Bressan, A., Chiosi, C., Groenewegen, M. A. T., Marigo, P., Salasnich, B., & Weiss, A. 2002, A&A, 391, 195
- Gonzalez, G. 1997, MNRAS, 285, 403
- Gonzalez, G. 2006, PASP, 118, 1494
- Gonzalez, G., & Vanture, A. D. 1998, A&A, 339, L29
- Hakkila, J., Myers, J. M., Stidham, B. J., & Hartmann, D. H. 1997, AJ, 114, 2043
- Hébrard, G., et al. 2010, A&A, 512, A46
- Holweger, H., Bard, A., Kock, A., & Kock, M. 1991, A&A, 249, 545
- Howard, A. W., et al. 2009, ApJ, 696, 75
- Ida, S., & Lin, D. N. C. 2004, ApJ, 616, 567
- Johnson, J. A., & Apps, K. 2009, ApJ, 699, 933
- Kaufer, A., Stahl, O., Tubbesing, S., Nørregaard, P., Avila, G., Francois, P., Pasquini, L., & Pizzella, A. 1999, The Messenger, 95, 8
- Kurucz, R. L., Furelind, I., Brault, J., & Testerman, L. 1984, Solar Flux Atlas from 296 to 1300 nm (Cambridge: Harvard Univ. Press)

- Kupka, F., Piskunov, N., Ryabchikova, T A., Stempels, H. C., & Weiss, W. W. 1999, A&AS, 138, 119
- Lambert, D. L., Heath, J. E., Lemke, M., & Drake, J. 1996, ApJS, 103, 183
- Laws, C., Gonzalez, G., Walker, K. M., Tyagi, S., Dodsworth, J., Snider, K., & Suntzeff, N. B. 2003, AJ, 125, 2664
- Léger, A., et al. 2009, A&A, 506, 287
- Lo Curto, G., et al. 2010, A&A, 512, A48
- Lovis, C., & Mayor, M. 2007, A&A, 472, 657
- Luck, R. E., & Heiter, U. 2006, AJ, 131, 3069
- Marcy, G. W., Butler, R. P., Vogt, S. S., Fischer, D. A., Henry, G. W., Laughlin, G., Wright, J. T., & Johnson, J. A. 2005, ApJ, 619, 570
- May, M., Richter, J., Wichelmann, J. 1974 , A&AS, 18, 405
- Mayor, M., et al. 2009, A&A, 493, 639
- Meléndez J., Asplund, M., Gustafsson, B., & Yong, D. 2009, ApJ, 704, L66
- Meléndez J., & Barbuy B. 2009, A&A, 497, 611
- Mishenina, T. V., Soubiran, C., Bienaymé, O., Korotin, S. A., Belik, S. I., Usenko, I. A., & Kovtyukh, V. V. 2008, A&A, 489, 923
- Mordasini, C., Alibert, Y., & Benz, W. 2009, A&A, 501, 1139
- Mordasini, C., Alibert, Y., Benz, W., & Naef, D. 2009, A&A, 501, 1161
- O'Brian, T. R., Wickliffe, M. E., Lawler, J. E., Whaling, W., Brault J. W., 1991, J. Opt. Soc. Am. B, 8, 1185
- Pasquini, L., Döllinger, M. P., Weiss, A., Girardi, L., Chavero, C., Hatzes, A. P., da Silva, L., Setiawan, J. 2007, A&A, 473, 979
- Perryman, M. A. C., et al. 1997, A&A, 323, L49
- Pinsonneault, M. H., DePoy, D. L., & Coffee, M. 2001, ApJ, 556, L59
- Raassen, A. J. J., & Uylings, P. H. M. 1998, A&A, 340, 300

- Reddy, B. E., Tomkin, J., Lambert, D. L., & Allende Prieto, C. 2003, MNRAS, 340, 304
- Santos, N. C., Israelian, G., & Mayor, M. 2001, A&A, 373, 1019
- Santos, N. C., Israelian, G., & Mayor, M. 2005, A&A, 415, 1153
- Santos, N. C., Israelian, G., Mayor, M., Bento, J. P., Almeida, P. C., Sousa, S. G., & Ecuvillon, A. 2005, A&A, 437, 1127
- Smith, V. V., Cunha, K., Lazzaro, D. 2001, AJ, 121, 3207
- Sneden, C. 1973, PhD thesis, Univ. Texas, Austin
- Sousa, S. G., Santos, N. C., Israelian, G., Mayor, M., & Monteiro, M. J. P. F. G. 2008, A&A, 469, 783
- Sousa, S. G., Santos, N. C., Mayor, M., Udry, S., Casagrande, L., Israelian, G., Pepe, F., Queloz, D., & Monteiro, M. J. P. F. G. 2008, A&A, 487, 373
- Takeda, Y., Ohkubo, M., Sato, B., Kambe, E., Sadakane, K. 2005, PASJ, 57, 27
- Udry, S., & Santos, N. C., 2007, ARA&A, 45, 397
- Udry, S., et al. 2006, A&A, 447, 361
- Valenti, J. A., et al. 2009, ApJ, 702, 989
- Valenti, J. A., & Fischer, D. A. 2005, ApJS, 159, 141
- van Leeuwen, F. 2007, Ap&SSLlibrary, Vol. 350, Hipparcos, the New Reduction of the Raw Data
- van Leeuwen, F., Evans, D. W., Grenon, M., Großmann, V., Mignard, F., & Perrymann, M. A. C. 1997, A&A, 323, L61
- Woolf, V. M., & Wallerstein, G. 2006, PASP, 118, 218
- Yi, S. K., Kim, Y.-C., & Demarque, P. 2003, ApJS, 144, 259

Table 1. Log of Observations

Star	<i>V</i>	Observation Date	<i>T_{exp}</i> (s)	S/N (~ 6700 Å)
<i>Planet Hosting Stars</i>				
HD 142	5.70	2007 Aug 30	200	367
HD 1237	6.59	2007 Aug 30	480	466
HD 2039	9.00	2007 Aug 28	3000	362
HD 2638	9.44	2007 Aug 29	3000	276
HD 3651	5.88	2007 Aug 29	200	356
<i>Control Sample</i>				
HD 1581	4.23	2008 Aug 20	30	216
HD 1835	6.39	2007 Oct 02	200	388
HD 3823	5.89	2007 Oct 02	200	452
HD 4628	5.74	2008 Aug 20	200	375
HD 7199	8.06	2008 Aug 19	1200	348

Note. — Table 1 is published in its entirety in the electronic edition of the Astrophysical Journal. A portion is show here for guidance regarding its form and content.

Table 2. Selected Fe lines and Measured Equivalent Widths for the Sun.

λ (Å)	Ion	LEP (eV)	$\log gf$ (dex)	$W_{\lambda}\odot$ (mÅ)
4779.439	Fe I	3.415	−2.020	40.4
4788.751	Fe I	3.237	−1.763	63.3
4802.875	Fe I	3.695	−1.514	58.3
4962.572	Fe I	4.178	−1.182	52.7
5054.642	Fe I	3.640	−1.921	39.6
5247.049	Fe I	0.087	−4.946	65.8
5379.574	Fe I	3.694	−1.514	59.8
5618.631	Fe I	4.209	−1.276	48.4
5741.846	Fe I	4.256	−1.670	30.8
5775.081	Fe I	4.220	−1.298	57.9
5778.453	Fe I	2.588	−3.430	21.3
5855.076	Fe I	4.608	−1.478	21.4
5916.247	Fe I	2.453	−2.994	55.0
5956.692	Fe I	0.859	−4.605	51.3
6120.246	Fe I	0.915	−5.970	5.2
6151.617	Fe I	2.176	−3.299	48.7
6173.334	Fe I	2.223	−2.880	67.2
6200.313	Fe I	2.608	−2.437	72.5
6219.279	Fe I	2.198	−2.433	89.8
6240.645	Fe I	2.223	−3.170	48.0
6265.131	Fe I	2.176	−2.550	84.2
6380.743	Fe I	4.186	−1.376	51.8
6593.870	Fe I	2.433	−2.422	84.5
6699.141	Fe I	4.593	−2.101	7.7
6739.520	Fe I	1.557	−4.794	11.7
6750.150	Fe I	2.424	−2.621	73.2
6858.145	Fe I	4.607	−0.930	51.1
4993.358	Fe II	2.807	−3.670	37.6
5132.669	Fe II	2.807	−4.000	26.9
5284.109	Fe II	2.891	−3.010	62.6

Table 2—Continued

λ (Å)	Ion	LEP (eV)	$\log gf$ (dex)	$W_{\lambda} \odot$ (mÅ)
5325.553	Fe II	3.221	−3.170	39.2
5414.073	Fe II	3.221	−3.620	27.6
5425.257	Fe II	3.199	−3.210	41.5
5991.376	Fe II	3.153	−3.560	30.4
6084.111	Fe II	3.199	−3.800	20.5
6149.258	Fe II	3.889	−2.720	35.0
6369.462	Fe II	2.891	−4.190	19.9
6416.919	Fe II	3.892	−2.680	38.5
6432.680	Fe II	2.891	−3.580	40.4

Table 3. Atmospheric Parameters.

Star	T_{eff} (K)	log g	ξ (km s $^{-1}$)	A(Fe)	σ (Fe I)	N (Fe I)	σ (Fe II)	N (Fe II)	[Fe/H]
<i>Planet Hosting Stars</i>									
HD 142	6338 ± 46	4.34 ± 0.14	2.27 ± 0.08	7.46	0.09	23	0.07	10	0.03 ± 0.04
HD 1237	5572 ± 40	4.58 ± 0.09	1.34 ± 0.04	7.55	0.09	27	0.05	9	0.12 ± 0.04
HD 2039	5934 ± 36	4.30 ± 0.13	1.26 ± 0.04	7.73	0.08	27	0.05	12	0.30 ± 0.03
HD 2638	5236 ± 70	4.38 ± 0.19	0.86 ± 0.04	7.65	0.07	26	0.07	9	0.22 ± 0.05
HD 3651	5252 ± 65	4.32 ± 0.18	0.81 ± 0.02	7.62	0.08	27	0.05	10	0.19 ± 0.03
<i>Control Sample</i>									
HD 1581	5908 ± 31	4.26 ± 0.13	1.17 ± 0.04	7.23	0.08	25	0.08	12	-0.20 ± 0.03
HD 1835	5829 ± 41	4.39 ± 0.16	1.24 ± 0.04	7.65	0.07	22	0.05	10	0.22 ± 0.03
HD 3823	6012 ± 31	4.18 ± 0.08	1.92 ± 0.10	7.08	0.07	25	0.05	11	-0.35 ± 0.02
HD 4628	5055 ± 40	4.33 ± 0.19	0.88 ± 0.04	7.14	0.08	25	0.06	5	-0.29 ± 0.02
HD 7199	5349 ± 65	4.09 ± 0.19	1.04 ± 0.04	7.74	0.09	26	0.05	10	0.31 ± 0.05

Note. — Table 3 is published in its entirety in the electronic edition of the Astrophysical Journal. A portion is shown here for guidance regarding its form and content.

Table 4. Evolutionary Parameters.

Star	π (mas)	σ_π (mas)	A_V	BC_V	$\log(L/L_\odot)$	$\sigma_{\log(L/L_\odot)}$	R (R_\odot)	σ_R (R_\odot)	M_{spec} (M_\odot)	$\sigma(M_{spec})$ (M_\odot)	M_{track} (M_\odot)	$\sigma(M_{track})$ (M_\odot)	$\log g_{Hipp}$	$\sigma(\log g_{Hipp})$	Age (Gyr)	Δ Age (Gyr)
<i>Planet Hosting Stars</i>																
HD 142	38.89	0.37	0.05	0.017	0.462	0.061	1.41	0.11	1.59	0.77	1.25	0.10	4.24	0.08	2.5	2.0-3.5
HD 1237	57.15	0.31	0.04	-0.075	-0.196	0.060	0.86	0.07	1.02	0.49	1.00	0.10	4.57	0.08	< 1.0	0.0-3.0
HD 2039	9.75	0.95	0.11	-0.004	0.376	0.104	1.46	0.18	1.55	0.81	1.25	0.10	4.21	0.11	3.5	3.0-4.5
HD 2638	20.03	1.49	0.10	-0.159	-0.368	0.089	0.80	0.09	0.55	0.28	0.90	0.10	4.59	0.11	< 1.0	0.0-4.0
HD 3651	90.42	0.32	0.02	-0.153	-0.287	0.060	0.87	0.07	0.57	0.28	0.90	0.10	4.51	0.08	5.0	0.0-12.0
<i>Control Sample</i>																
HD 1581	116.46	0.16	0.01	-0.037	0.102	0.060	1.08	0.08	0.76	0.37	1.00	0.10	4.38	0.08	6.5	4.0-9.0
HD 1835	47.93	0.53	0.08	-0.025	0.033	0.061	1.02	0.08	0.93	0.45	1.10	0.10	4.47	0.08	1.0	0.0-3.5
HD 3823	40.07	0.34	0.04	-0.035	0.376	0.061	1.42	0.11	1.11	0.54	1.00	0.10	4.13	0.08	7.5	6.5-9.0
HD 4628	134.14	0.51	0.01	-0.226	-0.549	0.060	0.69	0.06	0.37	0.18	0.70	0.10	4.60	0.09	9.0	0.0-14.0
HD 7199	28.33	0.57	0.10	-0.122	-0.132	0.063	1.00	0.08	0.45	0.22	0.95	0.10	4.41	0.08	9.0	5.0-13.0

Note. — Table 4 is published in its entirety in the electronic edition of the Astrophysical Journal. A portion is show here for guidance regarding its form and content.

Table 5. Comparison with other results in the literature.

Study	$\langle \Delta T_{eff} \rangle$ (K)	$\langle \Delta \log g \rangle$	$\langle \Delta [\text{Fe}/\text{H}] \rangle$	N_{Stars}
Laws et al. (2003)	-5 ± 74	-0.10 ± 0.15	-0.03 ± 0.05	23
Santos et al. (2004, 2005)	-2 ± 72	-0.08 ± 0.13	-0.02 ± 0.06	113
Takeda et al. (2005)	-8 ± 65	-0.05 ± 0.16	-0.03 ± 0.07	35
Valenti & Fischer (2005)	10 ± 65	-0.11 ± 0.14	-0.01 ± 0.06	223
Luck & Heiter (2006)	-32 ± 84	-0.11 ± 0.15	-0.02 ± 0.07	56
Bond et al. (2006)	74 ± 113	0.01 ± 0.19	0.09 ± 0.09	90
Sousa et al. (2008)	-14 ± 61	-0.11 ± 0.11	0.00 ± 0.06	119

Note. — Δ = This study - Literature Study

Table 6. Neptunian-mass Planet Hosts

Star	$M_P \sin i$ (M_\oplus)	Jupiter	[Fe/H]	Reference [Fe/H]
<i>Results from This Work</i>				
HD 4308	12.87	no	−0.31	
HD 16417	21.93	no	0.14	
HD 40307	4.20	no	−0.35	
HD 47186	22.78	yes	0.21	
HD 69830	10.49	no	0.00	
HD 125612	21.29	yes	0.25	
HD 160691	10.56	yes	0.23	
HD 181433	7.56	yes	0.46	
HD 219828	20.98	no	0.14	
<i>Literature Results</i>				
HD 7924	9.22	no	−0.15	Howard et al. (2009)
HD 1461	7.60	no	0.18	Valenti & Fischer (2005)
			0.21	Luck & Heiter (2006)
			0.19	Sousa et al. (2008)
			0.19	Average
CoRoT-7	4.80	no	0.05	Léger et al. (2009)
55 Cnc	7.63	yes	0.33	Santos et al. (2004)
BD-082823	14.30	yes	−0.07	Hébrard et al. (2010)
HD 90156	17.48	no	−0.24	Encyclopaedia
61 Vir	5.09	no	0.01	Santos et al. (2004, 2005)
			0.05	Takeda et al. (2005)
			0.11	Valenti & Fischer (2005)
			−0.02	Sousa et al. (2008)
			0.04	Average
HD 125595	14.30	no	0.02	Encyclopaedia
HD 156668	4.16	no	−0.07	Mishenina et al. (2008)
Kepler-4	24.47	no	0.17	Borucki et al. (2010)
HD 179079	25.43	no	0.25	Valenti et al. (2009)

Table 6—Continued

Star	$M_P \sin i$ (M_\oplus)	Jupiter	[Fe/H]	Reference [Fe/H]
HAT-P-11	25.74	no	0.31	Bakos et al. (2010)
HD 190360	18.12	yes	0.24	Sousa et al. (2008)
HD 215497	5.40	yes	0.23	Lo Curto et al. (2010)
<i>Literature Results for M Stars</i>				
HD 285968	8.42	no	-0.10	Endl et al. (2008)
			0.18	Johnson & Apps (2009)
			0.04	Average
GJ 436	22.88	no	0.02	Bonfils et al. (2005)
			-0.32	Bean et al. (2006)
			0.25	Johnson & Apps (2009)
			-0.02	Average
Gl 581	1.94	no	-0.25	Bonfils et al. (2005)
			-0.33	Bean et al. (2006)
			-0.10	Johnson & Apps (2009)
			-0.23	Average
GJ 674	11.76	no	-0.28	Bonfils et al. (2007)
			-0.11	Johnson & Apps (2009)
			-0.20	Average
Gliese 876	6.36	yes	-0.03	Bonfils et al. (2005)
			-0.12	Bean et al. (2006)
			0.37	Johnson & Apps (2009)
			0.07	Average

Capítulo 3

Metalicidades de Estrelas Evoluídas com Planetas

Neste capítulo, é apresentado o artigo (sumbeto ao *Astrophysical Journal*) que analisa as metalicidades da subamostra de 46 estrelas evoluídas, a qual é composta por 31 estrelas com planetas e 15 objetos de comparação. No primeiro grupo, temos 15 subgigantes e 16 gigantes. O segundo contém 14 subgigantes e apenas 1 gigante. Os parâmetros atmosféricos e as metalicidades destas estrelas evoluídas foram determinados através do mesmo método automático apresentado e discutido no Artigo I. Este estudo contém, pela primeira vez, uma análise homogênea das estrelas com planetas em 3 estágios evolutivos distintos (as anãs foram discutidas no capítulo anterior). Como consequência, foi possível verificar se o processo da diluição é observado nestes objetos, o que seria um importante indício da ocorrência da poluição nas atmosferas estelares. Adicionalmente, este trabalho contém a mais completa análise homogênea, até o momento, das estrelas gigantes com planetas. As metalicidades e massas destes objetos sugeriram vínculos adicionais para os processos de formação planetária.

Metallicities of Planet Hosting Stars: A Sample of Giants and Subgiants¹

L. Ghezzi¹, K. Cunha^{1,2,3}, S. C. Schuler² & V. V. Smith²

ABSTRACT

This work presents a homogeneous derivation of atmospheric parameters and iron abundances for a sample of giant and subgiant stars which host giant planets, as well as a control sample of subgiant stars not known to host giant planets. The analysis is done using the same technique as for our previous analysis of a large sample of planet-hosting and control sample dwarf stars. A comparison between the distributions of [Fe/H] in planet-hosting main-sequence stars, subgiants, and giants within these samples finds that the main-sequence stars and subgiants have the same mean metallicity of $\langle \text{[Fe/H]} \rangle \simeq +0.11$ dex, while the giant sample is typically more metal poor, having an average metallicity of $\text{[Fe/H]} = -0.06$ dex. The fact that the subgiants have the same average metallicities as the dwarfs indicates that significant accretion of solid metal-rich material onto the planet-hosting stars has not taken place, as such material would be diluted in the evolution from dwarf to subgiant. The lower metallicity found for the planet-hosting giant stars in comparison with the planet-hosting dwarfs and subgiants is interpreted as being related to the underlying stellar mass, with giants having larger masses and thus, on average larger-mass protoplanetary disks. In core accretion models of planet formation, larger disk masses can contain the critical amount of metals necessary to form giant planets even at lower metallicities.

Subject headings: Planets and satellites: formation – Stars: abundances – Stars: atmospheres – Stars: fundamental parameters – (Stars): planetary systems

¹Observatório Nacional, Rua General José Cristino, 77, 20921-400, São Cristóvão, Rio de Janeiro, RJ, Brazil; luan@on.br

²National Optical Astronomy Observatory, 950 North Cherry Avenue, Tucson, AZ 85719, USA

³Steward Observatory, University of Arizona, Tucson, AZ 85121, USA

¹Based on observations made with the 2.2 m telescope at the European Southern Observatory (La Silla, Chile), under the agreement ESO-Observatório Nacional/MCT.

1. Introduction

A physical property of planetary systems that has yet to be fully understood is a connection between planetary formation and the metallicities of the host stars. There is now unequivocal evidence that main sequence (MS) FGK-type dwarfs known to have at least one giant planet (i.e., $M_p \geq 1 M_J$, where M_p is the planetary mass and M_J is a Jupiter mass) companion discovered via the radial velocity method are metal-rich compared to similar stars in the disk field not known to harbor close-in giant planets (e.g., Fischer & Valenti 2005; Ghezzi et al. 2010). Contrary to this observation, there is increasing evidence that this planet-metallicity correlation does not extend to evolved giant stars; giants with planets tend to be more metal-poor than their main sequence counterparts (e.g., Schuler et al. 2005; Pasquini et al. 2007).

The metallicity distribution of planetary host stars may hold critical clues to planet formation processes and the subsequent evolution of planetary systems. Indeed, the favored interpretation of the planet-metallicity correlation observed for MS dwarfs is that planets form more readily in high-metallicity environments (e.g., Fischer & Valenti 2005), in agreement with predictions of core accretion planet formation models (e.g., Ida & Lin 2004; Ercolano & Clarke 2010). A competing interpretation, however, holds that the enhanced metallicity results from the accretion of H-depleted rocky material onto the star and pollution of the thin convective envelopes of FGK dwarfs (e.g., Gonzalez 1997). This scenario would be supported by the lower metallicities of giants with planets, which having been enhanced on the MS, would be diluted by the deepening convection zones as the stars evolve up the red giant branch.

An observational result that has been used as an argument in favor of the primordial enrichment hypothesis and against the pollution hypothesis is the observed metallicities of subgiants: subgiants with planetary companions have been shown to have enhanced metal abundances, similar to those of MS dwarfs with planets (Fischer & Valenti 2005). If the difference in metallicities of planet hosting dwarfs and giants results from the pollution and subsequent dilution of the stars' convective envelopes, one might expect the subgiants to have intermediate metallicities, forming a metallicity gradient from the metal-rich MS dwarfs, to the increasingly diluted subgiants, and finally to the fully diluted giants. Heretofore, this pattern has not been observed. In this paper, we present the results of a homogeneous metallicity ([Fe/H]) analysis of 15 subgiants and 16 giants with planetary companions, as well as a control sample of 14 subgiants not known to harbor closely orbiting giant planets. This sample constitutes the largest number of evolved stars with planets for which metallicities have been derived in a consistent fashion within a single study. These metallicities are compared to those of a large sample of main sequence dwarfs with and without planets that

have been derived as part of the same analysis and have been recently reported in Ghezzi et al. (2010) (Paper I).

2. Observations

The sample of planet hosting stars studied here contains 31 targets. The target list was compiled from the Extrasolar Planet Encyclopaedia², and these stars were originally part of the larger sample analyzed in Ghezzi et al. (2010): the latter study focused on the analysis of dwarf stars while the more evolved objects, giants and subgiants, are presented here. A sample of disk subgiants ($N=14$) observed to not host closely orbiting giant planets was also observed with the same set-up, and the target list was obtained from the list of candidates deemed to be “RV stable” from Fischer & Valenti (2005). The list with all stars analyzed in this study can be found in Table 1.

The observations consist of high-resolution spectra ($R = \lambda/\Delta\lambda \sim 48,000$) obtained with the FEROS spectrograph (Kaufer et al. 1999) MPG/ESO-2.20 m telescope (La Silla, Chile)³. The spectra were reduced in a standard way. A more detailed account of the observations and the data reduction is provided in Paper I. A log of the observations with V magnitudes, observation dates, integration times and signal-to-noise ratios can be found in Table 1.

3. Stellar Parameters and Metallicities

The derivation of stellar parameters and metallicities ([Fe/H]) in this study followed the same methodology presented and discussed in Paper I. The same selection of Fe I and Fe II lines was analyzed and their equivalent widths were also measured using the automatic code of equivalent width measurement ARES (Sousa et al. 2007). In order to further test the quality of automatic equivalent width measurements for the parameter space covered by this particular set of subgiant and giant stars, equivalent widths of two sample targets HD 188310 (with T_{eff} typical of the giants in our sample and a spectrum with high S/N) and HD 27442 (typical T_{eff} but with a lower S/N spectrum) were measured manually (using the task `splot` on IRAF). Our results indicate that equivalent widths measured with IRAF compare favorably with the automatic ones: $\langle EW_{ARES} - EW_{Manual} \rangle = -0.43 \pm 2.28$ mÅ for HD 188310 and $+0.15 \pm 3.42$ mÅ for HD 27442, which is consistent with previous results in

²Available at <http://exoplanet.eu>

³Under the agreement ESO-Observatório Nacional/MCT.

Sousa et al. (2007).

Effective temperatures, surface gravities, microturbulent velocities and iron abundances were derived under the assumption of LTE and self-consistently from the requirement that the iron abundance be independent of the line excitation potential and measured equivalent widths, as well as from the forced agreement between Fe I and Fe II abundances. Although this analysis uses the approximation of LTE, a discussion of possible non-LTE effects in the Fe abundances will be presented in Section 4.1.3. Table 2 lists the derived stellar parameters for the target stars. The number of Fe I and Fe II lines (and the standard deviations in each case) for each star is also listed.

Uncertainties in the derived parameters T_{eff} , $\log g$, ξ and $[\text{Fe}/\text{H}]$ can be estimated as in Gonzalez & Vanture (1998), similarly to Paper I. The typical values for the internal errors in this study are ~ 50 K in T_{eff} , 0.15 dex in $\log g$, 0.05 km s^{-1} for ξ , and 0.05 dex in $[\text{Fe}/\text{H}]$. (See Paper I for a discussion of these internal uncertainties). We note, however, that the real uncertainties are expected to be somewhat larger (100 K in T_{eff} , 0.20 dex in $\log g$, 0.20 km s^{-1} in ξ and 0.10 dex in $[\text{Fe}/\text{H}]$) than the internal errors. The sensitivity of Fe I abundances to changes in the parameters T_{eff} , $\log g$ and ξ is also investigated. For this exercise, we use 2 giants that span the T_{eff} interval of most of the giant sample: HD 11977 ($T_{\text{eff}} = 4972$ K), NGC 2423 3 ($T_{\text{eff}} = 4680$ K), and the subgiant HD 11964 ($T_{\text{eff}} = 5318$ K). A variation of ± 100 K in T_{eff} induces a change of ± 0.03 and ± 0.05 dex in $A(\text{Fe I})$ for the coolest (HD 122430) and hottest (HD 11977) giants, respectively. For the subgiant, the sensitivity is ± 0.09 dex. A variation of ± 0.2 dex in $\log g$ does not affect significantly the Fe abundances: $A(\text{Fe})$ changes by ~ 0.01 dex for the hotter stars and ~ 0.03 dex for the cooler stars. As expected, a decrease in the microturbulence causes an increase in $A(\text{Fe I})$; for the subgiant star, a change of $\pm 0.20 \text{ km s}^{-1}$ causes a variation of ∓ 0.08 dex in the Fe I abundance, while for the giants, this variation is around ∓ 0.10 . The total errors in $A(\text{Fe})$ from these typical uncertainties are ± 0.11 dex for the subgiants and ± 0.13 dex for the giants. As the results in this study for the giants and subgiants will be compared to those for the dwarfs in Paper I, we repeat the above exercise for a typical dwarf with solar parameters (HD 106252; Paper I). Variations of ± 100 K in T_{eff} , ± 0.20 dex in $\log g$ and $\pm 0.20 \text{ km s}^{-1}$ in ξ cause changes of, respectively, ± 0.08 , ≤ 0.01 and ∓ 0.05 dex in $A(\text{Fe I})$; or a total error of ± 0.1 dex. These total uncertainties for the dwarfs in Paper I are slightly lower but not significantly different from the total uncertainties estimated for the subgiants (0.11 dex) and giants (0.13 dex).

The derived effective temperatures for the stars in our sample can be compared with independent results from photometric $V - K$ calibrations. Several photometric calibrations are available in the literature (e.g. Alonso et al. 1999; Ramírez & Meléndez 2005). González Hernández & Bonifacio (2009) presented a new implementation of the infrared flux method

using 2MASS magnitudes and Kurucz models. A comparison of the derived spectroscopic effective temperatures with their photometric calibration is shown in the top panel of Figure 1. Results are shown for all stars in our sample which have unsaturated K_s 2MASS magnitudes (with errors in $K_s < 0.1$ mag); reddening corrections from Arenou et al. (1992) were applied to obtain the de-reddened colors. The comparison between the two scales is quite good for the entire T_{eff} range, with agreement for most of the stars within ± 100 K (shown as the dashed lines in the figure). There is not a significant systematic difference in the effective temperatures between giants and subgiants, but we note a few outliers falling above the dashed lines (mostly subgiants) and 2 results for subgiants which fall below. The average difference between the two scales is well within the expected errors and overall agree with the variations typically found between different T_{eff} scales in the literature: $\langle \delta T_{\text{eff}} \rangle$ (This Study - González Hernández & Bonifacio 2009) = -48 ± 136 K.

The more recent calibration by Casagrande et al. (2010) is hotter than that of González Hernández & Bonifacio (2009); a comparison with our results for the subgiants (the calibration of Casagrande et al. 2010 only applies for dwarfs and subgiants) shows a larger systematic difference of $\langle \delta T_{\text{eff}} \rangle$ (This Study - Casagrande et al. 2010) = -106 ± 147 K. For the calibration of González Hernández & Bonifacio 2009, we find $\langle \delta T_{\text{eff}} \rangle_{\text{subgiants}} = -55 \pm 142$ K. This difference of ~ 50 K is consistent with the discussion presented in section 2.5 of Casagrande et al. (2010). Reddening corrections applied to (V-K) influence the derived photometric temperatures: a change of 0.01 mag in E(B-V) can lead to a change of 50 K in the effective temperature (Casagrande et al. 2010). Note that Casagrande et al. (2010) have not adopted reddening corrections for stars in their samples closer than ~ 75 pc. If we also neglect reddening corrections for those stars in our sample which are closer than ~ 75 pc and recompute the photometric T_{eff} s, the average differences become $\langle \delta T_{\text{eff}} \rangle$ (This Study - Casagrande et al. 2010) = -33 ± 144 K.

The bottom panel of Figure 1 shows the comparison of our derived effective temperatures with those obtained by Valenti & Fischer (2005); the latter study also derived T_{eff} spectroscopically, although their analysis followed a different method which consisted in fitting the observed spectra by adjusting 41 free parameters (one of them being the effective temperature). The T_{eff} results in the two spectroscopic analyses agree well: $\langle \delta T_{\text{eff}} \rangle$ (This Study - Valenti & Fischer 2005) = -18 ± 67 K.

3.1. Evolutionary Parameters

As mentioned previously, Paper I analyzed unevolved stars with and without planets, while the present study focuses on more evolved stars, also both with and without giant

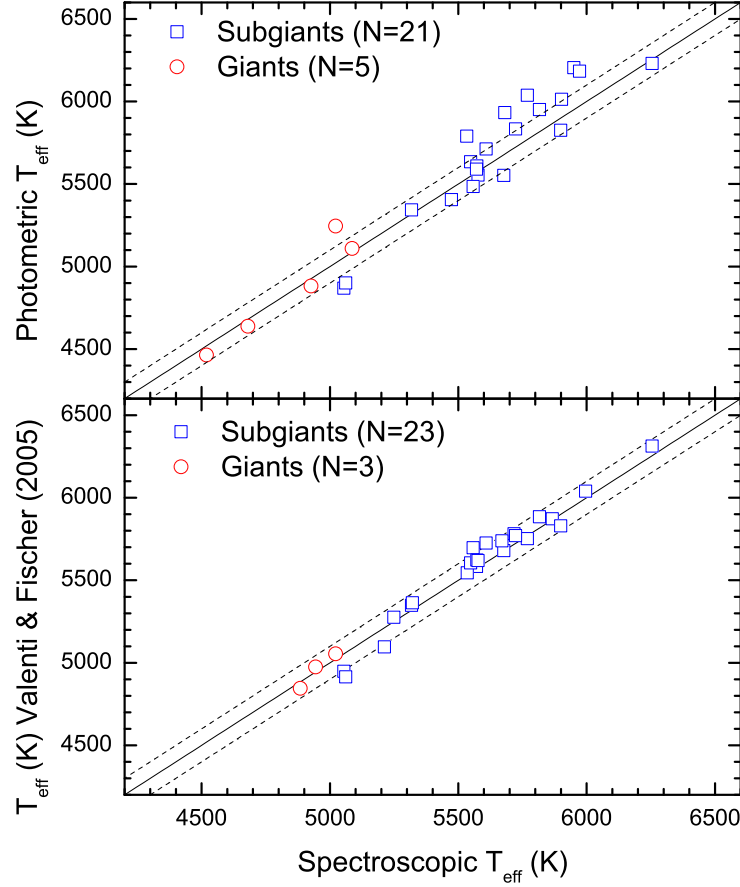


Fig. 1.— Top Panel: Comparison between the spectroscopic effective temperatures derived in this study with T_{eff} 's derived from the $V - K$ calibration by González Hernández & Bonifacio (2009). Subgiants are the open blue squares and giants are the open red circles. Bottom Panel: Comparison between the effective temperatures derived in this study with the stars in common with Valenti & Fischer (2005). The solid line represents perfect agreement and the dashed lines ± 100 K. The three effective temperature scales shown in the top and bottom panels show good agreement within the expected errors in the determinations.

planets. Figure 2 shows the location of the sample stars in an HR diagram with the bolometric magnitudes versus effective temperatures. The bolometric magnitudes for the stars were calculated using the bolometric corrections of Girardi et al. (2002, see details in Paper I). This figure also includes for comparison the sample of stars which was studied in Paper I (represented by black filled circles), and these generally define the location of the main sequence. The target stars analyzed here are obviously more evolved. In this study, a star is classified as a subgiant (represented as red triangles in Figure 2) if it is 1.5 mag above the lower boundary of the main sequence and has $M_{bol} > 2.82$; the 17 stars which have $M_{bol} < 2.82$ are classified as giants (represented as blue squares in Figure 2). This boundary transition between the main-sequence and the subgiant branch is somewhat uncertain and for two stars in particular we adopted a different classification: HD 2151 was classified as a subgiant (although it is not 1.5 mag above the lower boundary of the main sequence) because of its low derived values of $\log g$ (~ 4.0), and HD 205420 (the isolated star with $T_{eff} = 6255$ K and $M_{bol} < 2.82$) is considered as a subgiant. The transition between the subgiant and giant branches is also uncertain. In particular, the classification of two stars (HD 177380 and HD 208801) which lie close to the base of the red-giant branch is uncertain; however, their derived surface gravities are more compatible with their classification as subgiants. (Nevertheless, the implications of including these stars as giants in our analysis is discussed in Section 4.1.2). The adopted classification of the sample stars in giants and subgiants can be found in the last column of Table 1.

Table 3 summarizes the evolutionary parameters calculated for the studied stars. The parallaxes are from the Hipparcos catalogue; the luminosities are calculated using the parallax, V magnitudes, reddening and the derived effective temperatures (see Paper I for details). Three stars (namely NGC 2423 3, NGC 4349 127 and HD 171028) were not present in the Hipparcos catalogue, thus their V magnitudes and parallaxes come from the references in the Extrasolar Planet Encyclopaedia. Note also that the Arenou et al. (1992) model for reddening is accurate to distances within 1 kpc of the Sun. The radii, masses, as well as Hipparcos gravities and estimated ages in Table 3 were calculated using L. Girardi's web code PARAM⁴, which is based on a Bayesian parameter estimation method (da Silva et al. 2006). We note that the Y^2 evolutionary tracks (Yi et al. 2003) were not used in this paper because these do not follow evolution through the red clump.

The surface gravity values obtained here from the ionization equilibrium of Fe I and Fe II and in LTE (column 3; Table 2) can be compared with gravities which are based on Hipparcos parallaxes (column 11; Table 3); such a comparison is shown in Figure 3. The agreement

⁴Available at <http://stev.oapd.inaf.it/cgi-bin/param>

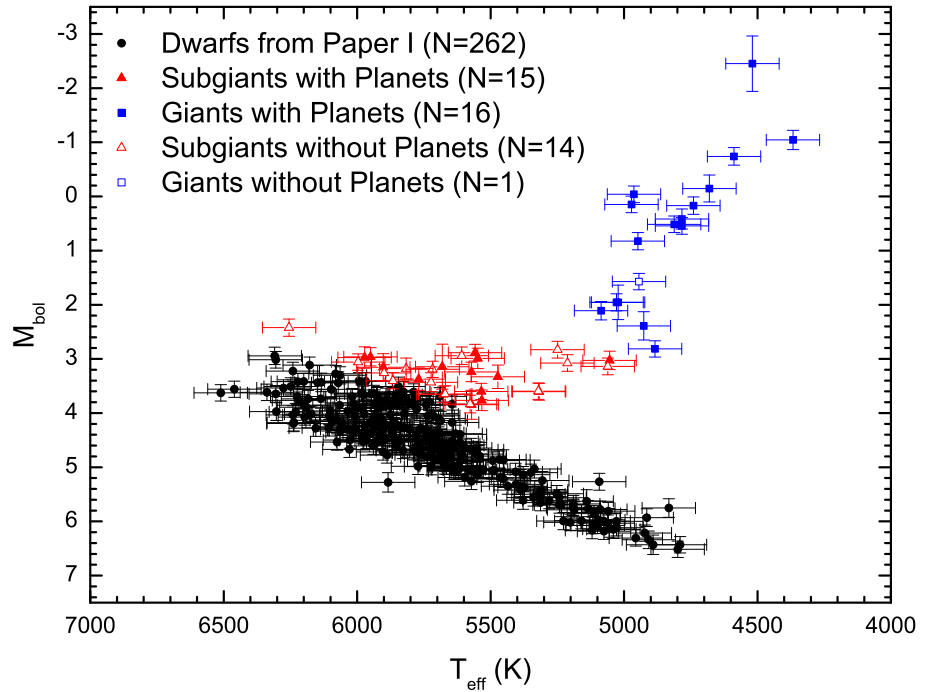


Fig. 2.— Location of studied stars in an H-R diagram. The targets analysed in this study are evolved away from the main sequence. The samples are segregated in dwarfs (black circles; analyzed in Paper I), subgiants (red triangles) and giants (blue squares). All giant stars in our sample, except one, host giant planets; the sample of subgiants include both planet hosting stars as well as a control sample of subgiant stars known to not host giant planets.

between the average values for the two scales is found to be good: $\langle \delta (\log g \text{ Hipparcos} - \log g \text{ This Study}) \rangle = -0.04 \pm 0.12$ dex. Such an agreement between the Hipparcos gravities and spectroscopic values derived from the agreement between Fe I and Fe II suggest the absence of strong non-LTE effects (see discussion in Section 4.1.3).

Concerning their masses and ages, the sample of giants studied here is more massive and younger than the subgiants and dwarfs (from Paper I). The giants in our sample have an average mass of $1.82 \pm 0.68 M_{\odot}$ and a distribution ranging between $\sim 1.1 - 3.8 M_{\odot}$; their average age is $\langle \text{Age} \rangle_{\text{giants}} = 2.22 \pm 1.37$ Gyr. For comparison we note that the sample dwarfs (Paper I) have $\langle M \rangle_{\text{dwarfs}} = 1.03 \pm 0.17 M_{\odot}$ (encompassing the interval $\sim 0.6 - 1.4 M_{\odot}$) and $\langle \text{Age} \rangle_{\text{dwarfs}} = 5.34 \pm 2.70$ Gyr. The overlap in the mass range between the samples of giants and dwarfs is therefore small. We note that the masses and ages of the dwarfs were derived in a different way (Y^2 evolutionary tracks and isochrones). However, it was shown in Paper I that the results from the two methods are consistent for dwarfs: ΔM (Y^2 - Girardi's Code) = $0.03 \pm 0.05 M_{\odot}$ and ΔAge (Y^2 - Girardi's Code) = 0.37 ± 1.46 Gyr (see last paragraph of Section 3.4 in Paper I).

In terms of their average masses, the sample of subgiants studied here falls technically in between the sample of giants and dwarfs but there is considerable overlap in the mass range of the dwarf sample (the subgiant sample encompasses the interval $\sim 1.0 - 1.5 M_{\odot}$; with an average mass of $1.20 \pm 0.14 M_{\odot}$). It is interesting to note that the subgiants in our sample are on average slightly older than the dwarfs ($\langle \text{Age} \rangle_{\text{subgiants}} = 5.46 \pm 1.92$ Gyr), representing the oldest population in this study. In summary, the sample subgiants are a more evolved population of the previously studied dwarfs from Paper I as these dwarfs and subgiants have approximately the same mass ranges. The sample giants, however, are evolved from stars which are more massive and are on average the youngest of all target stars.

4. Discussion

4.1. Metallicity Distributions of Evolved Stars Hosting Planets

As the number of discovered planet hosting stars increases and samples include a larger number of stars which are on the red-giant branch, metallicity distributions of evolved stars hosting planets have started to appear in the literature. Because the samples are still relatively small, and the abundance analyses are not always homogeneous, there is some controversy in some of the conclusions of recent studies of giants, which are briefly summarized as follows. Schuler et al. (2005) compared the iron abundances of 7 giants with planets known at the time and found that their metallicity distribution was on average lower than

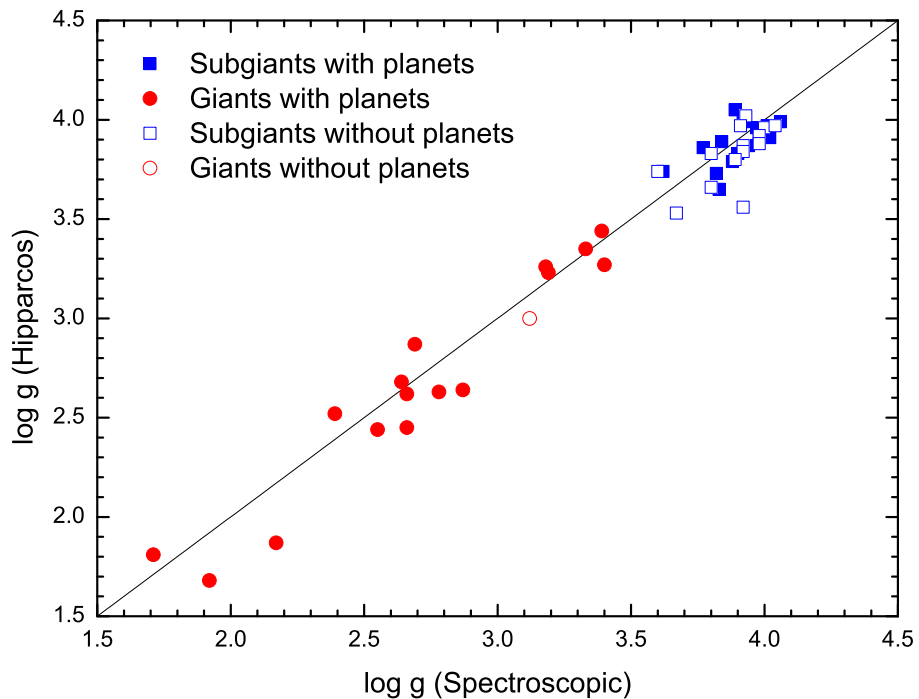


Fig. 3.— Comparison between the spectroscopic gravities derived in this study with those derived using Hipparcos parallaxes. The agreement between the two scales is good with no significant offsets. Perfect agreement is represented by the solid line.

that of dwarfs with planets. This result was later confirmed by Pasquini et al. (2007) who concluded that the metallicity distributions of giants with planets do not favor metal-rich systems. Their results were based on a sample of 14 giants with planets (10 of which analyzed by their group) and are interpreted as possible evidence for pollution. Hekker & Meléndez (2007) analyzed 380 G-K giants as part of the radial velocity survey at Lick Observatory. Five of these stars host planets; they also gather abundances from the literature for another 15 giants and obtain an average metallicity for the sample of -0.05 dex. In addition, this study concludes that there is an offset of 0.13 dex between the metallicity distributions of giants with and without planets; the latter are found to be generally more metal poor. Such an offset in the metallicity distributions is not confirmed in the recent study by Takeda et al. (2008), who analyzed a sample of 322 intermediate-mass late-G giants; ten of these stars host planets. Their comparisons between the metallicity distributions of giants with and without detected planets reveals no significant difference between the two samples; both distributions have average metallicities around -0.12 dex. In the following sections we discuss the metallicity distributions for the giant and subgiant planet-hosting stars in our sample.

4.1.1. Giants

The iron abundance distribution derived from the sample of giant stars hosting planets ($N=16$) is shown in the top panel of Figure 4 as a red dotted line histogram; the average value for this distribution is $\langle \text{[Fe/H]} \rangle_{\text{giants}} = -0.06$ dex. For comparison, the iron abundances obtained for the sample of dwarf stars hosting giant planets ($N=117$) from Paper I are also shown (black solid line histogram). It is apparent from the figure that the metallicity distribution of the giant stars peaks at a lower metallicity value when compared to the dwarf stars; the difference between the average [Fe/H] is 0.17 dex. The application of a Kolmogorov-Smirnov (K-S) test gives a probability of only 1% that the main-sequence dwarfs and giants are drawn from the same parent Fe-abundance population. It is important to recognize, however, the relatively small number of giant stars in this comparison, although this contains $\sim 45\%$ of the total number of giant stars hosting giant planets found to date.

In order to improve the giant star statistics as much as possible, iron abundances for the remaining giants known to have planets were collected from different studies in the literature; their metallicities are listed in Table 4. Literature results for the giant star sample studied here are also presented for comparison. The histogram in the bottom panel of Figure 4 shows the metallicity distribution for the sample including both the giants in this study and for all other literature giants in Table 4 ($N=37$; blue dashed line). The metallicity distribution for the planet-hosting dwarfs from Paper I is shown again for comparison. Using the extended

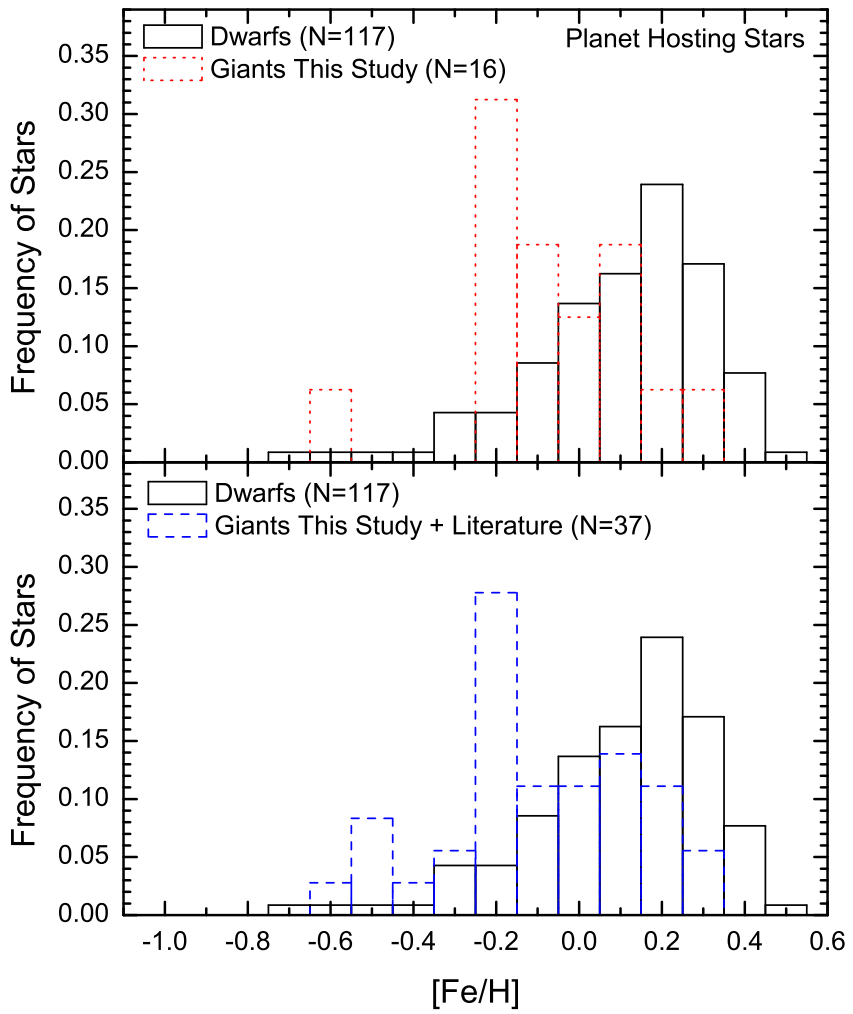


Fig. 4.— Top panel: Metallicity distributions obtained for planet hosting dwarfs (black solid line), and giants (red dotted line). All abundance results in these distributions were derived homogeneously. Bottom panel: Metallicity distributions for planet hosting dwarfs (black solid line; same as top panel), and all giant star hosting giant planets known to date (blue dashed line). The metallicities for those planet-hosting giants not analyzed in this study are taken as the average of the iron abundance values found in the literature (see Table 4).

giant sample yields a similar conclusion: the metallicities of giant stars with planets are on average lower than dwarfs with planets. In particular, the average metallicity for the extended sample (giants from this study plus literature) is somewhat lower ($\langle \text{[Fe/H]} \rangle = -0.12$ dex), but not significantly so, than the average metallicity obtained using only the giants from this study by 0.06 dex. The results from this extended giant sample reinforce the premise that giant stars with giant planets seem to have on average lower iron abundances than dwarf stars with giant planets. The application of a K-S test using the extended giant sample gives a very small probability of $1.91 \times 10^{-5}\%$ that the main-sequence dwarfs and giants are drawn from the same parent population. Such results are in line with the conclusions by Pasquini et al. (2007, see also Schuler et al. 2005) who discuss that the metallicity distributions of planet hosting dwarfs and giants are different; with the giant stars having a distribution shifted to lower metallicites by 0.2–0.3 dex with respect to the dwarfs.

As a final note, we recall the discussion about uncertainties in Section 3. It was shown that our spectroscopic temperatures for the giants would be ~ 20 K cooler if we considered the photometric temperatures as the “correct” scale. This would result in underestimated Fe I abundances by 0.02 dex at most. The sensitivity of this parameter to T_{eff} , $\log g$ and ξ was also discussed and the conclusion was that relative systematic effects of up to 0.1 dex can exist when comparing abundances of dwarfs and giants. Comparisons of our metallicities with those from many studies in the literature (see Table 5 of Paper I and Table 4 of this study) do not show evidence for these possible systematic effects in our metallicities. Even if they existed, neither would be sufficient to explain the differences of 0.17 – 0.23 dex found between the average metallicities of dwarfs and giants.

4.1.2. Subgiants

An additional important aspect of the present study is the homogeneous abundance analysis for samples of subgiants with and without giant planets. A comparison of the metallicity distributions for the two samples (Figure 5 top panel) points to a similarity to that found for dwarfs; namely that subgiant stars without planets are on average more metal poor than the sample of subgiants hosting planets. The results from Paper I showed that the metallicity distribution of dwarfs hosting planets was more metal rich by 0.15 dex than that for dwarfs not hosting planets. This abundance offset found previously for unevolved stars compares well with the difference obtained here for subgiants: the average metallicity for our sample of subgiants hosting planets ($N=15$) is $\langle \text{[Fe/H]} \rangle = +0.12$ dex and for subgiants without planets ($N=14$) it is more metal poor by 0.21 dex ($\langle \text{[Fe/H]} \rangle = -0.09$ dex). Fischer & Valenti (2005) also analyzed a sample of 86 subgiants, nine of which host giant planets.

They find that the median metallicity of their sample of subgiants without detected planets is -0.01 dex, while that of the sample of subgiants with planets is +0.35 dex. This is more metal rich than the results found here for planet hosting subgiants: the median metallicity of the subgiant distribution obtained here is 0.20 dex.

As discussed in the previous section, the sample of subgiants studied here is in fact on average older than the sample of dwarfs (from Paper I), as well as the giant star sample. In terms of their mass distribution the subgiants, although including a few more massive stars, constitute the same general population as the dwarfs, but are just older and more evolved. A comparison of the metallicities of subgiants in our sample and dwarfs from Paper I is shown in Figure 5 (bottom panel), and the distributions are not significantly different. A K-S test gives a probability of 56% that the two samples belong to the same parent population. Based on a K-S test applied to their samples, Fischer & Valenti (2005) also find that the metallicity distributions of main-sequence and subgiant stars with planets are consistent, and that both samples are more metal-rich than their counterparts without detected planets.

There is presently a negligible offset (0.01 dex) between the averages of the metallicity distributions of dwarfs with planets (from Paper I) and the subgiants with planets studied here: both have $\langle [\text{Fe}/\text{H}] \rangle \simeq +0.11$ dex. In general terms, this is what would be expected if dwarfs and subgiants come from the same population if there are no effects related to age-metallicity. It should be recognized, however, that the subgiant sample is significantly smaller than the dwarf sample and that this offset in metallicity, which is found to be zero for the stars with planets, could in fact be as large as ~ 0.05 dex given the uncertainties in the analysis and the small number statistics. In fact, there is a small offset of 0.05 dex between the averages of the metallicity distributions of dwarfs and subgiants without planets (with the latter being more metal poor). For example, if the the planet hosting star (HD 177830) which lies in the transition between the subgiant and red-giant branches (previously noted in Section 3.1; Figure 2) is instead classified as a giant (as in Hekker & Meléndez 2007), this will affect the average metallicity of the sample of subgiants with planets which will change to a slightly lower value: $\langle [\text{Fe}/\text{H}] \rangle = +0.10$ dex ($N=14$); or an offset between subgiants and dwarfs with planets of 0.01 dex (note also that in this case the giants will have an average metallicity which is slightly higher of $\langle [\text{Fe}/\text{H}] \rangle = -0.03$ dex). If this offset in the metallicities between the dwarfs and subgiants is small but real, a possible interpretation for the lower metallicity found for the subgiants is that these small differences in the abundances are the result of chemical evolution, since the sample subgiant stars are older they would be on average slightly more metal poor.

We note that the discusson about uncertainties presented in Section 3 revealed that no significant systematic effects should be expected in the comparison of metallicities of sub-

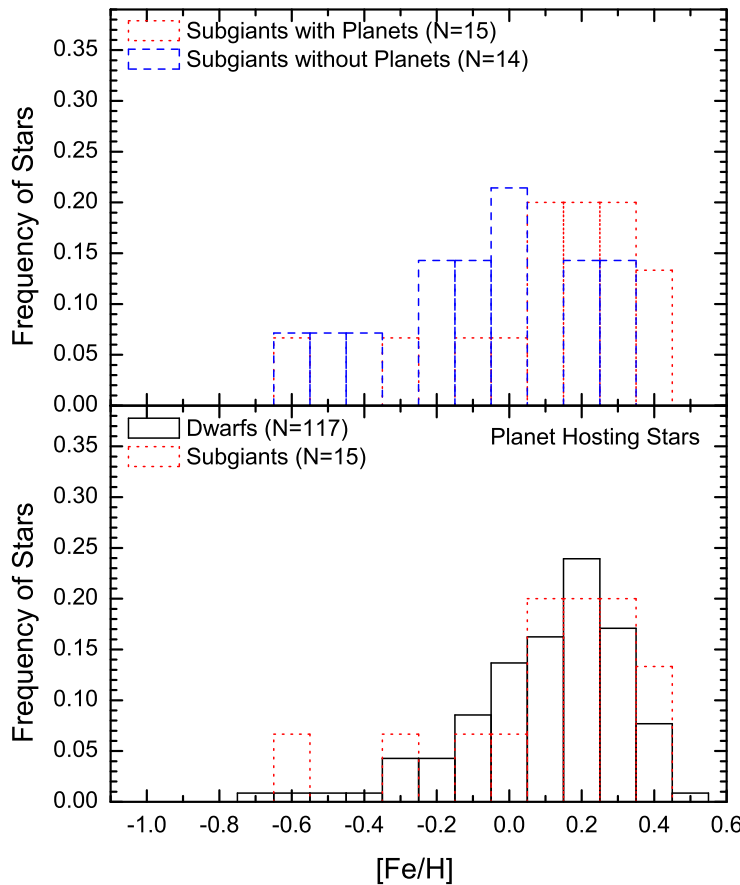


Fig. 5.— Top panel: Metallicity distributions obtained for the sample of subgiant stars hosting planets (red dotted line histogram) and the control sample of subgiants not known to have giant planets (blue dashed line histogram). The planet-hosting stars are found to be on average more metal rich than the control sample by 0.21 dex. Bottom panel: Metallicity distributions of subgiant stars with planets (red dotted line histogram) in comparison with the dwarf star planet hosting sample (black solid line histogram) analyzed in Paper I. The two distributions are similar with no obvious abundance shifts.

giants and dwarfs. It was also shown that our spectroscopic temperatures for the subgiants would be ~ 50 K cooler if we considered the photometric temperatures as the “correct” scale. This would result in underestimated Fe I abundances by 0.05 dex at most. Therefore, if possible systematic effects do exist in our metallicities (which does not seem to be true), they would not change the main point of the above discussion: the average metallicities of dwarfs and subgiants are equal within the expected uncertainties.

4.1.3. Departures from LTE in Fe I and Fe II in Dwarfs, Subgiants, and Giants

Given the comparisons in the metallicity distributions (primarily from Fe I but also from Fe II lines) between the dwarf, subgiant, and giant samples discussed here, it is important to assess non-LTE Fe I and Fe II line-formation as a function of T_{eff} , surface gravity, and stellar metallicity. Within the homogeneous LTE analysis conducted in this study, planet-hosting dwarf and subgiant stars display the same [Fe/H] distributions, while there is an overall difference of ~ 0.2 dex in the Fe-abundance distributions of dwarfs and subgiants with planets when compared to giants with planets. Could this difference be due simply to different non-LTE effects between dwarfs/subgiants and giants?

Non-LTE Calculations

Non-LTE calculations for iron contain uncertainties due to such quantities as electronic collisional cross-sections, in particular for dipole-forbidden transitions; photoionization cross-sections, in particular those from the excited states; a treatment of upper states (particularly those for which no laboratory-measured energies are available); recombination to the upper levels; a treatment of autoionizing levels and related photoionization resonances; and, most importantly, uncertainties due to treatment of collisions with neutral hydrogen atoms, which are poorly known (Hubeny 2010, private communication). Within these uncertainties, however, results from non-LTE calculations in cool stars (e.g., Mashonkina et al. 2010a; Gehren et al. 2001a,b) generally find that departures from LTE become larger in very metal poor stars, evolved stars, and stars with effective temperatures $T_{\text{eff}} > 6000$ K. In the temperature and gravity regimes considered here, non-LTE departures are much less important for Fe II lines, which are generally found to be closer to LTE.

Certain studies of non-LTE in Fe I and Fe II find rather small departures from LTE, even in rather metal-poor stars, such as globular cluster stars. For example, Korn et al. (2003) analyze main-sequence turn-off stars, subgiants, and giants in the globular cluster NGC 6397 (with [Fe/H] = -2.35) and find total corrections to LTE of Fe I of only 0.03 - 0.05

dex, with no differential non-LTE effects between the main-sequence turn-off and giant stars. A more recent analysis of this cluster by Lind et al. (2009) notes that such small corrections found by Korn et al. (2003) were probably due to their adoption of rather high efficiencies of collisions between iron atoms and neutral hydrogen atoms, as parameterized by the H I collision enhancement factor of $S_H = 3$.

Given that one of the major uncertainties in non-LTE calculations, as discussed above, is the efficiency of collisions of Fe I with neutral hydrogen, Mashonkina et al. (2010a) present results for H I collision enhancement factors, S_H , varying between 0 (which corresponds to the strongest non-LTE case) and 2 (corresponding to a situation closer to LTE), as well as LTE. Figure 1 in their study illustrates differences between non-LTE Fe I and Fe II abundances for 4 different stars: Procyon ($T_{\text{eff}} = 6510$ K, $\log g = 3.96$, $[\text{Fe}/\text{H}] = -0.10$), β Vir ($T_{\text{eff}} = 6060$ K, $\log g = 4.11$, $[\text{Fe}/\text{H}] = +0.04$), τ Cet ($T_{\text{eff}} = 5377$ K, $\log g = 4.53$, $[\text{Fe}/\text{H}] = -0.43$), and HD 84937 ($T_{\text{eff}} = 6350$ K, $\log g = 4.00$, $[\text{Fe}/\text{H}] = -1.94$). It is clear from this figure that non-LTE Fe I abundances of the most metal poor stars in the sample can be affected by as much as 0.15 dex when $S_H = 0$, however this is only for the most metal-poor star in the sample, HD 84937; the effect of non-LTE on Fe I decreases significantly for increasing metallicities, due to increasing electron densities. In addition, values of S_H as low as 0.1 lead to very small non-LTE corrections for Fe I for all stars. Although uncertain, the value $S_H=0.1$ is favored (Mashonkina et al. 2010c) and this would suggest that differences in the iron abundances between the samples of near-solar metallicity dwarfs, subgiants, and giants caused by non-LTE corrections would be less than 0.1 dex.

The calculations presented in Mashonkina et al. (2010a) predict that non-LTE corrections for Fe I increase strongly with decreasing metallicity and, therefore, should be minimal at solar metallicities. In addition, the corrections become increasingly important for effective temperatures greater than $T_{\text{eff}} = 6000$ K, as well as $\log g \leq 2.00$. The sample analyzed here is dominated by stars with $\log g \geq 2.00$, $T_{\text{eff}} = 4500 - 6000$ K, and near-solar metallicities, where the predicted effects on Fe I are less than 0.1 dex. More recent results presented in Mashonkina et al. (2010b) increase the number of stars to five and indicate that LTE can be considered “as good as non-LTE” for $S_H > 0.1$ and metallicities between solar and -0.5 dex, based on the analysis of stars such as Procyon and τ Cet. With values of $S_H \sim 0.1$, combined with the points described above, LTE abundances from Fe I and Fe II are expected to be very close to those derived from non-LTE (within hundredths of a dex) for the samples of stars with planets studied here.

Observations of Fe in dwarfs and giants in clusters

The theoretically predicted small non-LTE effects on Fe I described above for near-solar metallicity stars are born out by observations of real stars in clusters which contain uniform Fe abundances. One recent result relevant to this discussion is the abundance analysis of giants, subgiants, and main-sequence stars from a number of open clusters by Santos et al. (2009), as well as the results from the analysis of main-sequence turn-off stars, subgiants, and giants in the globular cluster M71 (one of the more metal-rich globular clusters) by Ramírez et al. (2001). A short summary of these studies would note that no significant abundance differences (i.e., $\Delta[\text{Fe}/\text{H}] \geq 0.05$ dex) were found in LTE analyses of Fe I lines between stars with $T_{\text{eff}} \sim 6000\text{--}6100$ K and $\log g \sim 4.2\text{--}4.6$ when compared to those with $T_{\text{eff}} \sim 4500\text{--}4600$ K and $\log g \sim 1.7\text{--}2.5$ in any of the studied clusters. Iron abundances from these studies are illustrated in Figure 6 for the globular cluster M71 (Ramírez et al. 2001) and the open clusters NGC 2682 and IC 4651 (Santos et al. 2009); these particular clusters are shown as the numbers of stars studied in each cluster were the largest, and the clusters span a range in [Fe/H] overlapping that of the sample stars included here. The top panel shows Fe abundances (as [Fe/H]) plotted versus T_{eff} and the bottom panel is [Fe/H] versus $\log g$. The points are average values for stars found along the major phases of stellar evolution (main sequence, turn-off, subgiant and giant branches), with the standard deviations in [Fe/H], T_{eff} , and $\log g$ shown for each sub-sample. Linear least-squares fits were carried out for each cluster and the derived slopes are labelled. For the near-solar metallicity open clusters, in particular, the slopes are very small and not significant indicating a good agreement between the LTE Fe abundances in dwarfs and giants.

Another piece of evidence that the Fe abundances of the stars analyzed here are not affected by significant non-LTE effects is the comparison of stellar surface gravities derived from the enforcement of LTE ionization equilibrium between Fe I and Fe II, with surface gravities derived from fitting stellar models to luminosities obtained from Hipparcos parallaxes (so-called Hipparcos gravities), as illustrated here in Figure 3. If Fe I and/or Fe II suffer from significant departures from LTE, gravities may be adversely affected. The mean difference in $\log g$ between these methods for subgiants and giants is $\log g_{\text{Hipp}} - \log g_{\text{Spec}} = -0.04 \pm 0.12$ dex. The standard deviation in this difference compares well with the expected uncertainty in defining $\log g$ by any method, while the small offset of 0.04 dex indicates excellent agreement between the two surface gravity methods. This small difference indicates that there are not significant departures from LTE populations in Fe I and Fe II in the line-forming regions of near-solar metallicity dwarfs, subgiants, and giants in the T_{eff} and $\log g$ regimes analyzed here.

As the analysis of all stars in the present study was done in a strictly homogeneous

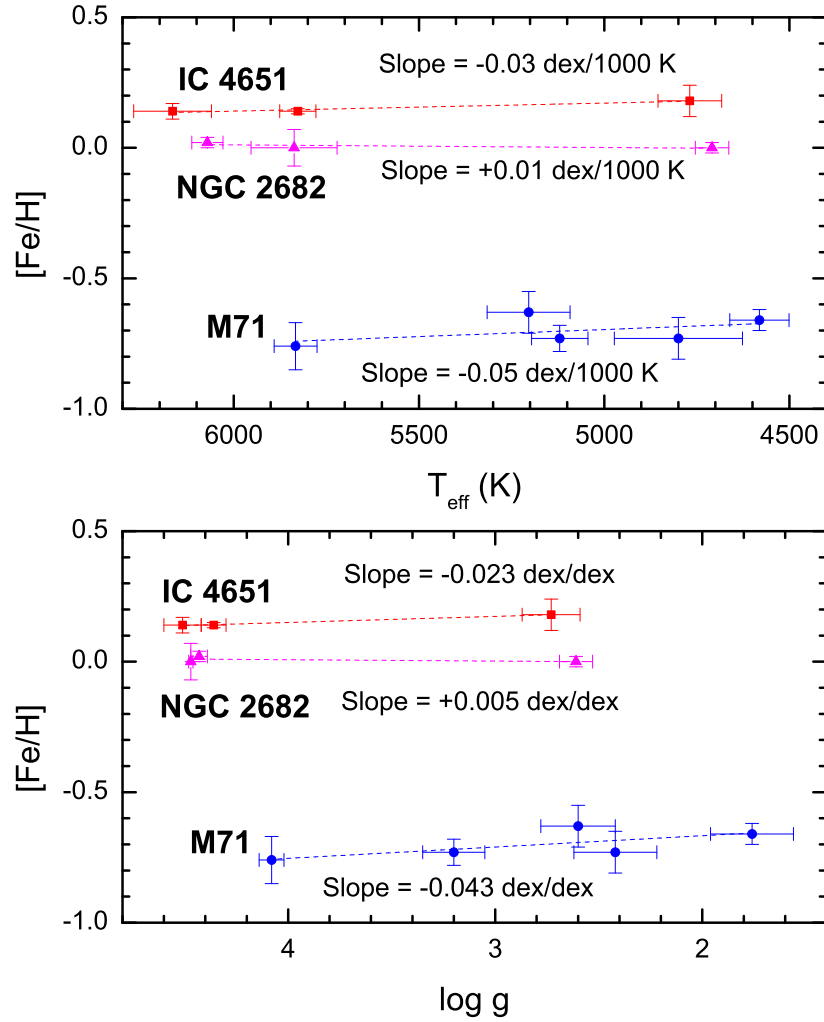


Fig. 6.— Iron abundances versus effective temperatures (top panel) and surface gravities (bottom panel) for the globular cluster M71 (Ramírez et al. 2001; blue circles) and the open clusters NGC 2682 and IC 4651 (Santos et al. 2009; respectively, magenta triangles and red squares). The dashed lines show the linear fit to the points for each case. No significant slopes are observed for any of the clusters.

manner, when coupled to the predictions that non-LTE corrections to Fe I in near-solar metallicity dwarfs and giants with the range of stellar parameters studied here will be small (much less than 0.1 dex), and the observations of rather uniform LTE iron abundances derived in cluster dwarfs and giants, it is unlikely that non-LTE departures can explain the differences observed here in the iron abundances of dwarfs and subgiants with planets, when compared to giants with planets (~ 0.2 dex).

4.1.4. Dwarfs, Subgiants, Giants, Dilution and Other Possibilities

The fact that the metallicity distribution of giant stars with planets in our sample is generally more metal poor than the metallicity distribution found for the dwarfs cannot be explained in terms of Galactic chemical evolution, as these results are opposite from what would be expected from chemical evolution: the giant sample stars being younger (on average) than the sample dwarfs would be more metal rich if one considers the effects of an age-metallicity relation. Haywood (2009) propose, on the other hand, that the difference in the metallicity distributions of dwarfs and giants with planets is not related to the formation process of giant planets themselves, but results from a galactic effect instead. His conclusions are based on ages and metallicities of sample giants and dwarfs analyzed by Takeda (2007) and Takeda et al. (2008). As radial mixing is a secular process, the sample of giants would be less contaminated by old, metal-rich wanderers of the inner disk. This scenario would only hold, however, if stars from the inner disk have a higher percentage of giant planets than stars born at the solar radius and assumes a metallicity gradient for the Galactic disk.

A relevant question concerning metallicity distributions of planet hosting stars in different evolutionary stages connects the possibility of late accretion of metal rich material onto the star to the dilution of this abundance signature as the star develops a deeper convective envelope. The expectation in such a scenario would be that the metal rich signature which is due to accretion would vanish as stars become giants; their convective zones become larger and the metal rich material becomes diluted. If the high metallicity observed for the main-sequence stars hosting giant planets is indeed restricted to the outer envelope it is expected that subgiants will have a systematically lower metallicity than the dwarfs.

Taken at face value, the metallicity distributions of planet hosting dwarfs, subgiants and giants obtained in this study are not in line with the dilution picture as there is not a consistent decrease in the average metallicities for planet-hosting stars going from dwarfs (+0.11 dex) to subgiants (+0.12 dex), to giants (-0.06 dex); in particular between the dwarfs and subgiants. In addition, the absence of a trend in the plot of effective temperature versus stellar metallicity for sample subgiants (shown in Figure 7) indicates the absence of dilution

on the subgiant branch. A trend in the run of metallicity with effective temperature would be expected if the stars experienced increased dilution as they evolve redward on the subgiant branch, but this gradient is flat. The giants in our sample which are at the base of the red giant branch (with $M_{bol} \simeq 2.82$; see Figure 2), are also shown in Figure 7 as it is at this stage that the convective zone deepens significantly. Note that a similar range in metallicity (roughly between $[Fe/H] = -0.3$ to $+0.3$ dex) is encompassed by the subgiants and giants in the figure, which indicates no significant differences between the metallicities of subgiants and giants at the base of the RGB. This result is in agreement with the findings of Fischer & Valenti (2005) who also do not find a metallicity gradient as a function of T_{eff} along the subgiant branch and conclude that subgiants do not exhibit any evidence for dilution.

Without evidence for dilution along the subgiant branch, the observations point to a scenario to explain the more metal poor distribution observed for giant stars in comparison with dwarfs which is related to the fact that the higher masses of the giant stars compensate for the lower metallicities by allowing, or favoring, the formation of planets because higher mass stars have on average disks with larger masses. A number of studies (e.g. Natta et al. 2000) find that disk mass increases with stellar mass. As disk mass increases, the surface density (σ) within typical protoplanetary disks also increases and larger values of σ favor the formation of giant planets in the core accretion model of planetary formation (Ida & Lin 2004; Laughlin et al. 2004). The precipitation of a substantial planetary core which begins to accrete gas requires a threshold density of solid material (which consists of the heavier elements, or metals).

The observation that the average metallicity of planet-hosting stars is related to the average mass within a stellar sample, with giants representing the more massive but lower metallicity population, is taken as an observational signature of core-accretion as the main mechanism for planetary formation, at least for planets which form relatively close to their parent stars. The disk instability mechanism (see review by Boss 2010) may still be important for the massive planets which form at large distances from their parent stars. Examples of such systems may be the recently imaged planets found around HR 8799 (Marois et al. 2008) and Fomalhaut (Kalas et al. 2008). The nature of planetary system architectures is quite likely a function of both stellar mass and metallicity.

5. Conclusions

It is now well established that stars hosting giant planets have on average higher metallicities than stars which do not host closely orbiting giant planets (see, e.g. Gonzalez 2006; Udry & Santos 2007; Valenti 2010 for reviews). So far, however, most of the studies have

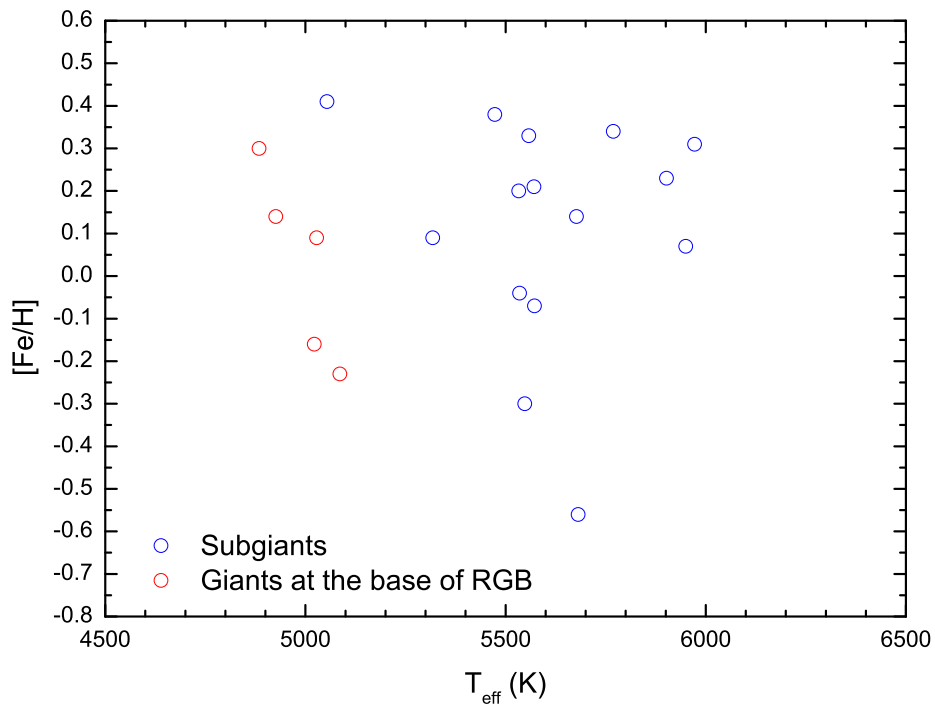


Fig. 7.— Metallicities versus effective temperatures for the studied sample of subgiant stars hosting planets (blue open circles). The absence of a trend in this figure indicates the stars are not experiencing increasing dilution of their convective zones. Sample giants (red open circles) which are at the base of the red giant branch ($M_{\text{bol}} \simeq 2.82$) are also shown for comparison.

concentrated on host stars which are on the main sequence. Such a finding was recently corroborated from metallicities obtained in the homogeneous analysis of a large sample of main-sequence planet hosts and a control sample of stars without closely orbiting giant planets, which was presented in Paper I. The present study extends the main-sequence sample in Paper I by adding planet hosting stars which are evolved from the main sequence.

We have determined stellar parameters and metallicities for a sample of 15 subgiants and 16 giants with planets discovered via radial velocity surveys and 14 comparison subgiants which have been found to exhibit nearly constant radial velocities and are not likely to host large, closely orbiting planets. The stellar parameters and iron abundances were derived from a classical spectroscopic analysis (similar to Paper I).

Our results are summarized as follows:

- 1) One strong point of the present study is the strictly homogeneous abundance analyses performed for the samples of dwarfs (Paper I), subgiants and giants. An additional important aspect is the sample of disk subgiant stars which are known to be RV stable (Fischer & Valenti 2005) and can be used as a comparison sample for the subgiant planet-hosting stars.
- 2) The subgiant sample in this study is found to be a slightly older population which has evolved mostly from the same underlying population as the dwarfs analyzed in Paper I; the sample dwarfs and subgiants have significant overlap in their mass ranges. The sample giants, however, are evolved from stars which are more massive and are, on average, the youngest of all studied targets.
- 3) The metallicity distribution obtained for our sample of 16 giant planet-hosting stars displays an average that is more metal poor by 0.17 dex than the metallicity distribution obtained in Paper I for the sample of planet-hosting dwarfs ($N=117$). When literature iron abundance results for all other presently known giant planet-hosting stars are included, in order to improve the giant star statistics to a total of 37 stars, the offset in the average metallicities between dwarf and giant planet-hosting stars is confirmed and becomes marginally larger (0.23 dex).
- 4) The average metallicity of the planet-hosting subgiant sample is metal-rich relative to the Sun, $\langle [Fe/H] \rangle = +0.12$ dex. The latter distribution is similar to that obtained for the planet hosting dwarf sample, and on average more metal rich than that of subgiants without planets by 0.21 dex. This abundance difference between the subgiants with and without planets is in general agreement, within the uncertainties, with the abundance shift that is found for dwarfs with and without planets.
- 5) The absence of a trend in the derived iron abundances with effective temperature

for the sample subgiant stars shows no evidence for dilution on the subgiant branch. This flat gradient plus the fact that there is not a significant difference between the metallicity distributions of subgiant planet-hosting stars in comparison to dwarf planet-hosting stars, as would be expected from the more extended convective envelopes of subgiants in comparison with dwarfs, weakens the possibility of dilution as a viable explanation for the lower metallicity found for the giant stars.

6) In the absence of substantial evidence for the dilution of accreted metal-rich material, the results in this study favor a scenario to explain the more metal poor distribution observed for giant stars in comparison with that of dwarfs which is related to the fact that the higher masses of the giant stars compensate for the lower metallicities, as higher mass stars have on average more massive disks with more metals available for planet formation through core accretion.

We thank Leo Girardi for helping with the computation of the evolutionary parameters. K.C. thanks Andreas Korn and Ivan Hubeny for discussions concerning non-LTE effects and for Joan Najita and Luca Pasquini for fruitful discussions. L.G. thanks Oliver Schütz for his valuable help in using the FEROS DRS package and Cláudio Bastos for conducting the observations for target star HD 114613. L.G. acknowledges financial support by CNPq. Research presented here was supported in-part by NASA grant NNH08AJ581.

REFERENCES

- Alonso, A., Arribas, S., & Martínez-Roger, C. 1999, *A&AS*, 140, 261
Arenou, F., Grenon, M., & Gómez, A. 1992, *A&A*, 258, 204
Boss, A. P. 2010, in IAU Symp. 265, Chemical Abundances in the Universe: Connecting First Stars to Planets, ed. K. Cunha, M. Spite & B. Barbuy (Cambridge:Cambridge University Press), 391
Casagrande, L., Ramírez, I., Meléndez, J., Bessel, M., & Asplund, M. 2010, *A&A*, 512, A54
da Silva, L., et al. 2006, *A&A*, 458, 609
Döllinger, M. P., Hatzes, A. P., Pasquini, L., Guenther, E. W., Hartmann, M., Girardi, L., & Esposito, M. 2007, *A&A*, 472, 649
Döllinger, M. P., Hatzes, A. P., Pasquini, L., Guenther, E. W., & Hartmann, M. 2009a, *A&A*, 505, 1311

- Döllinger, M. P., Hatzes, A. P., Pasquini, L., Guenther, E. W., Hartmann, M., & Girardi, L. 2009b, *A&A*, 499, 935
- Ercolano, B., & Clarke, C. J. 2010, *MNRAS*, 402, 2735
- Fischer, D. A., & Valenti, J. 2005, *ApJ*, 622, 1102
- Fuhrmann, K. 2004, *AN*, 325, 3
- Gehren, T., Butler, K., Mashonkina, L., Reetz, J., & Shi, J. 2001, *A&A*, 366, 981
- Gehren, T., Korn, A.J., & Shi, J. 2001, *A&A*, 380, 645
- Ghezzi, L., Cunha, K., Smith, V. V., de Araújo, F. X., Schuler, S., & de la Reza, R. 2010, *ApJ*, in press
- Girardi, L., Bertelli, G., Bressan, A., Chiosi, C., Groenewegen, M. A. T., Marigo, P., Salasnich, B., & Weiss, A. 2002, *A&A*, 391, 195
- Gonzalez, G. 1997, *MNRAS*, 285, 403
- Gonzalez, G. 2006, *PASP*, 118, 1494
- Gonzalez, G., & Vanture, A. D. 1998, *A&A*, 339, L29
- González Hernández, J. I., & Bonifacio, P. 2009, *A&A*, 497, 497
- Han, I., Lee, B. C., Kim, K. M., Mkrtichian, D. E., Hatzes, A. P., & Valyavin, G. 2010, *A&A*, 509, A24
- Hatzes, A. P., et al. 2006, *A&A*, 457, 335
- Haywood, M. 2009, *ApJ*, 698, L1
- Hekker, S., & Meléndez, J. 2007, *A&A*, 475, 1003
- Ida, S., & Lin, D. N. C. 2004, *ApJ*, 616, 567
- Johnson, J. A., et al. 2007, *ApJ*, 665, 785
- Johnson, J. A., Howard, A. W., Bowler, B. P., Henry, G. W., Marcy, G. W., Wright, J. T., Fischer, D. A., & Isaacson, H. 2010, *PASP*, 122, 701
- Kalas, P., et al. 2008, *Science*, 322, 1345

- Kaufer, A., Stahl, O., Tubbesing, S., Nørregaard, P., Avila, G., Francois, P., Pasquini, L., & Pizzella, A. 1999, *The Messenger*, 95, 8
- Korn, A. J. 2010, IAU Symp. 268, Light Elements in the Universe, ed. C. Charbonnel, M. Tosi, F. Primas & C. Chiappini (Cambridge:Cambridge University Press), 249
- Korn, A. J., Shi, J., & Gehren, T. 2003, *A&A*, 407, 691
- Laughlin, G., Bodenheimer, P., & Adams, F. C. 2004, *ApJ*, 612, L73
- Lind, K., Primas, F., Charbonnel, C., Grundahl, F., & Asplund, M. 2009, *A&A*, 503, 545
- Liu, Y.-J., Sato, B., Zhao, G., & Ando, H. 2009, *RAA*, 9, 1
- Luck, R. E., & Heiter, U. 2007, *AJ*, 133, 2464
- McWilliam, A. 1990, *ApJS*, 74, 1075
- Marois, C., Macintosh, B., Barman, T., Zuckerman, B., Song, I., Patience, J., Lafreniére, D., Doyon, R. 2008, *Science*, 322, 1348
- Mashonkina, L., Gehren, T., Shi, J., Korn, A., & Grupp, F. 2010a, IAU Symp., 265, Chemical Abundances in the Universe: Connecting First Stars to Planets, ed. K. Cunha, M. Spite & B. Barbuy (Cambridge:Cambridge University Press), 197
- Mashonkina, L., Gehren, T., Shi, J., Korn, A., & Grupp, F. 2010b, in workshop “The Chemical Enrichment of the Milky Way Galaxy”, Ringberg Castle, Germany (http://www.mpa-garching.mpg.de/~cemw10/talks/Mashonkina_rindberg2010.pdf)
- Mashonkina, L., et al. 2010, *A&A*, submitted
- Mishenina, T. V., Bienaymé, O., Gorbaneva, T. I., Charbonnel, C., Soubiran, C., Korotin, S. A., & Kovtyukh, V. V. 2006, *A&A*, 456, 1109
- Natta, A., Grinin, V., & Mannings, V. 2000, in Protostars and Planets IV, ed. V. Mannings, R. P. Boss, & S. S. Russell (Tucson: Univ. Arizona Press), 559
- Niedzielski, A., Goździecki, K., Wolszczan, A., Konacki, M., Nowak, G., & Zieliński, P. 2009a, *ApJ*, 693, 276
- Niedzielski, A., Nowak, G., Adamów, M., & Wolszczan, A. 2009b, *ApJ*, 707, 768
- Niedzielski, A., et al. 2007, *ApJ*, 669, 1354

- Pasquini, L., Döllinger, M. P., Weiss, A., Girardi, L., Chavero, C., Hatzes, A. P., da Silva, L., & Setiawan, J. 2007, *A&A*, 473, 979
- Ramírez, I., & Meléndez, J. 2005, *ApJ*, 626, 465
- Ramírez, S. V., Cohen, J. G., Buss, J., & Briley, M. M. 2001, *AJ*, 122, 1429
- Robinson, S. E., et al. 2007, *ApJ*, 670, 1391
- Sadakane, K., Ohnishi, T., Ohkubo, M., & Takeda, Y. 2005, *PASJ*, 57, 127
- Santos, N. C., Israelian, G., Mayor, M., Rebolo, R., & Udry, S. 2003, *A&A*, 398, 363
- Santos, N. C., Israelian, G., & Mayor, M. 2005, *A&A*, 415, 1153
- Santos, N. C., Israelian, G., Mayor, M., Bento, J. P., Almeida, P. C., Sousa, S. G., & Ecuvillon, A. 2005, *A&A*, 437, 1127
- Santos, N. C., Lovis, C., Pace, G., Meléndez, J., & Naef, D. 2009, *A&A*, 493, 309
- Sato, B., et al. 2003, *ApJ*, 597, L157
- Sato, B., et al. 2007, *ApJ*, 661, 527
- Sato, B., et al. 2008a, *PASJ*, 60, 539
- Sato, B., et al. 2008b, *PASJ*, 60, 1317
- Schuler, S. C., Hatzes, A. P., King, J. R., Kürster, M., & The, L.-S. 2006, *AJ*, 131, 1057
- Schuler, S. C., Kim, J. H., Tinker, M. C., Jr., King, J. R., Hatzes, A. P., & Guenther, E. W. 2005, *ApJ*, 632, L131
- Setiawan, J., et al. 2005, *A&A*, 437, L31
- Sousa, S. G., Santos, N. C., Israelian, G., Mayor, M., & Monteiro, M. J. P. F. G. 2006, *A&A*, 458, 873
- Sousa, S. G., Santos, N. C., Israelian, G., Mayor, M., & Monteiro, M. J. P. F. G. 2007, *A&A*, 469, 783
- Takeda, Y. 2007, *PASJ*, 59, 335
- Takeda, Y., Sato, B., Kambe, E., Izumiura, H., Masuda, S., & Ando, H. 2005, *PASJ*, 57, 109

- Takeda, Y., Sato, B., & Murata, D. 2008, PASJ, 60, 781
- Udry, S., & Santos, N. C., 2007, ARA&A, 45, 397
- Valenti, J. A. 2010, in IAU Symp. 265, Chemical Abundances in the Universe: Connecting First Stars to Planets, ed. K. Cunha, M. Spite & B. Barbuy (Cambridge:Cambridge University Press), 403
- Valenti, J. A., & Fischer, D. A. 2005, ApJS, 159, 141
- Yi, S. K., Kim, Y.-C., & Demarque, P. 2003, ApJS, 144, 259

Table 1. Log of Observations

Star	<i>V</i>	Observation Date	T_{exp} (s)	S/N ($\sim 6700 \text{ \AA}$)	Classification
<i>Planet Hosting Stars</i>					
HD 5319	8.05	2007 Aug 28	1200	282	G
HD 10697	6.27	2007 Aug 29	200	277	SG
HD 11977	4.68	2007 Aug 30	80	344	G
HD 11964	6.42	2007 Aug 30	200	313	SG
HD 16400	5.65	2008 Aug 19	200	352	G
HD 23127	8.58	2007 Aug 30	1800	291	SG
HD 27442	4.44	2007 Oct 02	15	138	G
HD 28305	3.53	2007 Aug 30	30	291	G
HD 33283	8.05	2007 Aug 30	1200	385	SG
HD 38529	5.95	2007 Oct 02	200	314	SG
HD 47536	5.25	2007 Apr 08	80	369	G
HD 59686	5.45	2007 Apr 08	80	217	G
NGC 2423 3	10.04	2007 Aug 28	3000	183	G
HD 73526	8.99	2007 Apr 08	3000	301	SG
HD 88133	8.01	2007 Apr 07	1200	290	SG
NGC 4349 127	10.83	2008 Apr 06	10800	196	G
HD 117176	4.97	2007 Apr 06	80	415	SG
HD 122430	5.47	2007 Apr 06	80	199	G
HD 154857	7.24	2007 Apr 06	480	439	SG
HD 156846	6.50	2008 Apr 06	500	417	SG
HD 159868	7.24	2007 Apr 06	480	460	SG
HD 171028	8.31	2007 Aug 28	1200	331	SG
HD 175541	8.02	2007 Aug 28	1200	291	G
HD 177830	7.18	2007 Aug 29	480	207	SG
HD 188310	4.71	2008 Apr 06	100	344	G
HD 190647	7.78	2007 Aug 28	1200	363	SG
HD 192699	6.44	2007 Aug 28	200	259	G
HD 199665	5.51	2008 Apr 06	200	320	G
HD 210702	5.93	2007 Aug 28	200	280	G

Table 1—Continued

Star	<i>V</i>	Observation Date	<i>T_{exp}</i> (s)	S/N (~ 6700 Å)	Classification
HD 219449	4.24	2007 Aug 30	60	316	G
HD 224693	8.23	2007 Aug 29	1200	336	SG
<i>Control Sample</i>					
HD 2151	2.82	2008 Aug 20	15	363	SG
HD 18907	5.88	2008 Aug 20	200	407	SG
HD 33473	6.75	2008 Aug 20	500	441	SG
HD 114613	4.85	2008 Feb 21	100	446	SG
HD 121384	6.00	2008 Apr 07	200	414	SG
HD 140785	7.38	2008 Apr 07	500	371	SG
HD 168060	7.34	2008 Aug 20	500	331	SG
HD 168723	3.23	2008 Aug 20	15	326	G
HD 188641	7.34	2008 Aug 19	500	409	SG
HD 196378	5.11	2008 Aug 19	100	433	SG
HD 205420	6.45	2008 Aug 19	200	307	SG
HD 208801	6.24	2008 Aug 19	200	301	SG
HD 212330	5.31	2008 Aug 20	100	273	SG
HD 219077	6.12	2008 Aug 19	200	372	SG
HD 221420	5.82	2008 Aug 20	200	307	SG

Note. — SG = Subgiant; G = Giant.

Table 2. Atmospheric Parameters and Metallicities

Star	T _{eff} (K)	log g	ξ (km s ⁻¹)	A(Fe)	σ (Fe I)	N (Fe I)	σ (Fe II)	N (Fe II)	[Fe/H]
<i>Planet Hosting Stars</i>									
HD 5319	4926	3.33	1.17	7.57	0.10	23	0.06	9	0.14
HD 10697	5677	4.06	1.28	7.57	0.08	27	0.05	12	0.14
HD 11977	4972	2.64	1.42	7.27	0.08	25	0.07	11	-0.16
HD 11964	5318	3.77	1.12	7.52	0.07	27	0.05	11	0.09
HD 16400	4783	2.39	1.46	7.36	0.11	25	0.09	7	-0.07
HD 23127	5769	4.01	1.30	7.77	0.09	27	0.06	10	0.34
HD 27442	4884	3.39	1.31	7.73	0.12	22	0.07	6	0.30
HD 28305	4963	2.87	1.68	7.60	0.13	25	0.07	7	0.17
HD 33283	5972	4.02	1.42	7.74	0.08	27	0.06	12	0.31
HD 38529	5558	3.62	1.32	7.76	0.09	26	0.06	10	0.33
HD 47536	4588	2.17	2.03	6.82	0.10	23	0.04	4	-0.61
HD 59686	4740	2.66	1.58	7.57	0.14	22	0.04	5	0.14
NGC 2423 3	4680	2.55	1.67	7.43	0.13	25	0.05	8	0.00
HD 73526	5571	3.89	1.15	7.64	0.07	26	0.05	10	0.21
HD 88133	5473	3.94	1.09	7.81	0.07	24	0.04	8	0.38
NGC 4349 127	4519	1.92	2.08	7.22	0.12	17	0.08	6	-0.21
HD 117176	5535	3.98	1.12	7.39	0.07	27	0.06	12	-0.04
HD 122430	4367	1.71	1.71	7.27	0.14	17	0.08	7	-0.16
HD 154857	5548	3.82	1.34	7.13	0.07	26	0.05	12	-0.30
HD 156846	5950	3.84	1.62	7.50	0.09	24	0.07	11	0.07
HD 159868	5572	3.90	1.21	7.36	0.06	26	0.06	12	-0.07
HD 171028	5681	3.88	1.71	6.87	0.06	24	0.06	10	-0.56
HD 175541	5022	3.19	1.15	7.27	0.05	24	0.06	11	-0.16
HD 177830	5054	3.83	1.30	7.84	0.11	20	0.05	6	0.41
HD 188310	4783	2.66	1.57	7.30	0.12	23	0.07	7	-0.13
HD 190647	5533	3.92	1.12	7.63	0.06	25	0.04	10	0.20
HD 192699	5086	3.18	1.17	7.20	0.07	25	0.06	11	-0.23
HD 199665	4948	2.69	1.31	7.34	0.09	24	0.09	8	-0.09
HD 210702	5028	3.40	1.24	7.52	0.09	26	0.05	7	0.09

Table 2—Continued

Star	T_{eff} (K)	$\log g$	ξ (km s $^{-1}$)	A(Fe)	σ (Fe I)	N (Fe I)	σ (Fe II)	N (Fe II)	[Fe/H]
HD 219449	4812	2.78	1.72	7.48	0.11	23	0.06	5	0.05
HD 224693	5902	3.97	1.36	7.66	0.10	27	0.06	12	0.23
<i>Control Sample</i>									
HD 2151	5866	4.00	1.51	7.32	0.08	24	0.06	10	-0.11
HD 18907	5212	3.92	1.20	6.87	0.06	24	0.04	10	-0.56
HD 33473	5608	3.60	1.36	7.21	0.08	26	0.05	12	-0.22
HD 114613	5717	3.92	1.30	7.61	0.07	26	0.07	12	0.18
HD 121384	5249	3.67	1.24	6.93	0.07	27	0.05	12	-0.50
HD 140785	5723	3.98	1.18	7.40	0.05	23	0.04	12	-0.03
HD 168060	5577	3.93	1.14	7.72	0.09	27	0.04	10	0.29
HD 168723	4944	3.12	1.25	7.26	0.08	26	0.04	8	-0.17
HD 188641	5816	3.98	1.37	7.31	0.06	24	0.05	12	-0.12
HD 196378	5996	3.92	1.78	6.99	0.04	20	0.05	10	-0.44
HD 205420	6255	3.89	1.99	7.43	0.06	20	0.07	12	0.00
HD 208801	5061	3.80	1.08	7.59	0.08	21	0.06	8	0.16
HD 212330	5670	3.91	1.33	7.41	0.07	27	0.05	12	-0.02
HD 219077	5321	3.80	1.13	7.27	0.08	27	0.04	11	-0.16
HD 221420	5899	4.04	1.48	7.77	0.05	20	0.06	12	0.34

Table 3. Evolutionary Parameters.

Star	π (mas)	σ_π (mas)	A_V (mag)	$\log(L/L_\odot)$	$\sigma_{\log(L/L_\odot)}$	R (R_\odot)	σ_R (R_\odot)	M (M_\odot)	$\sigma(M)$ (M_\odot)	$\log g_{Hip}$	$\sigma(\log g_{Hip})$	Age (Gyr)	$\sigma(\text{Age})$ (Gyr)
<i>Planet Hosting Stars</i>													
HD 5319	8.74	0.86	0.10	0.952	0.105	3.97	0.43	1.40	0.14	3.35	0.10	3.30	1.11
HD 10697	30.70	0.43	0.00	0.446	0.061	1.69	0.06	1.11	0.03	3.99	0.03	6.75	0.71
HD 11977	14.91	0.16	0.16	1.849	0.061	11.04	0.43	2.27	0.29	2.68	0.07	0.83	0.27
HD 11964	30.44	0.60	0.10	0.466	0.062	1.97	0.08	1.12	0.03	3.86	0.03	7.02	0.67
HD 16400	10.81	0.45	0.08	1.741	0.074	10.50	0.45	1.43	0.31	2.52	0.11	2.66	1.46
HD 23127	10.13	0.67	0.21	0.559	0.083	1.81	0.13	1.21	0.05	3.97	0.06	4.66	0.81
HD 27442	54.83	0.15	0.03	0.782	0.060	3.50	0.15	1.35	0.08	3.44	0.06	3.79	0.85
HD 28305	22.24	0.25	0.06	1.924	0.061	12.69	0.46	2.75	0.11	2.64	0.03	0.51	0.09
HD 33283	10.62	0.62	0.21	0.718	0.079	2.08	0.13	1.39	0.06	3.91	0.05	2.93	0.41
HD 38529	25.46	0.40	0.03	0.754	0.062	2.49	0.10	1.37	0.02	3.74	0.03	3.35	0.14
HD 47536	8.11	0.23	0.11	2.204	0.065	19.84	1.09	1.15	0.25	1.87	0.12	4.38	2.58
HD 59686	10.32	0.28	0.00	1.840	0.064	11.80	0.60	2.27	0.30	2.62	0.09	0.92	0.33
NGC 2423 3	1.31	0.03	0.39	1.966	0.099	14.11	0.88	2.16	0.38	2.44	0.11	0.96	0.40
HD 73526	9.93	1.01	0.06	0.369	0.107	1.53	0.16	1.05	0.05	4.05	0.08	8.50	1.34
HD 88133	12.28	0.88	0.04	0.576	0.087	2.04	0.15	1.20	0.06	3.87	0.04	5.22	0.90
NGC 4349 127	0.45	0.01	1.08	2.889	0.205	44.72	2.46	3.77	0.36	1.68	0.07	0.20	0.05
HD 117176	55.60	0.24	0.01	0.467	0.060	1.83	0.06	1.08	0.03	3.91	0.03	7.83	0.63
HD 122430	7.42	0.33	0.28	2.325	0.071	24.49	1.78	1.53	0.31	1.81	0.12	2.18	1.11
HD 154857	15.57	0.71	0.12	0.712	0.075	2.40	0.14	1.21	0.06	3.73	0.04	4.43	0.63
HD 156846	21.00	0.51	0.14	0.724	0.067	2.11	0.08	1.36	0.06	3.89	0.04	3.17	0.47
HD 159868	17.04	0.76	0.08	0.612	0.072	2.11	0.11	1.19	0.04	3.83	0.04	5.31	0.76
HD 171028	11.10	1.85	0.31	0.651	0.165	2.06	0.28	1.03	0.09	3.79	0.08	7.25	2.44
HD 175541	7.87	0.95	0.32	1.126	0.127	4.55	0.57	1.37	0.16	3.23	0.11	3.11	1.16
HD 177830	16.94	0.63	0.08	0.698	0.068	2.85	0.16	1.41	0.03	3.65	0.04	3.14	0.20
HD 188310	17.77	0.29	0.09	1.690	0.062	10.23	0.39	1.16	0.28	2.45	0.11	4.63	2.88
HD 190647	17.46	0.81	0.15	0.402	0.076	1.68	0.09	1.07	0.03	3.99	0.04	7.96	0.81

Table 3—Continued

Star	π (mas)	σ_π (mas)	A_V (mag)	$\log(L/L_\odot)$	$\sigma_{\log(L/L_\odot)}$	R (R_\odot)	σ_R (R_\odot)	M (M_\odot)	$\sigma(M)$ (M_\odot)	$\log g_{Hip}$	$\sigma(\log g_{Hip})$	Age (Gyr)	$\sigma(\text{Age})$ (Gyr)
HD 192699	15.24	0.57	0.04	1.064	0.068	4.41	0.23	1.38	0.13	3.26	0.07	2.90	0.88
HD 199665	13.28	0.31	0.05	1.578	0.063	8.29	0.31	2.01	0.10	2.87	0.04	1.10	0.16
HD 210702	18.20	0.39	0.05	1.125	0.063	4.83	0.24	1.72	0.13	3.27	0.06	1.68	0.36
HD 219449	21.77	0.29	0.10	1.702	0.061	10.16	0.45	1.74	0.35	2.63	0.11	1.69	0.81
HD 224693	10.16	0.91	0.10	0.646	0.101	1.90	0.17	1.30	0.08	3.96	0.06	3.54	0.68
<i>Control Sample</i>													
HD 2151	134.07	0.11	0.02	0.547	0.060	1.77	0.05	1.13	0.04	3.96	0.03	6.13	0.88
HD 18907	31.06	0.36	0.09	0.678	0.061	2.66	0.10	1.02	0.06	3.56	0.05	7.62	1.51
HD 33473	18.69	0.49	0.09	0.731	0.064	2.41	0.10	1.25	0.04	3.74	0.03	4.06	0.37
HD 114613	48.38	0.29	0.04	0.631	0.060	2.06	0.07	1.26	0.03	3.87	0.03	4.22	0.27
HD 121384	25.84	0.48	0.07	0.776	0.062	2.95	0.12	1.15	0.08	3.53	0.06	4.90	1.21
HD 140785	17.54	0.56	0.12	0.536	0.070	1.85	0.08	1.13	0.03	3.92	0.04	6.33	0.75
HD 168060	21.07	0.65	0.06	0.375	0.066	1.61	0.07	1.07	0.02	4.02	0.04	7.92	0.56
HD 168723	53.93	0.18	0.06	1.279	0.060	6.00	0.24	1.41	0.16	3.00	0.07	2.81	1.01
HD 188641	16.14	0.82	0.16	0.637	0.078	1.98	0.12	1.18	0.04	3.88	0.04	5.30	0.75
HD 196378	40.55	0.27	0.05	0.684	0.060	2.01	0.06	1.10	0.03	3.84	0.03	5.62	0.43
HD 205420	15.81	0.39	0.04	0.939	0.064	2.47	0.09	1.53	0.05	3.80	0.03	2.09	0.22
HD 208801	27.11	0.41	0.05	0.653	0.061	2.73	0.13	1.34	0.05	3.66	0.04	3.61	0.41
HD 212330	48.63	0.34	0.04	0.449	0.060	1.71	0.06	1.07	0.03	3.97	0.03	7.78	0.80
HD 219077	34.07	0.37	0.05	0.470	0.061	1.99	0.08	1.06	0.04	3.83	0.03	8.27	0.70
HD 221420	31.81	0.27	0.07	0.605	0.060	1.88	0.05	1.31	0.04	3.97	0.03	3.43	0.47

Table 4. Giant Stars Comparison with the Literature

Star	[Fe/H]	Reference
<i>Results from This Work</i>		
HD 5319	0.14	This study
	0.15	Valenti & Fischer (2005)
HD 11977	-0.16	This study
	-0.21	da Silva et al. (2006)
	-0.09	Sousa et al. (2006)
HD 16400	-0.07	This study
	-0.06	Takeda et al. (2008)
HD 27442	0.30	This study
	0.42	Santos et al. (2003)
	0.42	Valenti & Fischer (2005)
HD 28305	0.17	This study
	0.11	Mishenina et al. (2006)
	0.20	Schuler et al. (2006)
	0.17	Sato et al. (2007)
	0.05	Hekker & Meléndez (2007)
	0.13	Takeda et al. (2008)
HD 47536	-0.61	This study
	-0.54	Santos et al. (2004)
	-0.54	Sadakane et al. (2005)
	-0.68	da Silva et al. (2006)
HD 59686	0.14	This study
	0.28	Santos et al. (2005)
	0.11	Sadakane et al. (2005)
	0.02	Mishenina et al. (2006)
	0.15	Hekker & Meléndez (2007)
NGC 2423 3	0.00	This study
	0.00	Santos et al. (2009)
NGC 4349 127	-0.21	This study
	-0.14	Santos et al. (2009)
HD 122430	-0.16	This study

Table 4—Continued

Star	[Fe/H]	Reference
HD 175541	-0.05	da Silva et al. (2006)
	-0.16	This study
	-0.07	Valenti & Fischer (2005)
	-0.07	Johnson et al. (2007)
HD 188310	-0.13	This study
	-0.21	Sato et al. (2008a)
	-0.18	Takeda et al. (2008)
HD 192699	-0.23	This study
	-0.15	Johnson et al. (2007)
HD 199665	-0.09	This study
	-0.05	Sato et al. (2008a)
	-0.05	Takeda et al. (2008)
HD 210702	0.09	This study
	0.06	Luck & Heiter (2007)
	+0.12	Johnson et al. (2007)
HD 219449	0.05	This study
	0.05	Santos et al. (2005)
	0.09	Sadakane et al. (2005)
	0.05	Luck & Heiter (2007)
	-0.03	Hekker & Meléndez (2007)
<i>Literature Results</i>		
HD 13189	-0.58	Schuler et al. (2005)
	-0.39	Sousa et al. (2006)
	-0.49	Average
HD 17092	0.22	Niedzielski et al. (2007)
HD 32518	-0.15	Döllinger et al. (2009a)
HD 62509	0.05	Sadakane et al. (2005)
	0.19	Hatzes et al. (2006)
	0.17	Luck & Heiter (2007)
	0.07	Hekker & Meléndez (2007)
	0.12	Average

Table 4—Continued

Star	[Fe/H]	Reference
4 UMa	-0.16	Luck & Heiter (2007)
	-0.25	Döllinger et al. (2007)
	-0.21	Average
HD 81688	-0.36	Sato et al. (2008a)
BD+20 2457	-1.00	Niedzielski et al. (2009b)
gamma 1 Leo	-0.49	McWilliam (1990)
	-0.51	Han et al. (2010)
	-0.50	Average
HD 102272	-0.26	Niedzielski et al. (2009a)
HD 104985	-0.35	Sato et al. (2003)
	-0.28	Santos et al. (2005)
	-0.15	Takeda et al. (2005)
	-0.26	Luck & Heiter (2007)
	-0.26	Average
HD 110014	0.19	da Silva et al. (2006)
11 UMi	0.04	Döllinger et al. (2009a)
HIP 75458	0.03	McWilliam (1990)
	0.09	Santos et al. (2003)
	0.13	Santos et al. (2004)
	0.12	Sadakane et al. (2005)
	0.11	Hekker & Meléndez (2007)
	0.10	Average
HD 139357	-0.13	Döllinger et al. (2009b)
42 Dra	-0.46	Döllinger et al. (2009b)
HD 173416	-0.22	Liu et al. (2009)
HD 180902	0.04	Johnson et al. (2010)
HD 181342	0.26	Johnson et al. (2010)
HD 240210	-0.18	Niedzielski et al. (2009b)
14 And	-0.24	Sato et al. (2008b)
HD 222404	+0.18	Fuhrmann (2004)
	+0.16	Santos et al. (2004)

Table 4—Continued

Star	[Fe/H]	Reference
	+0.17	Average

Capítulo 4

Abundâncias de Lítio em Estrelas com Planetas

Este capítulo apresenta o artigo (sumetido ao *Astrophysical Journal*) no qual são determinadas as velocidades de rotação projetadas e as abundâncias de lítio para a subamostra de 262 estrelas de seqüência principal (a tabela 1 é reproduzida por completo no apêndice C). As subgigantes e gigantes não foram incluídas porque as suas abundâncias superficiais de lítio podem ser alteradas pelos processos físicos característicos destes estágios evolutivos. Por exemplo, o progressivo aprofundamento das zonas convectivas das estrelas durante a passagem nos ramos das subgigantes e gigantes vermelhas faz com que o lítio seja transportado para regiões mais profundas e quentes, onde ele é destruído. Este processo, chamado de diluição, causaria uma diminuição da abundância superficial de lítio.

A amostra analisada contém 117 estrelas com planetas, o que faz deste trabalho o mais completo até o presente momento. Particularmente, o intervalo de temperaturas efetivas $T_{\text{ef}} \lesssim 5600$ K possui 41 objetos, o que faz deste o estudo com o maior número de estrelas com planetas neste regime. As velocidades de rotação projetadas e as abundâncias de lítio foram derivadas através do ajuste de perfis sintéticos aos espectros observados na região que contém o duploto do Li I (~ 6708 Å). Novamente, um método automático foi utilizado e correções manuais foram necessárias em apenas 10% dos casos. Os resultados nos permitiram investigar se as estrelas com planetas e temperaturas efetivas próximas da solar realmente possuem menores velocidades de rotação projetadas e abundâncias de lítio.

Lithium Abundances in a Sample of Planet Hosting Dwarfs

L. Ghezzi¹, K. Cunha^{2,1}, V. V. Smith², & R. de la Reza¹

ABSTRACT

This work presents a homogeneous determination of lithium abundances in a large sample of giant-planet hosting stars ($N=117$), and a control sample of disk stars without detected planets ($N=145$). The lithium abundances, as well as projected rotational velocities, were derived using a detailed profile fitting of the Li I doublet at $\lambda 6708 \text{ \AA}$. The planet hosting and comparison stars were chosen to have significant overlap in their respective physical properties, including effective temperatures, luminosities, masses, metallicities, ages, and chromospheric activity levels. The combination of uniform data and homogeneous analysis with well selected samples, makes this study well-suited to probe for possible differences in the lithium abundances found in planet hosting stars. An overall broad comparison between the two samples reveals no obvious differences between stars with and without planets. Closer examination of the behavior of the Li abundances over a narrow range of effective temperature ($5700 \text{ K} \leq T_{\text{eff}} \leq 5850 \text{ K}$), however, reveals subtle differences between the two stellar samples; this temperature range is particularly sensitive to various physical processes that can deplete lithium. Planet hosting stars have lower Li abundances (by ~ 0.26 dex on average) than the comparison stars. This difference is mirrored in the chromospheric activity levels, with the planet hosting stars also exhibiting somewhat lower levels of activity relative to the comparison stars without planets. This is interpreted as a manifestation of slightly lower rotational velocities among the planet hosting stars. Different rotational velocity histories would lead to different behaviors of the Li abundances over time, particularly within the mass and age range defined by this interval in effective temperature.

Subject headings: line: profiles – planetary systems: formation – stars: abundances – stars: atmospheres

¹Observatório Nacional, Rua General José Cristino, 77, 20921-400, São Cristóvão, Rio de Janeiro, RJ, Brazil; luan@on.br

²National Optical Astronomy Observatory, 950 North Cherry Avenue, Tucson, AZ 85719, USA

1. Introduction

The physical processes that both create and destroy lithium lead to a complex behavior of its chemical abundance in a variety of astrophysical sites. The abundance of Li in stellar photospheres, in particular, holds important clues to the understanding of various processes, from Big Bang Nucleosynthesis to the formation and evolution of planetary systems (see, e.g., Meléndez et al. 2009; Santos et al. 2010). The determination of lithium abundances in FGK dwarfs is challenging as it requires high-resolution and high signal-to-noise (S/N) stellar spectra. In addition, the interpretation of the results is not straightforward as lithium abundances are known to depend on several variables, such as the effective temperature (T_{eff}), metallicity ([Fe/H]¹), stellar mass, age, rotation and activity level.

This complexity in the interpretation of lithium abundance results has led to conflicting conclusions concerning possible differences between lithium abundances in planet hosting stars when compared with stars not known to host giant planets. In this introduction, we briefly discuss the results in these previous studies. One of the first papers to focus on the element lithium in stars with planets was Gonzalez & Laws (2000). This study compared Li abundances in a sample of 8 stars with planets to a sample of field stars taken from the literature. After correcting for systematic differences in T_{eff} , [Fe/H] and the Ca II H+K emission index, $\log R'_{HK}$ (which is a measurement of the chromospheric emission), from the different studies, the conclusion was that stars with planets have lower Li abundances than non-planet hosts. This initial result, however, was not confirmed by Ryan (2000), who compared Li abundances (from the literature) of planet hosting stars with those of open cluster and field stars carefully selected to span similar intervals in temperature, age and chemical composition and found no differences in A(Li)².

As more planet hosting stars were discovered, the work by Israelian et al. (2004) obtained lithium abundances for a larger sample of 79 stars hosting planets and 38 stars without planets. This study did not find significant differences between the Li abundances in the two samples, but noted that the control sample had too few stars with detectable Li to be used as a comparison. The authors then compared their Li abundances for their sample of planet hosting stars with a sample of 157 field stars from Chen et al. (2001) and concluded that planet hosting stars with effective temperatures in the range between 5600 K and 5850 K exhibit an excess of Li depletion. Two possible hypotheses were proposed for explaining this result: increased mixing due to rotational breaking caused by the interaction (during pre-

¹Here, we adopt the usual notation $[Fe/H] = \log(N_{Fe}/N_H)_\star - \log(N_{Fe}/N_H)_\odot$

²A(Li)= log[N(Li)/N(H)]+12

main-sequence evolution) of the host stars with their proto-planetary disks; effective mixing generated by tidal forces resulting from planet migration.

The findings of Israelian et al. (2004) were further confirmed by Takeda & Kawanomoto (2005) with Li abundances derived for a sample of 160 FGK dwarfs and subgiants in the Galactic disk, among which there were only 27 planet hosting stars. The lithium abundance distributions for planet-hosting and non planet-hosting stars in that study were found to be very similar; the size of the planet hosting stellar sample in Takeda & Kawanomoto (2005), however, was not large enough in order to make meaningful statistical comparisons. If instead of using their own derived Li abundances for the planet-hosting stars, the authors adopted the Li results from Israelian et al. (2004), for planet hosting stars only, a similar tendency of finding an excess of Li depletion in the planet hosting star sample was obtained, although this was only observed for stars within the narrow range in effective temperature between $5800 \text{ K} \lesssim T_{\text{eff}} \lesssim 5900 \text{ K}$. The study by Chen & Zhao (2006) analyzed smaller samples but also found a higher frequency of Li poor stars within their sample of 16 planet hosting stars in comparison with 20 control stars, but in this case for stars with effective temperatures ranging between 5600 K and 5900 K.

Contrary results to these findings were obtained by Luck & Heiter (2006), continuing the controversy about Li in planet-hosting stars. This study derived Li abundances homogeneously for a sample of 216 nearby dwarf stars, 55 of which host close giant planets. They found no differences between lithium abundances of stars with and without planets and argued that the low-Li tendency observed by Israelian et al. (2004) was caused by a systematic difference between the temperature scales adopted in the latter work and the study of Chen et al. (2001) (from which the Li abundances for the control sample were drawn).

The topic was revisited by Gonzalez (2008) who combined samples of stars from the literature (gathering a total of 37 stars with planets and 147 stars without planets) and corrected for systematic offsets between the T_{eff} , $\log g$, [Fe/H] and A(Li) from the different published analyses. Gonzalez (2008) found that planet hosting stars with $T_{\text{eff}} \sim 5800 \text{ K}$ tend to have lower Li abundances compared to stars not hosting planets. It was suggested in that study that stars with planets also exhibit larger Li abundances near $T_{\text{eff}} \simeq 6100 \text{ K}$, with the transition occurring at $T_{\text{eff}} \simeq 5950 \text{ K}$, and that $v \sin i$ and $\log R'_{HK}$ seem to correlate with the lithium abundance.

More recently, Meléndez et al. (2009), on the other hand, presented results for 4 and 6 stars with and without planets, respectively, with effective temperatures near $T_{\text{eff}} \sim 5800 \text{ K}$ (the same effective temperature regime for which Gonzalez 2008 finds differences). Based on this much smaller but homogeneous set of results, Meléndez et al. (2009) argue that stars with planets do not show anomalously low Li abundances. A much larger sample observed

with HARPS (GTO; Sousa et al. 2008) has been analyzed by Israelian et al. (2009). Lithium abundances were obtained for 451 stars, among which there are 70 stars which host planets. This sample was extended to include 16 stars hosting planets and 13 stars without planets (with $5600 \text{ K} \lesssim T_{\text{eff}} \lesssim 5900 \text{ K}$). The results obtained from this sample confirmed the low-Li tendency for planet hosting stars with effective temperatures in the range between 5600 - 5900 K and $T_{\text{eff}} = 5777 \pm 80 \text{ K}$ (solar analogues). The question about differences in other parameters being responsible for the effect was addressed by Sousa et al. (2010), who showed that differences in mass and age could not be responsible for this enhanced depletion and proposed that the low lithium abundance is directly related to the presence of planets. Finally, Gonzalez et al. (2010) performed a homogeneous analysis and derived Li abundances and $v \sin i$ for a large sample of stars with and without planets (with 90 and 60 stars, respectively). They basically confirm the results of Gonzalez (2008), although finding a lower temperature ($T_{\text{eff}}=5850 \text{ K}$) for the transition region between low and high Li abundances in stars with planets (relative to comparison stars).

In Ghezzi et al. (2010a, hereafter Paper I), we performed a homogeneous determination of stellar parameters and metallicities for a large sample of dwarf stars hosting giant planets close in, as well as a sample of control disk stars not known to host large planets. The spectra analyzed in that study had high S/N and covered the spectral region containing the Li I feature at 6707.8 \AA . The present study presents the homogeneous determination of lithium abundances for all the stars in Paper I based on a detailed profile fitting of the Li I resonance doublet at $\lambda 6707.8 \text{ \AA}$. This paper is organized as follows: in Section 2, the sample and observational data are briefly described. The profile fitting techniques and resulting lithium abundances and projected rotational velocities are presented in Section 3. Section 4 contains the discussion and interpretation of the results. Finally, concluding remarks are presented in Section 5.

2. Sample and Observational Data

The sample of stars analyzed in this study is comprised of 117 stars hosting large planets and 145 comparison disk stars. The target stars were previously analyzed in Paper I, where stellar parameters and iron abundances were derived. The sample of main-sequence stars with planets were selected (until August 2008) from the Extrasolar Planet Encyclopaedia³ given the constraints on object observability from La Silla Observatory. In addition, a control sample of main-sequence stars without detected planets so far was compiled from the subset

³Available at <http://exoplanet.eu>

of 850 nearby FGK stars in Fischer & Valenti (2005), which has been monitored in planet search programmes. The selection criteria were such that the stellar properties of the control stars matched those of stars with planets (which makes this comparison sample adequate for the lithium study presented here).

High-resolution ($R \sim 48,000$) and high signal-to-noise ($S/N \sim 200$) spectra were obtained with the Fiber-fed Extended Range Optical Spectrograph (FEROS) attached to the MPG/ESO-2.20m telescope (La Silla, Chile) during 6 observing runs between April 2007 and August 2008⁴. The data reduction was done with the FEROS Data Reduction System (DRS)⁵ and followed standard procedures for echelle spectra. A complete description of the sample selection, observations and data reduction can be found in Paper I and we refer to this previous study for details.

3. Analysis

The determination of Li abundances from synthetic spectra requires a line list for the spectral region around the Li I feature at 6707.8 Å. The line list adopted here was taken from Ghezzi et al. (2009), but removing the ^6Li components (not measurable at the resolution of FEROS spectra). The model atmospheres adopted in the calculations were interpolated from the ODFNEW grid of ATLAS9 models⁶ (Castelli & Kurucz 2004). Stellar parameters and metallicities ([Fe/H]) for the target stars were taken from Table 3 of Paper I. Briefly, the atmospheric parameters (T_{eff} , $\log g$ and ξ) were derived in Local Thermodynamic Equilibrium (LTE) following standard spectroscopic methods (excitation and ionization equilibria based on Fe I and Fe II lines; see Paper I for all the details on these determinations). The 2002 version of the code MOOG⁷ (Sneden 1973) was used to compute synthetic spectra in the Li region. We note that limb darkening was not considered, as the impact on the derived lithium abundances is negligible.

In this study, we adopted the following procedure in order to determine Li abundances and projected rotational velocities for the target stars. First, it was assumed that the broadening of spectral lines was represented by a single Gaussian smoothing function which combined the effects of stellar rotation, macroturbulence and instrumental profile. A grid

⁴Under the agreement ESO-Observatório Nacional/MCT

⁵Available at <http://www.eso.org/sci/facilities/lasilla/instruments/feros/tools/DRS/index.html>

⁶Available at <http://kurucz.harvard.edu/>

⁷Available at <http://verdi.as.utexas.edu/moog.html>.

of synthetic spectra was then computed for combinations of the Gaussian Full-Width at Half-Maximum ($\text{FWHM}_{\text{Gauss}}$) and lithium abundance. The best fit between the synthetic and observed profiles was obtained through a reduced χ^2 -minimization in the spectral interval between 6707.3 - 6708.4 Å (including mainly, besides the Li I doublet, a Fe+CN and a Ca+CN feature). Small adjustments in the continuum level were allowed in order to compensate for possible errors in the continuum normalization. Also, wavelength shifts of the observed spectra were needed in order to account for radial velocity shifts. The abundances of Fe, CN, Si, Ca and V were kept as free parameters in this first step in order to properly match their contributions and improve the overall quality of the fits. Such adjustments in the elemental abundances, however, do not affect the derivation of the Li abundances, as their contributions to the global feature are clearly distinguishable from the Li I line.

This first step provided the best-fit lithium abundance, as well as values of r (continuum displacement), w (wavelength shift) and $\text{FWHM}_{\text{Gauss}}$. Such quantities were then kept fixed but in order to estimate $v \sin i$, the broadening was then separated into the contributions of macroturbulence and instrumental profile (combined as a single gaussian) and the stellar rotational velocity profile. A new grid of synthetic spectra was computed for combinations of values of $\text{FWHM}_{\text{Macro+Inst}}$ and $v \sin i$. The best fit between synthetic and observed profiles was again obtained through a reduced χ^2 -minimization in the spectral interval between 6707.3 - 6708.4 Å.

The determination of Li abundances and $v \sin i$ described above was done in an automated way with the aid of BASH and FORTRAN codes: lithium abundances for the entire sample of 262 stars studied here could be derived in ~ 2 days. All automatically obtained fits were inspected visually and manual corrections were needed for approximately 10% of the cases. The stars with non-optimum fits generally had spectra with low S/N values, or extremely weak or non-measurable Li lines for which only upper limits to the Li abundances could be derived. Figure 1 shows the best fit between observed and synthetic spectrum obtained for target star HD 52265 as an example. Table 1 lists the final values of $\text{FWHM}_{\text{Macro+Inst}}$ (column 2), $v \sin i$ (column 3), and $A(\text{Li})$ (column 4) for all studied stars.

The Li abundance in the Sun was also derived using a solar spectrum observed with the FEROS spectrograph on August 20, 2008. The result obtained for the Sun is $A(\text{Li}) = 0.99 \pm 0.16$, which is in agreement with recent solar abundance determinations which are based on 3D hydrodynamical models and take non-LTE effects into account ($A(\text{Li}) = 1.05 \pm 0.10$ from Asplund et al. 2009; $A(\text{Li}) = 1.03 \pm 0.03$ from Caffau et al. 2010). The projected rotational velocity obtained was $v \sin i = 1.20 \pm 4.00 \text{ km s}^{-1}$; this is lower than the canonical $v \sin i$ for the Sun of $1.7 - 1.8 \text{ km s}^{-1}$, but the difference between the values is well within the formal uncertainties in our determination.

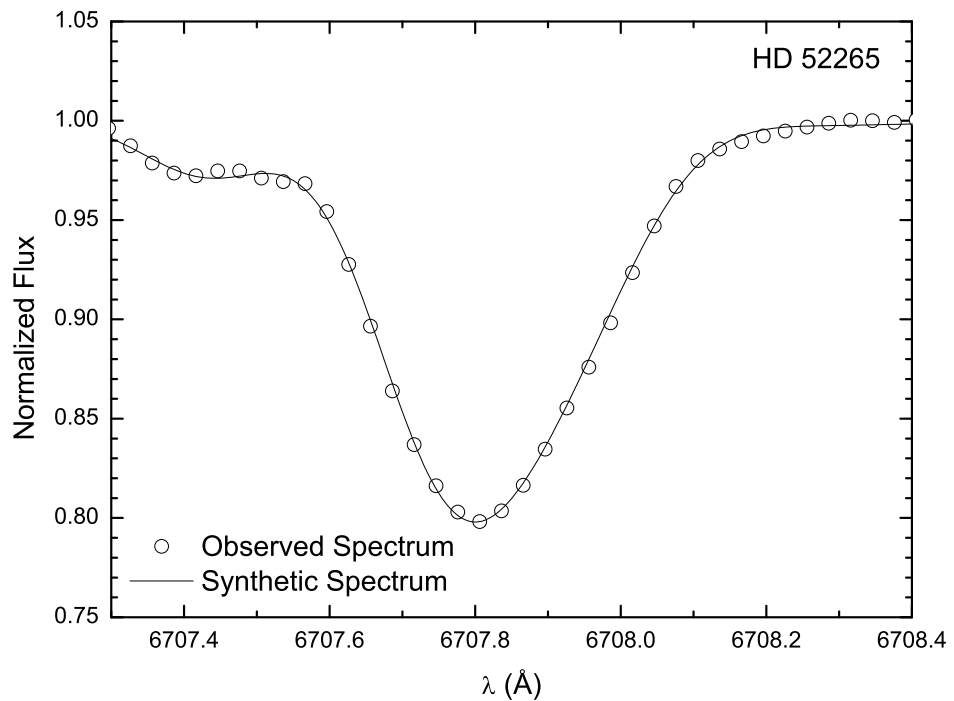


Fig. 1.— The best fit obtained between observed (open circles) and synthetic (solid line) spectra for target star HD 52265. The best-fit Li abundance displayed corresponds to $A(\text{Li}) = 2.65$. The derived $v \sin i = 4.00 \text{ km s}^{-1}$.

We compared the results obtained here with those from Ghezzi et al. (2009), which were based on much higher quality bHROS spectra ($R \sim 150,000$ and $S/N \gtrsim 700$). For the six stars in common (namely HD 17051, HD 36435, HD 74156, HD 82943, HD 147513 and HD 217107), we find the average differences (in the sense “FEROS - bHROS” spectra) to be: $\langle A(Li) \rangle = 0.01 \pm 0.09$ and $\langle v \sin i \rangle = 0.64 \pm 2.04 \text{ km s}^{-1}$. The agreement between these two sets of results is very good. We also compared our values of $v \sin i$ with the projected rotational velocities obtained in Valenti & Fischer (2005); such a comparison is shown in Figure 2. The mean difference between these two sets of $v \sin i$ ’s (in the sense “This Study - Valenti & Fischer”) is $-0.61 \pm 2.00 \text{ km s}^{-1}$ ($N=223$). One of the differences in the methods adopted to obtain $v \sin i$ ’s in the two studies is that Valenti & Fischer (2005) fix the macroturbulence from a calibration prior to the determination of the projected rotational velocities, while here the macroturbulent velocity is kept as a free parameter. We note that the comparison between the $v \sin i$ results from Valenti & Fischer (2005) with those in Takeda et al. (2010) is of similar quality as what is found here (see figure 4 in Takeda et al. 2010).

3.1. Uncertainties

The formal uncertainties in the derived best-fit lithium abundances can be calculated by varying $A(Li)$ around its best value and computing, for each lithium abundance tested, the quantity $\Delta\chi_r^2 = \chi_r^2 - \chi_{r,\min}^2$. The difference between $A(Li)$ and $A(Li)_{best}$ that gives $\Delta\chi_r^2 = 1$ is taken as the 1σ uncertainty. The derived lithium abundances and their formal uncertainties are presented in column 4 of Table 1. The lithium abundances, however, are also sensitive to uncertainties in the effective temperature parameter: $\delta T_{eff} = \pm 100 \text{ K}$ introduces an uncertainty of $\sim \pm 0.1 \text{ dex}$ in the derived lithium abundances for most sample stars; for the cooler stars ($T_{eff} \sim 5000 \text{ K}$) the sensitivity to T_{eff} is slightly larger ($\sim 0.15 \text{ dex}$). The sensitivity of $A(Li)$ to variations in the adopted $\log g$ ’s and microturbulent velocities is only marginal: a change in $\log g$ of $\pm 0.5 \text{ dex}$ changes the lithium abundance by 0.01-0.02 dex, with a slightly larger sensitivity of ~ 0.05 for the coolest stars in our sample. A change in the microturbulent velocity by $\pm 0.5 \text{ km s}^{-1}$ has virtually no effect on the derived $A(Li)$. The total uncertainties in the derived lithium abundances are then calculated by the addition of all these uncertainties in quadrature, assuming the errors are independent. The total estimated uncertainties in the derived Li abundances in this study are in column 5 of Table 1.

Non-LTE effects have not been considered in this Li abundance analysis and these will contribute to the total error budget. Takeda & Kawanomoto (2005) calculated non-LTE Li abundances for their sample of stars with effective temperatures ranging between 5000

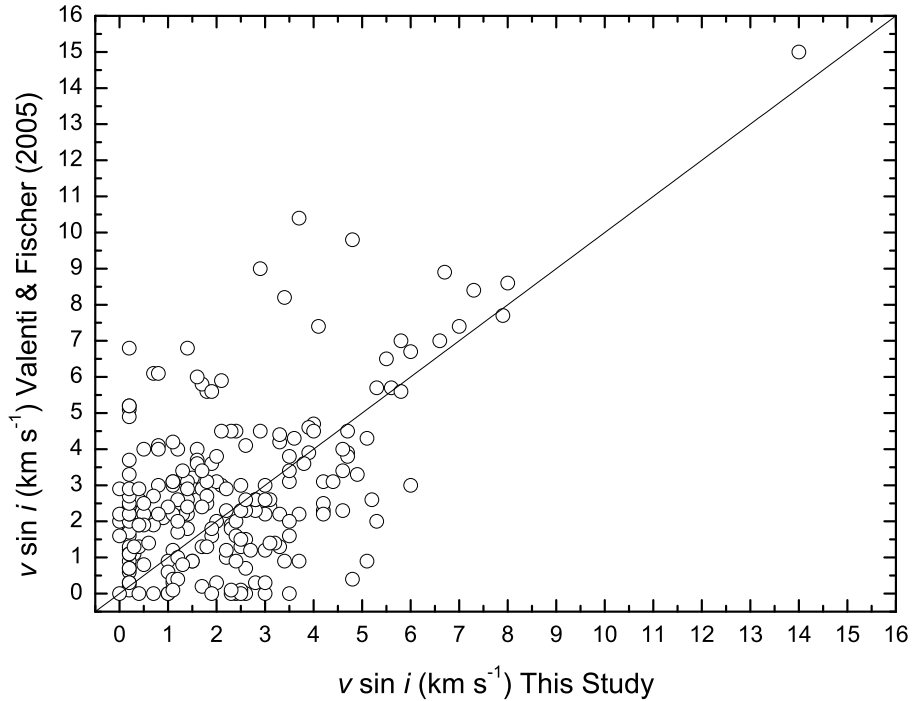


Fig. 2.— Comparison between the $v \sin i$ values derived in this study with the results from Valenti & Fischer (2005). The scatter is large but generally compatible with the uncertainties expected from $v \sin i$ determinations which are not based on a Fourier analysis; the solid line represents perfect agreement. One difference between the methods adopted in the determinations is that Valenti & Fischer (2005) fix the value of macroturbulence from a calibration, while macroturbulence is kept as a free parameter in this analysis.

K and 7000 K, and metallicities $-1.0 < [Fe/H] < +0.40$ dex. The non-LTE corrections in that study were found to range between $-0.1 < \Delta < +0.1$ dex. Stars in restricted ranges in effective temperatures and metallicities, however, have similar non-LTE corrections. The stars with detected Li I lines in this study have effective temperatures roughly between 5700 K and 6200 K (as will be shown in Figure 8). For these hotter dwarfs, with $A(\text{Li}) < 3.00$, the non-LTE corrections are found to be small in the recent study of Lind et al. (2009).

When considering the uncertainties in the derived projected rotational velocities, we note that the velocity resolution in FEROS is approximately 6.25 km s^{-1} , while only ~ 10 of our targets have projected rotational velocities higher than this value (Table 1; column 3). The instrumental profile of FEROS spectrograph, however, is very well defined and constant and estimates of $v \sin i$ values can be determined even below the resolution limit. Formal errors in the derived $v \sin i$ can be obtained in a similar manner as described above for $A(\text{Li})$. Such uncertainties in the $v \sin i$ obtained from profile fitting in this study are of the order of many of the $v \sin i$ values listed in Table 1 (column 3): the average of the 1σ uncertainties for our sample ($N=249$; 13 stars with very weak Li lines were not included) is $\langle \delta_{v \sin i} \rangle = 3.34 \pm 1.54 \text{ km s}^{-1}$. We take this value as an estimate of the $v \sin i$ detectability limit in this study. We note, however, that it is possible to distinguish between different fits even below this limit.

4. Discussion

4.1. Comparisons within the Samples: Metallicities, Masses, Ages and Activity

As mentioned previously, interpreting lithium abundances can be a complex process because these abundances depend on a number of parameters, such as effective temperature, metallicity, mass, age, rotation, as well as the stellar activity level. The behavior of Li with T_{eff} and $v \sin i$ can only be isolated if samples with similar metallicities, masses, ages and activity level are compared. The stars in the sample considered here are dwarfs, as shown in Figure 3; all targets lie on the main sequence.

The metallicity distributions of the studied stars are shown in panel ‘a’ of Figure 4 (same as figure 9 of Paper I). As discussed in Paper I there is a visible offset between the distributions of stars with and without planets; the average metallicity of stars hosting giant planets is 0.15 dex higher than that of the comparison stars. This metallicity offset, however, has a negligible effect on the Li abundances, as can be noted from panel ‘b’ of Figure 4 where Li is shown *versus* [Fe/H]. The samples of stars with and without planets have considerable

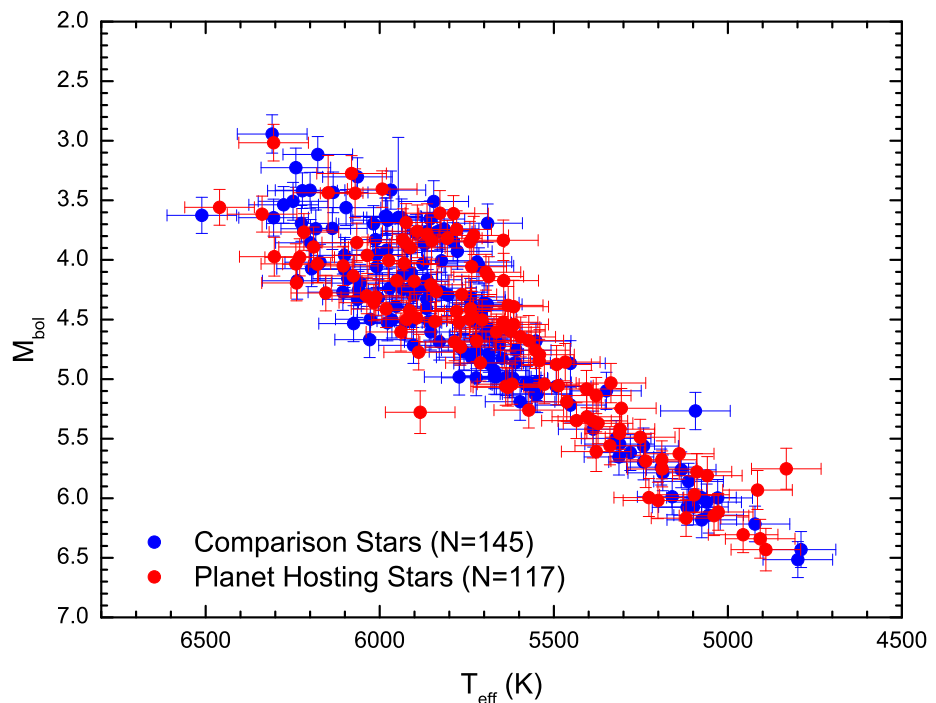


Fig. 3.— Location of the target stars in an H-R diagram represented by the bolometric magnitudes and effective temperatures. The planet hosting stars (red filled circles; $N=117$) and comparison stars not known to have giant planets (blue filled circles; $N=145$) analyzed in this study are all unevolved.

overlap with no significant trend of the lithium abundance with metallicity found over the roughly 1.0 dex change in [Fe/H] for the stars studied here. Also, the Sun does not exhibit any peculiarity in this plot.

Panel ‘c’ of Figure 4 presents the mass distributions for the two studied samples. The adopted values for the stellar masses correspond to the M_{track} values presented in Table 4 of Paper I (see that paper for details on the derived masses). The samples of stars hosting planets (represented by the red solid line histogram) and without planets (represented by the blue dashed line histogram) overlap closely in mass. The average masses for stars with and without planets are, respectively, $\langle M \rangle = 1.05 \pm 0.16$ and $1.02 \pm 0.17 M_{\odot}$; there is a probability of 92%, based on a Two-Sample Kolmogorov-Smirnov (KS) test that they are drawn from the same parent population of mass distributions. Panel ‘d’ of Figure 4 reveals a tendency of higher Li abundances with increasing mass. This is expected (see, e.g., Lambert & Reddy 2004), as lower mass stars have deeper convective zones in which Li is destroyed more efficiently. The location of the Sun in this diagram (represented by the black star symbol) indicates it to be a normal star when compared to the samples of stars with and without planets.

The age distributions for the sample stars are shown in panel ‘a’ of Figure 5. The stellar ages were taken from Table 4 of Paper I (see that paper for details). An inspection of the two histograms in this panel (red solid line representing stars with planets and blue dashed line representing stars without planets) indicates that overall there is not a significant difference between the age distributions of the two samples; the average values are: $\langle Age \rangle_{P-Hstars} = 5.24 \pm 2.48$ Gyr and $\langle Age \rangle_{nonP-Hstars} = 5.41 \pm 2.86$ Gyr. The probability that these two samples belong to the same parent population (from a KS test) is 84%. In panel ‘b’ of Figure 5, we observe an expected slight dependence of A(Li) upon age, with lower abundances being found for older stars. However, the behavior of stars with and without planets seems indistinguishable.

Panel ‘c’ of Figure 5 shows histograms comparing the chromospheric activity indices ($\log R'_{HK}$) for the two samples studied here. The values of $\log R'_{HK}$ for the target stars were taken, whenever available, from Henry et al. (1996), Tinney et al. (2002) and Wright et al. (2004). An evaluation of possible systematic differences between the chromospheric activity indices in these studies follows. Tinney et al. (2002) find that the activity indices in their study are consistent with those from Henry et al. (1996). A comparison of indices for 13 stars in our sample which appear in both studies finds good agreement: the linear fit to the two datasets has a slope of 0.98 ± 0.12 ; a correlation coefficient $R = 0.92$ and a mean difference (in the sense “Tinney et al. - Henry et al.”) of -0.01 dex. The works of Henry et al. (1996) and Wright et al. (2004) have 17 stars in common with our sample. A linear fit for these

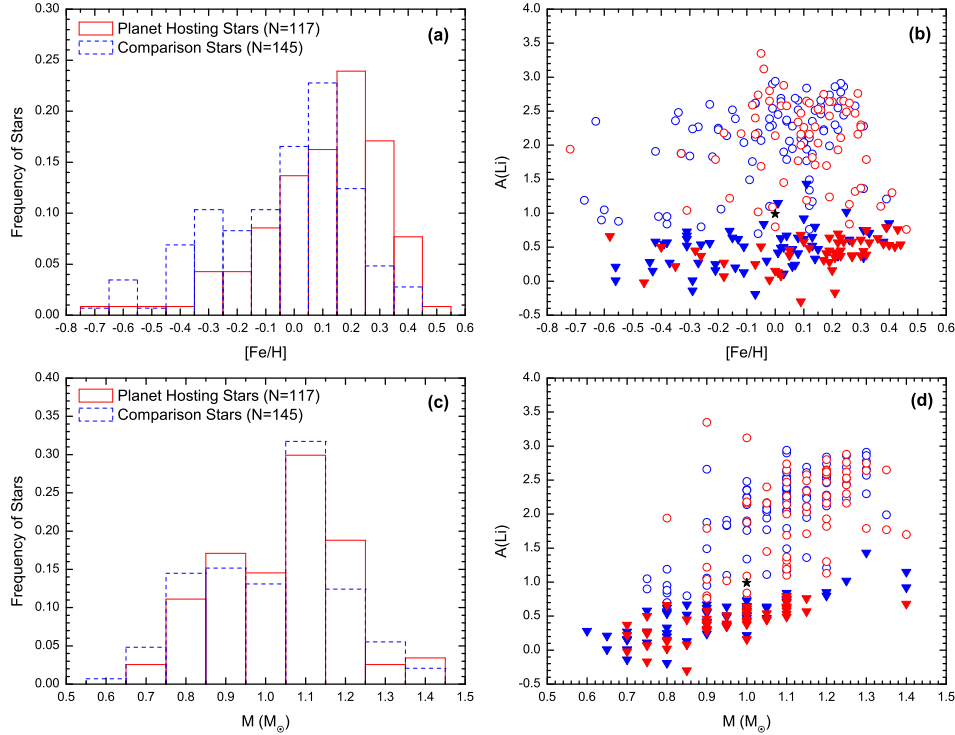


Fig. 4.— (a) Metallicity distributions of planet hosting (solid red line) and comparison (blue dashed line) stars from Paper I. (b) Lithium abundances *versus* metallicity for stars with (red symbols) and without (blue symbols) planets. Open circles are detected abundances and inverted triangles denote upper limits. The Sun is represented by a black star. (c) Same as panel (a) but for masses. (d) Same as panel (b) but replacing metallicity with mass.

values reveals no significant trend, having a slope of 0.99 ± 0.04 and a correlation coefficient $R = 0.99$. There is just an offset in the averages of ~ 0.04 dex, with the indices from Henry et al. (1996) being higher than those in Wright et al. (2004). Henry et al. (1996) derived an error of 0.052 for $\log R'_{HK}$, while Wright et al. (2004) state that the uncertainties in R'_{HK} are not larger than 13% (which would correspond to ~ 0.057 for $\log R'_{HK} \simeq -4.90$). As the offset between the two studies is compatible with the errors in $\log R'_{HK}$, no corrections in the indices were attempted in order to bring them to a consistent scale. In this study, whenever a star had more than one $\log R'_{HK}$ value, the average value was adopted.

Inspection of Panel ‘c’ of Figure 5 indicates that there is a visible offset between the distributions of $\log R'_{HK}$ for stars with and without planets, with a probability of 6.80×10^{-5} that they are drawn from the same population. This result is a consequence of the greater number of planet hosting stars with low activity levels. We note that this fact may be related to a possible bias in the Doppler detection method, which is more accurate for inactive stars. In spite of this offset, the average chromospheric activity indices for planet hosting and comparison stars are, respectively, $\langle \log R'_{HK} \rangle -4.94 \pm 0.16$ and -4.87 ± 0.17 dex. The overall global difference of 0.07 dex is interesting but cannot be considered as significant since it is roughly of the same order of the uncertainties discussed above. Panel ‘d’ of Figure 5 shows that there is no clear correlation between Li abundances and $\log R'_{HK}$ and no visible difference in the behavior of stars with and without planets. Finally, the Sun ($\log R'_{HK} = -4.96$; Wright et al. 2004) does not seem to be anomalous.

The comparisons of the various quantities discussed above show that the samples of planet host and comparison stars are similar in their mass and age distributions, although the metallicities do show a significant difference, with the planet hosting stars being on average more metal rich (as discussed in Paper I). Small differences are found in their respective activity levels, but neither the metallicity nor the activity levels produce obvious trends with the lithium abundances. Therefore, it is concluded that this comparison sample is well suited to search for possible anomalies in the Li abundances of stars with planets as a function of T_{eff} and $v \sin i$. An interesting result is that the Sun does not seem to exhibit any peculiarities and follows the global behaviors of target stars.

4.2. Projected Rotational Velocities

In Section 3.1, it was discussed that the detectability limit for $v \sin i$ determinations in this study is estimated to be 3.5 km s^{-1} . In spite of this relatively high limit, the homogeneity of the present analysis allows us to make relevant comparisons between rotational velocities in stars with and without planets. The behavior of $v \sin i$ as a function of T_{eff} is shown in

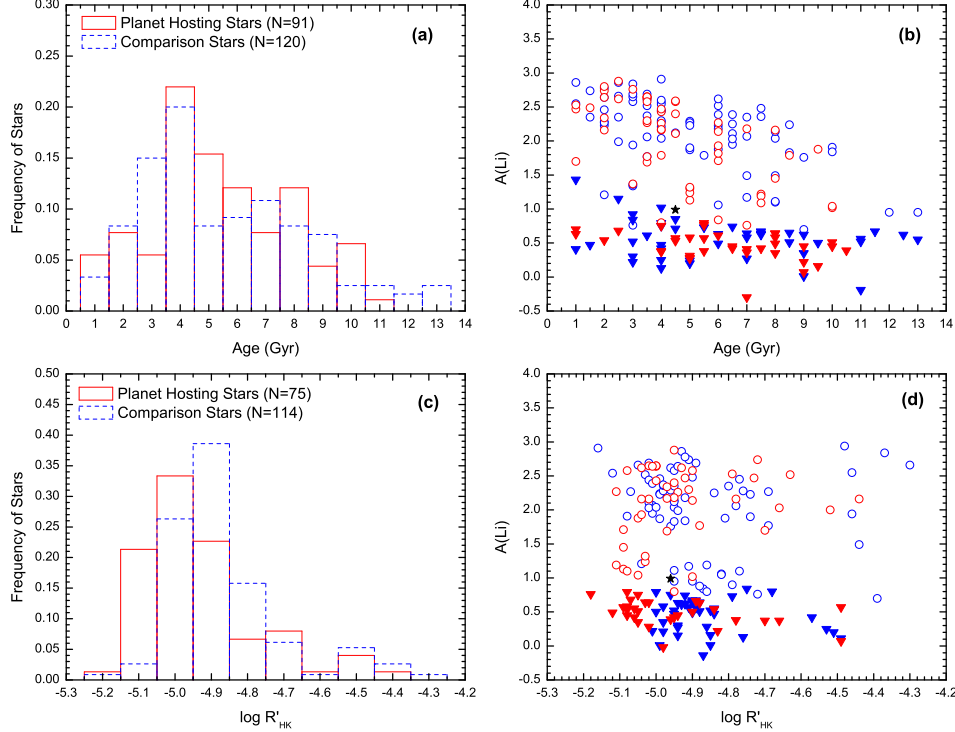


Fig. 5.— (a) Age distributions of planet hosting (solid red line) and comparison (blue dashed line) stars. (b) Lithium abundances *versus* age for stars with (red symbols) and without (blue symbols) planets. Open circles are detected lithium abundances and inverted triangles denote upper limit lithium abundances. The Sun is represented by a black star symbol. (c) Same as panel (a) but with the Ca II H+K emission index $\log R'_{HK}$. (d) Same as panel (b) but replacing age with $\log R'_{HK}$.

the upper panel of Figure 6. A clear positive correlation can be seen in the upper envelope of the distribution, with hotter stars having higher rotational velocities, as expected. The only three exceptions are the stars AB Pic, HD 70573 and HD 120136, which have rather high $v \sin i$ values. AB Pic is a young star identified as a member of the Tucana-Horologium association (Song et al. 2003), which has an estimated age of ~ 30 Myr; its rotational velocity is consistent with its youth. HD 70573 was identified as a member of the Hercules-Lyra Association, which is a young (~ 200 Myr) moving group (López-Santiago et al. 2006) with a derived upper limit of 1 Gyr for its age in Paper I. HD 120136 is also relatively young (with an age of 1 Gyr; Paper I) and active ($\log R'_{HK} = -4.70$; Wright et al. 2004). Finally, the projected rotational velocities obtained for these two stars are in close agreement with those derived by Gonzalez et al. (2010). We also note that none of the comparison stars have $v \sin i \gtrsim 10$ km s $^{-1}$ due to our selection criterium, which restricted the observed sample to having low values of $v \sin i$, as derived in Valenti & Fischer (2005, see Section 2.1 of Paper I).

No global differences between stars with and without planets are observed in the upper panel of Figure 6. Following the discussion in Gonzalez et al. (2010), we exclude those stars with $T_{\text{eff}} \leq 5650$ K, as well as the three target stars with planets which have the highest $v \sin i$ discussed above. The remaining stars are divided into two groups: one with those stars with $T_{\text{eff}} \leq 6000$ K and another with stars having $T_{\text{eff}} \geq 6000$ K. For the first group ($T_{\text{eff}} \leq 6000$ K), planet hosting (N=43) and comparison (N=70) stars have average projected rotational velocities of, respectively, $\langle v \sin i \rangle = 2.10 \pm 1.42$ and 2.16 ± 1.58 km s $^{-1}$. For the second group ($T_{\text{eff}} \geq 6000$ K), the average $\langle v \sin i \rangle = 3.87 \pm 2.26$ and 3.03 ± 2.15 km s $^{-1}$ for stars with (N=20) and without (N=34) planets, respectively. These differences cannot be considered significant given that the uncertainties in the derived $v \sin i$ are relatively large; we are unable to determine if there are differences between the projected rotational velocities of stars with and without planets below the estimated level in the uncertainties.

As a final test, the dependence of the lithium abundances on the projected rotational velocities of the stars is investigated; this is shown in the lower panel of Figure 6. There is a lower envelope in which A(Li) increases with increasing $v \sin i$. Such result agrees with the findings of Takeda et al. (2010), although their correlation is much tighter than the one in this study. An interesting feature is the absence of planet hosting stars with $4 \text{ km s}^{-1} \lesssim v \sin i \lesssim 8 \text{ km s}^{-1}$ and upper limits for Li abundances. We are unsure if this fact is related to any physical effect or selection bias. Finally, the Sun does not seem to be peculiar in either of the panels of Figure 6.

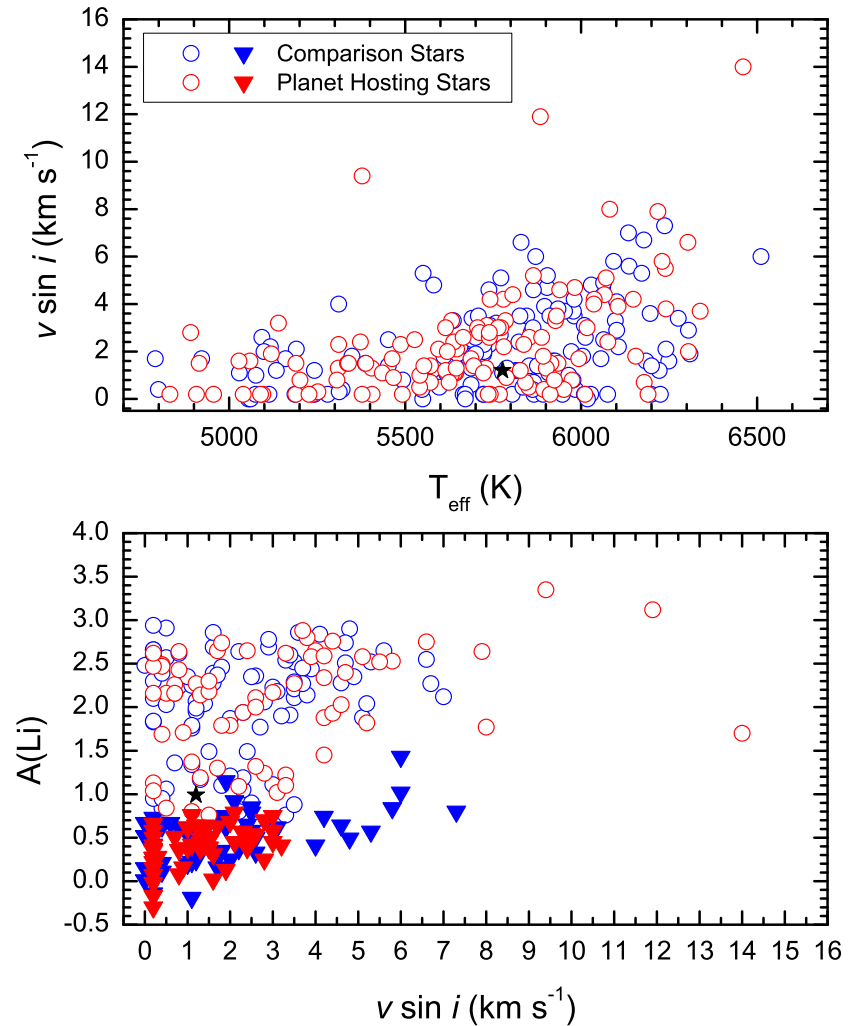


Fig. 6.— Upper Panel: Projected rotational velocities for the studied sample *versus* the adopted effective temperatures. Lower Panel: Lithium abundances *versus* rotational velocities. Stars with and without planets are shown as red symbols and blue symbols, respectively. Determined abundances are represented by circles and upper limits are denoted by downward triangles. The black star represents the Sun.

4.3. Lithium Abundances

Possible differences between Li abundances in stars with and without planets remains an open question. In order to investigate such possible differences, we first examine the lithium abundance distributions for all stars in our sample, which are shown as the histograms in panel ‘a’ of Figure 7. In this initial discussion, upper limits were included in the construction of this plot. An inspection of panel ‘a’ reveals two interesting features. First, we can clearly see a bimodal distribution, with peaks located at $A(Li) \sim 0.5$ and 2.4 dex. Second, the similarity between the distributions of stars with and without planets is evident, with a significant difference being visible only in the bin centered at $A(Li) = 0.4$ dex, which is dominated by upper limits; these facts become more evident if we analyze the cumulative distributions which are shown in panel ‘b’ of Figure 7. The differences between the distributions are probably a result of the inclusion of those stars with only upper limits to the Li abundances. In fact, if only detected Li abundances are considered, the distributions become more similar, as can be seen in panels ‘c’ (histogram) and ‘d’ (cumulative distribution) of Figure 7. The average lithium abundances of stars with and without planets are $\langle A(Li) \rangle = 2.06 \pm 0.63$ and 2.06 ± 0.60 dex, respectively, and the probability that the two samples belong to the same parent population is 87% (KS test). Therefore, this broad comparison does not seem to reveal any anomaly in the Li abundances of planet hosting stars.

Differences between Li abundances in stars with and without planets is usually seen in the effective temperature range $5600 \text{ K} \lesssim T_{eff} \lesssim 5900 \text{ K}$. In order to investigate this behavior in our samples, the lithium abundances derived in this study are plotted versus the effective temperatures of the target stars in Figure 8. This plot holds some interesting features. First, the detection limit of our method varies with T_{eff} roughly as $0.07 \text{ dex}/100 \text{ K}$, increasing from ~ 0.3 dex at $\sim 4800 \text{ K}$ to ~ 1.5 dex at $\sim 6500 \text{ K}$. Also, the well known decrease in lithium abundances with declining temperatures is recovered (see, e.g., Takeda & Kawanomoto 2005; Luck & Heiter 2006). This behavior is ultimately a reflection of the trend seen in panel ‘d’ of Figure 4, as higher mass stars on the main sequence also have higher effective temperatures. This dependency is also responsible for the bimodal distribution observed for Li abundances in panel ‘a’ of Figure 7. The peaks at $A(Li) \sim 0.5$ and 2.4 dex correspond to stars with low and high effective temperatures or masses, respectively. As there are three clearly distinct Li regimes, in the following we discuss them separately (see Figure 9).

For $T_{eff} \lesssim 5600 \text{ K}$ (upper most panel of Figure 9), almost all stars have low Li abundances ($\lesssim 0.7$ - 0.8 dex) and only upper limits could be derived in most cases. The exceptions are: HD 1237, HIP 14810, AB Pic, HD 69830 and HD 181433 (stars with planets); HD 17925, HD 36435, HD 118972 and HD 128674 (stars without planets). The two stars exhibiting extremely high Li abundances are AB Pic ($A(Li)=3.35$ dex) and HD 17925 ($A(Li)=2.66$ dex).

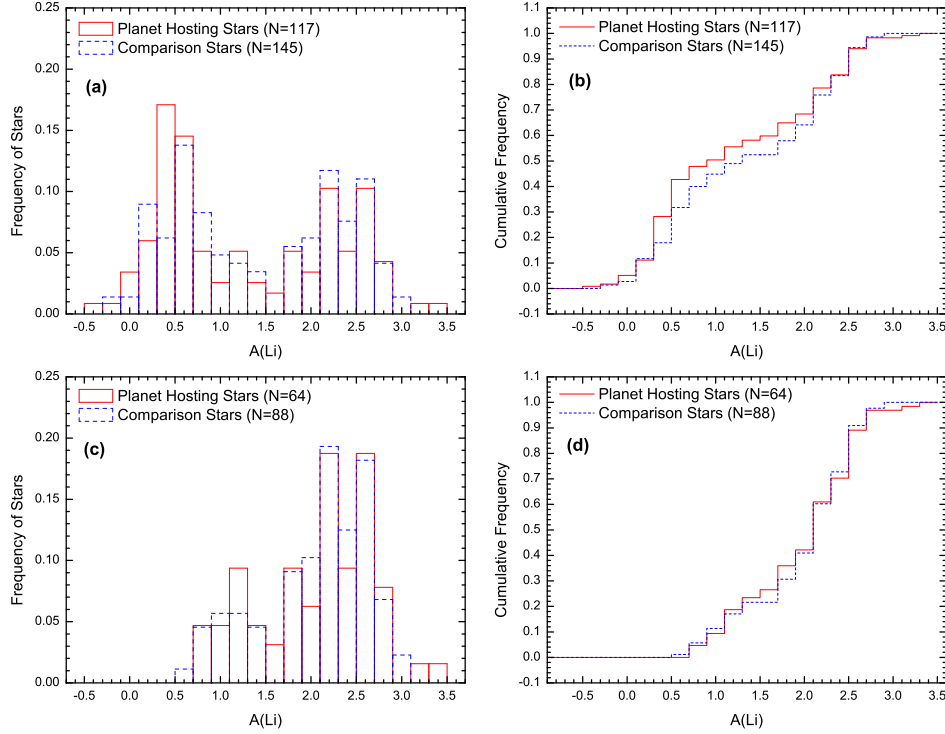


Fig. 7.— Distributions of lithium abundances for planet hosting (red solid lines) and comparison (blue dashed lines) stars. Panels (a) and (b) show the frequency and cumulative distributions, respectively, for all stars in our sample. Panels (c) and (d) presents the same plots, but only for those stars with detected Li abundances.

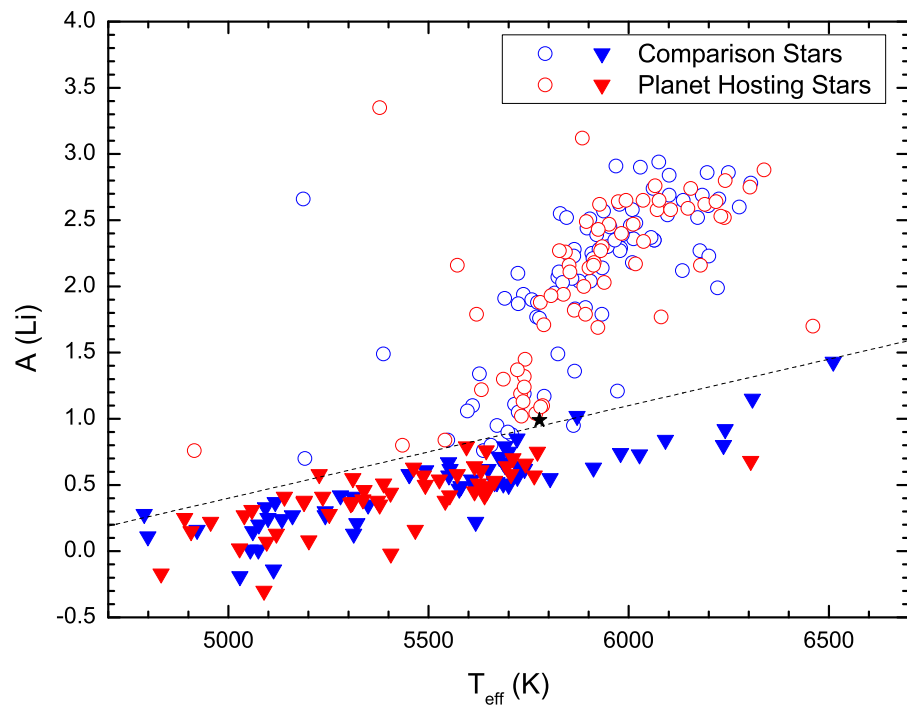


Fig. 8.— Lithium abundances versus effective temperatures for planet hosting (red symbols) and comparison (blue symbols) stars. Determined abundances are represented by circles and upper limits are denoted by downward triangles. The dashed line shows the detection limit of our method. The black star represents the Sun.

As already noted by Takeda & Kawanomoto (2005), HD 17025 is a young star with high activity level ($\log R'_{HK} = -4.30$; Henry et al. 1996). As previously mentioned AB Pic has an estimated age of ~ 30 Myr. In Paper I, upper limits of 1 Gyr were derived for the ages of these two stars. The same age upper limit is derived in Paper I for HD 1237, which has $A(Li) = 2.16$ dex and is also a young, active star (Age=0.02 Gyr and $\log R'_{HK} = -4.27$; Naef et al. 2001). The stars HD 36435 and HD 181433 have uncertain ages because they are located in crowded regions of their respective grids of isochrones. Based on their chromospheric activity level ($\log R'_{HK} = -4.44$; Henry et al. 1996), HD 36435 is most likely young, which would explain its relatively high Li abundance ($A(Li) = 1.49$ dex). HD 181433, on the other hand, has $\log R'_{HK} = -5.11$ (Bouchy et al. 2009) and does not seem to be young. Although consistent with the chromospheric activity level, its lithium abundance ($A(Li) = 0.76$ dex) is relatively high when compared to stars of the same temperature (difference of ~ 0.35 dex). Finally, the four remaining stars (HIP 14810, HD 69830, HD 118972 and HD 128674) have Li abundances consistent with those of other stars within the same temperature range. In this lower temperature regime ($T_{eff} \lesssim 5600$ K), there are 41 and 34 stars with and without planets, respectively; this corresponds to the largest sample analyzed to date. If we do not consider the stars with high Li abundances (HD 1237 and AB Pic; HD 17925 and HD 36435), a general overlap of the two samples is clear. Taking the upper limits as real detections, we find that the average Li abundances of planet hosting and comparison stars are, respectively, $\langle A(Li) \rangle = 0.37 \pm 0.25$ and 0.35 ± 0.28 dex.

For $T_{eff} \gtrsim 5900$ K (bottom most panel of Figure 9), it can be seen that stars are divided into two clearly distinct groups, one with $A(Li) \gtrsim 2.00$ and the other with $A(Li) \lesssim 1.50$. This Li gap was already observed by Chen et al. (2001) and Takeda & Kawanomoto (2005). We note that some of the stars with low Li abundance and $T_{eff} \gtrsim 6300$ K may be in the Li dip (see Boesgaard & Tripicco 1986; Balachandran 1995). In this temperature interval, there are 34 and 54 planet hosting and comparison stars, respectively, with considerable overlap. It is clear that the number of stars with planets diminishes with increasing temperature, reflecting the limitation of radial velocity surveys. Also, we notice that 8 comparison stars belong to the low-Li group, while only one star with a planet has an upper limit on its Li abundance. Although this feature can also be seen in Takeda & Kawanomoto (2005) and Luck & Heiter (2006), we are not sure if this is related to any physical effect or selection bias. Considering only detected lithium abundances, we obtain $\langle A(Li) \rangle = 2.42 \pm 0.31$ and 2.44 ± 0.32 for stars with and without planets, respectively. Thus, we do not find the excess Li abundances for planet hosting stars with $T_{eff} \sim 6000$ K discussed in Gonzalez (2008) and Gonzalez et al. (2010).

A more complicated behavior of the Li abundance occurs in the transition region between high and low Li, at the temperature interval $5600 \text{ K} \lesssim T_{eff} \lesssim 5900 \text{ K}$ (middle panel of

Figure 9). In this temperature regime, there are 42 and 57 stars with and without planets, respectively in our sample. The overlap is considerable, except in the narrow range of $T_{eff} \sim 5700 - 5800$ K. Over the entire temperature range shown in this panel ($T_{eff} = 5600 - 5900$ K), 26 planet hosting stars (or 62%) have detected Li abundances, with an average value of $\langle A(Li) \rangle = 1.68 \pm 0.53$ dex. For the comparison stars, the average lithium abundance for 37 stars (65%) with detections is $\langle A(Li) \rangle = 1.69 \pm 0.54$ dex. Treating the upper limits as actual detections, we derive $\langle A(Li) \rangle = 0.58 \pm 0.11$ and 0.62 ± 0.17 dex for stars with and without planets. Finally, it is interesting to note that the Sun does not exhibit an excessive Li depletion; actually, it looks like a “normal” main-sequence star.

Within this complex temperature transition region for Li, if we now follow the analysis of Israeli et al. (2009) and keep only stars within the very narrow range of $T_{eff} = 5777 \pm 80$ K, the sample here is left with 21 planet hosting and 27 comparison stars. For the sample of stars with planets, the average is $\langle A(Li) \rangle = 1.50 \pm 0.44$ dex for the 16 detections (76%) and $\langle A(Li) \rangle = 0.65 \pm 0.08$ dex for the 5 upper limits. For the control sample, the average is $\langle A(Li) \rangle = 1.76 \pm 0.48$ dex for the 19 detections (70%) and $\langle A(Li) \rangle = 0.64 \pm 0.11$ dex for the 8 upper limits. Following the analysis of Gonzalez et al. (2010), on the other hand, we have 20 and 30 planet hosting and comparison stars, respectively, in the temperature interval 5650 - 5800 K. For the former group, we obtain $\langle A(Li) \rangle = 1.30 \pm 0.26$ dex for the 13 detections (65%) and $\langle A(Li) \rangle = 0.63 \pm 0.08$ dex for the 7 upper limits. For the control sample, we derive $\langle A(Li) \rangle = 1.45 \pm 0.47$ dex for the 16 detections (53%) and $\langle A(Li) \rangle = 0.64 \pm 0.11$ dex for the 14 upper limits.

The above comparisons between Li abundances in planet hosting and comparison stars using the different T_{eff} boundaries as defined by Israeli et al. (2009) and Gonzalez et al. (2010) is intriguing, with average differences of +0.26 dex and +0.15 dex (in the sense of “comparison - planet hosting” stars) in $A(Li)$, respectively. It is interesting to investigate in more detail the Li abundances derived here for stars falling in the narrow T_{eff} range centered on the solar effective temperature as used by Israeli et al. (2009), since this temperature interval resulted in the larger difference of 0.26 dex. The Israeli et al. sample in this T_{eff} interval contains more stars than analyzed here, with 23 planet hosting stars and 60 comparison stars, compared to 21 and 25 stars here. The Li abundance distribution from Israeli et al. (2009) is heavily influenced by non-detections of Li I and thus, upper limits to $A(Li)$, with 17 and 28 upper limits for planet hosting stars and comparison stars, respectively. Taking the remaining Li I detections from Israeli et al., which span values of $A(Li) \sim 1.0 - 3.0$, and examining the cumulative fraction of $A(Li)$ reveals a shift towards larger Li abundances in the stars without planets, as discussed in Israeli et al. (2009). This same procedure is carried out for the samples of stars here, where there are only 5 upper limits in planet hosting stars and 6 upper limits in comparison stars. The cumulative fractions

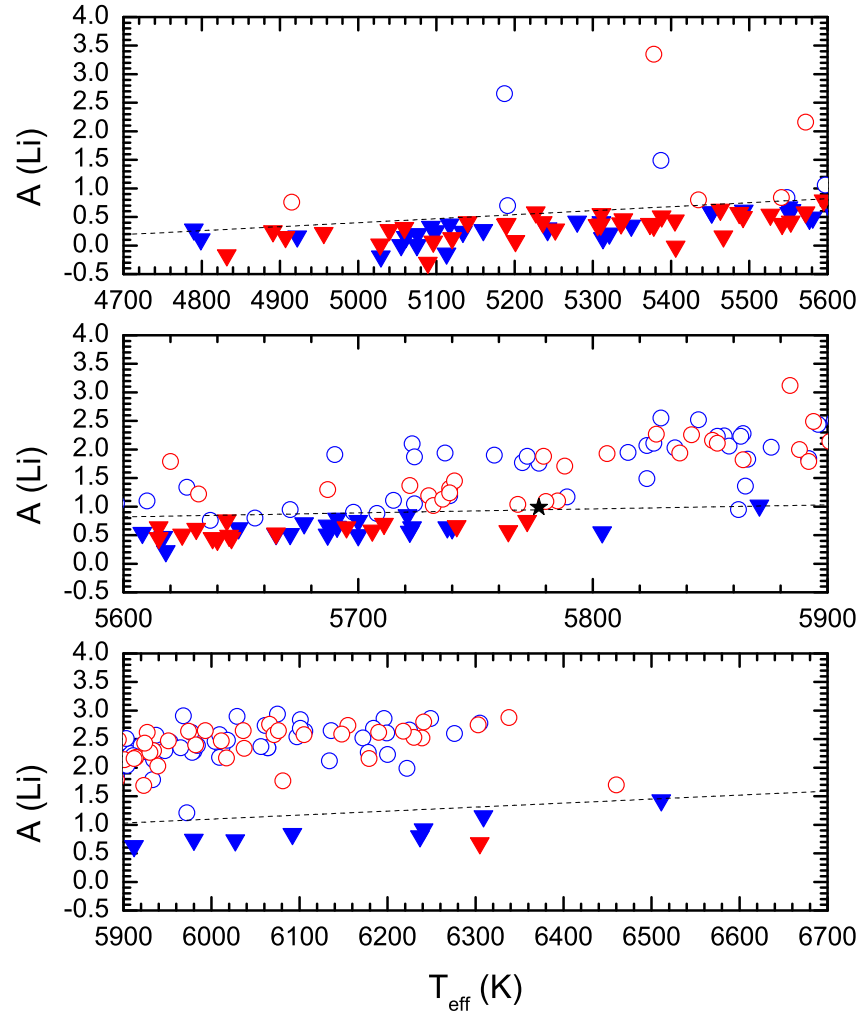


Fig. 9.— Lithium abundances versus effective temperatures for the intervals $T_{\text{eff}} \lesssim 5600$ K (upper panel), 5600 K $\lesssim T_{\text{eff}} \lesssim 5900$ K (middle panel) and $T_{\text{eff}} \gtrsim 5900$ K (lower panel). The symbols and dashed line have the same meaning as in Figure 8.

of A(Li) in the two sets of stars also show that the comparison stars are shifted towards somewhat larger values of A(Li), but not as large a shift as found by Israelian et al. (2009). Taken together, we find the same effect as found by Israelian et al., however the difference in the samples here is not as large. It is worthwhile to probe for other differences between planet hosting and comparison stars that might pertain to these possibly real differences in Li abundances between the two sets of stars.

Stellar rotation would be an obvious candidate on which to focus more closely in trying to understand why there might be differences in A(Li) between the planet hosting and comparison star samples, however all stars analyzed in the narrow T_{eff} range discussed above rotate slowly ($v \sin i \leq 4 \text{ km s}^{-1}$). It is not possible with the spectral resolution used here to accurately gauge differences between, say, $v \sin i = 3 \text{ km s}^{-1}$ or 1 km s^{-1} . A possible proxy for underlying stellar rotation is the stellar activity index, $\log R'_{HK}$. In Figure 10, $\log R'_{HK}$ is plotted versus T_{eff} for the range 5700 – 5850 K (the same temperature interval on which Israelian et al. 2009 focus their discussion). It is clear from this figure that the planet hosting stars tend to fall towards lower values of $\log R'_{HK}$ relative to the comparison stars.

This point about differences in stellar activity levels is made more clear by the respective frequency distributions and cumulative fractions of $\log R'_{HK}$ shown in the top and bottom panels of Figure 11, respectively. The comparison stars are shifted significantly towards larger levels of stellar activity when compared to the planet hosting stars. There is no significant difference in ages between these two groups over this temperature range and the values of $\log R'_{HK}$ are likely related to underlying stellar rotation. Although the projected rotational velocities within this T_{eff} interval are generally below our ability to accurately measure, the differing values of $\log R'_{HK}$ may reflect real differences in rotational velocities for the two groups of stars. If the planet hosting stars tend to rotate more slowly than the comparison stars in this narrow window in T_{eff} , it could be due to either 1) a selection bias, or 2) a real physical effect. A selection bias could occur if the lower activity levels lead to stars with more constant spectral line profiles (perhaps due to fewer distortions from cool spots or active regions rotating across the disk) and a higher success rate of detecting planets. The comparison stars studied here are taken from the stable radial velocity list of Fischer & Valenti (2005) and have velocity stabilities better than 30 m s^{-1} , so it is not obvious that this level of stability would lead to a significant selection effect. The other possibility is that the planet hosting stars do indeed tend to rotate more slowly, with the presence of large, closely orbiting planets, or their formation, having led to different rotational histories relative to “single” stars (see also Takeda et al. 2010). In addition, we note that da Silva et al. (2009) found that rapidly rotating pre-main sequence stars had undergone less Li depletion than those with lower rotational velocities (see also Cunha et al. 1995 for Orion). Our results are suggestive of subtle connections between the presence of giant, closely orbiting planets,

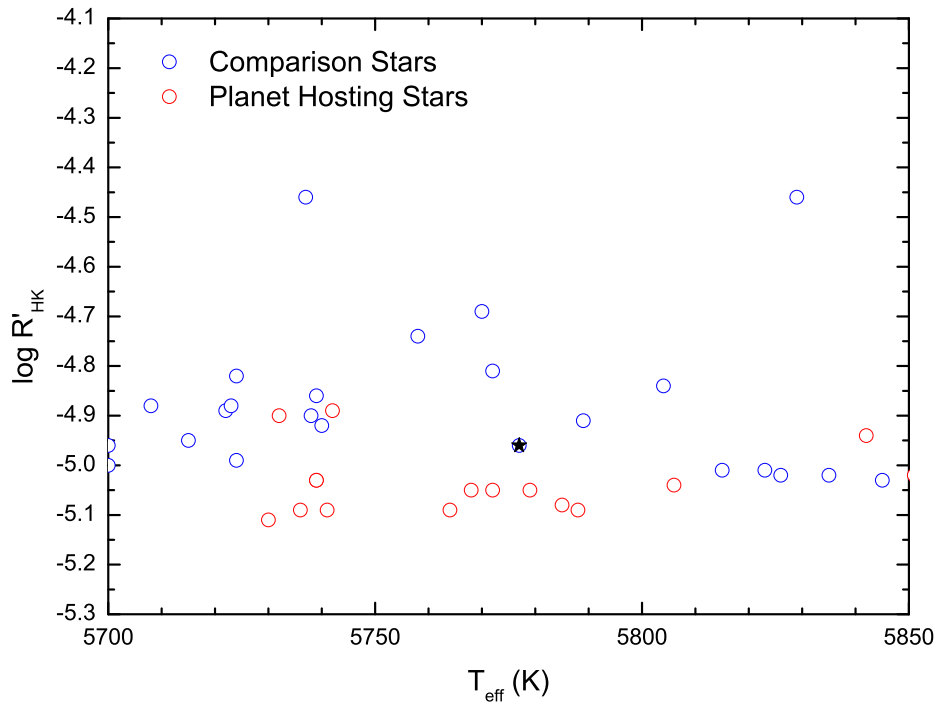


Fig. 10.— Ca II H+K emission indices *versus* the effective temperatures for planet hosting (red symbols) and comparison (blue symbols) stars in the effective temperature between 5700 – 5850 K. The black star represents the Sun.

stellar activity (and presumably rotation), and lithium abundances. More work, with both well-defined samples of larger numbers and homogeneous analyses needs to be carried out to either confirm, or refute, the trends that may have been observed here and in other studies (e.g., Gonzalez 2008; citealti09; Takeda et al. 2010; Gonzalez et al. 2010).

5. Conclusions

This paper is the third in a series which analyzes chemical abundances in a sample of planet hosting stars and a comparison sample of disk stars. Paper I (Ghezzi et al. 2010a) presented metallicities, [Fe/H], for dwarf stars; Paper II (Ghezzi et al. 2010b) analyzed samples of subgiants and giant stars and the present paper analyzes the element lithium in the same main-sequence targets as in Paper I. These targets consist of 117 planet hosting stars and 145 comparison stars known not to host giant planets.

Lithium abundances are potentially important for a better understanding of processes involved in the formation and evolution of planetary systems. Several recent studies in the literature have looked into possible differences between Li abundances of stars with and without planets, but so far have yet to reach a full consensus regarding a possible excess Li depletion in planet hosting stars (see e.g. reviews by Meléndez et al. 2010 and Santos et al. 2010). The combination of uniform data and homogeneous analysis with well-selected samples makes the results in this study well-suited to investigate possible differences in the Li abundances found in planet hosting stars.

Lithium abundances and projected rotational velocities were derived through an automated profile fitting of the Li I resonance doublet at $\lambda 6707.8 \text{ \AA}$. As a test, the automated analysis of the Sun as a normal target star yields a lithium abundance $A(\text{Li}) = 0.99 \pm 0.16$; this result is in good agreement with recent NLTE 3D abundance determinations done by Asplund et al. (2009) and Caffau et al. (2010). When compared to stars with similar properties in our sample (irrespective of the presence of planets), the Sun appears to have a normal Li abundance and rotational velocity.

Lithium abundances were not found to exhibit significant trends with metallicity and activity levels. It is possible, though, to identify a slight negative correlation with age. The most significant dependence is with effective temperature or, alternatively, mass. Hotter (more massive) stars have higher Li abundances. This is a well known effect related to the variation of the depth of the convective zone as a function of mass. We have also observed evidence that $A(\text{Li})$ increases with $v \sin i$, which is in line with the results of Takeda et al. (2010).

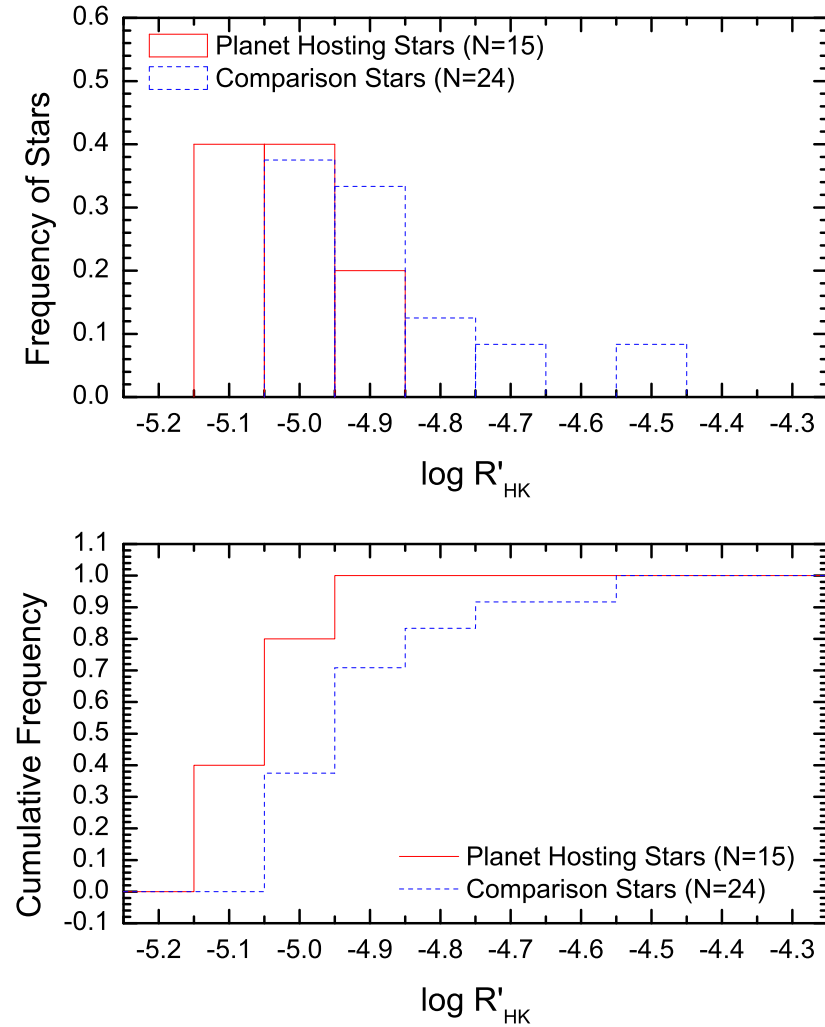


Fig. 11.— Frequency (upper panel) and cumulative (lower panel) distributions of the Ca II H+K activity indices for planet hosting (red solid line) and comparison (blue dashed line) stars in the range between $T_{\text{eff}} = 5700 - 5850$ K.

The most suggestive difference between planet hosting stars and the comparison stars occurs in the narrow T_{eff} range from 5700 K to 5850 K, where the behavior of the Li abundance is perhaps the most complex. Within this restricted temperature range, we find that the comparison stars tend to have somewhat larger Li abundances than the planet hosting stars; this is similar to earlier results from Israeli et al. (2009) and Gonzalez et al. (2010), although the differences found here are smaller. It is also found that, within this sample of stars, the planet hosting stars tend to exhibit lower levels of stellar chromospheric activity $\log R'_{HK}$ relative to the comparison stars. We suggest that, if this difference is not a selection effect, it is due to underlying differences in the stellar rotation rates, which would influence the evolution of the lithium abundances in the stellar photospheres (see also Bouvier 2008). It is worth considering whether the protoplanetary disks that form closely orbiting giant planets might affect the early spin-down histories of such planet hosting stars.

It is important to note that the comparisons conducted here are sensitive to the adopted samples of stars and choice of temperature intervals. As the number of stars with planets continues to grow, more homogeneous analyses based on high quality spectra are needed in order to fully understand the influence of planets on the lithium abundances of their host stars.

We thank Simon Schuler for discussions. We acknowledge the financial support of CNPq. Research presented here was supported in part by NASA grant NNH08AJ581.

REFERENCES

- Asplund, M., Grevesse, N., Sauval, A. J., & Scott, P. 2009, *ARA&A*, 47, 481
Balachandran, S. 1995, *ApJ*, 446, 203
Boesgaard, A. M., Tripicco, M. J. 1986, *ApJ*, 302, L49
Bouchy, F. 2009, *A&A*, 496, 527
Bouvier, J. 2008, *A&A*, 489, L53
Caffau, E., Ludwig, H.-G., Steffen, M., Freytag, B., Bonifacio, P. 2010, *Sol. Phys.*, tmp, 66
Castelli, F., & Kurucz, R. L. 2004, in Proc. IAU Symp. 210, Modelling of Stellar Atmospheres ed. N. Piskunov, et al. (Dordrecht: Kluwer), poster A20 (arXiv:astro-ph/0405087)
Chen, Y. Q., Nissen, P. E., Benoni, T., & Zhao, G. 2001, *A&A*, 371, 943

- Chen, Y. Q., & Zhao, G. 2006, AJ, 131, 1816
- Cunha, K., Smith, V.V., & Lambert, D.L. 1995, ApJ, 452, 634
- da Silva, L., Torres, C. A. O., de La Reza, R., Quast, G. R., Melo, C. H. F., & Sterzik, M. F. 2009, A&A, 508, 833
- Fischer, D. A., & Valenti, J. 2005, ApJ, 622, 1102
- Ghezzi, L., Cunha, K., Smith, V. V., de Araújo, F. X., Schuler, S., & de la Reza, R. 2010, ApJ, submitted
- Ghezzi, L., Cunha, K., Schuler, S., & Smith, V. V. 2010, ApJ, submitted
- Ghezzi, L., Cunha, K., Smith, V.V., Margheim, S., Schuler, S., de Araújo, F.X., & de la Reza, R. 2009, ApJ, 698, 451
- Gonzalez, G. 2008, MNRAS, 386, 928
- Gonzalez, G., & Laws, C. 2000, AJ, 119, 390
- Gonzalez, G., Carlson, M. K., & Tobin, R. W. 2010, MNRAS, 403, 1368
- Gonzalez, G., Laws, C., Tyagi, S., & Reddy, B. E. 2001, AJ, 121, 432
- Henry, T. J., Soderblom, D. R., Donahue, R. A., & Baliunas, S. L. 1996, AJ, 111, 439
- Israelian, G., et al. 2009, Nature, 462, 189
- Israelian, G., Santos, N. C., Mayor, M., & Rebolo, R. 2004, A&A, 414, 601
- Lambert, D. L., & Reddy, B. E. 2004, MNRAS, 349, 757
- Lind, K., Asplund, M., & Barklem, P.S. 2009, A&A, 503, 541
- López-Santiago, J., Montes, D., Crespo-Chacón, I., & Fernández-Figueroa, J. 2006, ApJ, 643, 1160
- Luck, R. E., & Heiter, U. 2006, AJ, 131, 3069
- Meléndez, J., Ramírez, I., Asplund, M., Baumann, P. 2010, in IAU Symp. 268, Light Elements in the Universe, ed. C. Charbonnel, M. Tosi, F. Primas & C. Chiappini (Cambridge:Cambridge University Press), 341
- Meléndez, J., et al. 2009, Ap&SS, tmp, 221

- Naef, D., Mayor, M., Pepe, F., Queloz, D., Santos, N. C., Udry, S., & Burnet, M. 2001, A&A, 375, 205
- Ryan, S. G. 2000, MNRAS, 316, L35
- Santos, N. C., et al. 2010, in IAU Symp. 268, Light Elements in the Universe, ed. C. Charbonnel, M. Tosi, F. Primas & C. Chiappini (Cambridge:Cambridge University Press), 291
- Sneden, C. 1973, PhD thesis, Univ. Texas, Austin
- Song, I., Zuckerman, B., & Bessel, M. S. 2003, ApJ, 599, 342
- Sousa, S. G., Fernandes, J., Israelian, G., & Santos, N. C. 2010, A&A, 512, L5
- Sousa, S. G., et al. 2008, A&A, 487, 373
- Takeda, Y., & Kawanomoto, S. 2005, PASJ, 57, 45
- Takeda, Y., Honda, S., Kawanomoto, S., Ando, H., & Sakurai, T. 2010, arXiv:1003.1564 (astro-ph)
- Takeda, Y., Kawanomoto, S., Honda, S., Ando, H., & Sakurai, T. 2007, A&A, 468, 663
- Tinney, C. G., McCarthy, C., Jones, H. R. A., Butler, R. P., Carter, B. D., Marcy, G. W., & Penny, A. J. 2002, MNRAS, 332, 759
- Valenti, J. A., & Fischer, D. A. 2005, ApJS, 159, 141
- Wright, J. T., Marcy, G. W., Butler, R. P., & Vogt, S. S. 2004, ApJS, 152, 261

Table 1. Rotational velocities and lithium abundances.

Star	$\text{FWHM}_{Macro+Inst}$ (Å)	$v \sin i$ (km s ⁻¹)	A(Li)	$\delta A(\text{Li})$
<i>Planet Hosting Stars</i>				
HD 142	0.341	3.70	2.88 ± 0.03	0.11
HD 1237	0.208	0.70	2.16 ± 0.02	0.10
HD 2039	0.156	1.50	2.30 ± 0.03	0.11
HD 2638	0.140	0.20	≤ 0.41	...
HD 3651	0.149	0.30	≤ 0.28	...
<i>Comparison Sample</i>				
HD 1581	0.203	1.10	2.25 ± 0.05	0.11
HD 1835	0.145	6.60	2.55 ± 0.02	0.10
HD 3823	0.147	2.60	2.36 ± 0.02	0.10
HD 4628	0.167	0.00	≤ 0.01	...
HD 7199	0.140	1.80	≤ 0.35	...

Note. — Table 1 is published in its entirety in the electronic edition of the Astrophysical Journal. A portion is shown here for guidance regarding its form and content.

Capítulo 5

Razões Isotópicas de ${}^6\text{Li}/{}^7\text{Li}$ em Estrelas com Planetas

Neste capítulo, é apresentado o artigo (publicado no *Astrophysical Journal*) em que são derivadas razões isotópicas de ${}^6\text{Li}/{}^7\text{Li}$ para 5 estrelas com planetas (inclusive HD 82943). Os espectros das estrelas da amostra possuem uma resolução $R \simeq 143.000$ e relações sinal-ruído entre 700 e 1100. Estas duas características fazem com que estes sejam os dados de melhor qualidade já utilizados para a obtenção de razões isotópicas nas estrelas com planetas. Juntamente com uma lista de linhas mais completa, eles nos permitiram derivar um valor de ${}^6\text{Li}/{}^7\text{Li}$ bastante preciso para HD 82943 (assim como para outras 4 estrelas com planetas e 1 sem planeta) e resolver a controvérsia a respeito da possibilidade de poluição na atmosfera desta estrela. Os gráficos que contêm os ajustes dos espectros sintéticos aos observados para as outras 5 estrelas analisadas não aparecem neste artigo, mas podem ser vistos no apêndice D.

Os espectros de altíssima qualidade usados neste artigo foram obtidos com o espectrógrafo bHROS (*bench-mounted High-Resolution Optical Spectrograph*) acoplado ao telescópio Gemini Sul (8,1 m), que fica localizado em Cerro Pachón (Chile). Apesar de os dados terem sido coletados no modo “fila”, pude acompanhar as observações durante as noites de 10 – 12 de dezembro de 2006, sob a supervisão do Dr. Steven Margheim (astrônomo do Gemini responsável pelo bHROS) e da Dra. Katia Cunha. Vale ressaltar que espectros bHROS de outras 5 estrelas com planetas foram obtidos pelo nosso colaborador Simon Schuler e as suas razões isotópicas de ${}^6\text{Li}/{}^7\text{Li}$ devem ser publicadas em um futuro próximo.

MEASUREMENTS OF THE ISOTOPIC RATIO ${}^6\text{Li}/{}^7\text{Li}$ IN STARS WITH PLANETS

L. GHEZZI¹, K. CUNHA^{1,2}, V. V. SMITH², S. MARGHEIM³, S. SCHULER², F. X. DE ARAÚJO¹, AND R. DE LA REZA¹

¹ Observatório Nacional, Rua General José Cristino, 77, 20921-400 São Cristóvão, Rio de Janeiro, RJ, Brazil; luan@on.br

² National Optical Astronomy Observatory, 950 North Cherry Avenue, Tucson, AZ 85719, USA

³ Gemini Observatory, Casilla 603, La Serena, Chile

Received 2009 February 10; accepted 2009 March 30; published 2009 May 20

ABSTRACT

High-resolution ($R = 143,000$), high signal-to-noise ratio ($\text{S/N} = 700\text{--}1100$) Gemini-S bench-mounted High-Resolution Optical Spectrograph spectra have been analyzed in a search for ${}^6\text{Li}$ in five stars which host extrasolar planets. The presence of detectable amounts of ${}^6\text{Li}$ in these mature, solar-type stars is a good monitor of accretion of planetary disk material, or solid bodies themselves, into the outer layers of the parent stars. Detailed profile fitting of the Li I resonance doublet at $\lambda 6707.8 \text{ \AA}$ reveals no detectable amounts of ${}^6\text{Li}$ in any star in our sample. The list of stars analyzed includes HD 82943 for which ${}^6\text{Li}$ has been previously detected at the level of ${}^6\text{Li}/{}^7\text{Li} = 0.05 \pm 0.02$. The typical limits in the derived isotopic fraction are ${}^6\text{Li}/{}^7\text{Li} \leq 0.00\text{--}0.02$. These upper limits constrain the amount of accreted material to less than $\sim 0.02\text{--}0.5$ Jovian masses. The presence of detectable amounts of ${}^6\text{Li}$ would manifest itself as a red asymmetry in the Li I line profile and the derived upper limits on such asymmetries are discussed in light of three-dimensional hydrodynamic model atmospheres, where convective motions also give rise to slight red asymmetries in line profiles.

Key words: line: profiles – planetary systems: formation – stars: abundances – stars: atmospheres

1. INTRODUCTION

One of the interesting properties of the known stars with planets concerns their metallicity distribution. Several studies (Santos et al. 2000, 2005; Gonzalez et al. 2001; Laws et al. 2003; Fischer & Valenti 2005) have confirmed the result first shown by Gonzalez (1997): stars with giant planets are systematically metal-rich (by ~ 0.2 dex) relative to field FGK dwarfs not known to harbor planets. Two hypotheses have been proposed to explain this excess: primordial enrichment or pollution. The first indicates that the probability of forming giant planets is a steeply rising function of the intrinsic metallicity of the gas and dust cloud which gave birth to the system. This possibility is in agreement with the core-accretion scenario (e.g., Pollack et al. 1996). The higher metal content would raise the surface density of solid material in the disk, leading to a more efficient agglomeration of the cores onto which the gas will be accreted. The pollution scenario, on the other hand, indicates that the presence of planets could alter the metallicity of their hosting stars. During the inward migration process of giant planets, solid material from the protoplanetary disk or even inner planetesimals and planets could be accreted into the convective envelope of the hosting star. As this material is depleted in H and He, the star’s metallicity would be enhanced.

Current results (e.g., Fischer & Valenti 2005) show that the frequency of planets increases significantly for higher metallicities, thus giving strong support for the primordial hypothesis. Evidence for the occurrence of pollution is still ambiguous. For instance, Ecuillon et al. (2006) studied the relation between chemical abundances of several elements and their respective condensation temperatures in stars with and without planets, finding no significant differences in the two groups. On the other hand, Pasquini et al. (2007) analyzed the metallicity distributions of planet-hosting dwarfs and giants and found that the latter do not favor metal-rich systems. The authors argue that this result could be a strong indication of pollution, as the metal excess could be erased by the dilution process that takes place during the later stages of stellar evolution.

Another ambiguous result is the possible detection of ${}^6\text{Li}$ in the atmospheres of stars with planets, which is a sensitive test of the pollution hypothesis. Both lithium isotopes are destroyed at relatively low temperatures ($T = 2 \times 10^6 \text{ K}$ for ${}^6\text{Li}$ and $T = 2.5 \times 10^6 \text{ K}$ for ${}^7\text{Li}$) in stellar interiors. During the early stages of evolution in solar-type stars (specifically, before entering the main sequence), these stars are entirely convective and most of the primordial Li is transported to deeper and hotter layers, where it is rapidly burned. The fraction of lithium destruction is, however, a strong function of the stellar mass. For a given metallicity, there is a mass range in which the ${}^6\text{Li}$ is completely destroyed, while a significant amount of ${}^7\text{Li}$ is preserved. The lower edge of this range falls just above the solar mass (corresponding to main-sequence late-F spectral types) for near solar metallicities. Thus, one should not expect to find any ${}^6\text{Li}$ in the atmospheres of solar-type stars. Any positive detection could indicate an external contamination or pollution process.

Israelian et al. (2001) measured the isotopic ratio ${}^6\text{Li}/{}^7\text{Li}$ in HD 82943 (with two close-in giant planets) and found ${}^6\text{Li}/{}^7\text{Li} = 0.126 \pm 0.014$. This can be compared with a solar system (meteoritic) ratio of ${}^6\text{Li}/{}^7\text{Li} = 0.08$. The positive ${}^6\text{Li}$ detection for this star was interpreted as observational evidence of the pollution process. Reddy et al. (2002) studied ${}^6\text{Li}$ in eight planet-hosting stars (HD 82943 included) and found no significant amount of this isotope in HD 82943, nor in any of the targets analyzed. The difference from the previously published ${}^6\text{Li}$ detection for HD 82943 was attributed to the use of a more complete line list, although it noted the presence of an unidentified absorption in the Li region. Israelian et al. (2003) investigated the nature of the unidentified absorption feature at 6708.025 \AA , which affects the Li I line, by observing several stars of different effective temperatures. They concluded that a high excitation Si I line first proposed by Müller et al. (1975) is more adequate than the Ti I line used by Reddy et al. (2002). Adopting a revised line list and higher quality spectra, the authors performed a new analysis of HD 82943 and measured ${}^6\text{Li}/{}^7\text{Li} = 0.05 \pm 0.02$. Thus, this most recent result for HD 82943 gave additional support to the pollution scenario.

More recently, Mandell et al. (2004) made a major extension of the previous line lists (especially for the CN contribution) and tested three different possibilities for the unidentified feature at 6708.025 Å (Si I, Ti I, and Ti II): for all of the three different line lists no ${}^6\text{Li}$ was detected in a sample of three planet-hosting stars. These results are generally consistent with Reddy et al. (2002) and argue against the pollution scenario. Unfortunately, HD 82943 was not analyzed by Mandell et al. (2004).

In this paper, the ${}^6\text{Li}/{}^7\text{Li}$ isotopic ratio in HD 82943 is analyzed, as well as in other four planet-hosting stars and one star not known to have giant planets. The observations and the data reduction are described in Section 2. The analysis procedures including the derivation of atmospheric and broadening parameters and compilation of the line list for the Li I region are presented in Section 3. The abundance results are presented in Section 4 and discussed in Section 5.

2. OBSERVATIONS AND DATA REDUCTION

2.1. Observations

Spectra of the program stars were obtained at the Gemini-S telescope with the bench-mounted High-Resolution Optical Spectrograph (bHROS). Given the brightness of these targets, the “object-only” mode was used for observations; for this mode, a 0''.9 fiber is fed into an image slicer that produces a “slit,” measuring $0''.14 \times 6''.5$ as projected to the camera focal plane. The spectrograph is cross dispersed by a set of fused silica prisms and an image slicer rotation mechanism is used to produce a “vertical” slit at the observed central wavelength on the detector, a single 2048×4608 E2V CCD with $13.5 \mu\text{m}$ pixels.

The instrument was configured to produce a central wavelength on the detector of 6501 Å. In this configuration, eight incomplete spectral orders were obtained, covering the interval between 5580 and 7230 Å. The continuous coverage available within a single echelle order varies from ~ 50 to 70 Å depending on the order. The detector was used with 1×1 binning to achieve a resolution close to the spectrograph’s nominal resolution of $R = \lambda/\delta\lambda = 150,000$ (three pixel sampling) and minimize the impact of cosmic rays. The actual resolution was measured using 10 ThAr lines in the order containing the Li I feature and this resolution was found to be $R = 143,000 \pm 5000$. The spectra were obtained in a wide range of observing conditions during both classical (2006 May) and queue operations (2006 December and 2007 January). Table 1 contains a detailed log of the observations including spectral types, V magnitudes, number of exposures, integration times, and the resulting signal-to-noise ratios (S/Ns; per resolution element). The quoted S/N values are based on direct measurements of the rms in sample continuum regions which were selected based on inspection of the Solar Atlas. The measured values of S/N are compatible with the S/N based on Poisson statistics.

In addition to the target spectra, calibration sets of biases, flats, and ThAr arcs were obtained each night. When the observations were done in queue mode, only a single ThAr spectrum was taken each night as only a single object was observed per night. When observations were done in classical mode, ThAr spectra were taken which bracketed the observations. For example, the observations of HD 82943 obtained on 2006 May 9 were bracketed with ThAr spectra and this provides a measure of the spectrograph stability. A direct measurement of the stability can be found when combining multiple spectra via cross-correlation. The largest drift found was about $3 \text{ m}\text{\AA}$ or $1/5$ of a pixel. Telluric

Star	Spectral Type	V	Observation Date	N	T_{int} (s)	Observing Log	
						($\sim 6708 \text{ \AA}$)	S/N
HD 17051	F9V	5.40	2006 Dec 13	1	600	740	
HD 36435	G9V	7.01	2006 Dec 15	2	1050	560	
HD 74156	G0	7.62	2007 Jan 30	3	1320	710	
HD 82943	F9V	6.54	2006 May 9, 10	8	600	1130	
HD 147513	G1V	5.37	2006 May 10	4	600	1100	
HD 217107	G8IV	6.16	2006 May 10	3	600	750	

spectra were also obtained and, as expected, demonstrated no significant atmospheric contamination in the region of the lithium feature.

2.2. Reduction

The data were processed using standard echelle reduction practices with IRAF⁴ packages, following the recipe developed by the bHROS science demonstration team.⁵ The raw spectra were corrected by overscan and bias-image subtraction. The images were then flat-fielded to remove both pixel-to-pixel variations and small amounts of fringing present in the spectra; since the illumination pattern on the detector is nearly identical for the flat and target spectra, the fringe pattern can be very well removed. Scattered light was then sampled, fit, and subtracted from our images before extraction.

The use of the prism cross-disperser combined with the long “slit” length causes the spectral orders to become tilted away from the central order. The severity of this tilt can potentially result in the loss of resolution in the extraction process. To reduce the impact of the tilts, each of the eight spectral orders was divided into 14 subapertures, for a total of 112 resulting subapertures. Each subaperture was individually extracted with optimal extraction method and blaze corrected with similarly extracted flat-field spectra. The ThAr spectra were also subdivided into the same subapertures and wavelength solutions were derived for each of the 112 subapertures, with a typical rms scatter of 0.001 Å. These wavelength solutions were applied to the target subapertures and combined to produce a reduced one-dimensional echelle spectrum composed of eight spectral orders. Rejection methods employed in the combination process ensured the removal of cosmic rays from the final spectra. Finally, the spectra were continuum normalized and corrected for radial velocity shifts. More details about the bHROS data reduction process can be found in Schuler et al. (2008). The final processed spectrum for a target star is shown in Figure 1, as an example.

3. ANALYSIS

The first step in the analysis is to derive effective temperatures, surface gravities, and microturbulent velocities for the sample stars. In addition, broadening parameters affecting the observed spectral lines also need to be defined. A crucial point in the determination of ${}^6\text{Li}/{}^7\text{Li}$ isotopic ratios is the construction of a detailed line list for the region around the Li I feature. This

⁴ Image Reduction and Analysis Facility (IRAF) is distributed by the National Optical Astronomy Observatory (NOAO), which is operated by the Association of Universities for Research in Astronomy, Inc. (AURA) under cooperative agreement with the National Science Foundation (NSF).

⁵ Available at <http://www.gemini.edu/sciops/instruments/hros/hrosIndex.html>.

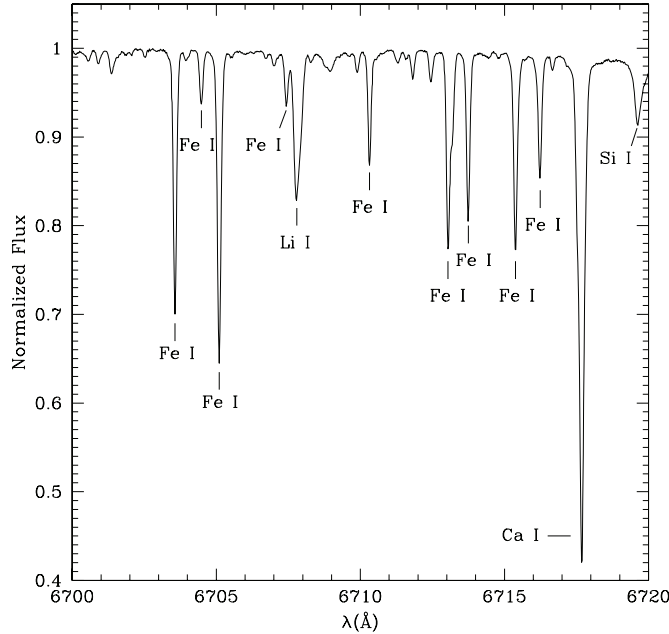


Figure 1. Gemini bHROS spectrum of HD 82943 ($R \simeq 143,000$ and $S/N \simeq 1130$), showing part of the spectral order which contains the lithium feature. The main spectral lines in this region are identified.

section presents a discussion of the analysis method adopted in this study.

3.1. Line Selection and Derivation of Stellar Parameters

The bHROS spectra have incomplete wavelength coverage (Section 2.1) which restricts the selection of iron lines to derive stellar parameters and metallicities. A sample of Fe I and Fe II lines was compiled from the list in Thévenin (1990) and equivalent widths were measured in the solar spectrum (Kurucz et al. 1984) in order to select suitable lines and gf -values which produced an abundance scatter of less than or equal to 0.05 dex. The final list of adopted Fe lines, as well as the measured equivalent widths for the target stars and the Sun are presented in Table 2. The wavelengths, lower excitation potentials (LEPs), and gf -values were taken from the Vienna Atomic Line Database⁶ (VALD-2; Kupka et al. 1999). As a reference note that the adopted line list yields a solar abundance $A(\text{Fe})^7 = 7.48 \pm 0.05$ and $\xi = 1.24 \text{ km s}^{-1}$ using a Kurucz model atmosphere with $T_{\text{eff}} = 5777 \text{ K}$, $\log g = 4.44$, $\xi = 2.00 \text{ km s}^{-1}$, and $l/H_p = 1.25$.

Stellar parameters for the target stars were derived spectroscopically and followed standard techniques. Effective temperatures were obtained from zero slopes in diagrams of Fe abundance versus excitation potential and surface gravities from ionization equilibrium between Fe I and Fe II species. The microturbulent velocities were varied until the slopes of $A(\text{Fe I})$ versus $\log(W_{\lambda}/\lambda)$ were zero. The abundances were derived in LTE using an updated version of the spectrum synthesis code MOOG⁸ (Sneden 1973). The model atmospheres adopted in the analysis were interpolated from the ODFNEW grid of ATLAS9 models⁹ (Castelli & Kurucz 2004). Figure 2 shows the iterated result of $A(\text{Fe I})$ versus LEP (top panel) and $A(\text{Fe I})$ versus

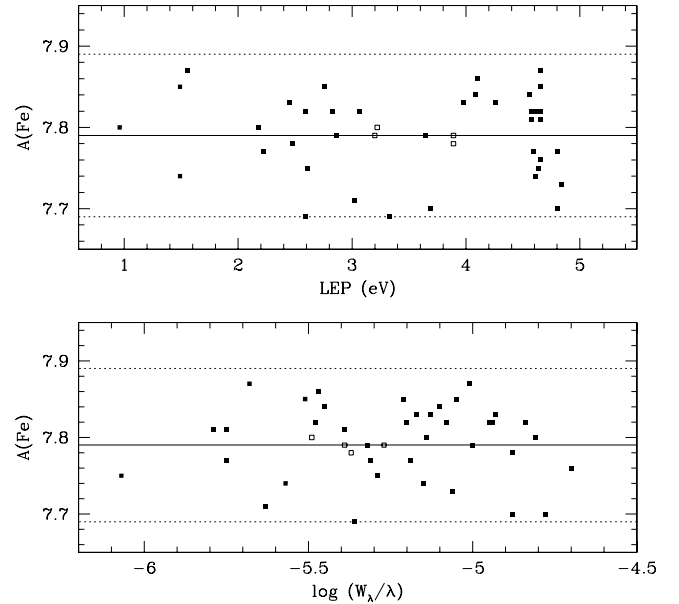


Figure 2. Spectroscopic determination of the effective temperature and microturbulent velocity for HD 82943 obtained from zero slopes in the runs of Fe I abundances with excitation potential of the transitions (upper panel) and reduced equivalent widths (lower panel). Fe I (filled squares) and Fe II (open squares) abundances are consistent and the slopes are zero for $A(\text{Fe}) = 7.79$.

$\log(W_{\lambda}/\lambda)$ (bottom panel) for the star HD 82943, as an example. The adopted stellar parameters for all target stars are given in Table 3. Our adopted values for effective temperatures are in good agreement (within $\sim 100 \text{ K}$) with the derived values using the photometric correlations presented in Ramírez & Meléndez (2004). Differences of this amount have no significant effect in the derived isotopic fractions.

The Fe abundance uncertainties can be estimated from the errors in T_{eff} , $\log g$, ξ , line gf -values, continuum placement, and equivalent width measurements, among others. We estimate the uncertainties in T_{eff} to be $\pm 100 \text{ K}$; $\log g \pm 0.2 \text{ dex}$; and $\xi \pm 0.2 \text{ km s}^{-1}$. The combined uncertainties in the derived Fe abundances are typical for this type of classical spectroscopic analysis and are estimated to be about $\pm 0.1 \text{ dex}$.

The luminosities of the program stars were calculated using apparent V magnitudes, *Hipparcos* parallaxes, bolometric corrections from Girardi et al. (2002), and using $M_{\text{bol},\odot} = 4.77$. No interstellar extinction was included as the most distant star has $d = 65 \text{ pc}$. Utilizing these luminosities and the T_{eff} values from Table 3, stellar masses were derived by placing the stars in a grid of evolutionary tracks from Girardi et al. (2000) for $[\text{Fe}/\text{H}] = 0.00$ and 0.20 , with stellar masses covering $M = 0.8\text{--}1.4 M_{\odot}$. Stellar ages were estimated by using the values of effective temperature and luminosity to place the stars in a grid of isochrones from Girardi et al. (2000) for $[\text{Fe}/\text{H}] = 0.00$ and 0.20 , with ages from 0.063 to 7 Gyr . In addition, stellar masses were calculated using the relation between luminosity, surface gravity, and effective temperature:

$$\log \frac{M}{M_{\odot}} = \log \frac{L}{L_{\odot}} + \log \frac{g}{g_{\odot}} - 4 \log \frac{T_{\text{eff}}}{T_{\text{eff},\odot}}, \quad (1)$$

with $T_{\text{eff},\odot} = 5777 \text{ K}$ and $\log g_{\odot} = 4.44$. The masses and ages estimated for the targets stars are presented in Table 3.

3.2. Spectrum Synthesis

Lithium isotopic ratios are measured via spectrum synthesis analysis. The Li I doublet at $\sim 6708 \text{ \AA}$ is an asymmetric blend

⁶ <http://ams.astro.univie.ac.at/~vald/>

⁷ $A(\text{Fe}) = \log [N(\text{Fe})/N(\text{H})] + 12$.

⁸ Available at <http://verdi.as.utexas.edu/moog.html>.

⁹ <http://kurucz.harvard.edu/>

Table 2
Selected Fe Lines and Measured Equivalent Widths

λ (Å)	Ion	LEP (eV)	$\log gf$ (dex)	W_λ (mÅ)						
				Sun	HD 17051	HD 36435	HD 74156	HD 82943	HD 147513	HD 217107
5741.848	Fe I	4.26	-1.730	32.9	35.4	41.9	30.8	38.8	32.1	52.7
5760.345	Fe I	3.64	-2.490	23.8	23.5	34.9	23.4	27.6	22.7	42.0
5778.453	Fe I	2.59	-3.430	22.7	20.9	35.6	20.7	25.0	20.8	45.5
5905.672	Fe I	4.65	-0.863	57.9	59.9	67.9	58.3	67.3	58.1	76.7
5916.247	Fe I	2.45	-2.832	62.2	62.9	77.6	58.5	70.0	62.7	86.2
5927.789	Fe I	4.65	-1.090	43.1	...	52.0	42.1	57.7	42.7	67.3
5930.180	Fe I	4.65	-0.028	105.7	112.1	129.4	103.2	119.4	107.7	136.1
6079.009	Fe I	4.65	-1.120	46.2	48.3	57.6	46.0	54.7	46.8	64.3
6082.711	Fe I	2.22	-3.573	34.8	28.8	52.1	29.8	39.4	33.5	60.9
6093.644	Fe I	4.61	-1.252	31.2	33.7	40.5	34.5	43.6	31.2	54.7
6094.374	Fe I	4.65	-1.661	20.2	21.7	25.3	20.2	25.1	19.5	36.9
6096.665	Fe I	3.98	-1.890	38.3	37.8	49.9	36.8	44.9	38.3	58.4
6098.245	Fe I	4.56	-1.859	16.2	18.8	23.3	16.8	21.8	16.3	33.0
6265.134	Fe I	2.18	-2.550	94.0	86.0	118.6	89.4	97.6
6270.225	Fe I	2.86	-2.576	57.6	48.7	68.0	54.8	62.2	54.6	78.0
6271.279	Fe I	3.33	-2.703	23.3	23.4	34.5	21.2	27.6	22.1	42.5
6297.793	Fe I	2.22	-2.740	81.0	...	104.0	78.2	...	85.1	105.7
6302.494	Fe I	3.69	-0.973	96.1	89.8	...	91.5	103.4	101.9	123.0
6315.812	Fe I	4.08	-1.710	41.7	41.9	52.3	43.0	50.4	42.4	62.6
6322.686	Fe I	2.59	-2.304	84.5	74.0	103.6	81.5	92.1	86.0	108.4
6495.742	Fe I	4.84	-0.801	48.4	45.0	58.9	...	57.2	...	72.4
6496.467	Fe I	4.80	-0.348	75.6	75.6	90.8	73.4	84.8	77.8	101.6
6498.939	Fe I	0.96	-4.699	45.6	34.8	72.6	39.8	47.2	42.3	76.5
6518.367	Fe I	2.83	-2.460	66.1	62.6	80.5	62.0	72.5	62.8	87.8
6699.142	Fe I	4.59	-2.101	9.1	9.2	11.9	8.2	12.0	8.0	18.0
6703.567	Fe I	2.76	-3.141	37.4	32.2	50.9	33.5	41.6	35.2	59.4
6710.320	Fe I	1.49	-4.764	16.1	11.6	27.3	12.3	18.0	13.7	35.4
6713.745	Fe I	4.80	-1.338	21.8	22.5	28.6	24.0	33.1	21.4	44.1
6716.237	Fe I	4.58	-1.836	16.0	17.3	22.6	16.6	22.1	15.3	31.6
6725.357	Fe I	4.10	-2.300	17.5	16.7	23.9	17.0	22.8	17.7	34.3
6726.666	Fe I	4.61	-1.133	46.6	47.6	59.8	45.8	56.0	46.6	66.6
6732.065	Fe I	4.58	-2.210	7.7	8.2	9.1	7.7	10.8	7.5	16.0
6733.151	Fe I	4.64	-1.437	26.4	26.8	32.7	25.9	34.5	25.5	48.6
6739.522	Fe I	1.56	-4.950	12.0	9.8	19.4	8.0	14.0	10.6	26.9
6745.101	Fe I	4.58	-2.160	9.0	10.6	11.3	8.9	11.9	8.3	18.1
6746.955	Fe I	2.61	-4.262	4.9	4.1	9.4	4.0	5.8	3.8	11.5
6971.950	Fe I	3.02	-3.340	13.8	11.7	21.1	12.5	16.5	12.3	29.4
6978.852	Fe I	2.48	-2.413	86.4	84.1	113.4	79.3	92.8	88.8	108.5
7179.995	Fe I	1.49	-4.780	20.4	14.9	33.0	14.6	22.3	19.2	42.4
7189.146	Fe I	3.07	-2.771	40.4	35.3	53.7	37.5	45.5	38.5	62.8
6084.111	Fe II	3.20	-3.780	22.0	32.2	18.5	31.7	32.8	21.6	31.0
6113.322	Fe II	3.22	-4.110	12.5	21.0	9.6	19.1	19.8	12.0	19.0
7222.394	Fe II	3.89	-3.276	19.7	29.6	29.1	19.2	27.1
7224.487	Fe II	3.89	-3.226	21.3	32.4	16.3	31.8	30.5	20.0	...

of two ^7Li lines which consist of seven hyperfine components, spanning a separation of approximately 0.15 Å between stronger blue and weaker red components. The ^6Li lines present the exact same configuration, except with three hyperfine levels, with a total separation of approximately 0.15 Å between stronger blue and weaker red components. As the ^6Li lines are much weaker, with the stronger one situated almost at the same wavelength as the weaker ^7Li component, the former isotope appears as a perturbation, providing an additional small asymmetry to the blend. In addition, the lithium region suffers from the contribution of several blends from metal and molecular CN lines.

3.2.1. Broadening Parameters

The stellar projected rotational velocity, $v \sin i$, and macroturbulent velocity, V_m , are broadening parameters which need to be defined for modeling spectral lines via spectrum synthesis. A good strategy to estimate rotation and macroturbulent veloc-

Table 3
Adopted Stellar Parameters and Derived Metallicities

Star	T_{eff} (K)	$\log g$ (cm s $^{-2}$)	ξ (km s $^{-1}$)	M (M_\odot)	Age (Gyr)	A(Fe)
HD 17051	6197	4.49	1.24	1.2	1.0	7.73
HD 36435	5503	4.56	1.46	1.0	1.0	7.52
HD 74156	6100	4.36	1.38	1.4	2.5	7.64
HD 82943	6055	4.56	1.33	1.2	1.5	7.79
HD 147513	5904	4.63	1.48	1.0	2.0	7.52
HD 217107	5690	4.44	1.25	1.1	5.5	7.87

ties is to analyze lines which are isolated, unblended, and with similar strengths to the Li line and then apply the same broadening parameters to the Li I synthesis. A few Fe I lines which fall in the same echelle order as the Li I feature were investigated and the Fe I at 6703.567 Å was identified as a clean line which was used to estimate $v \sin i$ and V_m for the studied stars.

A grid of synthetic spectra was computed for combinations of $v \sin i$ and V_m varying between 0 and 10 km s⁻¹ (with steps of 0.1 km s⁻¹). Also, we let the iron abundance vary within 0.05 dex of the abundance value which was obtained for that line. Best fits between synthetic and observed line profiles were obtained from a χ^2 minimization as follows:

$$\chi_r^2 = \frac{1}{(d-1)} \sum_{i=1}^n \frac{(O_i - S_i)^2}{\sigma^2}, \quad (2)$$

where O_i and S_i are, respectively, the observed and synthetic normalized fluxes at a wavelength point i across the line profile; σ is rms error of the continuum, given by $(S/N)^{-1}$; $d = n - p$ is the number of degrees of freedom in the fit, where n is the number of points in the observed spectra used in the fit and p is the number of free parameters in the calculation of the synthetic spectra. In this case, $p = 5$: $v \sin i$ and V_m ; r (continuum level), w (wavelength), and iron abundance $A(\text{Fe})$. Small adjustments in the continuum level ($r \leq 0.4\%$), to account for possible errors in the normalization process were allowed. In addition, shifts in the central wavelengths of the Fe I lines were needed in order to properly match the observed lines.

Since the resolution of the bHROS spectra is $R \sim 143,000$, the velocity resolution is just a bit larger than 2 km s⁻¹. Thus, at low values of $v \sin i$ and typical macroturbulent velocities in stars of the type studied here, the spectra will not be sensitive to changes in low projected rotational velocities found in the program stars. In order to estimate a lower limit to $v \sin i$ that can be detected significantly with the data here, synthetic spectra were computed for the Fe I 6703.567 Å line with a range of values of $v \sin i$, from 1.0 to 3.0 km s⁻¹, a single macroturbulent velocity of 3.0 km s⁻¹ and additionally smoothed to the bHROS resolution, using a model with solar parameters. The synthetic spectra were then sampled at the same scale as bHROS, after which noise was added such that $S/N = 1000$. These “degraded” synthetic spectra were then subjected to the same analysis as the real spectra, with the result that for $v \sin i$ values of 3.0 and 2.5 km s⁻¹ the proper rotational velocities were recovered to within 0.3 km s⁻¹ (close to what the estimated uncertainties are for the target stars). For values of 2.0 and 1.5 km s⁻¹, the analysis yielded a lower and constant value of 1.3 km s⁻¹, indicating that the bHROS spectra are not necessarily sensitive to values of $v \sin i \leq 1.5\text{--}2.0$ km s⁻¹ for typical macroturbulent velocities.

We note, however, that even though the bHROS spectra are not sensitive to projected rotational velocities of less than about 2.0 km s⁻¹, it is still found in the real data that small values of $v \sin i$ provide somewhat better fits to the Fe I line profiles than a combination of larger $v \sin i$ and lower macroturbulence. Although these lower values of $v \sin i$ provide better fits, their detection should not be considered significant, with realistic lower limits of $v \sin i = 1.5$ km s⁻¹.

Figure 3 shows the fit obtained for the star HD 74156. The top panel plot both the observed and best-fit synthetic Fe I line profile as an illustration of the quality of the fits that are obtained in the analysis. The bottom panel illustrates the χ^2 -minimization techniques used for estimating both projected rotational velocity (left) and macroturbulence (right).

The uncertainties in the overall line broadening caused by macroturbulent and projected rotational velocities can be estimated by varying $v \sin i$ (while keeping V_m fixed) in an interval of 1.0 km s⁻¹ around its best value, with steps of 0.05 km s⁻¹. For each value of $v \sin i$, $\Delta\chi_r^2 = \chi_r^2 - \chi_{r,\min}^2$ was calculated

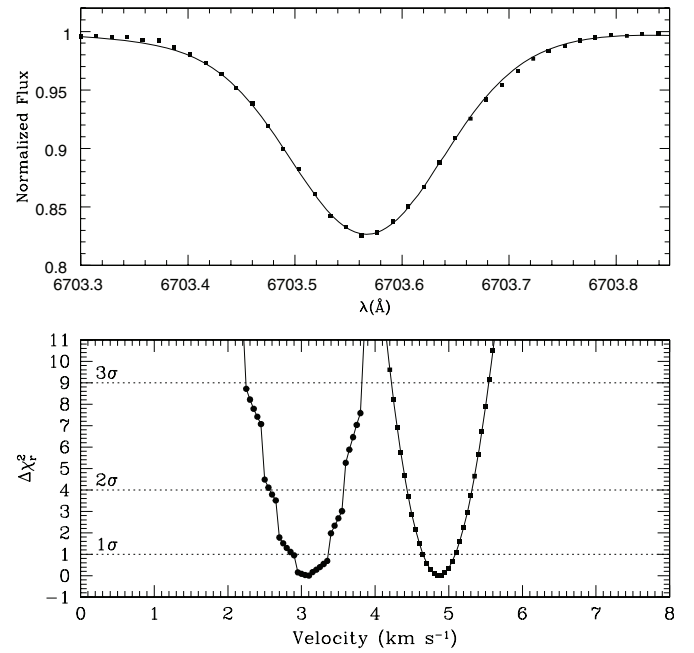


Figure 3. Top panel: observed (filled squares) and synthetic (solid line) spectra for the selected Fe I line which was used to define the broadening parameters in target star HD 74156. The χ_r^2 minimization used for estimating $v \sin i$ (filled circles; left) and V_m (filled squares; right) is shown in the bottom panel.

Table 4
Elemental Abundances and Isotopic Ratios

Star	$v \sin i$ (km s ⁻¹)	V_m (km s ⁻¹)	$A(\text{Li})$	⁶ Li/ ⁷ Li
Sun	1.70	2.80	0.96	0.00
HD 17051	4.90 ± 0.25	5.25 ± 0.30	2.48 ± 0.01	0.03 ± 0.04
HD 36435	4.25 ± 0.20	2.95 ± 0.30	1.60 ± 0.03	0.06 ± 0.08
HD 74156	3.10 ± 0.25	4.85 ± 0.25	2.59 ± 0.01	0.00 ± 0.03
HD 82943	≤ 1.5	3.60 ± 0.10	2.49 ± 0.01	0.00 ± 0.02
HD 147513	≤ 1.5	3.05 ± 0.10	2.03 ± 0.01	0.02 ± 0.03
HD 217107	≤ 1.5	2.85 ± 0.10	≤ 0.36	0.00 ± 0.04

and the velocity change which produced a 1σ change in $\Delta\chi_r^2$ was taken as the uncertainty. The uncertainties in V_m were obtained in a similar manner. The adopted broadening parameters and uncertainties are presented in Table 4.

3.2.2. Convection and Line Asymmetries

The additional small radial velocity shifts noted above represent convective shifts which are related to the effects of granulation in the stellar atmospheres (see discussion in Allende Prieto et al. 2002). Figure 4 shows the trend of radial velocity shifts applied as a function of the measured equivalent widths for target star HD 82943 and the Sun. The trend of increasingly positive radial velocities as the equivalent widths increase has been noted previously by Allende Prieto et al. (2002), Reddy et al. (2002), and Mandell et al. (2004). All three of these studies measured the Sun and fit straight lines to the trends with slopes and intercepts, respectively, of: $2.9 \text{ m s}^{-1} (\text{mÅ})^{-1}$ and 80 m s^{-1} (Allende Prieto et al. 2002); $2.8 \text{ m s}^{-1} (\text{mÅ})^{-1}$ and 120 m s^{-1} (Reddy et al. 2002); $4.2 \text{ m s}^{-1} (\text{mÅ})^{-1}$ and 30 m s^{-1} (Mandell et al. 2004). Since different Fe lines were used by the different groups, as well as different fitting techniques, the differences between the trends are not surprising and do not lead to significant differences in convective shifts. The results reported here

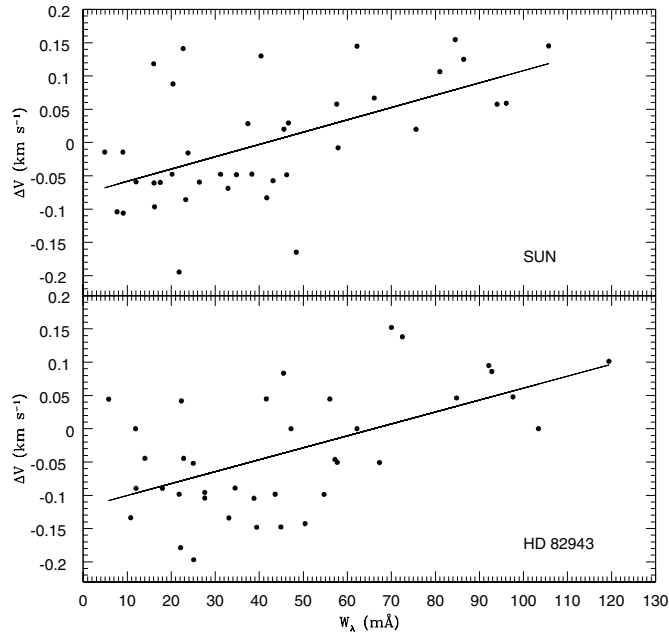


Figure 4. Convective shifts measured for Fe I lines in the solar spectrum (top panel) and HD 82943 (bottom panel). The solid lines in each panel represent the least-squares fits to the points.

for the Sun are a slope of $2.0 \text{ m s}^{-1} (\text{m}\text{\AA})^{-1}$ and an intercept of -80 m s^{-1} .

Solar-type stars are known to display slight red asymmetries in spectral lines due to the convective motions of granules (e.g., Allende Prieto et al. 2002); the flux across the line is dominated by hot, rising granules, while the cooler, falling (i.e., redshifted) intergranular regions produce the small red asymmetries. The line bisector for the Fe I 6703.567 Å line is shown in Figure 5, where it is plotted as flux level versus velocity (in m s $^{-1}$) instead of wavelength. A detailed discussion of stellar line bisectors can be found in Gray (2005). The filled squares are the observed points in HD 82943, while the open squares were derived from a synthesis of this region using a standard one-dimensional model, which necessarily produces a symmetric line profile. The synthetic profile shows a vertical bisector, indicating an isolated symmetric line (demonstrating that the Fe I 6703.567 Å line is good for determining broadening parameters). The observed line bisector in HD 82943 deviates to the red due to convective granules; the magnitude of the convective asymmetry is manifested as an $\sim 200 \text{ m s}^{-1}$ excursion in the line bisector. The shape and amplitude of this bisector are typical for stars of this type and represent a rather small perturbation of the line profile.

3.3. The Line List

The determination of the ${}^6\text{Li}/{}^7\text{Li}$ isotopic ratio rests upon modeling the shape of the Li I line profile, which depends not only on the isotopic ratios themselves, but also on the stellar broadening mechanisms discussed in the previous section. In addition, the shape of the Li I profile is affected by several weak absorption features that fall within the wavelength region of the various lithium transitions. There are several weak lines of CN and other metal absorption lines that will blend with ${}^6\text{Li}$, thus a detailed compilation and careful assessment of line lists is a critical ingredient for the analysis.

As mentioned in Section 1, the search for ${}^6\text{Li}$ in planet-hosting stars has been the subject of a few recent studies and line lists for the Li I region are available in the literature. As a starting point

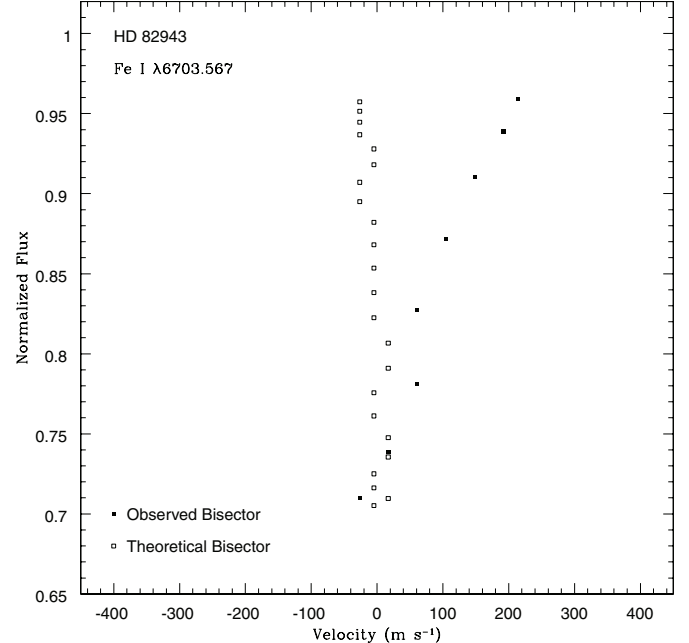


Figure 5. Synthetic (open squares) and observed (filled squares) line bisectors measured for Fe I at 6703.567 Å. The asymmetry to the red in the observed profile is indicative of photospheric velocity fields. The errors in the bisectors are largest in the central portion of the line.

in this analysis, we adopted the line list from the most recent and complete study to date by Mandell et al. (2004). The list of lines and atomic data (gf -values and wavelengths) carefully compiled by the authors were adjusted in that study to fit the Kurucz et al. (1984) solar spectrum. In addition, a laboratory carbon arc spectrum was used to adjust the CN lines (in both wavelengths and gf -values) in comparison to theoretical line lists. As for the three possibilities for the unidentified feature at 6708.025 Å listed by Mandell et al. (2004; Si I, Ti I, and Ti II) we adopted the Si I line. Recall that Mandell et al. (2004) found no significant differences in the ${}^6\text{Li}/{}^7\text{Li}$ ratios derived using the three different lines. The first step here was to return all atomic data in their line list to those values appearing in the original references. The CN molecular data were kept the same as in Mandell et al. (2004).

This initial line list was checked via comparisons between the solar flux spectrum from Kurucz et al. (1984) and synthetic spectra which are based on the models and synthesis code adopted in this analysis. The solar spectrum was modeled using an ATLAS9 ODFNEW model with $T_{\text{eff}} = 5777 \text{ K}$, $\log g = 4.44$, and $\xi = 1.24 \text{ km s}^{-1}$. The broadening parameters adopted were obtained from fits to the unblended Fe I line at 6703.567 Å: $v \sin i = 1.70 \text{ km s}^{-1}$, $V_m = 2.80 \text{ km s}^{-1}$. The limb darkening coefficient, ϵ , was taken from Van Hamme (1993); however, the choice of ϵ has little effect on the Li I line profile and no measurable impact on the estimation of ${}^6\text{Li}$ isotopic fractions. The comparison of observed solar spectrum and synthesis in the small wavelength interval around the Li I feature was improved by a small continuum adjustment of 0.25%. In addition, small wavelength corrections to the nearby Fe I line (-0.003 \AA) and to Li I ($+0.002 \text{ \AA}$) line led to a better fit; these wavelength corrections are those expected due to convective shifts in the solar photosphere (see Section 3.2.2). A small change in the Fe I gf -value of +0.015 dex improved the fit to the Fe I profile, while the accurate laboratory gf -values for the Li I components were maintained.

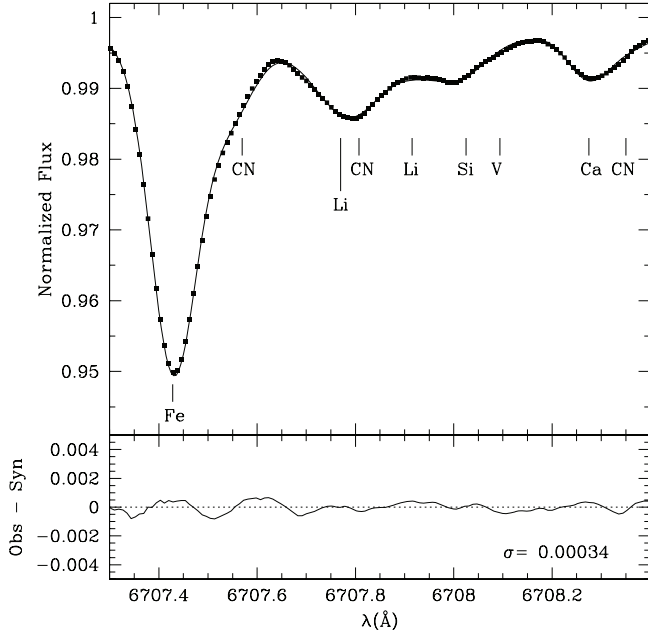


Figure 6. Synthetic solar spectrum (solid line) computed with the line list in Table 5. The main lines contributing to the synthesis are identified. The observed solar spectrum (filled squares) is from Kurucz et al. (1984). The bottom panel shows the differences between model and observations; the overall agreement is excellent.

Within the scope of the above changes, the fit to the solar spectrum exhibited some small mismatch, especially near 6708.275 Å, where there appeared additional absorption. The absorption in this region was attributed to an Mg I line by Mandell et al. (2004) and a V I line by Reddy et al. (2002). No references to either of these lines could be found in a literature search, whereas King et al. (1997) attributed the absorption at this wavelength to a Ca I line (present in VALD-2). There were other small differences between the line lists: in the narrow region from 6708.31 to 6708.54 Å the Mandell et al. list contained four CN lines while King et al. had two (at 6708.375 and 6708.635 Å). We included the Ca I line plus the two adjacent CN lines; some of the gf -values were changed somewhat and wavelengths allowed to shift by 0.001 Å in order to improve the fit to the solar spectrum. The final line list adopted in this study is presented in Table 5. The best fit to the solar spectrum achieved with this line list was excellent and this is shown in Figure 6. The best fit was obtained for $A(\text{Li}) = 0.96$, which is very close to what was found by both King et al. (1997) and Reddy et al. (2002), and within 0.1 dex of the recommended value in Asplund et al. (2005).

4. LITHIUM ABUNDANCES AND ISOTOPIC RATIOS

As discussed previously, several blending lines due to metals and CN affect the shape of the Li I feature in metal-rich stars. It is possible to study which of these potentially offending lines have the largest effects on the ^6Li absorption via test spectrum syntheses which can isolate each of the nearby lines.

Synthetic spectra were generated to focus on lithium and each of the possible blending species in turn: CN, Si I, Ca I, and V I. In the case of CN, the main impact on ^6Li comes from 6707.807 Å which falls slightly blueward (~ 0.10 Å) of most of the ^6Li absorption and does not affect the derived abundances significantly. The Ca I line at 6708.275 Å falls too far to the red to affect ^6Li , while V I at 6708.094 Å is too weak to even be detectable. The biggest effect on ^6Li absorption comes from the

Table 5
The Line List

λ (Å)	Identification	LEP (eV)	$\log g f$ (dex)	Original Reference
6706.548	CN $Q_2(93)$ (11,5)	3.130	-1.359	M04
6706.567	CN $Q_2(80)$ (8,3)	2.190	-1.650	M04
6706.657	CN $R_{12}(22)$ (7,3)	0.870	-3.001	M04
6706.733	CN $Q_1(22)$ (7,3)	0.870	-1.807	M04
6706.844	CN $R_1(34)$ (12,7)	1.960	-2.775	M04
6706.863	CN $P_2(83)$ (7,2)	2.070	-1.882	M04
6706.880	Fe II	5.956	-4.504	V
6706.980	Si I	5.954	-2.797	V
6707.205	CN $Q_2(47)$ (11,6)	1.970	-1.222	M04
6707.282	CN $Q_2(60)$ (10,5)	2.040	-1.333	M04
6707.371	CN $Q_1(85)$ (12,6)	3.050	-0.522	M04
6707.431	Fe I	4.608	-2.268	R02
6707.457	CN $P_{12}(13)$ (7,3)	0.790	-3.055	M04
6707.470	CN $Q_1(28)$ (12,7)	1.880	-1.451	M04
6707.473	Sm II	0.933	-1.477	V
6707.518	V I	2.743	-1.995	V
6707.545	CN $Q_2(44)$ (6,2)	0.960	-1.548	M04
6707.595	CN $Q_2(29)$ (12,7)	1.890	-1.851	M04
6707.596	Cr I	4.208	-2.767	V
6707.645	CN $P_2(44)$ (6,2)	0.960	-2.460	M04
6707.740	Ce II	0.500	-3.810	R02
6707.752	Sc I	4.049	-2.672	V
6707.756	^7Li	0.000	-0.428	H99
6707.768	^7Li	0.000	-0.206	H99
6707.771	Ca I	5.796	-4.015	R02
6707.807	CN $R_1(64)$ (5,1)	1.210	-1.853	M04
6707.848	CN $R_1(61)$ (19,12)	3.600	-2.417	M04
6707.899	CN $P_2(39)$ (20,13)	3.360	-3.110	M04
6707.907	^7Li	0.000	-1.509	H99
6707.908	^7Li	0.000	-0.807	H99
6707.919	^7Li	0.000	-0.807	H99
6707.920	^6Li	0.000	-0.479	H99
6707.920	^7Li	0.000	-0.807	H99
6707.923	^6Li	0.000	-0.178	H99
6707.930	CN $Q_2(35)$ (12,7)	1.980	-1.651	M04
6707.964	Ti I	1.879	-6.903	V
6707.980	CN $R_{21}(72)$ (10,5)	2.390	-2.027	M04
6708.023	Si I	6.000	-2.910	I03
6708.026	CN $R_2(35)$ (12,7)	1.980	-2.031	M04
6708.073	^6Li	0.000	-0.303	H99
6708.094	V I	1.218	-3.113	V
6708.147	CN $P_2(42)$ (11,6)	1.870	-1.434	M04
6708.275	Ca I	2.710	-3.377	K97
6708.375	CN	1.979	-1.097	K97
6708.499	CN	1.868	-1.423	K97
6708.577	Fe I	5.446	-2.728	V
6708.635	CN $P_2(42)$ (11,6)	1.870	-1.584	M04

References. (H99) Hobbs et al. (1999); (I03) Israelian et al. (2003); (K97) King et al. (1997); (M04) Mandell et al. (2004); (R02) Reddy et al. (2002); and (V) VALD-2 (Kupka et al. 1999).

blending line due to Si I at 6708.023 Å, where its absorption falls on the red side of possible ^6Li absorption. Even here, absorption from ^6Li that is about 1% deep would compete with Si I (at solar metallicity) and be detectable. These tests indicate that ^6Li absorption which is $\sim 1\%$ deep would be marginally detected, while larger amounts of ^6Li that would produce absorption of only a few percent would be detectable.

The important goal is to obtain an overall good fit across the entire Li region from 6707.3 Å to 6708.4 Å and this includes fitting the nearby feature just blueward of Li I which is mainly Fe I with some contribution from CN. Also, a close region nearly free of spectral lines (6706.40–6706.55 Å) is useful

for providing an estimate of the local continuum level, while the wavelengths of Fe I (6707.431 Å) and Li I were adjusted slightly to take into account convective shifts (see Figure 4). The abundances of Ca and V were allowed to vary within ± 0.2 dex in order to improve the overall fits to the observed spectra, as well as adjusting C and N to fit the blue CN feature. The final values, or limits, to ${}^6\text{Li}$ were set by a χ^2 minimization of $A(\text{Li})$, ${}^6\text{Li}/{}^7\text{Li}$, and $A(\text{Si})$ simultaneously.

Lithium abundances and isotopic ratios are given in Table 4 for the six target stars and the best fit obtained for HD 82943 is shown in Figure 7 as an example. The uncertainties estimated for the Li abundances and isotopic ratios were derived in a manner similar to that used for the rotational and macroturbulent velocities. The total lithium abundance was varied (but keeping ${}^6\text{Li}/{}^7\text{Li}$ fixed) in steps of 0.001 dex, with the χ^2 computed for each value. A change in χ^2 of 1 was taken to define the $\pm 1\sigma$ value of $A(\text{Li})$. The uncertainty in the isotopic ratio was determined in an analogous way, with ${}^6\text{Li}/{}^7\text{Li}$ values varied in steps of 0.005 and the total Li abundance being fixed. The errors in $A(\text{Li})$ and ${}^6\text{Li}/{}^7\text{Li}$ are also shown in Table 4.

In order to further test the sensitivity of our method to the isotopic ratios, synthetic spectra were computed for six values of the ${}^6\text{Li}/{}^7\text{Li}$ ratio (between 0.00 and 0.05 with a step of 0.01) adopting the stellar parameters derived for HD 82943. These model spectra were then sampled at the same scale as bHROS, after which noise was added such that $S/N = 750$ (typical S/N for our observations). These “degraded” synthetic spectra were then subjected to the same analysis as the real spectra and we were able to recover isotopic ratios within ± 0.01 , demonstrating an analysis sensitivity of 0.01 for ${}^6\text{Li}/{}^7\text{Li}$.

As an additional test, we used the line list in Israelian et al. (2003) in order to analyze the target star HD 82943. The line list adopted in that study is identical to that used by Reddy et al. (2002), except for having a Si I line at 6708.025 Å instead of a Ti I line. All the input parameters (model atmospheres, broadening parameters, and convective shifts for the Li I and the nearby Fe I line) and the analysis method employed were the same as described above; the only difference being the removal of the Ca abundance as a free parameter because the feature at ~ 6708.275 Å is attributed to V I in Israelian et al.’s list. The best fit between model and observations was achieved for $A(\text{Li}) = 2.49$ and ${}^6\text{Li}/{}^7\text{Li} = 0.01$, which are in excellent agreement with the obtained results using the line list in Table 5. The derived isotopic ratio for this star, however, is significantly lower than the value derived in Israelian et al. (2003); although the Li abundances in the two studies agree well.

5. DISCUSSION

5.1. Three-Dimensional Model Atmospheres and their Impact on the One-Dimensional ${}^6\text{Li}$ Results

As discussed in Section 3.2.2, convective granules result in small red asymmetries in the spectral lines of solar-type stars, such as those analyzed here for ${}^6\text{Li}$. Since the ${}^6\text{Li}$ components of the neutral lithium ground-state doublet fall to the red of the ${}^7\text{Li}$ transitions and because ${}^6\text{Li}$ is expected to be much less abundant than ${}^7\text{Li}$, the presence of ${}^6\text{Li}$ will result in a slight red asymmetry to the combined Li I feature. Since both convection and ${}^6\text{Li}$ can result in a red asymmetric profile, a discussion of the expected convective asymmetries to the Li I feature must be included in order to interpret either detections or upper limits to ${}^6\text{Li}$ fractions.

A more realistic theoretical treatment of the convective motions that cause red asymmetric line profiles has been included

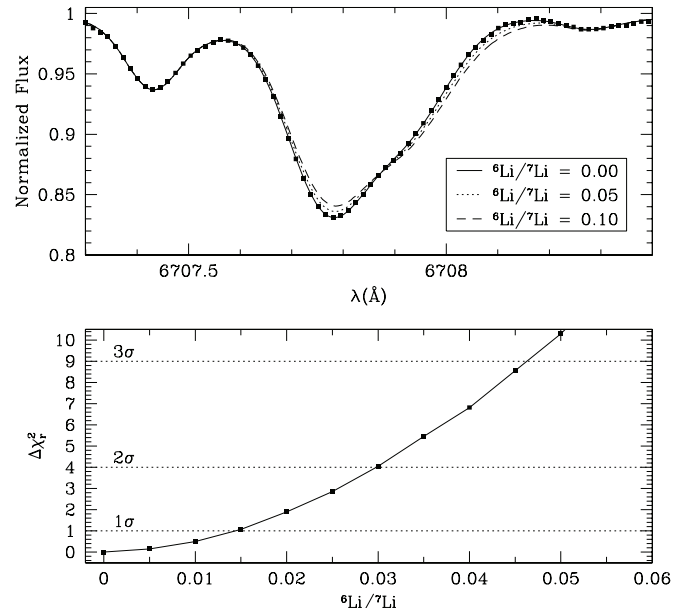


Figure 7. Observed and synthetic Li I profiles for HD 82943. The syntheses were calculated for ${}^6\text{Li}/{}^7\text{Li}$ isotopic ratios of 0%, 5%, and 10%. The χ^2 minimization of the ${}^6\text{Li}/{}^7\text{Li}$ isotopic ratio is shown in the bottom panel. The best fit is obtained for a synthetic spectrum with zero contribution from ${}^6\text{Li}$.

in model stellar atmospheres via the incorporation of radiative hydrodynamical convection, e.g., Stein & Nordlund (1998) or Asplund et al. (2000). The resulting model atmospheric structures are three-dimensional, time-dependent and contain self-consistent convective flows; such models, often referred to as “3-dimensional models,” naturally produce absorption lines with small red asymmetries. Recent analyses of the Li I line profiles in stars that span the T_{eff} range of the program stars here (although mostly for much more metal-poor halo dwarfs and subgiants) have included a discussion of effects due to three-dimensional models (Asplund et al. 2006; Cayrel et al. 2007, 2008).

Asplund et al. (2006) determined ${}^6\text{Li}$ abundances for a set of 24 metal-poor halo dwarfs and subgiants based on very high quality spectra acquired with the ESO VLT/UVES. The authors found detections of ${}^6\text{Li}$ at the 2σ significance level in nine stars. They also showed that the isotopic ratio ${}^6\text{Li}/{}^7\text{Li}$ is effectively immune to changes in the stellar parameters (at the levels of ± 100 K, ± 0.2 dex, ± 0.2 dex, and $\pm 0.5 \text{ km s}^{-1}$ in T_{eff} , $\log g$, [Fe/H], and microturbulent velocity, respectively). Another important result is that the usage of three-dimensional model atmospheres in LTE (when compared with one-dimensional models also in LTE) does not change significantly the derived ${}^6\text{Li}$ fractions from synthesis of the Li I 6707.8 Å line, suggesting that one-dimensional models are essentially as good as three-dimensional models when employing LTE analyses. Finally, the authors observe that one-dimensional ${}^6\text{Li}/{}^7\text{Li}$ isotopic ratios are, in general, similar or lower than those derived from three-dimensional LTE calculations. The average three-dimensional – one-dimensional difference is +0.008 and the largest value is +0.033. In only three cases are the three-dimensional values smaller (-0.010 , -0.015 , and -0.017) than the corresponding ones for the one-dimensional case. These results suggest that the upper limits for the isotopic ratios set here would probably increase if the analysis had been done with three-dimensional models. However, the maximum increase would be compatible with the typical errors in the isotopic ratios.

More recently, Cayrel et al. (2007) showed that convection-induced line asymmetries could mimic the presence of ${}^6\text{Li}$,

at the few percent level, for the halo turnoff metal-poor star HD 74000. Note that Smith et al. (1998) found $^6\text{Li}/^7\text{Li} = 0.00 \pm 0.02$ for this star via a one-dimensional analysis, similar to the analysis performed in this study. The Cayrel et al. (2007) result was based on a three-dimensional hydrodynamical simulation for a single set of atmospheric parameters, while Cayrel et al. (2008) presented theoretical line asymmetries for a range of atmospheric parameters that cover the values of the stars from Asplund et al. (2006). Note that a three-dimensional-non-LTE (NLTE) treatment, the most adequate for the Li I analysis according to Asplund et al. (2006), is used by Cayrel et al. (2007, 2008). The authors compute an asymmetry of about 2%, which is exactly the mean value of $^6\text{Li}/^7\text{Li}$ for the stars from Asplund et al. (2006). Also, Cayrel et al. (2008) investigate the dependence of these asymmetries on the stellar parameters T_{eff} , $\log g$, and $[\text{Fe}/\text{H}]$. Based on a small grid of eight hydrodynamical simulations, they predict an increase in the Li I line asymmetry with metallicity for $[\text{Fe}/\text{H}] \geq -2.0$. Also, they find that hotter stars with lower gravities show larger asymmetries than cooler stars with higher gravities.

Given the tight limits on ^6Li fractions derived here via one-dimensional measurements, combined with the Cayrel et al. (2008) predictions that there may be expected line asymmetries of the order of or larger than $\sim 2\%$ for more metal-rich stars, there is no evidence of detectable ^6Li in the six stars studied here. The average value of $^6\text{Li}/^7\text{Li}$ for the six stars in Table 5, inversely weighted by their respective uncertainties, is $^6\text{Li}/^7\text{Li} = 0.012$, which is consistent with zero ^6Li within the errors. If the nonplanet-hosting star, HD 36435, is rejected from the average due to its low S/N spectrum (Table 1), the weighted average for the five stars with planets is even lower: $^6\text{Li}/^7\text{Li} = 0.008$. With limits close to zero, these results can also provide tests on the three-dimensional models and NLTE analyses.

5.2. Limits on Accreted Mass

An approximate upper limit to the number of ^6Li atoms in the atmospheres of the target stars can be estimated by combining limits to the number of ^6Li atoms with the convective zone masses. To carry out this exercise, we use the convective zone masses for main-sequence stars presented in Pinsonneault et al. (2001) in their Figure 1. This is a simple estimate which assigns a single convective zone mass to the target stars (see Table 6) based on their effective temperatures, but will provide a rough upper limit on the number of ^6Li atoms present in the outer layers of stellar atmospheres. The ^6Li abundance is set by the $^6\text{Li}/^7\text{Li}$ values in Table 4; in those stars where this value is 0.00, the limit is set to the 1σ uncertainty. Table 6 presents the resulting limits to the number of ^6Li atoms. In addition, the ^6Li abundances are translated to upper limits of accreted mass in Jovian masses. This is an admittedly naive estimate, but does provide a framework in which to limit the amount of accretion that could have occurred on the surfaces of these five planet-hosting stars.

Accretion limits of a fraction of a Jovian mass are typical values derived by both Mandell et al. (2004) and Reddy et al. (2002). The tightest accretion limit set here is for the coolest star, HD 217107, due to the increasing strength of the Li I line with decreasing T_{eff} ; this star has a very low total lithium abundance with a corresponding low limit of ^6Li . The tighter limit on HD 217107 is perhaps also the most interesting from this sample, as this star is the only one with a very closely orbiting massive planet, with a $\sin i = 0.073$ AU and $M_{\text{planet}} \sin i = 1.33 M_{\text{Jup}}$.

Table 6
Mass Accretion Limits

Star	$\log M_{\text{CZ}}$ (M_{\odot})	N (^6Li)	M_{acc} (M_{Jup})
HD 17051	-2.44	$< 4.6 \times 10^{43}$	< 0.33
HD 74156	-2.23	$< 1.0 \times 10^{44}$	< 0.71
HD 82943	-2.15	$< 6.2 \times 10^{43}$	< 0.44
HD 147513	-1.90	$< 3.8 \times 10^{43}$	< 0.27
HD 217107	-1.66	$< 2.9 \times 10^{42}$	< 0.02

While the nondetections of ^6Li , at levels 1%–2% of total lithium, are secure limits, the interpretation of this lack of ^6Li in light of accretion rests on details of stellar evolution. Montalbán & Rebolo (2002) have presented calculations of the expected evolution of the ^6Li abundance as a function of time after ingestion for various stellar model masses and metallicities. Within the standard model framework of stellar evolution, where there is no exchange of material between the convective envelope and the radiative interior, accreted ^6Li would survive for gigayears in main-sequence stars with $M \geq 1.0\text{--}1.1 M_{\odot}$ and having metallicities of $[\text{Fe}/\text{H}] = 0.0$ and $+0.3$ (Montalbán & Rebolo 2002). These types of stellar masses encompass most of the target stars studied here, thus the limits would suggest that any accretion of planetary material was typically less than a few to several tenths of a Jovian mass.

When stellar evolution with nonstandard transport processes, such as microscopic diffusion or turbulent mixing, is used to investigate the fate of ^6Li on the surface of solar-type stars, the interpretation becomes more complex, as discussed by Montalbán & Rebolo (2002). Both diffusion and turbulent mixing act to move material between the convective surface layer and the deeper radiative interior, with the result that accreted ^6Li will be removed from the photosphere and destroyed. The efficiency of this destruction is a function of stellar mass, metallicity, and the time at which ^6Li is accreted. For warmer effective temperatures, $T_{\text{eff}} \geq 6100$ K, the survival of detectable quantities of ^6Li can exceed a gigayear, thus if accretion takes place after such stars settle onto the main sequence, there would be measurable amounts of ^6Li in some of these stars. Large, sensitive surveys for ^6Li remain useful ways to probe and constrain accretion.

6. CONCLUSIONS

The main conclusion drawn from the analysis presented here is that no detections of ^6Li are found in five planet-hosting stars which span the T_{eff} range of 5700–6100 K, masses from ~ 1.1 to $1.4 M_{\odot}$, and metallicities from $[\text{Fe}/\text{H}] \sim +0.1$ to $+0.4$. Since the hotter, more massive of the solar-type stars have the least-massive convection zones, the stars studied here would be some of the best candidates for detecting signatures of accretion. The combination of high spectral resolution with high S/N makes this search one of the most sensitive and the results here can be combined with previous studies (Reddy et al. 2002; Mandell et al. 2004) to provide strong limits on accretion of ^6Li .

We acknowledge the financial support of CNPq. We thank Jeremy King for discussions and for providing the line list for the spectral region between 6700 and 6720 Å. K.C. thanks Martin Asplund for discussions. We thank the anonymous referee for useful comments that helped improve the paper.

This study is based on observations obtained at the Gemini Observatory, which is operated by the Association of Universities for Research in Astronomy, Inc., under a cooper-

ative agreement with the NSF on behalf of the Gemini partnership: the National Science Foundation (USA), the Science and Technology Facilities Council (UK), the National Research Council (Canada), CONICYT (Chile), the Australian Research Council (Australia), Ministério da Ciência e Tecnologia (Brazil), and Ministerio de Ciencia, Tecnología e Innovación Productiva (Argentina). Observations were obtained in the following Gemini programs: GS-2006A-C-5 and GS-2006B-Q-47. Research here is supported in-part by NASA grant NNG08AJ58I. Support for Simon C. Schuler has been provided by the NOAO Leo Goldberg Fellowship; NOAO is operated by the Association of Universities for Research Astronomy (AURA), Inc., under a cooperative agreement with the National Science Foundation.

Facility: Gemini:South(bHROS)

REFERENCES

- Allende Prieto, C., Asplund, M., García López, R. J., & Lambert, D. L. 2002, *ApJ*, **567**, 544
- Asplund, M., Grevesse, N., & Sauval, A. J. 2005, in ASP Conf. Ser. 336, Cosmic Abundances as Records of Stellar Evolution and Nucleosynthesis, ed. F. N. Bash & T. G. Barnes (San Francisco, CA: ASP), 25
- Asplund, M., Lambert, D. L., Nissen, P. E., Primas, F., & Smith, V. V. 2006, *ApJ*, **644**, 229
- Asplund, M., Nordlund, Å., Trampedach, R., Allende Prieto, C., & Stein, R. F. 2000, *A&A*, **359**, 729
- Castelli, F., & Kurucz, R. L. 2004, in Proc. IAU Symp. 210, Modelling of Stellar Atmospheres ed. N. Piskunov, et al. (Dordrecht: Kluwer), poster A20 (arXiv:[astro-ph/0405087](#))
- Cayrel, R., Steffen, M., Bonifacio, P., Ludwig, H.-G., & Caffau, E. 2008, arXiv:[0810.4290](#)
- Cayrel, R., et al. 2007, *A&A*, **473**, L37
- Ecuillon, A., Israeli, G., Santos, N. C., Mayor, M., & Gilli, G. 2006, *A&A*, **449**, 809
- Fischer, D. A., & Valenti, J. 2005, *ApJ*, **622**, 1102
- Girardi, L., Bertelli, G., Bressan, A., Chiosi, C., Groenewegen, M. A. T., Marigo, P., Salasnich, B., & Weiss, A. 2002, *A&A*, **391**, 195
- Girardi, L., Bressan, A., Bertelli, G., & Chiosi, C. 2000, *A&AS*, **141**, 371
- Gonzalez, G. 1997, *MNRAS*, **285**, 403
- Gonzalez, G., Laws, C., Tyagi, S., & Reddy, B. E. 2001, *AJ*, **121**, 432
- Gray, D. F. 2005, The Observation and Analysis of Stellar Photospheres (3rd ed.; Cambridge: Cambridge Univ. Press)
- Hobbs, L. M., Thorburn, J. A., & Rebull, L. M. 1999, *ApJ*, **523**, 797
- Israelian, G., Santos, N. C., Mayor, M., & Rebolo, R. 2001, *Nature*, **411**, 163
- Israelian, G., Santos, N. C., Mayor, M., & Rebolo, R. 2003, *A&A*, **405**, 753
- King, J. R., Deliyannis, C. P., Hiltgen, D. D., Stephens, A., Cunha, K., & Boesgaard, A. M. 1997, *AJ*, **113**, 1871
- Kupka, F., Piskunov, N., Ryabchikova, T. A., Stempels, H. C., & Weiss, W. W. 1999, *A&AS*, **138**, 119
- Kurucz, R. L., Furenlind, I., Brault, J., & Testerman, L. 1984, Solar Flux Atlas from 296 to 1300 nm (Cambridge: Harvard Univ. Press)
- Laws, C., Gonzalez, G., Walker, K. M., Tyagi, S., Dodsworth, J., Snider, K., & Sunzrteff, N. B. 2003, *AJ*, **125**, 2664
- Mandell, A. M., Ge, J., & Murray, N. 2004, *AJ*, **127**, 1147
- Montalbán, J., & Rebolo, R. 2002, *A&A*, **386**, 1039
- Müller, E. A., Peytremann, E., & de la Reza, R. 1975, *Sol. Phys.*, **41**, 53
- Pasquini, L., Döllinger, M. P., Weiss, A., Girardi, L., Chavero, C., Hatzes, A. P., da Silva, L., & Setiawan, J. 2007, *A&A*, **473**, 979
- Pinsonneault, M. H., DePoy, D. L., & Coffee, M. 2001, *ApJ*, **556**, L59
- Pollack, J. B., Hubickyj, O., Bodenheimer, P., Lissauer, J. J., Podolak, M., & Greenzweig, Y. 1996, *Icarus*, **124**, 62
- Ramírez, I., & Meléndez, J. 2004, *ApJ*, **609**, 417
- Reddy, B. E., Lambert, D. L., Laws, C., Gonzalez, G., & Covey, K. 2002, *MNRAS*, **335**, 100
- Santos, N. C., Israeli, G., & Mayor, M. 2000, *A&A*, **363**, 228
- Santos, N. C., Israeli, G., Mayor, M., Bento, J. P., Almeida, P. C., Sousa, S. G., & Ecuvillon, A. 2005, *A&A*, **437**, 1127
- Schuler, S. C., Margheim, S. J., Thirupathi, S., Asplund, M., Smith, V. V., Cunha, K., & Beers, T. C. 2008, *AJ*, **136**, 2244
- Smith, V. V., Lambert, D. L., & Nissen, P. E. 1998, *ApJ*, **506**, 405
- Sneden, C. 1973, PhD thesis, Univ. Texas, Austin
- Stein, R. F., & Nordlund, Å. 1998, *ApJ*, **499**, 914
- Thévenin, F. 1990, *A&AS*, **82**, 179T
- Van Hamme, W. 1993, *AJ*, **106**, 2096

Capítulo 6

Conclusões e Perspectivas Futuras

Nesta tese, determinamos parâmetros atmosféricos e evolutivos, metalicidades, abundâncias de lítio e velocidades de rotação projetadas para uma amostra de 148 estrelas com planetas e 160 estrelas de comparação do disco Galáctico (sem planetas detectados). Adicionalmente, derivamos razões isotópicas de ${}^6\text{Li}/{}^7\text{Li}$ para 5 destas estrelas com planetas. Os resultados desta análise homogênea foram divididos em 4 artigos (apresentados nos capítulos 2, 3, 4 e 5 desta tese) e nos permitem obter as seguintes conclusões:

1. Uma diferença de 0,15 dex foi encontrada para as metalicidades médias das estrelas de seqüência principal com ($N = 117$) e sem ($N = 145$) planetas, sendo as primeiras mais ricas. Este resultado basicamente confirma as conclusões obtidas por inúmeros estudos anteriores na literatura (por exemplo, Santos et al. 2005, Fischer & Valenti 2005 e Sousa et al. 2008). Devemos ressaltar que as amostras analisadas não foram selecionadas com base em nenhum critério rigoroso, a não ser a presença ou não de planetas. A lista de estrelas sem planetas possui uma tendência a incluir objetos mais ricos, ao passo que algumas estrelas com planetas faziam parte dos programas de procura por planetas devido às suas altas metalicidades.
2. A variação da metalicidade com a massa é muito similar para as anãs com e sem planetas. Este resultado indica que não houve acresção de material sólido às atmosferas das primeiras. Caso este fenômeno tivesse ocorrido, deveríamos observar metalicidades maiores para as estrelas de maior massa com planetas (pois elas possuem as menores zonas convectivas).

3. A amostra estudada contém 9 estrelas de seqüência principal com pelo menos um planeta netuniano. Dentre estes sistemas, 4 também possuem planetas gigantes e 5 têm apenas planetas netunianos. Testes estatísticos revelaram que, provavelmente, há uma diferença real entre as distribuições de metalicidades das estrelas que têm apenas planetas netunianos ($N = 5$) e aquelas que possuem pelo menos um planeta gigante ($N = 112$). As primeiras parecem não favorecer objetos mais ricos em metais. Este resultado é diferente do que foi obtido por Sousa et al. (2008). Os autores mostram que tanto estrelas com apenas planetas netunianos ou pelo menos um objeto deste tipo possuem metalicidades mais baixas do que as estrelas com planetas gigantes somente. Esta tese confirma apenas a primeira conclusão.
4. A inclusão de metalicidades da literatura para estrelas de tipo F, G e K com apenas planetas netunianos estende esta amostra para 15 objetos e confirma os resultados anteriores. Algumas estrelas de tipo M também possuem apenas planetas netunianos ($N = 4$). Entretanto, nossos resultados mostram que a consideração destes objetos deve ser feita com cautela, visto que as determinações de suas metalicidades ainda possuem elevadas incertezas.
5. Os resultados dos dois itens anteriores sugerem uma possível conexão entre as metalicidades das estrelas e as massas dos maiores planetas do sistema. Valores menores de $[Fe/H]$ produziriam massas menores para o maior planeta do sistema. Estas conclusões estão de acordo com o cenário do enriquecimento primordial e o modelo de acresção do núcleo. No entanto, elas devem ser analisadas com cautela devido ao pequeno número de estrelas com planetas netunianos apenas. O aumento da precisão nos métodos de detecção de planetas deve mudar drasticamente esta situação nos próximos anos.
6. As metalicidades médias das anãs ($N = 117$) e gigantes ($N = 16$) com planetas diferem por 0,17 dex, sendo as últimas mais pobres. Se incluirmos as metalicidades da literatura para outras gigantes que têm planetas (totalizando 37 objetos), a diferença fica um pouco maior (0,23 dex), mas confirma o resultado anterior.
7. A metalicidade média das subgigantes com planetas ($N = 15$) é idêntica a das anãs ($N = 117$) e 0,21 dex maior do que a metalicidade média das subgigantes sem planetas (N

$= 14$). Esta diferença entre as subgigantes com e sem planetas é consistente (dentro das incertezas) com aquela que encontramos para as anãs (0,15 dex). Além disso, nenhuma tendência foi observada no gráfico $[Fe/H]$ versus T_{ef} para as subgigantes com planetas. Estes dois resultados indicam que não houve o processo de diluição, favorecendo o cenário do enriquecimento primordial. Esta conclusão é contrária a de Pasquini et al. (2007).

8. Na ausência de indícios de diluição, uma possível explicação para as metalicidades mais baixas das gigantes com planetas estaria nas maiores massas destes objetos e dos seus respectivos discos protoplanetários. As maiores massas destes discos aumentariam a quantidade de metais disponíveis para a formação de planetas através do mecanismo de acresção do núcleo, compensando o efeito das baixas metalicidades.
9. As abundâncias de lítio das estrelas com e sem planetas não apresentam nenhuma dependência significativa com a metalicidade ou o nível de atividade cromosférica medido a partir das linhas H e K do Ca II ($\log R'_{HK}$). Por outro lado, é possível observar uma pequena correlação negativa destas abundâncias com a idade. A dependência mais significativa é com a temperatura efetiva ou, alternativamente, a massa. As estrelas mais quentes (ou de maior massa) possuem as maiores abundâncias de lítio. Este efeito é bem conhecido e está relacionado com a variação da profundidade da zona convectiva em função da massa. Por fim, também encontramos uma evidência de que a abundância de lítio cresce com a velocidade de rotação projetada (consistente com os resultados de Takeda et al. 2010).
10. A diferença mais sugestiva entre as estrelas com e sem planetas foi encontrada para o intervalo $5700 \text{ K} \lesssim T_{ef} \lesssim 5850 \text{ K}$, no qual o comportamento das abundâncias de lítio é bastante complexo. Em média, as estrelas com planetas possuem abundâncias de lítio menores. Esta conclusão é consistente com os resultados de Israeli et al. (2009) e Gonzalez et al. (2010a), embora a diferença encontrada em nosso trabalho seja menor.
11. Esta diferença nas abundâncias de lítio apresenta uma correlação com os níveis de atividade cromosférica. Em média, as estrelas com planetas e $5700 \text{ K} \lesssim T_{ef} \lesssim 5850 \text{ K}$ possuem menores valores de $\log R'_{HK}$. É possível que isto seja apenas um reflexo das

limitações do método de detecção de planetas baseado nas medidas de velocidades radiais (que é mais preciso para estrelas com menores níveis de atividade). Caso este resultado não seja um efeito de seleção, ele pode estar relacionado a diferenças nas velocidades de rotação projetadas das estrelas, que podem influenciar a taxa de depleção do lítio nas atmosferas estelares (ver, por exemplo, Bouvier 2008).

12. As comparações das abundâncias de lítio e velocidades de rotação projetadas são bastante sensíveis às amostras utilizadas e ao intervalo de temperaturas efetivas considerado.
13. A comparação do Sol com estrelas de propriedades similares (independentemente da presença de planetas) sugere que a sua abundância de lítio e sua velocidade de rotação projetada não apresentam nenhuma peculiaridade.
14. A qualidade dos espectros bHROS e a lista de linhas mais completa fazem com que a nossa análise do ${}^6\text{Li}$ seja a mais sensível já realizada. Não detectamos este isótopo em nenhuma das 5 estrelas com planetas analisadas (inclusive HD 82943), as quais possuem $5700 \text{ K} \lesssim T_{\text{ef}} \lesssim 6200 \text{ K}$ e $1,0 M_{\odot} \lesssim M \lesssim 1,4 M_{\odot}$. Como as estrelas mais quentes e de maior massa possuem as menores zonas convectivas, os objetos aqui analisados constituem ótimos candidatos para a detecção de indícios de poluição. Juntamente com os resultados de Reddy et al. (2002) e Mandell et al. (2004), o nosso trabalho fornece limites robustos para a quantidade de ${}^6\text{Li}$ que poderia ter sido acrescida às atmosferas das estrelas com planetas.

De uma maneira mais global, os resultados desta tese favorecem o cenário do enriquecimento primordial e o modelo de acresção do núcleo para a formação planetária. Nenhuma evidência de poluição foi encontrada. Observamos índices de que a metalicidade pode ser determinante no estabelecimento da massa máxima de um planeta no sistema e de que a massa da estrela hospedeira pode ter um papel importante na formação planetária. Por outro lado, as abundâncias de lítio representam uma sutil evidência de que a presença de planetas pode influenciar as abundâncias fotosféricas das estrelas (através de processos consideravelmente diferentes da poluição, no entanto).

A qualidade e a cobertura espectral dos espectros FEROS permitem a realização de uma grande variedade de estudos. A próxima etapa deste trabalho é a obtenção de abundâncias

químicas (através de medidas de larguras equivalentes) para os elementos C, Na, Mg, Al, Si, S, K, Ca, Ti, Cr, Ni, Zn, Y e Ba. Resultados preliminares indicam que não há diferenças nos padrões de evolução química (representados por gráficos do tipo $[X/\text{Fe}]$ versus $[\text{Fe}/\text{H}]$, onde X é um elemento químico qualquer) das estrelas com e sem planetas. As estrelas com planetas gigantes parecem apenas fazer parte do extremo mais rico das distribuições de abundâncias químicas do disco fino da Galáxia (o que está de acordo com os resultados recentes de Neves et al. 2009, por exemplo).

Em um segundo momento, pretendemos derivar as abundâncias químicas dos elementos N, O, Sc, V, Mn, Co e Cu através de síntese espectral para procurar possíveis anomalias nas estrelas com planetas. De posse deste vasto conjunto de abundâncias, faremos gráficos do tipo $[X/\text{H}]$ ou $[X/\text{Fe}]$ versus T_C para verificar os resultados recentes de Meléndez et al. (2009), Ramírez et al. (2009) e Gonzalez et al. (2010b). Além disso, poderemos testar as previsões de que as estrelas com planetas devem ser mais ricas em oxigênio (Robinson et al. 2006).

O grande volume de dados que temos nos permite fazer uma procura por análogas solares, através de um estudo comparativo detalhado de suas propriedades com as do Sol. Possuímos, ainda, espectros FEROS para 6 estrelas de tipo M com planetas. Pretendemos derivar as metalicidades destes objetos (o que é uma tarefa bastante complexa e sujeita a elevadas incertezas), uma vez que eles são de fundamental importância para um melhor entendimento das propriedades das estrelas com planetas netunianos. Finalmente, tentaremos estender a nossa amostra com a inclusão de estrelas com planetas do norte ($\delta > 26^\circ$) ou descobertas após agosto de 2008.

Apêndice A

Espectros FEROS

Neste apêndice, o espectro FEROS da estrela HD 2039 ($S/R \sim 350$) é mostrado como exemplo. As figuras apresentam todas as linhas do Fe I e Fe II usadas neste trabalho. No final, a região do Li I em $\sim 6708 \text{ \AA}$ também pode ser vista.

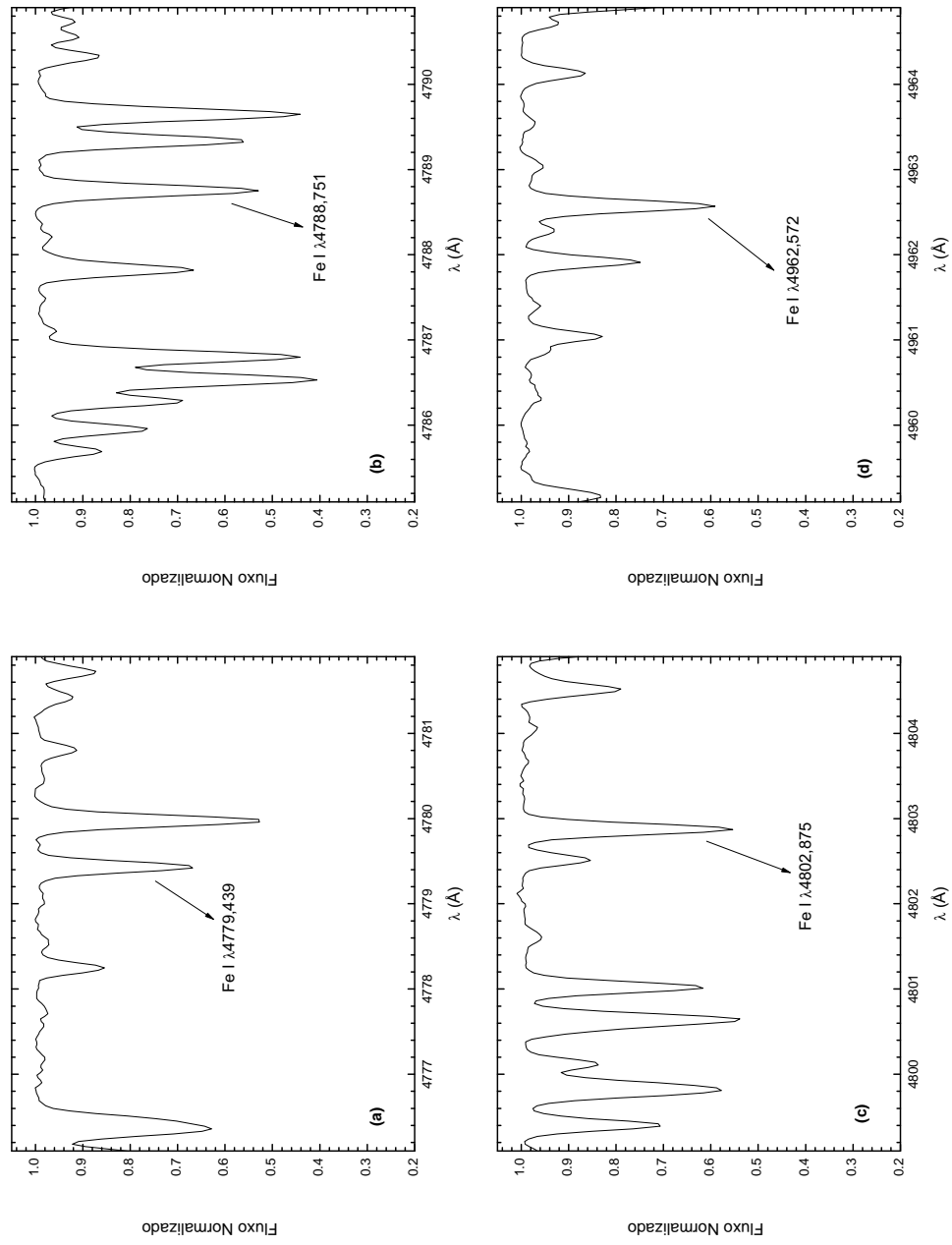


Figura A.1: Os painéis (a), (b), (c) e (d) mostram, respectivamente, as linhas do Fe I em 4779,439, 4788,751, 4802,875 e 4962,572 \AA .

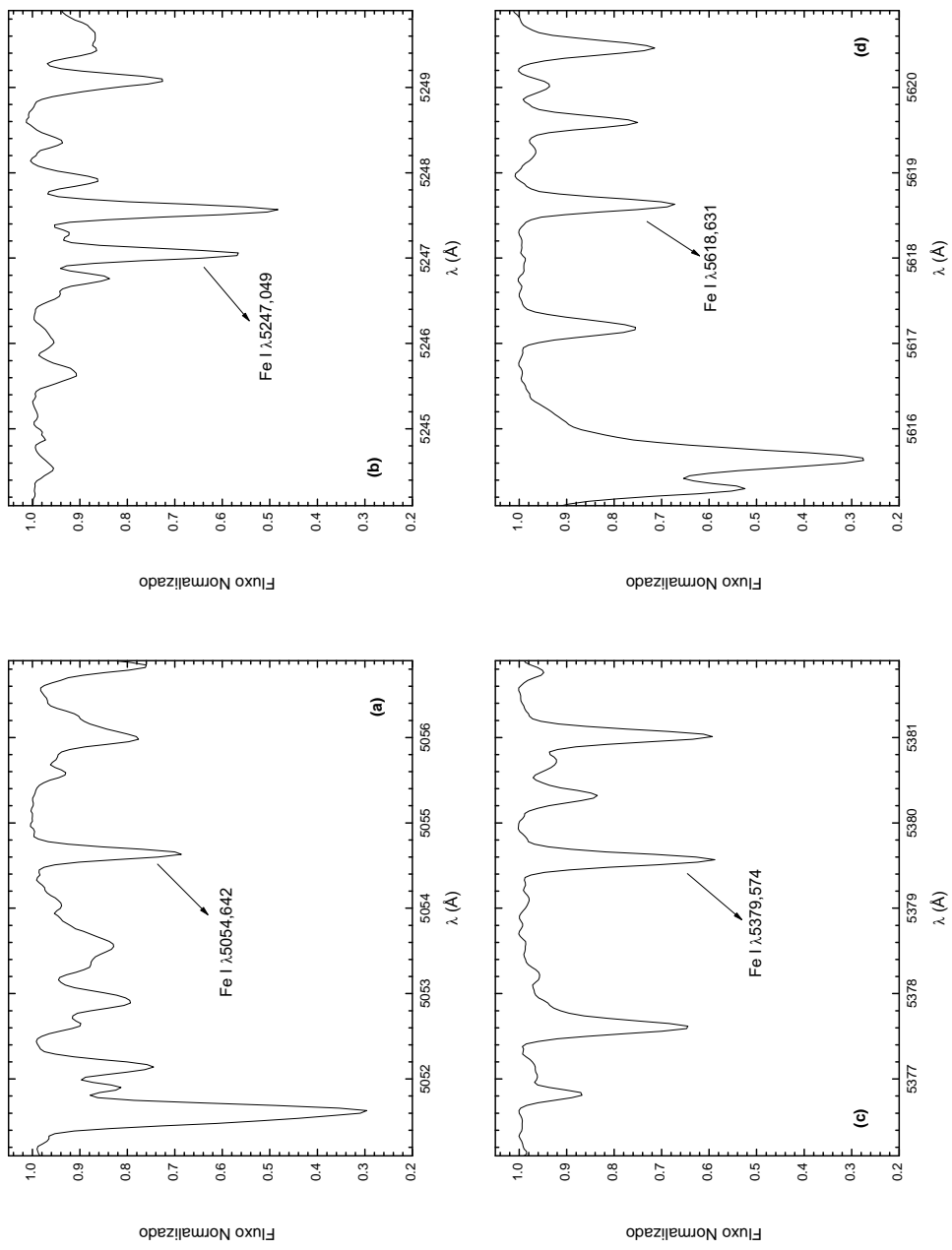


Figura A.2: Os painéis (a), (b), (c) e (d) mostram, respectivamente, as linhas do Fe I em 5054,642, 5247,049, 5379,574 e 5618,631 \AA .

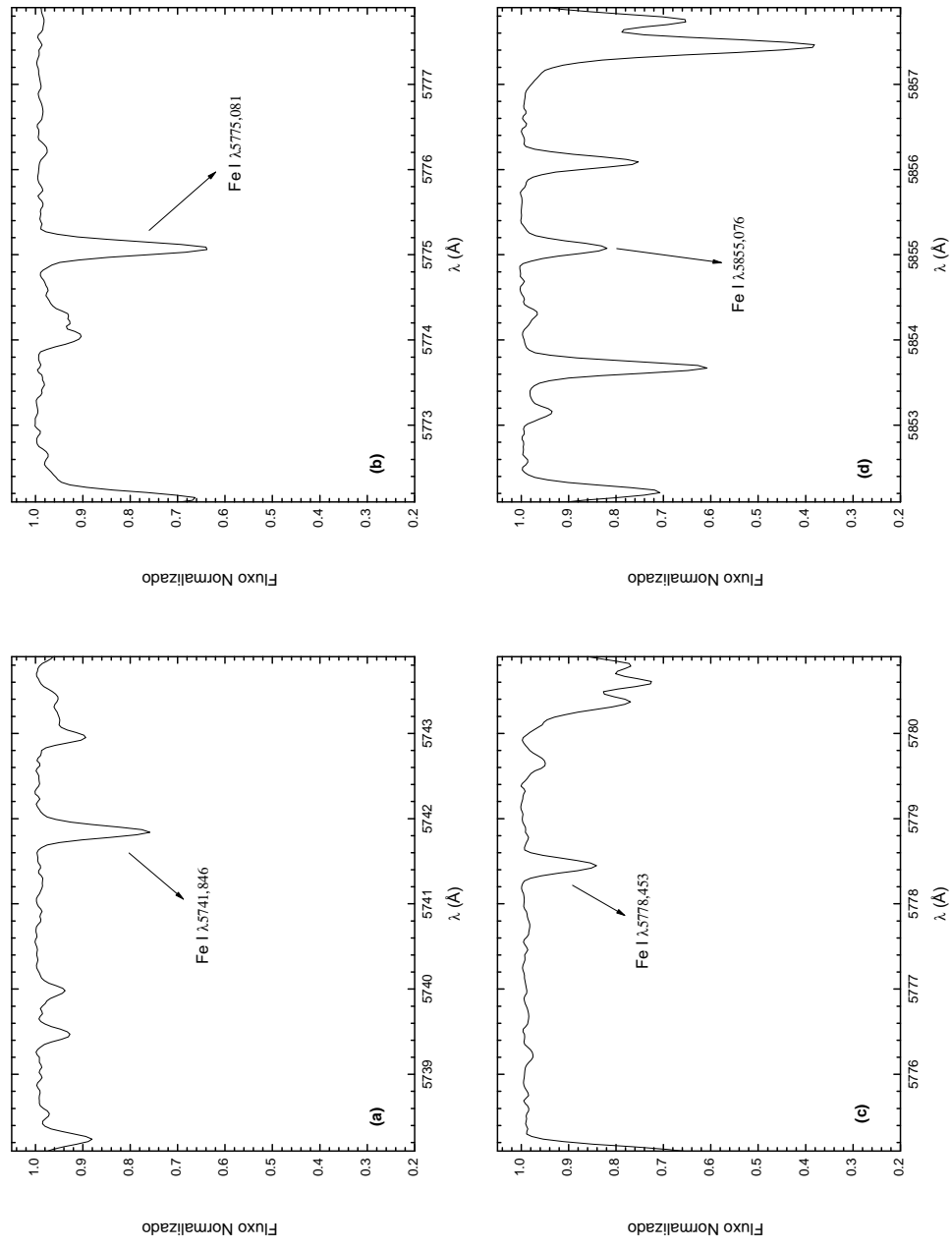


Figura A.3: Os painéis (a), (b), (c) e (d) mostram, respectivamente, as linhas do Fe I em 5741,846, 5775,081, 5778,453 e 5855,076 \AA .

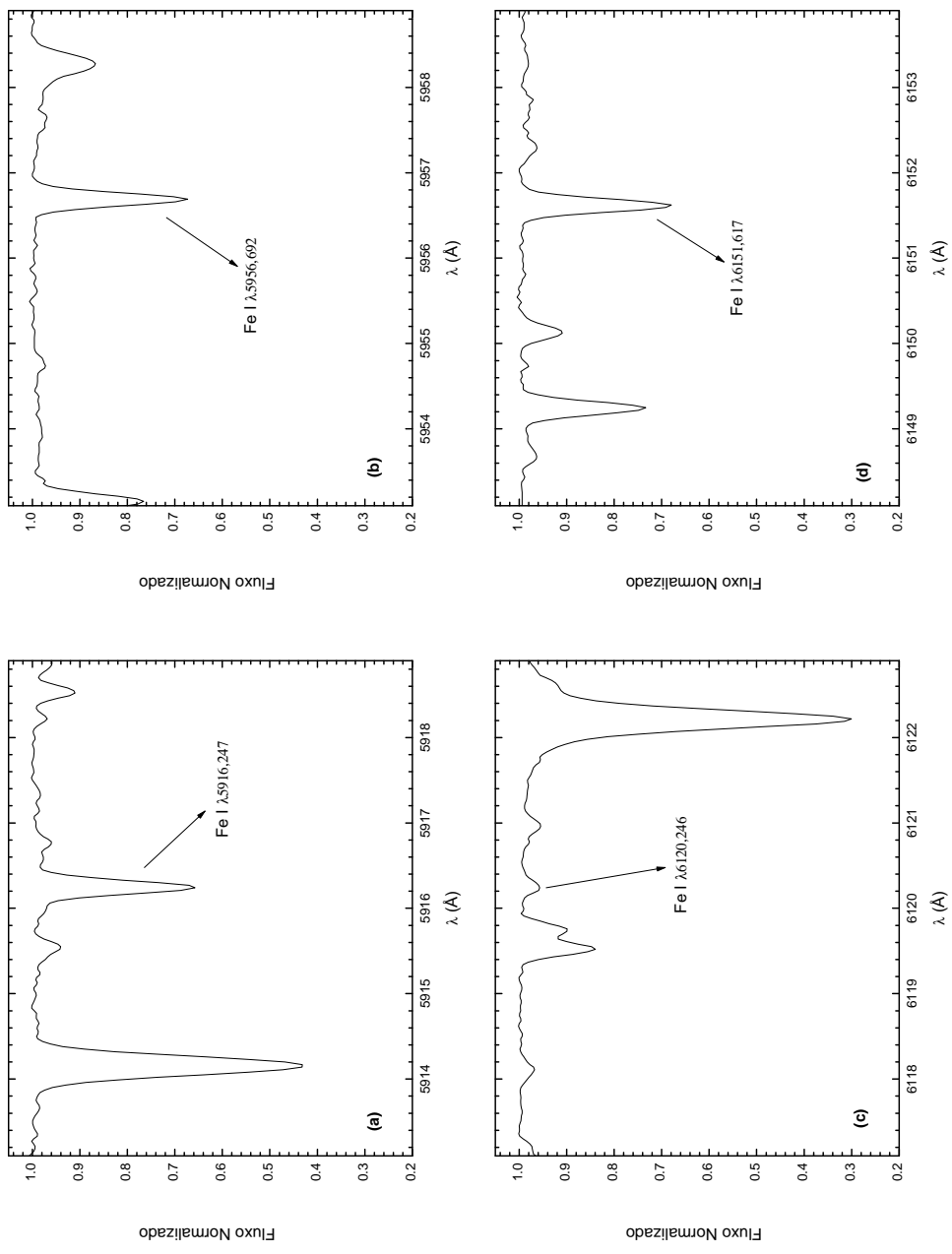


Figura A.4: Os painéis (a), (b), (c) e (d) mostram, respectivamente, as linhas do Fe I em 5916,247, 5956,692, 6120,246 e 6151,617 Å.

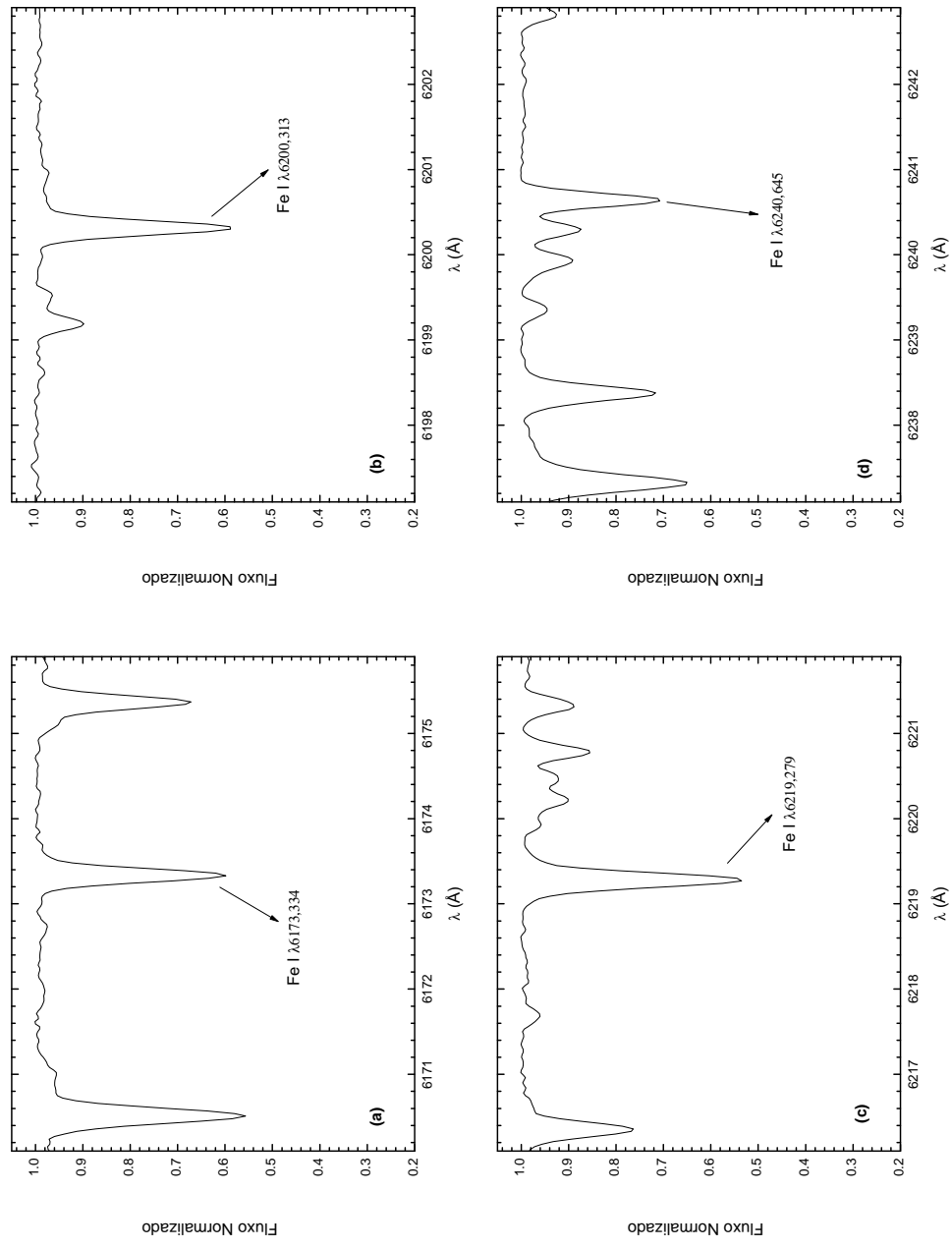


Figura A.5: Os painéis (a), (b), (c) e (d) mostram, respectivamente, as linhas do Fe I em 6173,334, 6200,313, 6219,279 e 6240,645 \AA .

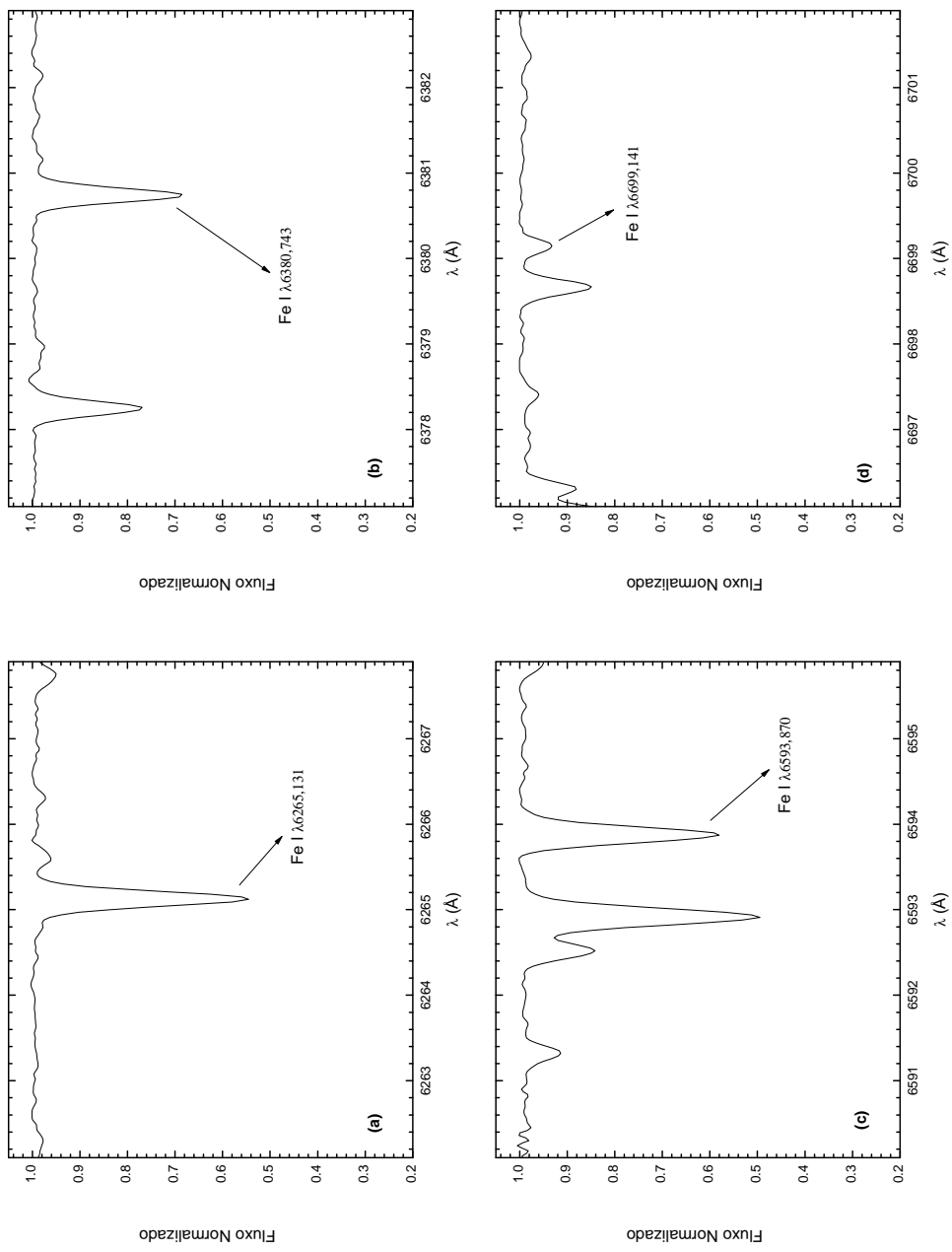


Figura A.6: Os painéis (a), (b), (c) e (d) mostram, respectivamente, as linhas do Fe I em 6265,131, 6380,743, 6593,870 e 6699,141 \AA .

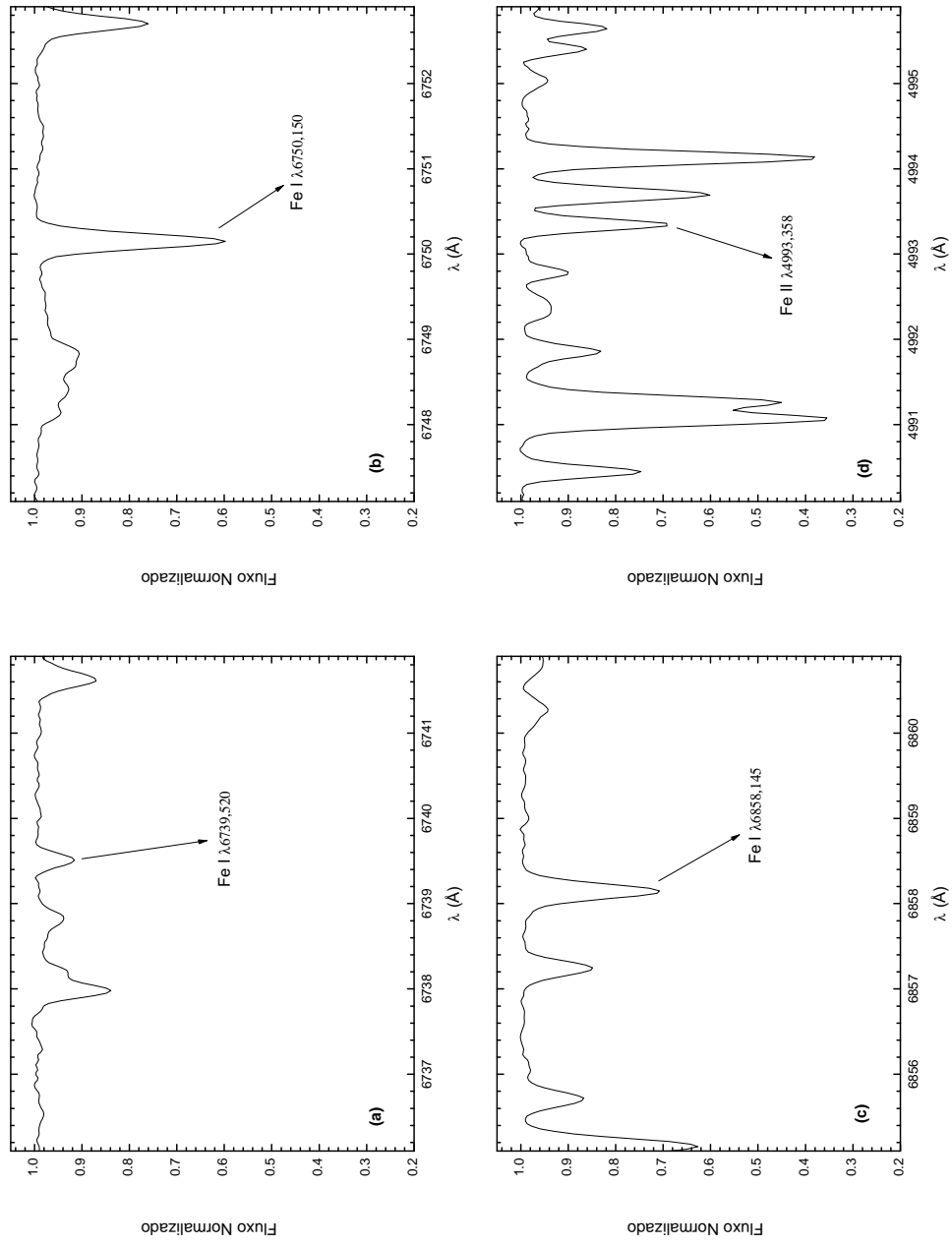


Figura A.7: Os painéis (a), (b) e (c) mostram, respectivamente, as linhas do Fe I em 6739,520, 6750,150 e 6858,145 \AA . O painel (d) apresenta a linha do Fe II em 4993,358 \AA .

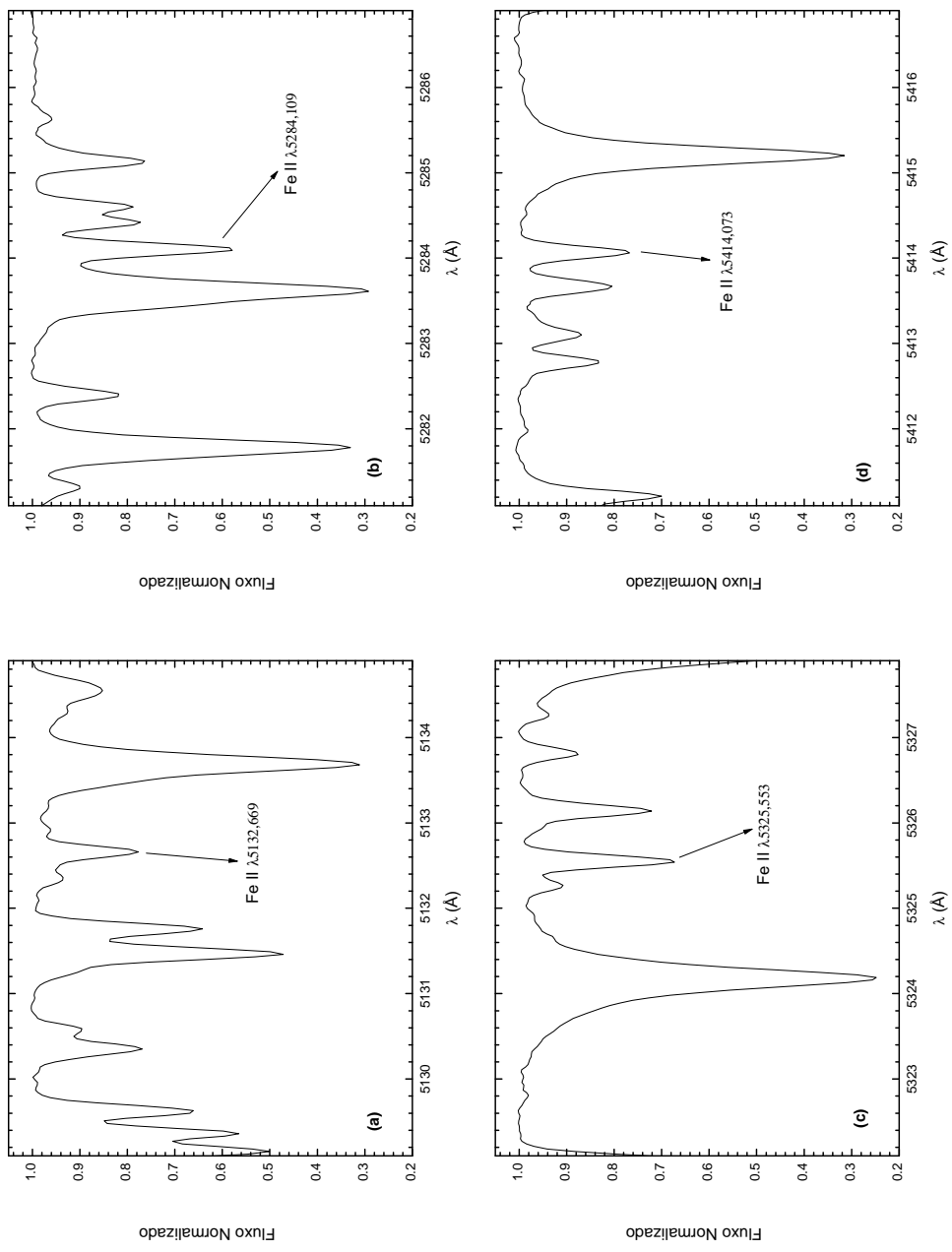


Figura A.8: Os painéis (a), (b), (c) e (d) mostram, respectivamente, as linhas do Fe II em 5132,669, 5284,109, 5325,553 e 5414,073 \AA .

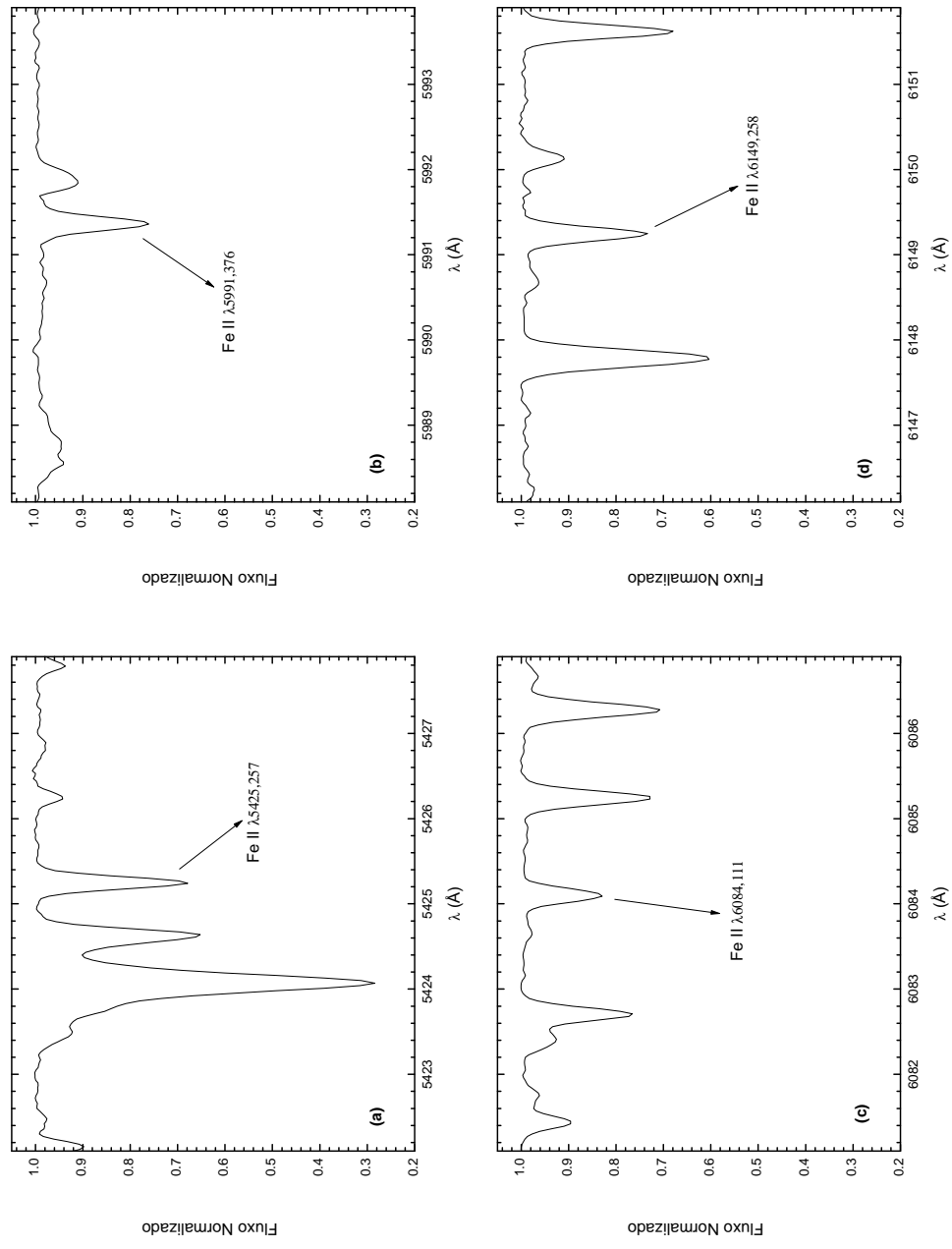


Figura A.9: Os painéis (a), (b), (c) e (d) mostram, respectivamente, as linhas do Fe II em 5425,257, 5991,376, 6084,111 e 6149,258 \AA .

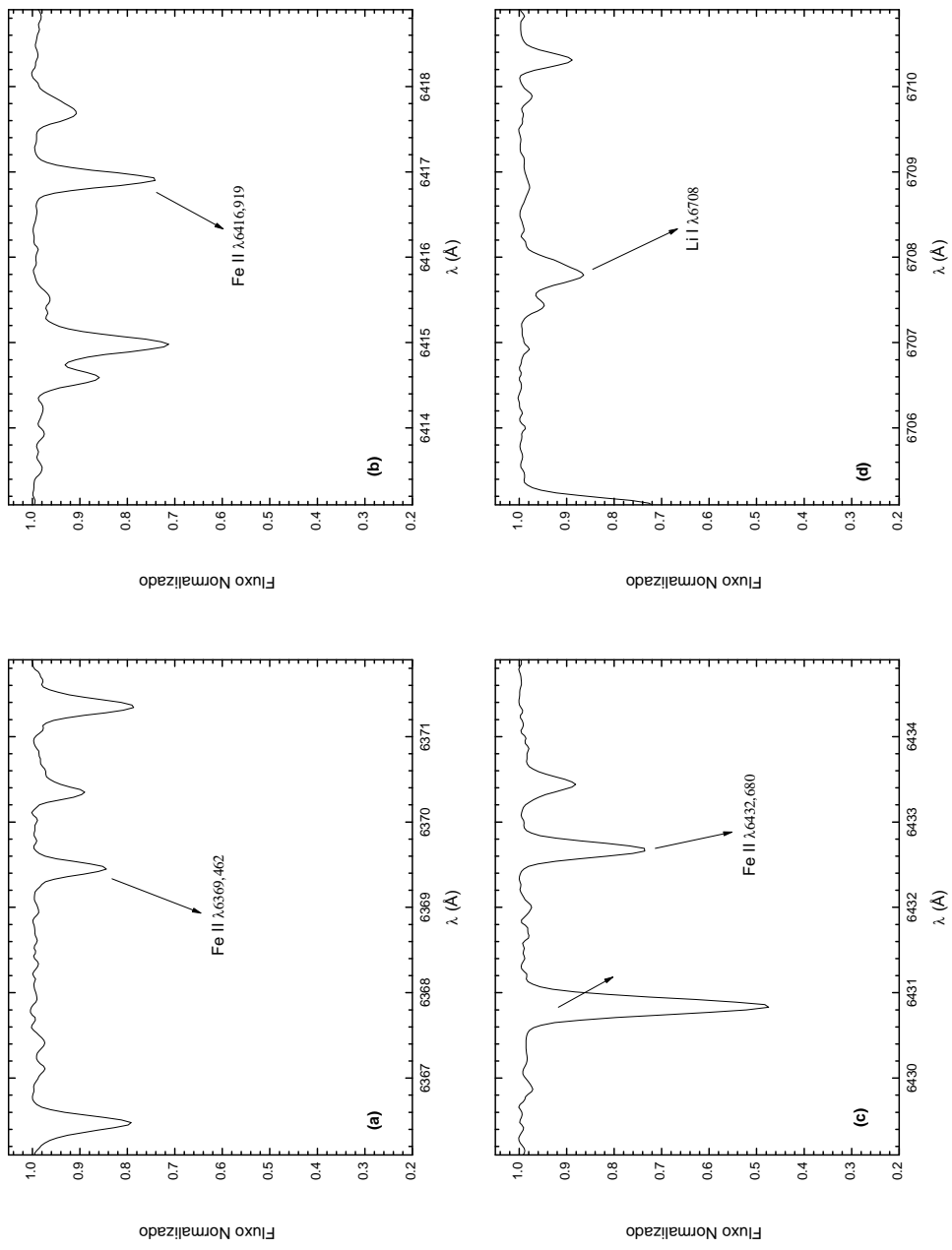


Figura A.10: Os painéis (a), (b) e (c) mostram, respectivamente, as linhas do Fe II em 6369,462, 6416,919 e 6432,680 Å. O painel (d) apresenta o dupletos do Li I em ~ 6708 Å.

Apêndice B

Medidas de Larguras Equivalentes

Este apêndice apresenta as tabelas com as larguras equivalentes das linhas do Fe I e Fe II para todas as 308 estrelas da nossa amostra. Os parâmetros atômicos das linhas, assim como as larguras equivalentes medidas no espectro solar, estão contidos na tabela 2 do artigo I.

Table 1. Larguras Equivalentes das Linhas de Fe I e Fe II.

λ (Å)	HD142	HD1237	HD2039	HD2638	HD3651	HD4113	HD4208	HD4308	HD4203	HD5319
4779.439	31.6	56.0	51.8	70.7	67.1	54.6	34.4	31.9	63.7	86.9
4788.751	57.2	79.9	74.9	88.2	85.4	77.1	61.8	57.5	86.5	98.1
4802.875	57.7	71.5	71.9	76.9	74.4	70.9	54.3	49.9	80.8	82.8
4962.572	57.3	63.8	69.8	75.7	73.6	68.2	48.5	44.3	79.1	79.0
5054.642	27.9	53.0	50.5	65.5	62.0	54.8	31.7	30.7	69.2	71.7
5247.049	45.6	96.1	74.3	100.8	95.7	82.5	64.7	59.8	98.3	...
5379.574	53.7	74.6	72.8	82.3	79.8	74.3	54.1	51.1	84.9	90.4
5618.631	42.7	63.8	62.6	69.8	67.2	62.4	40.3	38.4	71.9	70.7
5741.846	27.1	44.5	42.9	51.8	50.9	44.7	25.7	22.4	54.4	58.4
5775.081	53.3	76.7	72.0	...	77.7	48.0	83.6	84.9
5778.453	9.7	34.6	28.2	48.5	45.8	33.6	17.1	14.5	45.4	63.9
5855.076	17.0	32.2	33.1	38.1	36.7	32.5	15.8	13.4	42.6	43.5
5916.247	45.7	77.4	67.6	84.5	81.4	70.0	48.2	47.8	83.8	98.8
5956.692	29.6	71.8	59.7	85.1	80.1	65.7	46.8	44.8	76.8	105.5
6120.246	...	9.7	6.9	22.1	20.7	10.9	3.9	...	16.7	41.6
6151.617	33.8	67.4	59.1	77.5	74.6	63.4	43.9	39.9	73.6	90.3
6173.334	...	93.0	79.1	100.6	94.2	82.3	62.1	58.7	95.8	112.7
6200.313	63.3	97.8	80.2	98.3	94.4	89.6	66.1	63.4	102.4	110.1
6219.279	83.3	123.3	102.8	123.5	117.4	107.6	84.9	80.6	122.8	141.4
6240.645	41.2	66.9	58.0	74.9	71.6	63.8	42.6	38.9	74.4	...
6265.131	75.6	114.7	98.5	125.7	119.8	101.6	80.5	77.0	116.1	141.2
6380.743	45.9	66.6	65.3	71.2	70.2	66.6	44.8	40.6	78.5	83.2
6593.870	79.2	114.8	98.9	112.1	108.3	97.9	79.0	72.7	106.3	138.2
6699.141	...	12.7	12.9	17.4	15.9	13.2	5.6	...	21.2	23.1

Table 1—Continued

λ (Å)	HD142	HD1237	HD2039	HD2638	HD3651	HD4113	HD4208	HD4308	HD4203	HD5319
6739.520	...	22.0	15.3	34.5	33.2	20.0	9.3	6.8	29.0	...
6750.150	63.0	96.2	85.9	106.3	102.8	89.8	67.8	64.6	104.3	121.4
6858.145	48.5	66.9	64.6	71.5	69.4	...	42.2	40.9	76.5	...
4993.358	53.5	39.1	50.8	...	37.3	42.8	29.9	29.1	54.3	45.9
5132.669	36.0	10.2	40.7	25.2	40.0	18.5	18.6	57.5
5284.109	83.5	66.3	81.8	52.6	57.2	72.0	53.2	51.1	84.6	70.5
5325.553	64.3	38.1	56.1	...	27.9	44.6	31.4	30.9	53.7	...
5414.073	44.2	25.4	41.5	19.8	20.3	34.6	19.4	17.6	44.5	31.9
5425.257	59.1	42.4	56.3	38.5	38.3	49.1	30.8	30.5	60.0	45.0
5991.376	50.3	31.7	47.6	27.6	27.1	38.5	22.0	21.5	47.9	40.1
6084.111	35.2	18.7	32.1	16.1	16.7	26.7	14.6	13.4	34.9	26.9
6149.258	56.6	33.8	51.0	29.3	27.1	40.7	24.7	26.5	50.9	35.9
6369.462	32.4	19.6	30.4	15.8	15.0	25.2	12.9	13.1	31.9	23.5
6416.919	56.0	41.7	55.3	...	38.1	45.0	28.0	28.5	53.5	...
6432.680	61.4	38.5	56.3	29.9	32.6	46.8	29.1	29.3	56.4	44.6

Table 1. Larguras Equivalentes das Linhas de Fe I e Fe II.

λ (Å)	HD6434	HD10647	HD10697	HD11506	HD11977	HD11964	HD12661	HD13445	HD16141	HD16417
4779.439	53.5	...	71.1	62.9	60.2	53.8	50.0	48.5
4788.751	42.6	55.4	77.2	71.8	95.7	84.9	82.7	73.1	74.4	72.6
4802.875	36.9	50.4	72.3	67.7	84.2	75.3	75.8	62.2	69.7	67.2
4962.572	29.0	46.2	66.5	65.4	75.2	71.3	74.4	56.4	63.8	62.5
5054.642	16.6	...	53.2	44.3	62.0	61.1	62.0	41.2	47.7	46.5
5247.049	39.1	47.7	84.3	70.5	...	100.5	88.5	88.7	78.8	76.1
5379.574	34.8	49.8	73.9	68.4	85.9	79.1	81.3	64.3	69.1	68.8
5618.631	25.6	40.4	58.8	56.5	69.8	66.6	67.0	51.1	57.6	56.9
5741.846	12.8	23.5	44.0	39.3	52.9	46.9	52.1	36.3	39.4	37.8
5775.081	70.1	...	80.5	75.6	...	60.1	67.5	67.9
5778.453	...	11.2	32.3	24.6	55.0	44.8	40.1	29.4	27.9	26.2
5855.076	...	15.7	30.9	28.7	36.1	34.9	37.9	21.5	28.2	27.5
5916.247	27.3	41.7	71.1	63.8	96.6	79.7	...	65.6	66.1	66.3
5956.692	25.8	31.3	66.8	50.7	104.8	81.2	71.8	69.3	60.1	57.4
6120.246	8.9	4.7	29.4	17.6	9.7	11.8	8.1	7.5
6151.617	23.6	32.6	62.8	53.2	89.3	73.0	67.5	61.0	59.0	57.4
6173.334	42.2	52.3	82.2	74.5	110.9	92.8	88.1	80.1	77.2	76.6
6200.313	45.1	58.9	85.7	82.1	107.4	98.7	91.2	85.2	82.9	81.9
6219.279	64.8	76.7	104.4	98.1	136.4	116.5	114.2	107.7	100.5	101.3
6240.645	23.0	33.5	62.6	51.9	89.2	72.4	67.8	58.1	56.8	54.9
6265.131	60.2	71.5	101.4	92.3	134.4	112.9	110.1	102.9	94.9	93.7
6380.743	25.8	40.7	65.7	61.6	72.5	69.3	72.8	53.9	61.5	60.5
6593.870	...	71.2	103.7	94.0	124.2	107.4	111.1	99.9	89.8	96.8
6699.141	11.0	10.8	15.6	15.2	15.8	7.4	9.8	10.6

Table 1—Continued

λ (Å)	HD6434	HD10647	HD10697	HD11506	HD11977	HD11964	HD12661	HD13445	HD16141	HD16417
6739.520	19.5	33.2	24.1	21.5	15.9	15.8
6750.150	48.0	58.7	89.2	82.9	117.2	99.2	96.1	85.3	84.0	83.8
6858.145	24.1	42.2	61.8	61.1	69.8	67.4	70.6	51.8	59.0	59.1
4993.358	21.1	38.9	49.3	53.7	54.1	43.6	48.3	32.9	48.6	49.6
5132.669	11.2	26.2	40.7	43.1	47.7	37.1	45.3	6.8	38.2	38.9
5284.109	42.7	66.8	78.1	83.1	...	69.6	79.8	39.8	76.6	80.5
5325.553	25.2	49.6	52.5	60.3	58.1	41.7	50.6	19.8	52.5	54.2
5414.073	13.7	31.2	37.6	45.3	43.5	33.1	40.5	11.3	38.9	39.8
5425.257	24.1	46.9	55.7	60.7	57.3	47.1	56.0	24.0	53.7	56.9
5991.376	16.2	38.3	42.3	51.9	51.7	38.7	44.5	14.5	41.6	46.6
6084.111	9.5	23.4	30.8	36.6	36.2	25.8	31.5	9.4	29.8	31.5
6149.258	19.9	41.8	45.9	57.7	49.5	38.9	46.7	15.4	47.1	48.8
6369.462	10.5	24.3	28.4	35.4	34.3	23.5	27.6	9.2	28.5	29.0
6416.919	21.0	43.6	48.6	58.3	51.2	44.4	51.3	23.6	49.2	50.6
6432.680	23.5	46.9	51.5	61.8	59.5	45.8	52.7	18.8	53.6	55.6

Table 1. Larguras Equivalentes das Linhas de Fe I e Fe II.

λ (Å)	HD16400	HD17051	HIP14810	HD19994	HD20782	HD22049	HD23127	HD23079	HD27442	HD27894
4779.439	88.8	37.1	60.6	40.3	40.2	60.2	58.8	30.6
4788.751	108.6	63.9	82.0	67.6	67.1	84.0	83.4	58.1	109.5	97.6
4802.875	92.2	61.0	75.5	63.7	59.9	69.8	78.6	51.0	...	79.9
4962.572	87.3	55.9	74.1	65.1	56.2	60.9	76.2	45.0	86.3	80.3
5054.642	75.0	35.5	63.3	37.3	37.6	49.3	62.8	26.9
5247.049	...	58.0	90.4	61.5	66.8	109.2	88.4	54.2	136.9	113.5
5379.574	99.9	58.2	80.9	63.5	59.7	74.0	81.3	49.9	103.5	88.9
5618.631	79.9	49.9	68.3	52.8	48.9	61.2	69.3	39.7	80.6	71.8
5741.846	65.1	29.9	49.2	32.4	31.0	43.6	49.6	22.2	67.5	59.5
5775.081	91.9	57.9	...	61.6	...	69.9	79.8	47.8	95.7	...
5778.453	71.5	16.4	41.5	17.4	19.4	39.3	36.8	12.2	77.1	58.2
5855.076	48.1	20.7	37.4	22.7	21.1	29.1	38.4	15.3	51.3	44.1
5916.247	112.2	52.0	77.4	55.2	50.1	79.9	77.2	42.2	...	93.6
5956.692	120.7	39.8	72.2	43.5	49.2	81.7	67.5	36.3	116.2	95.7
6120.246	47.4	...	14.8	...	5.6	17.8	11.4	...	54.1	33.8
6151.617	103.6	42.2	68.2	45.1	49.3	71.8	66.1	36.8	100.6	85.2
6173.334	128.0	63.9	89.1	70.9	66.8	95.5	89.6	55.9	127.2	110.5
6200.313	115.9	70.6	87.6	76.1	72.4	97.0	91.6	60.9	130.2	105.2
6219.279	158.2	86.0	115.7	92.0	90.4	122.6	113.9	79.4	163.0	136.1
6240.645	100.8	41.0	68.3	52.1	46.3	70.5	66.4	36.4	100.7	85.0
6265.131	152.3	81.3	111.6	88.1	84.4	123.4	109.3	73.8	161.5	144.8
6380.743	90.5	50.6	71.0	55.6	50.7	57.1	74.2	43.0	97.9	78.0
6593.870	138.8	79.2	102.9	88.4	84.4	108.8	101.8	75.0	157.1	137.4
6699.141	24.7	7.9	16.1	6.9	8.1	9.3	16.1	6.0	32.7	22.7

Table 1—Continued

λ (Å)	HD16400	HD17051	HIP14810	HD19994	HD20782	HD22049	HD23127	HD23079	HD27442	HD27894
6739.520	...	7.4	26.7	...	12.6	27.5	20.9	6.6	66.0	49.7
6750.150	135.7	66.9	98.4	72.8	73.1	94.5	95.2	64.5	131.7	116.2
6858.145	70.7	51.5	70.2	56.2	49.2	62.7	73.2	41.3	...	61.9
4993.358	57.2	48.8	42.2	54.9	38.7	37.6	55.4	37.0	56.4	56.3
5132.669	...	23.7	13.3	45.1	25.5	...	52.0	22.7	59.7	...
5284.109	...	75.2	72.0	87.1	63.9	48.4	89.0	63.2	71.8	47.6
5325.553	56.8	58.7	42.2	66.8	42.5	16.8	59.5	40.7	33.4	20.6
5414.073	45.4	38.9	34.3	47.9	28.2	12.5	48.8	26.8	31.4	13.7
5425.257	60.0	53.7	48.5	63.3	42.5	27.9	63.7	41.4	48.8	40.0
5991.376	...	44.6	39.4	54.0	33.1	17.9	52.4	31.3
6084.111	41.1	30.7	26.5	37.2	21.1	8.3	38.8	19.9	30.2	13.8
6149.258	52.0	52.1	40.8	59.7	35.9	18.0	55.8	37.1	39.1	20.5
6369.462	38.5	29.2	22.8	37.5	20.4	10.2	36.7	18.2	27.3	9.3
6416.919	...	51.3	46.5	61.0	39.4	28.4	56.3	36.9	47.7	42.6
6432.680	61.2	56.2	45.8	63.6	41.1	22.0	62.2	41.4	42.4	27.5

Table 1. Larguras Equivalentes das Linhas de Fe I e Fe II.

λ (Å)	HD28185	HD28305	HD30177	HD32833	HD37124	HD39091	HD37605	HD38529	HD40307	HD4004A
4779.439	54.2	93.2	64.7	51.9	31.1	40.3	65.2	65.6	...	67.0
4788.751	78.7	114.4	87.2	77.2	57.0	65.6	86.9	89.2	77.5	85.9
4802.875	72.5	99.1	80.0	73.5	49.6	60.3	78.4	82.6	...	76.5
4962.572	70.1	95.5	80.2	69.4	42.9	55.4	78.4	79.3	71.5	74.1
5054.642	56.4	81.8	68.6	50.9	30.9	36.5	60.6	69.6	...	56.6
5247.049	84.8	...	97.1	77.4	62.2	63.1	100.3	98.0
5379.574	74.8	108.8	86.5	75.6	47.3	59.2	85.1	88.7	66.9	81.2
5618.631	63.6	...	73.0	61.6	36.0	50.1	71.6	73.1	50.9	66.7
5741.846	45.6	72.7	55.2	43.0	21.5	31.8	53.6	55.5	36.9	52.9
5775.081	...	101.8	...	72.8	44.5	82.9	60.2	...
5778.453	34.4	78.1	47.4	27.3	15.2	18.6	48.2	46.9	35.9	46.3
5855.076	32.8	54.7	42.3	31.8	13.5	22.5	41.5	42.7	23.2	37.3
5916.247	71.5	123.3	82.3	69.7	45.8	44.3	83.6	85.6	71.3	82.7
5956.692	66.9	127.5	81.1	57.7	42.7	47.7	79.9	80.8	76.3	81.9
6120.246	10.7	50.7	16.0	7.0	4.4	...	20.9	17.9	15.6	20.5
6151.617	64.9	109.5	73.4	60.0	38.8	47.5	75.8	77.0	67.2	74.0
6173.334	82.5	129.7	95.6	81.6	57.8	66.7	98.0	99.5	87.2	96.8
6200.313	86.2	137.5	96.1	88.7	63.3	73.0	95.8	91.8	93.4	93.5
6219.279	108.0	174.8	125.0	105.1	79.6	88.1	128.7	126.2	114.1	129.1
6240.645	62.9	107.2	74.5	59.2	39.0	43.9	74.8	76.8	66.7	...
6265.131	105.2	168.7	106.9	99.2	75.3	84.7	124.5	121.7	113.8	...
6380.743	66.8	103.7	78.2	67.8	38.7	53.9	76.5	80.4	45.5	70.3
6593.870	96.2	164.0	118.1	101.5	70.3	78.2	105.9	112.4	114.7	108.7
6699.141	14.6	33.3	19.2	13.2	5.5	7.8	19.4	19.0	8.0	17.5

Table 1—Continued

λ (Å)	HD28185	HD28305	HD30177	HD3283	HD37124	HD39091	HD37605	HD38529	HD40307	HD41004A
6739.520	22.0	65.9	31.4	14.3	10.8	9.4	33.9	30.8	25.7	33.4
6750.150	91.4	144.8	102.9	87.8	63.5	71.7	107.5	107.8	87.6	104.0
6858.145	66.7	81.2	77.4	65.9	34.2	51.3	75.9	76.2	51.0	69.4
4993.358	43.4	64.8	49.7	59.5	24.3	44.1	40.2	60.9	49.2	42.0
5132.669	36.8	...	42.3	50.5	22.5	31.1	33.3	64.4	...	29.6
5284.109	70.0	...	79.5	91.6	44.5	73.9	65.6	94.1	41.7	57.9
5325.553	44.3	67.1	49.5	66.6	24.7	49.4	35.7	62.0	12.5	28.7
5414.073	35.3	51.5	41.0	52.0	13.0	35.4	29.6	51.6	4.9	21.9
5425.257	49.0	67.5	56.3	66.2	24.9	50.0	46.9	66.9	24.0	38.8
5991.376	37.2	...	42.3	57.0	17.5	39.7	34.6	52.6	11.3	31.0
6084.111	26.6	...	32.2	40.8	10.0	26.1	23.5	41.4	4.3	19.3
6149.258	39.6	60.0	47.0	61.6	18.4	44.8	35.3	58.0	9.4	29.0
6369.462	23.7	45.1	28.1	40.2	8.5	24.2	21.2	39.7	5.6	16.6
6416.919	47.6	62.3	51.9	61.2	23.2	48.3	42.5	60.9	22.4	39.2
6432.680	46.6	69.2	50.9	67.7	24.5	52.9	39.7	64.2	13.8	32.2

Table 1. Larguras Equivalentes das Linhas de Fe I e Fe II.

λ (Å)	ABPic	HD45652	HD46375	HD47186	HD47536	HD50499	HD50554	HD52265	HD59686	NGC2423-3
4779.439	68.3	66.8	70.2	56.7	33.2	41.3
4788.751	99.0	87.4	86.4	78.8	107.4	75.4	61.4	...	121.6	122.4
4802.875	88.1	78.0	77.9	72.4	80.4	70.3	55.9	63.6	100.8	97.0
4962.572	...	78.5	80.4	71.0	69.8	67.0	50.8	59.6	95.9	94.6
5054.642	72.7	61.4	68.0	57.1	73.9	49.5	31.2	37.5	87.9	84.8
5247.049	151.2	95.4	97.3	83.7	...	73.3	56.9	63.5
5379.574	88.8	84.5	84.8	76.3	83.9	70.7	54.2	63.5	109.5	106.7
5618.631	75.0	71.0	66.6	65.5	62.4	60.1	44.5	50.9	88.8	84.9
5741.846	56.1	53.2	54.7	45.6	49.3	38.6	28.1	35.0	74.3	72.1
5775.081	...	82.6	84.0	74.5	73.7	100.5	100.7
5778.453	48.5	49.3	49.2	35.3	62.5	25.6	14.6	18.3	86.2	82.3
5855.076	33.4	40.4	39.5	34.5	28.4	30.8	17.7	24.3	...	52.3
5916.247	...	84.9	80.7	71.9	...	66.0	49.3	57.0	...	127.8
5956.692	108.6	79.3	83.2	68.0	136.5	...	39.0	52.2	...	143.7
6120.246	...	21.8	22.6	11.5	52.9	7.0	66.6	66.7
6151.617	92.6	75.4	76.1	65.0	101.3	54.4	38.7	47.3	118.0	118.6
6173.334	126.3	96.8	99.0	84.4	115.2	78.3	60.3	68.0	147.9	146.4
6200.313	133.2	97.0	95.4	91.6	119.8	84.9	65.7	76.1	128.3	129.7
6219.279	163.4	118.6	121.2	108.9	149.5	101.8	82.7	91.8	181.0	179.6
6240.645	96.3	74.4	75.2	64.8	101.2	56.1	38.8	46.7	115.4	116.2
6265.131	158.9	121.0	125.7	103.8	144.8	95.9	76.5	86.7	180.6	179.5
6380.743	77.7	74.5	74.7	69.4	70.1	65.6	47.3	57.2	106.7	100.1
6593.870	152.3	109.2	123.9	109.6	141.5	92.8	77.6	84.6	146.3	153.3
6699.141	...	20.8	20.5	13.5	...	11.8	6.5	9.3	33.4	31.6

Table 1—Continued

λ (Å)	ABPic	HD45652	HD46375	HD47186	HD47536	HD50499	HD5054	HD52265	HD59686	NGC2423-3
6739.520	...	35.4	34.7	21.1	60.7	14.1	...	10.4	78.1	78.6
6750.150	123.4	106.9	104.3	93.3	126.4	86.6	67.2	78.8	148.0	150.2
6858.145	73.7	65.5	71.7	67.5	53.5	61.6	41.5	54.6	88.3	83.5
4993.358	34.4	38.5	36.5	44.5	...	54.8	39.3	52.8	60.0	60.4
5132.669	...	32.9	28.7	43.4	...	45.7	26.9	38.8	...	46.8
5284.109	49.6	66.0	63.2	74.5	...	87.8	70.1	83.4	...	86.2
5325.553	...	33.5	30.8	45.5	...	61.5	46.4	63.7	...	50.8
5414.073	...	27.0	26.1	36.2	24.5	47.1	33.5	43.4	42.9	41.6
5425.257	41.5	44.2	41.1	50.1	40.5	62.1	47.2	58.9	...	57.2
5991.376	32.2	34.8	37.5	39.7	...	51.8	36.6	48.4
6084.111	...	22.0	20.5	28.5	20.4	37.1	24.4	34.6	...	41.9
6149.258	...	32.9	30.1	42.4	...	55.7	41.6	54.5	50.4	45.3
6369.462	19.8	19.2	18.2	24.9	18.3	33.7	22.3	31.9	33.9	34.3
6416.919	39.7	41.6	40.8	46.9	...	58.6	42.9	55.1	...	53.6
6432.680	...	37.7	34.6	48.2	...	61.1	47.8	61.0	60.6	56.8

Table 1. Larguras Equivalentes das Linhas de Fe I e Fe II.

λ (Å)	HD63454	HD65216	HD6428	HD69830	HD70642	HD70573	HD72659	HD73256	HD73526	HD74156
4779.439	56.9	51.4	38.0	62.2	59.6	37.5
4788.751	99.4	64.9	80.4	74.9	76.4	66.9	65.3	86.5	81.8	66.4
4802.875	78.8	56.3	74.7	66.0	70.3	58.8	58.6	77.3	74.9	60.4
4962.572	...	50.8	72.5	63.7	67.5	69.4	52.2	76.8	72.8	56.2
5054.642	...	36.7	57.5	48.9	52.6	36.8	36.2	61.9	59.9	36.3
5247.049	120.0	68.9	86.6	84.2	82.0	...	63.0	100.3	93.2	62.2
5379.574	86.0	57.8	77.0	68.0	74.0	63.2	58.4	81.5	78.6	60.2
5618.631	...	47.7	66.3	56.5	61.7	50.0	46.6	71.3	65.3	48.9
5741.846	...	30.4	46.2	40.1	42.7	32.3	30.0	51.4	49.0	31.9
5775.081	76.5	...	73.0	64.5	...	83.4	...	59.4
5778.453	54.1	20.3	37.5	31.8	33.5	18.8	17.0	41.4	36.5	17.8
5855.076	37.9	19.5	35.5	27.0	30.5	19.0	19.2	37.5	35.8	21.4
5916.247	...	53.8	69.6	68.2	69.4	63.2	...	81.1	74.5	53.7
5956.692	99.5	51.1	...	71.5	69.6	50.1	45.6	68.4	72.5	42.8
6120.246	30.8	5.0	11.9	11.1	9.8	...	3.6	15.4	13.8	...
6151.617	85.0	49.4	65.9	61.9	61.0	49.3	44.6	73.5	66.6	45.0
6173.334	113.8	67.6	86.5	80.5	82.2	76.1	63.9	97.5	89.0	66.0
6200.313	111.8	72.2	86.3	86.2	88.9	80.2	70.0	102.9	86.9	71.1
6219.279	142.5	86.8	111.9	106.6	109.0	105.8	85.5	119.2	113.8	89.3
6240.645	85.0	48.3	64.9	60.7	61.3	44.4	44.2	72.9	67.9	44.7
6265.131	141.9	86.4	106.1	101.2	103.9	97.1	82.6	121.3	108.6	83.3
6380.743	60.5	49.1	68.9	59.8	64.3	50.8	48.6	72.2	68.8	51.8
6593.870	141.1	81.7	101.9	94.4	99.5	95.1	79.1	112.7	103.5	81.7
6699.141	15.5	6.8	16.1	10.5	13.7	8.1	6.4	17.4	15.0	7.1

Table 1—Continued

λ (\AA)	HD63454	HD65216	HD66428	HD69830	HD70642	HD70573	HD72659	HD73256	HD73526	HD74156
6739.520	42.8	12.2	21.9	21.9	18.4	27.6	25.4	7.8
6750.150	114.7	74.3	95.1	85.3	87.9	76.8	70.5	103.9	94.7	70.6
6858.145	...	47.0	61.0	58.3	61.1	...	46.7	69.3	67.7	48.5
4993.358	54.4	31.3	47.7	34.4	42.2	30.6	45.4	41.3	53.3	46.3
5132.669	...	20.4	44.5	21.9	38.3	...	32.1	11.7	47.8	35.0
5284.109	54.9	56.0	76.8	58.1	71.9	...	72.1	70.9	77.5	79.3
5325.553	12.4	34.0	48.5	31.8	44.4	42.3	50.2	40.3	51.2	56.6
5414.073	6.9	19.2	38.9	20.8	33.5	22.3	36.6	30.1	39.8	37.6
5425.257	33.1	33.1	54.0	34.0	48.3	45.0	49.8	46.5	55.0	54.2
5991.376	25.2	24.1	41.6	24.7	35.0	37.7	38.6	34.7	48.3	47.9
6084.111	9.6	15.1	30.1	16.6	25.2	22.0	27.2	24.5	31.0	29.5
6149.258	17.1	28.1	45.3	26.0	39.3	39.9	44.9	37.5	47.7	50.9
6369.462	11.6	14.4	27.2	14.6	23.3	20.9	24.6	22.2	30.3	28.0
6416.919	34.9	32.9	50.3	33.9	45.7	...	47.1	46.0	50.0	52.3
6432.680	21.8	32.8	51.7	31.8	47.3	45.5	51.3	41.9	51.6	53.6

Table 1. Larguras Equivalentes das Linhas de Fe I e Fe II.

λ (Å)	HD75289	HD76700	HD8040	HD82943	HD83443	HD86081	HD88133	HD89307	HD92788	HD93083
4779.439	43.0	63.4	69.0	...	70.2	...	56.3	...
4788.751	70.2	84.5	65.0	73.1	88.4	72.6	89.7	57.7	78.6	92.5
4802.875	65.5	78.5	57.7	67.6	81.4	67.6	82.7	52.1	73.9	76.7
4962.572	61.8	77.0	52.7	65.9	81.5	62.8	82.5	46.1	71.2	77.1
5054.642	41.0	63.8	34.7	47.1	69.8	45.2	71.7	28.0	57.4	...
5247.049	65.5	93.9	66.4	71.0	92.0	71.6	...	53.7	83.7	106.3
5379.574	65.9	82.5	58.0	69.7	87.2	68.0	88.2	50.5	75.7	84.0
5618.631	54.5	70.1	47.5	59.0	75.0	55.1	71.9	39.9	66.2	67.6
5741.846	38.1	52.9	29.3	40.1	56.4	38.0	57.9	23.7	48.2	53.8
5775.081	65.2	80.4	75.5	75.3
5778.453	20.0	41.4	19.6	25.1	48.8	21.6	50.5	13.3	35.0	50.0
5855.076	25.0	40.3	19.6	29.2	43.3	25.9	44.7	15.7	33.9	37.8
5916.247	60.2	79.1	52.6	...	80.9	44.2	73.4	87.6
5956.692	47.0	75.5	55.6	53.5	81.6	57.8	85.5	35.6	67.5	87.7
6120.246	6.4	14.0	4.8	5.5	18.7	5.8	21.2	...	10.5	26.4
6151.617	49.4	71.7	46.8	55.3	77.4	52.3	79.3	38.3	64.5	80.1
6173.334	70.6	92.2	66.1	74.5	100.4	73.9	99.1	57.5	84.1	106.6
6200.313	76.9	92.6	71.4	82.6	96.9	79.9	102.0	61.5	86.0	100.4
6219.279	94.6	114.3	91.4	96.9	126.2	97.5	127.7	79.4	108.2	127.6
6240.645	49.1	71.2	45.7	54.5	77.6	51.0	77.5	36.5	63.1	...
6265.131	88.6	111.9	85.0	92.5	125.8	91.5	123.0	74.5	97.4	132.8
6380.743	58.4	73.5	50.1	63.0	77.8	59.3	78.7	41.6	69.2	65.3
6593.870	84.2	98.6	80.4	89.5	112.3	88.1	109.6	69.8	95.0	...
6699.141	10.3	19.1	5.7	11.4	21.7	9.9	21.2	5.3	14.7	18.0

Table 1—Continued

λ (\AA)	HD75289	HD76700	HD81040	HD82943	HD83443	HD86081	HD88133	HD89307	HD92788	HD93083
6739.520	11.7	27.8	12.9	13.0	34.5	14.4	36.9	8.0	20.5	39.6
6750.150	75.3	97.2	74.7	79.6	107.5	81.9	105.4	64.6	89.3	108.6
6858.145	54.9	72.0	48.3	59.1	75.0	57.0	74.2	40.2	66.5	67.5
4993.358	51.3	53.5	34.9	49.3	50.7	53.0	51.1	37.1	46.8	45.0
5132.669	29.7	51.4	23.2	39.1	22.0	41.2	32.1	21.3	42.4	...
5284.109	79.5	73.7	61.2	80.4	73.1	80.1	80.8	64.1	76.5	50.6
5325.553	60.8	53.7	37.4	55.4	41.2	60.0	50.6	44.1	49.1	17.0
5414.073	44.3	43.0	24.8	40.4	34.7	44.1	44.6	26.6	40.2	15.2
5425.257	58.9	57.1	37.9	55.1	49.9	59.2	57.6	39.7	53.5	35.3
5991.376	50.3	50.1	29.5	49.0	41.0	48.7	49.6	31.0	41.9	22.1
6084.111	35.5	33.4	19.0	32.4	27.1	35.6	33.4	20.2	29.7	13.5
6149.258	55.2	49.5	32.7	49.6	39.6	54.8	48.5	36.5	45.7	21.3
6369.462	32.3	31.5	17.0	30.2	22.5	32.6	28.8	19.0	27.2	11.5
6416.919	56.5	54.4	36.9	52.6	47.7	55.4	52.4	38.9	50.2	36.2
6432.680	59.6	54.5	37.2	54.9	45.3	59.6	55.4	39.7	52.9	26.0

Table 1. Larguras Equivalentes das Linhas de Fe I e Fe II.

λ (Å)	BD-10 3166	HD99109	HD100777	HD101930	HD102117	HD102195	HD106252	HD107148	NGC4349-127	HD108147
4779.439	71.3	73.7	...	77.2	59.0	59.4	34.9
4788.751	88.7	90.6	82.6	89.9	82.5	83.8	61.9	79.8	134.9	60.8
4802.875	81.5	81.2	76.8	77.1	76.2	71.7	56.2	73.4	...	57.6
4962.572	80.2	82.5	75.5	77.2	74.3	68.0	50.3	72.0	95.0	54.0
5054.642	71.0	66.9	63.0	62.7	60.1	56.0	33.6	56.9	91.4	31.1
5247.049	96.4	100.4	92.5	102.1	90.9	100.5	61.1	83.2	...	55.4
5379.574	88.6	84.1	80.1	82.7	78.9	75.3	56.2	75.8	117.4	56.5
5618.631	73.6	74.9	69.6	72.0	67.6	63.4	45.6	65.8	...	45.4
5741.846	58.9	58.2	51.0	55.4	50.3	47.8	27.5	47.6	82.9	28.0
5775.081	86.7	81.0	78.0	105.8	...
5778.453	51.2	52.9	41.6	50.8	37.9	38.5	16.6	34.4	90.9	14.2
5855.076	43.8	44.9	39.0	39.3	38.3	32.7	18.4	34.9	...	21.0
5916.247	84.7	88.3	...	88.1	75.7	73.7	51.3	71.4	...	47.7
5956.692	84.0	86.0	75.3	82.3	71.6	77.9	42.7	64.8	165.0	38.4
6120.246	22.1	25.9	13.7	25.6	13.5	15.1	...	10.1	81.9	...
6151.617	76.5	80.1	69.8	77.2	68.9	71.7	42.5	64.4	131.8	39.0
6173.334	100.9	105.2	89.5	100.7	88.7	93.0	62.5	84.4	164.9	60.9
6200.313	100.5	109.2	98.9	99.1	88.3	99.3	66.7	85.5	155.4	66.0
6219.279	123.5	137.8	115.5	125.9	111.8	117.7	84.1	109.4	200.5	84.8
6240.645	76.5	79.7	71.0	76.0	67.5	68.9	42.3	63.5	...	39.7
6265.131	130.0	132.3	111.9	128.5	109.5	119.0	79.6	103.1	202.1	78.1
6380.743	76.7	81.9	72.5	73.5	71.9	65.5	47.4	69.4	111.5	49.1
6593.870	119.5	120.5	104.8	115.3	97.3	100.4	79.7	103.3	188.6	75.0
6699.141	23.3	23.8	18.3	19.6	16.4	12.8	7.3	14.9	...	7.5

Table 1—Continued

λ (Å)	BD-10 3166	HD99109	HD100777	HD101930	HD102117	HD102195	HD106252	HD107148	NGC4349-127	HD108147
6739.520	37.2	40.7	30.2	39.3	25.6	27.4	8.8	20.8
6750.150	109.2	114.7	95.9	106.4	92.6	97.1	68.3	88.2	165.4	67.1
6858.145	74.5	74.3	64.7	70.7	68.0	64.1	44.0	65.2	...	51.2
4993.358	41.7	44.1	43.9	41.8	50.7	37.0	36.6	46.9	63.1	47.9
5132.669	26.2	28.3	12.6	38.8	45.9	25.8	26.0	42.0	...	34.2
5284.109	65.8	66.1	74.8	58.1	79.0	59.4	64.5	78.7	91.2	77.9
5325.553	34.1	35.2	42.0	25.4	49.8	29.3	42.9	51.4	59.7	56.3
5414.073	30.0	31.5	33.7	19.9	39.8	20.9	28.8	38.8	45.6	39.8
5425.257	43.6	46.5	49.1	37.4	53.1	35.0	43.3	53.0	60.2	55.1
5991.376	...	33.3	39.3	26.9	42.4	23.5	36.2	47.7	...	47.6
6084.111	22.6	24.3	27.1	16.7	30.1	14.5	21.3	30.0	48.6	30.5
6149.258	34.7	33.9	40.6	25.3	45.9	26.7	36.9	48.0	51.9	53.3
6369.462	19.0	19.8	17.9	11.8	30.5	14.5	19.9	27.5	38.0	29.5
6416.919	44.4	46.1	47.1	38.8	51.1	36.2	39.2	51.4	56.1	52.2
6432.680	38.6	37.8	46.3	30.7	51.5	33.2	42.4	51.2	63.3	57.0

Table 1. Larguras Equivalentes das Linhas de Fe I e Fe II.

λ (Å)	HD108874	HD109749	HD111232	HD114386	HD114762	HD114783	HD11479	HD117176	HD117207	HD117618
4779.439	57.6	51.0	33.8	74.4	27.8	48.0
4788.751	79.3	76.2	59.3	...	34.1	86.6	56.9	73.8	79.1	63.1
4802.875	73.6	70.4	50.4	69.9	27.1	74.6	48.6	65.2	72.7	58.2
4962.572	72.6	67.0	40.7	...	20.6	69.5	41.6	59.0	69.6	52.8
5054.642	57.2	51.7	34.5	68.8	26.1	46.2	56.4	34.9
5247.049	89.7	77.5	62.9	106.3	30.2	99.0	56.1	84.5	85.7	60.8
5379.574	77.0	72.7	51.8	76.6	25.1	79.9	47.9	66.1	75.3	58.1
5618.631	65.7	60.2	37.8	60.2	17.3	65.8	36.1	54.0	65.0	46.0
5741.846	46.9	41.1	23.5	...	8.5	49.7	20.5	36.9	45.1	28.4
5775.081	...	69.7	49.4	67.3	...	78.5	46.0	63.1	74.4	...
5778.453	38.1	29.6	16.1	47.2	...	46.9	11.6	28.2	35.7	16.5
5855.076	37.3	32.1	14.0	31.0	...	35.8	12.0	24.9	34.0	20.8
5916.247	69.4	63.0	46.9	81.6	21.3	82.1	42.6	58.6	74.1	50.9
5956.692	74.8	59.9	53.2	86.5	...	86.4	42.2	65.0	68.5	44.1
6120.246	13.6	8.1	5.5	22.4	...	9.2	11.1	3.7
6151.617	66.4	59.5	42.5	75.1	16.3	74.1	36.4	58.5	64.0	44.5
6173.334	85.8	79.5	61.1	96.7	31.6	96.2	55.3	77.5	84.6	64.0
6200.313	93.5	86.1	65.0	98.4	34.8	96.2	59.7	82.8	91.1	69.9
6219.279	111.8	103.5	81.7	126.3	...	121.5	77.6	99.9	110.7	85.6
6240.645	66.1	58.1	41.7	75.0	...	73.3	33.7	57.3	65.5	42.1
6265.131	108.5	98.1	78.9	125.7	...	122.9	74.3	96.3	105.5	82.0
6380.743	68.9	64.8	40.6	52.8	18.3	61.7	37.4	56.6	67.6	49.0
6593.870	102.8	90.0	81.0	104.4	...	109.8	69.1	91.3	97.8	75.2
6699.141	14.7	11.3	4.3	16.6	5.1	9.8	12.8	7.5

Table 1—Continued

λ (Å)	HD108874	HD109749	HD111232	HD114386	HD114762	HD114783	HD11479	HD117176	HD117207	HD117618
6739.520	24.7	14.9	9.7	34.6	...	34.6	...	17.7	23.0	...
6750.150	92.1	85.9	65.2	99.7	...	102.6	64.2	81.6	91.7	70.4
6858.145	68.2	64.5	36.0	58.6	17.6	59.4	36.4	53.3	68.8	48.8
4993.358	42.1	49.9	23.4	54.1	20.5	41.5	36.2	42.1	45.1	43.4
5132.669	52.9	41.0	18.3	22.4	34.0	42.2	31.7
5284.109	71.8	81.8	44.2	47.6	41.3	52.1	61.8	68.3	72.8	71.3
5325.553	42.0	54.3	24.0	9.3	23.8	22.9	43.3	43.0	45.1	48.4
5414.073	32.9	41.3	12.1	6.8	13.6	15.5	26.0	32.2	33.8	33.6
5425.257	47.8	56.3	25.0	29.4	24.2	33.6	41.0	45.1	49.5	47.6
5991.376	...	48.1	17.2	17.4	17.6	17.7	30.4	34.8	42.1	35.1
6084.111	25.1	31.4	10.7	6.4	...	13.2	20.1	24.6	27.0	24.9
6149.258	39.6	50.5	17.6	13.3	21.7	21.9	34.8	38.2	43.0	44.0
6369.462	22.7	30.6	11.0	9.7	9.6	11.1	17.6	22.4	25.1	23.3
6416.919	44.2	51.6	22.3	30.6	23.8	32.5	37.0	41.4	48.7	43.7
6432.680	45.3	55.5	23.2	18.7	24.1	27.4	40.4	45.0	47.7	48.3

Table 1. Larguras Equivalentes das Linhas de Fe I e Fe II.

λ (Å)	HD120136	HD121504	HD122430	HD125612	HD128311	HD130322	HD134987	HD330075	HD141937	HD142415
4779.439	33.3	50.1	...	54.9
4788.751	57.7	66.4	...	72.9	97.3	77.9	79.2	88.5	69.0	66.2
4802.875	...	61.7	98.7	69.8	...	69.4	73.7	74.2	64.1	63.5
4962.572	61.4	57.0	89.9	65.3	...	62.8	71.6	71.4	60.8	56.1
5054.642	30.8	...	97.8	46.5	...	51.7	59.7	83.3	42.4	38.7
5247.049	...	63.4	...	74.8	...	89.8	86.0	105.7	67.4	67.3
5379.574	57.7	60.2	110.2	69.0	82.2	73.2	77.8	81.2	64.9	62.5
5618.631	45.6	50.8	...	60.0	67.8	62.0	64.8	64.8	53.5	51.5
5741.846	28.2	32.9	78.7	42.1	52.0	42.3	45.7	52.2	35.0	32.5
5775.081	56.7	60.4	76.8	73.0
5778.453	...	19.2	93.8	25.6	50.9	36.4	35.2	48.4	24.7	20.5
5855.076	...	23.4	...	29.7	36.7	31.3	36.6	36.4	25.7	23.3
5916.247	...	55.9	...	56.1	...	71.3	...	82.6	58.9	...
5956.692	29.5	47.2	168.5	58.4	94.5	73.5	65.8	86.8	54.4	48.1
6120.246	...	4.5	86.8	8.1	...	13.9	10.9	21.8	5.6	5.1
6151.617	34.8	46.9	131.4	56.0	83.9	65.2	65.0	77.4	50.8	48.0
6173.334	61.8	67.3	157.9	76.4	103.5	85.2	85.5	93.8	69.8	68.2
6200.313	67.5	73.6	139.1	82.4	107.9	92.1	86.9	99.5	78.1	75.8
6219.279	88.5	91.2	195.7	100.2	156.2	107.6	109.4	125.6	94.6	94.4
6240.645	...	46.8	128.1	55.6	82.6	65.9	64.5	75.3	51.4	47.0
6265.131	81.4	84.4	192.6	93.9	144.4	108.0	106.2	127.6	89.7	89.0
6380.743	...	54.3	...	63.1	60.1	65.3	69.2	68.0	57.9	54.6
6593.870	71.8	79.8	183.3	92.8	123.1	98.9	97.3	111.7	83.7	81.4
6699.141	...	8.0	30.4	11.6	13.9	11.7	13.5	17.6	9.0	10.5

Table 1—Continued

λ (Å)	HD120136	HD121504	HD122430	HD125612	HD128311	HD130322	HD134987	HD330075	HD141937	HD142415
6739.520	...	10.0	...	14.0	37.8	25.2	...	38.4	13.2	13.0
6750.150	61.2	73.0	156.5	81.9	113.6	90.3	92.2	106.0	74.9	71.3
6858.145	...	52.8	...	63.1	...	64.2	70.3	67.6	58.5	57.5
4993.358	63.2	43.2	63.9	47.1	...	32.9	49.4	50.6	43.1	42.8
5132.669	41.3	31.8	55.2	37.0	...	24.3	48.7	...	33.1	32.5
5284.109	...	74.2	82.2	77.4	51.7	59.5	80.5	52.0	72.9	73.3
5325.553	72.4	50.1	40.1	52.6	...	30.2	49.7	15.6	46.6	46.1
5414.073	27.4	35.4	39.5	38.7	...	20.4	42.8	13.2	33.8	33.4
5425.257	65.0	49.5	48.8	53.7	31.4	36.8	56.2	33.0	48.4	48.6
5991.376	...	40.5	...	42.6	...	30.4	45.6	...	42.0	43.6
6084.111	...	27.4	33.4	27.8	...	17.2	30.8	12.2	26.3	26.0
6149.258	...	46.2	43.2	48.2	...	27.6	47.6	19.6	43.9	45.2
6369.462	...	25.4	33.3	27.5	10.4	15.9	30.5	13.0	25.2	26.0
6416.919	64.3	47.7	50.2	52.1	...	35.9	50.6	34.8	46.9	46.3
6432.680	67.5	50.8	51.3	54.1	23.4	33.4	53.4	22.8	49.1	48.8

Table 1. Larguras Equivalentes das Linhas de Fe I e Fe II.

λ (Å)	HD142022A	HD147513	HD149143	HD154857	HD156846	HD159868	HD160691	HD162020	HD164922	HD168443
4779.439	59.5	...	51.9	47.2	57.0	...	64.5	52.5
4788.751	81.2	66.7	76.8	66.3	70.0	72.4	79.5	97.0	82.0	77.4
4802.875	74.6	60.5	71.6	57.2	65.3	65.8	75.3	...	74.4	69.8
4962.572	74.0	57.6	69.7	48.5	59.4	59.4	71.8	...	74.3	63.5
5054.642	60.1	...	52.6	35.4	38.9	45.1	59.1	...	57.5	53.9
5247.049	92.4	64.8	77.7	73.4	67.8	82.5	86.6	...	90.6	87.1
5379.574	78.5	60.9	73.9	57.2	62.9	65.6	77.1	78.7	77.6	72.2
5618.631	66.8	50.4	61.2	44.0	54.2	52.8	66.0	...	66.1	58.7
5741.846	48.6	32.8	43.4	26.9	33.0	35.0	45.5	48.6	49.2	40.2
5775.081	52.7	63.5	...	74.1	70.3	78.4	67.5
5778.453	41.3	20.7	28.6	18.7	20.0	28.2	35.6	47.4	42.8	32.5
5855.076	37.3	23.6	33.0	16.9	22.3	24.0	34.8	31.7	36.7	28.9
5916.247	76.5	...	70.4	55.4	64.0	62.3	68.9	...	76.3	60.4
5956.692	76.4	49.2	62.9	54.5	56.6	62.2	66.0	92.7	77.3	68.6
6120.246	15.6	4.9	7.6	5.3	...	7.9	10.1	26.2	17.6	9.8
6151.617	69.2	49.3	60.0	48.0	48.3	57.4	65.6	79.5	71.8	62.2
6173.334	89.0	69.7	81.2	67.1	71.1	76.6	85.2	105.4	90.0	81.7
6200.313	90.6	74.8	88.4	71.5	77.6	81.3	91.4	104.1	91.7	86.4
6219.279	116.5	95.3	104.2	90.4	94.2	99.0	109.5	134.8	110.7	104.7
6240.645	68.8	48.3	59.4	46.6	49.6	57.0	66.0	79.9	70.5	62.5
6265.131	111.7	88.6	99.1	85.3	89.3	94.3	106.0	133.6	114.2	99.0
6380.743	70.3	52.8	66.7	46.0	57.3	56.7	70.6	...	68.6	63.2
6593.870	100.8	81.5	93.4	80.6	95.0	88.5	97.8	117.3	102.8	92.1
6699.141	14.5	8.8	12.8	5.5	...	8.2	12.9	...	15.4	12.2

Table 1—Continued

λ (Å)	HD142022A	HD147513	HD149143	HD154857	HD156846	HD159868	HD160691	HD162020	HD164922	HD168443
6739.520	27.2	10.8	...	12.0	14.3	17.2	20.8	...	30.7	18.0
6750.150	94.8	74.7	87.0	72.6	77.4	82.1	90.7	104.7	95.7	86.1
6858.145	70.1	54.7	66.5	43.1	53.0	56.0	69.0	63.8	69.2	58.3
4993.358	40.7	41.0	55.5	38.0	57.1	44.1	51.8	...	38.1	45.6
5132.669	11.8	26.7	49.2	28.4	35.1	34.7	46.8	...	25.0	42.6
5284.109	69.6	69.0	89.5	64.2	85.8	70.1	81.4	48.7	61.8	70.9
5325.553	39.6	43.5	60.6	41.0	63.6	45.0	52.5	...	34.1	44.4
5414.073	31.4	28.9	47.1	28.5	44.9	32.7	42.6	...	25.7	34.3
5425.257	45.2	43.6	61.7	41.4	64.2	46.4	57.0	...	39.5	49.3
5991.376	37.0	30.4	46.8	31.3	56.4	37.7	50.7	...	32.1	37.4
6084.111	23.9	21.2	37.8	20.7	40.0	24.7	32.8	...	20.6	26.7
6149.258	37.7	39.7	56.4	34.6	59.5	40.8	50.4	17.9	30.5	42.2
6369.462	23.0	20.1	35.8	19.4	37.3	24.5	31.1	...	18.0	24.4
6416.919	43.9	42.0	57.2	37.9	60.0	43.6	53.6	...	40.4	44.5
6432.680	41.7	43.7	61.9	42.0	65.8	44.4	54.8	21.5	35.9	45.1

Table 1. Larguras Equivalentes das Linhas de Fe I e Fe II.

λ (Å)	HD168746	HD169830	HD170469	HD171028	HD175541	HD177830	HD179949	HD181433	HD183263	HD231701
4779.439	45.3	33.6	56.1	26.5	66.4	30.7
4788.751	68.9	62.6	79.9	53.3	84.5	108.6	62.6	103.1	75.9	55.4
4802.875	62.1	58.4	73.0	45.0	74.8	...	58.8	83.8	69.9	52.3
4962.572	53.5	51.9	71.2	36.1	68.6	87.1	57.2	77.0	68.8	46.7
5054.642	41.2	32.9	55.0	22.1	58.0	77.0	33.9	...	51.7	28.0
5247.049	75.9	51.1	84.4	58.7	112.4	134.5	55.3	116.5	76.5	50.3
5379.574	62.8	57.0	75.7	44.4	77.7	94.7	58.5	95.9	73.1	51.3
5618.631	49.8	44.5	63.9	31.5	62.7	...	47.9	75.8	61.5	40.4
5741.846	33.4	26.2	46.7	16.6	48.0	67.7	29.9	63.3	42.2	20.7
5775.081	61.3	54.9	94.9	...	97.2	...	49.4
5778.453	25.0	13.6	35.6	10.0	46.1	75.5	15.9	63.1	28.9	13.6
5855.076	22.5	17.7	34.3	11.2	32.6	51.6	20.0	45.4	31.3	16.0
5916.247	56.4	49.5	...	38.5	81.5	103.0	...	47.0
5956.692	56.2	31.0	64.6	36.7	88.8	113.9	36.4	97.7	57.7	29.4
6120.246	5.9	...	8.5	...	23.8	39.3	6.9	...
6151.617	53.2	35.5	64.1	34.2	77.3	100.8	38.6	87.7	59.2	32.5
6173.334	72.6	59.2	84.8	54.1	95.6	127.1	62.0	126.4	78.4	55.9
6200.313	76.5	67.2	87.1	55.9	96.2	117.2	69.1	108.8	86.9	61.4
6219.279	94.7	85.1	109.1	74.4	120.4	162.5	85.0	160.1	104.8	81.1
6240.645	52.5	36.0	63.8	34.9	...	101.1	38.8	91.0	58.1	34.4
6265.131	89.9	79.3	102.8	72.0	116.2	162.3	80.4	157.9	97.7	72.1
6380.743	53.6	46.8	69.1	33.6	67.0	...	50.1	88.7	66.4	43.5
6593.870	83.4	73.9	95.5	69.1	113.8	158.4	74.3	125.1	88.9	73.9
6699.141	9.4	6.3	13.4	...	12.7	34.5	7.2	27.6	12.7	...

Table 1—Continued

λ (Å)	HD168746	HD169830	HD170469	HD171028	HD175541	HD177830	HD179949	HD181433	HD183263	HD231701
6739.520	15.8	7.7	...	66.7	9.2	52.1	16.8	...
6750.150	77.6	66.2	94.2	58.0	100.3	135.7	69.4	125.6	85.6	68.8
6858.145	52.6	50.4	69.0	30.9	63.8	...	52.0	...	64.9	41.7
4993.358	35.4	59.6	50.5	33.9	45.0	53.5	50.7	54.6	51.9	46.6
5132.669	26.1	41.3	47.4	20.1	21.9	...	37.1	...	42.0	30.1
5284.109	58.8	87.2	81.4	58.4	67.8	70.9	78.0	17.4	81.7	74.4
5325.553	34.4	67.1	52.7	40.2	43.3	...	59.9	21.7	54.4	54.9
5414.073	22.8	47.2	41.2	23.4	30.6	31.0	38.9	14.4	41.9	35.5
5425.257	37.7	65.6	56.1	38.3	44.4	48.6	55.7	42.3	58.4	50.5
5991.376	27.8	54.3	47.7	31.5	37.7	...	44.9	...	47.7	41.0
6084.111	17.4	38.9	31.7	19.0	26.3	...	31.2	19.2	34.8	27.5
6149.258	30.9	63.7	50.4	31.1	34.1	40.9	54.3	21.5	52.1	47.9
6369.462	17.1	36.6	31.6	17.8	22.3	24.6	30.6	8.7	32.3	27.6
6416.919	35.7	60.2	53.2	33.2	41.2	...	52.2	41.0	54.2	49.3
6432.680	34.8	66.2	55.3	37.6	43.8	43.4	56.5	29.5	57.4	49.8

Table 1. Larguras Equivalentes das Linhas de Fe I e Fe II.

λ (Å)	HD187085	HD188310	HD189733	HD190647	HD192263	HD192699	HD195019	WASP2	HD196050	HD196885
4779.439	36.2	95.3	67.8	59.0	72.4	59.9	...	67.1	50.7	37.0
4788.751	63.4	104.3	90.2	81.2	89.9	82.2	71.2	84.2	75.5	64.1
4802.875	59.9	88.2	72.5	74.1	...	71.9	64.7	73.5	69.1	62.1
4962.572	54.0	80.9	67.6	71.2	...	61.0	59.0	65.0	67.1	61.3
5054.642	33.1	75.2	69.1	60.6	...	52.0	43.9	55.4	49.9	34.7
5247.049	58.6	90.7	107.9	109.0	75.2	94.7	77.2	61.4
5379.574	59.1	96.2	78.0	79.5	80.4	73.5	64.7	78.7	73.1	62.1
5618.631	47.8	...	64.5	65.5	64.1	59.5	54.5	64.4	59.8	50.3
5741.846	28.8	60.0	47.7	48.2	46.9	43.1	35.4	49.0	43.1	32.4
5775.081	56.8	84.5	72.7	...	72.0	70.5	...	58.6
5778.453	15.1	69.9	42.8	38.7	45.6	40.8	25.2	43.6	27.8	14.9
5855.076	21.2	42.2	31.3	35.4	32.4	26.7	23.9	34.3	30.9	21.0
5916.247	51.5	...	85.4	75.1	...	79.8	...	79.9	66.3	42.9
5956.692	42.2	127.9	87.5	72.5	88.6	83.0	56.9	79.5	59.1	37.4
6120.246	...	45.7	14.7	12.1	22.9	18.9	4.9	18.1	7.3	...
6151.617	43.1	99.8	76.6	67.6	77.3	74.0	53.3	73.0	56.2	42.1
6173.334	63.2	117.7	101.4	88.5	102.2	90.5	72.5	91.9	79.2	66.5
6200.313	69.4	118.8	98.9	88.6	101.9	92.8	78.2	92.5	84.8	70.5
6219.279	87.3	156.4	127.1	112.3	127.8	112.6	93.9	124.6	103.4	89.3
6240.645	40.3	100.9	73.7	67.3	75.8	71.8	52.7	69.2	56.6	48.4
6265.131	80.7	160.4	127.7	108.1	121.8	110.7	92.5	117.5	98.2	83.5
6380.743	50.4	86.2	59.4	69.6	57.8	60.6	55.8	61.4	63.5	54.1
6593.870	80.5	155.6	110.9	106.8	113.5	110.5	85.8	119.6	94.7	76.0
6699.141	8.1	21.7	12.2	14.8	14.1	12.3	9.0	14.8	13.1	8.7

Table 1—Continued

λ (Å)	HD187085	HD188310	HD189733	HD190647	HD192263	HD192699	HD195019	WASP2	HD196050	HD196885
6739.520	7.8	...	29.9	...	32.5	...	19.2	31.9	16.7	11.5
6750.150	68.9	133.8	100.4	96.8	104.9	95.3	79.6	97.5	85.9	67.6
6858.145	53.0	75.1	66.8	67.9	63.9	58.9	55.0	67.0	60.5	54.1
4993.358	48.0	51.1	40.7	49.2	44.2	44.3	45.9	36.0	54.5	54.9
5132.669	33.8	48.2	...	21.1	35.1	...	42.3	32.7
5284.109	76.9	...	48.7	76.3	45.5	68.3	75.5	52.0	83.3	83.8
5325.553	55.0	48.1	12.7	49.0	18.0	43.8	49.5	25.2	55.5	64.5
5414.073	39.7	37.6	11.5	39.8	10.5	30.2	33.9	17.9	43.8	43.8
5425.257	54.8	55.1	30.8	54.8	30.2	44.6	50.6	32.7	57.9	61.4
5991.376	47.2	43.6	19.4	45.0	20.6	38.4	45.7	22.9	54.1	51.7
6084.111	31.0	...	9.2	28.7	8.1	26.1	26.5	15.7	34.0	35.8
6149.258	52.0	41.8	18.1	45.8	17.6	34.7	44.8	24.4	50.7	61.5
6369.462	29.0	32.0	9.3	29.2	...	22.9	25.9	13.3	30.8	36.1
6416.919	50.2	...	32.6	49.5	33.2	40.4	48.8	34.0	53.9	58.3
6432.680	56.8	52.3	23.0	52.5	22.0	44.0	50.9	29.4	56.3	65.3

Table 1. Larguras Equivalentes das Linhas de Fe I e Fe II.

λ (Å)	HD199665	HD202206	HD208487	HD209458	HD210277	HD210702	HD212301	HD213240	HD216435	HD216437
4779.439	72.0	...	34.9	...	59.0	79.5	35.4	...	47.5	51.7
4788.751	98.4	79.5	61.7	58.4	81.6	95.8	61.9	69.3	73.4	76.5
4802.875	85.8	74.4	56.2	54.0	73.2	82.9	57.7	65.0	69.2	71.5
4962.572	79.5	72.9	51.7	48.9	70.6	77.0	54.2	59.9	64.3	67.0
5054.642	66.4	55.3	32.5	30.5	60.4	68.5	33.0	...	46.4	52.2
5247.049	...	84.8	55.4	54.3	94.9	...	53.8	67.0	73.9	76.6
5379.574	89.3	75.9	57.9	54.3	78.6	87.9	56.5	64.5	68.7	72.2
5618.631	72.8	65.2	44.4	43.7	64.9	72.5	48.5	54.9	55.9	61.0
5741.846	56.9	48.4	27.1	25.9	45.2	57.3	29.1	35.0	38.6	41.9
5775.081	75.3	83.1	56.9	...	67.6	69.8
5778.453	59.6	35.1	15.2	14.3	38.8	60.0	14.3	...	22.9	29.6
5855.076	43.7	35.2	21.4	17.1	34.2	41.6	21.5	...	28.4	31.2
5916.247	90.6	...	37.4	41.3	66.1	95.1	50.5	58.5	64.9	67.5
5956.692	104.4	66.6	42.2	36.5	72.0	103.4	...	51.0	53.0	61.1
6120.246	32.6	11.1	12.8	34.8	5.6	8.8
6151.617	90.0	64.1	41.5	37.7	68.8	88.3	41.2	50.1	54.3	60.0
6173.334	110.5	85.7	61.2	58.0	87.6	108.5	61.9	72.3	76.5	80.8
6200.313	100.9	87.3	66.7	64.2	93.5	109.8	68.3	76.3	82.4	86.6
6219.279	141.1	112.6	86.3	81.4	114.3	137.6	87.9	94.9	100.3	104.5
6240.645	88.2	64.7	39.0	37.6	67.5	86.4	37.2	...	55.2	59.0
6265.131	137.3	107.0	81.8	77.4	110.2	134.9	82.1	88.9	93.2	97.9
6380.743	77.3	69.8	49.1	45.6	68.3	81.4	50.4	55.6	61.5	64.7
6593.870	125.7	106.0	76.8	75.3	102.7	135.3	78.7	83.0	95.8	92.8
6699.141	18.4	15.8	6.2	6.4	15.9	20.3	7.6	...	11.3	11.6

Table 1—Continued

λ (Å)	HD199665	HD202206	HD208487	HD209458	HD210277	HD210702	HD212301	HD213240	HD216435	HD216437
6739.520	...	22.3	7.5	...	25.1	49.4	12.7	16.0
6750.150	116.5	90.5	67.2	68.1	92.5	115.9	66.9	76.9	80.9	85.2
6858.145	66.2	68.5	49.2	45.2	69.0	72.2	52.8	55.2	61.6	64.1
4993.358	53.1	45.1	44.0	41.5	43.7	46.8	48.1	50.9	54.8	52.1
5132.669	24.8	39.9	24.4	28.3	12.1	16.6	36.0	38.0	44.8	44.3
5284.109	86.6	77.0	71.6	73.0	68.9	75.6	78.1	78.8	81.9	82.9
5325.553	54.6	49.2	51.1	49.9	38.7	43.9	55.6	54.7	60.6	55.6
5414.073	41.3	36.8	34.7	34.0	33.1	33.8	38.9	40.3	46.6	43.4
5425.257	57.0	51.5	49.7	48.3	46.4	47.7	55.6	55.7	61.2	57.5
5991.376	...	42.8	...	39.5	39.3	42.0	45.0	46.5	50.7	48.5
6084.111	37.5	29.4	27.7	23.6	23.4	28.9	32.2	31.1	37.5	33.3
6149.258	49.9	43.9	47.3	45.2	38.6	39.8	52.9	52.0	56.0	51.2
6369.462	35.9	28.0	26.5	25.1	23.7	28.4	27.5	30.4	36.9	...
6416.919	53.9	50.3	48.5	45.6	44.8	46.2	53.1	52.2	57.3	53.7
6432.680	59.5	51.1	51.7	48.5	42.7	49.2	55.6	56.1	62.3	57.0

Table 1. Larguras Equivalentes das Linhas de Fe I e Fe II.

λ (Å)	HD216770	HD217014	HD217107	HD219449	HD219828	HD221287	HD222582	HD224693
4779.439	66.7	50.7	62.3	...	49.5	...	41.8	49.0
4788.751	86.5	76.9	83.9	116.8	76.0	51.1	69.1	75.6
4802.875	78.0	69.2	77.5	98.5	68.7	48.8	61.6	71.4
4962.572	77.8	66.6	75.3	92.0	64.4	42.4	55.6	65.5
5054.642	66.1	50.4	63.3	85.0	46.1	...	41.4	47.5
5247.049	91.7	78.9	91.9	...	76.4	41.4	69.7	74.4
5379.574	83.5	71.6	78.5	106.5	68.5	47.5	61.5	71.4
5618.631	70.9	59.6	69.3	78.6	57.2	38.2	50.8	59.6
5741.846	52.3	40.7	52.2	70.4	38.4	20.5	31.7	40.1
5775.081	82.3	71.0	80.5	96.5	67.5	69.0
5778.453	46.9	29.7	43.0	82.5	24.7	11.9	21.3	25.1
5855.076	40.4	29.6	39.5	52.5	27.8	15.8	22.6	29.4
5916.247	77.8	68.4	78.5	123.3	68.4	36.5	57.3	66.4
5956.692	80.3	60.7	73.8	139.2	57.7	25.3	52.1	56.1
6120.246	18.7	9.9	14.3	...	6.9	...	4.9	8.4
6151.617	74.0	58.0	72.4	115.1	56.0	29.5	50.1	56.8
6173.334	96.2	78.4	91.5	142.0	77.8	49.3	69.0	78.8
6200.313	94.6	81.2	92.1	136.5	79.3	53.8	74.6	84.5
6219.279	124.3	101.3	116.2	174.7	101.7	73.2	91.5	100.9
6240.645	73.9	57.8	72.1	112.6	56.3	...	50.7	56.2
6265.131	120.1	96.8	113.3	170.7	93.8	68.3	86.9	96.0
6380.743	73.5	63.7	73.7	98.0	62.5	40.6	53.2	62.6
6593.870	108.6	98.4	103.4	166.3	97.8	65.2	88.2	99.7
6699.141	20.4	11.9	18.9	29.2	9.7	...	8.4	11.2

Table 1—Continued

λ (Å)	HD216770	HD217014	HD217107	HD219449	HD219828	HD221287	HD222582	HD224693
6739.520	32.4	18.6	26.9	75.8	15.3	...	11.8	12.6
6750.150	104.1	86.3	96.8	147.2	85.1	58.5	74.9	83.8
6858.145	72.5	63.0	73.1	...	60.9	39.1	53.9	63.0
4993.358	42.1	46.4	47.9	61.4	51.8	42.3	39.3	56.3
5132.669	19.9	39.1	49.0	...	40.2	26.9	27.1	47.6
5284.109	67.8	76.5	77.5	...	80.2	70.7	66.4	89.3
5325.553	37.0	49.2	47.7	...	55.4	49.4	43.1	61.1
5414.073	31.2	36.2	40.2	43.2	41.2	33.8	30.4	48.1
5425.257	44.7	51.3	53.9	57.3	56.4	48.7	43.9	62.2
5991.376	37.3	42.1	44.5	...	49.2	38.8	33.9	52.8
6084.111	23.9	29.6	30.2	...	32.4	24.2	21.6	38.5
6149.258	35.7	45.1	46.5	50.7	51.0	47.3	38.7	57.8
6369.462	21.7	27.1	28.2	...	30.9	24.3	21.0	36.5
6416.919	43.1	51.0	50.6	...	52.8	46.1	41.9	59.1
6432.680	39.7	50.9	51.3	59.6	57.6	46.8	43.2	61.9

Table 1. Larguras Equivalentes das Linhas de Fe I e Fe II.

λ (Å)	HD1581	HD1835	HD2151	HD3823	HD4628	HD7199	HD7693	HD7570	HD10180	HD10476
4779.439	28.1	...	36.4	23.1	62.7	72.8	73.8	...	43.0	59.9
4788.751	54.6	75.4	64.2	50.2	75.4	89.2	...	65.7	68.5	79.9
4802.875	49.5	68.2	56.7	43.8	61.1	78.5	...	62.3	62.4	68.4
4962.572	42.8	70.8	51.3	37.3	56.3	84.3	...	58.9	59.1	65.0
5054.642	25.7	48.0	34.3	21.5	...	64.6	78.9	38.4	41.5	56.6
5247.049	52.9	78.8	64.3	46.9	...	106.4	...	61.3	67.3	97.0
5379.574	48.3	69.3	57.2	42.1	66.2	83.3	...	61.4	64.5	73.7
5618.631	36.5	59.4	46.3	31.3	51.8	76.9	70.9	52.7	52.6	59.8
5741.846	21.1	40.9	27.0	17.6	34.5	57.2	53.8	32.2	32.2	43.4
5775.081	45.2	...	55.2	39.0	62.0	...	88.8
5778.453	12.2	27.4	...	9.1	33.8	51.5	49.5	17.2	20.1	38.1
5855.076	15.6	30.3	18.6	10.7	21.8	44.3	37.0	24.1	22.8	29.0
5916.247	39.3	67.2	53.5	33.9	71.4	87.8	91.7	47.8	...	75.3
5956.692	33.8	57.6	46.0	27.9	73.5	82.4	93.2	42.0	51.3	75.1
6120.246	...	7.1	14.3	23.4	27.8	15.1
6151.617	34.1	58.2	42.7	28.1	64.7	78.6	83.7	45.4	48.6	67.6
6173.334	53.4	80.7	66.4	47.1	84.0	101.3	111.3	67.8	69.9	88.4
6200.313	59.8	88.3	69.7	51.9	86.0	99.5	108.4	72.6	76.1	96.1
6219.279	77.7	108.2	84.2	71.0	108.7	136.0	...	90.6	91.8	119.3
6240.645	33.0	...	44.2	27.7	64.7	77.3	83.8	44.3	49.0	66.1
6265.131	72.1	101.8	82.8	67.0	108.6	124.5	143.9	84.5	87.9	110.0
6380.743	40.8	63.3	47.5	32.9	48.9	79.7	...	55.7	55.3	62.0
6593.870	69.8	...	81.7	64.9	95.5	112.9	...	79.5	87.4	101.7
6699.141	...	11.7	5.9	...	8.2	22.3	...	9.7	7.5	11.2

Table 1—Continued

λ (Å)	HD1581	HD1835	HD2151	HD3823	HD4628	HD7199	HD7693	HD7570	HD10180	HD10476
6739.520	10.6	4.1	22.7	36.4	38.9	11.5	...	25.8
6750.150	62.1	88.2	69.3	55.4	91.4	105.5	114.8	74.2	74.7	93.3
6858.145	41.7	64.3	45.4	32.4	52.7	68.7	73.8	53.2	53.1	62.0
4993.358	32.4	42.9	44.4	34.9	39.2	42.2	44.3	50.0	45.3	33.9
5132.669	21.1	40.8	31.5	21.2	...	35.8	...	37.5	33.2	19.2
5284.109	61.9	74.1	73.2	63.1	41.8	71.7	50.1	81.8	73.4	53.3
5325.553	37.5	47.4	50.5	42.4	12.3	38.0	20.5	57.0	48.9	23.0
5414.073	25.3	35.3	36.1	25.5	7.1	32.1	10.4	39.9	35.8	14.7
5425.257	37.5	51.3	51.7	41.6	22.7	48.6	33.9	57.3	50.7	30.2
5991.376	30.7	42.0	42.0	29.8	12.2	35.9	...	47.5	38.6	20.7
6084.111	21.6	27.7	28.8	19.9	5.1	24.5	11.1	33.4	28.1	11.1
6149.258	35.9	46.8	45.4	36.4	12.9	38.2	18.5	52.0	43.0	22.0
6369.462	17.6	26.1	25.8	17.2	6.5	22.3	9.4	29.7	25.3	10.6
6416.919	37.5	49.7	48.4	36.1	23.3	48.1	37.7	54.8	45.9	30.7
6432.680	44.7	50.5	53.9	40.4	13.4	43.4	26.4	59.1	50.0	26.9

Table 1. Larguras Equivalentes das Linhas de Fe I e Fe II.

λ (Å)	HD10700	HD11112	HD12387	HD16160	HD17925	HD18907	HD19632	HD20029	HD20201	HD20630
4779.439	34.3	49.2	34.2	...	68.1	43.1	...	37.6
4788.751	59.5	74.3	60.5	81.3	88.8	66.7	74.5	63.7	65.6	70.3
4802.875	49.3	69.3	53.1	...	77.6	53.8	67.6	59.0	61.9	64.2
4962.572	42.5	64.2	46.7	46.0	63.8	54.7	56.8	57.8
5054.642	31.6	46.9	33.7	...	69.5	38.4	46.4	33.2	...	43.4
5247.049	68.7	73.1	62.8	106.3	...	87.4	80.6	58.0	64.8	74.8
5379.574	51.3	69.7	52.8	72.5	81.8	54.9	68.6	58.5	59.8	66.4
5618.631	37.2	59.1	41.1	56.7	70.5	41.9	58.5	47.7	50.8	56.4
5741.846	21.9	40.4	23.7	42.4	49.7	24.8	39.2	28.3	32.1	36.6
5775.081	50.5	...	85.5	65.6
5778.453	19.7	25.9	17.3	41.4	46.4	24.3	25.9	15.1	19.0	27.1
5855.076	12.7	28.6	16.1	27.9	35.2	15.1	28.6	20.3	23.1	26.0
5916.247	51.3	64.8	49.7	80.6	50.8	57.1	...
5956.692	50.3	55.1	43.1	87.1	90.0	66.3	60.7	36.6	44.5	56.6
6120.246	5.6	6.6	4.3	17.9	20.2	9.0	8.8	8.0
6151.617	45.5	55.5	42.6	74.3	82.3	53.9	57.2	41.0	47.5	53.6
6173.334	62.3	76.3	61.4	94.4	109.5	70.0	79.5	63.1	67.0	77.6
6200.313	67.3	82.9	65.6	101.8	115.6	74.1	85.6	68.4	72.6	82.5
6219.279	87.4	99.6	82.7	127.8	135.6	91.5	109.0	86.7	90.7	104.1
6240.645	46.0	55.8	41.4	75.5	79.5	55.3	56.6	40.4	45.8	55.1
6265.131	80.7	94.2	78.2	116.7	136.1	89.1	100.4	80.9	84.7	97.4
6380.743	39.6	61.6	43.7	51.4	64.0	43.4	59.4	49.9	54.6	58.2
6593.870	75.0	91.6	72.8	121.8	120.5	85.6	100.5	74.9	85.5	...
6699.141	5.4	10.9	5.4	...	16.4	6.2	10.7	...	10.4	10.5

Table 1—Continued

λ (\AA)	HD10700	HD11112	HD12387	HD16160	HD17925	HD18907	HD19632	HD20029	HD20201	HD20630
6739.520	7.5	32.2	33.9	...	15.2	7.4	12.0	15.7
6750.150	71.4	82.0	68.8	91.5	108.3	75.9	84.1	71.5	74.3	85.2
6858.145	34.4	61.3	42.3	57.6	73.4	39.1	60.3	51.3	54.3	58.7
4993.358	22.8	49.3	33.4	...	39.3	28.9	40.9	49.5	44.1	38.7
5132.669	7.7	42.4	23.4	16.5	32.1	36.4	31.2	30.7
5284.109	38.6	82.3	55.8	37.0	56.4	44.8	70.9	77.5	76.6	70.0
5325.553	17.0	58.0	34.9	...	23.7	24.1	42.6	57.5	51.4	40.2
5414.073	9.4	42.0	21.6	...	15.9	14.5	31.7	40.2	35.5	30.1
5425.257	19.7	57.2	35.1	30.1	34.7	26.5	45.7	55.8	50.0	43.8
5991.376	13.5	48.9	24.6	...	24.4	18.7	36.7	47.1	42.5	34.1
6084.111	7.3	32.8	15.6	5.7	15.7	10.8	24.2	33.5	28.6	22.6
6149.258	15.0	50.3	29.2	12.2	24.3	19.3	40.8	53.4	47.9	38.1
6369.462	7.2	30.6	15.4	11.8	14.7	11.0	22.7	30.8	26.4	19.8
6416.919	21.5	53.6	30.9	...	37.2	23.1	46.3	54.0	49.7	43.2
6432.680	17.1	55.7	33.8	17.9	28.4	25.6	44.8	56.7	53.3	42.0

Table 1. Larguras Equivalentes das Linhas de Fe I e Fe II.

λ (Å)	HD20794	HD22104	HD22484	HD25587	HD25680	HD30876	HD31527	HD33473	HD36435	HD36889
4779.439	37.3	...	34.0	63.4	...	39.5	...	49.4
4788.751	61.2	81.5	60.3	56.1	68.2	86.4	58.0	67.2	77.2	74.6
4802.875	52.4	75.5	55.0	51.9	62.1	...	50.5	58.9	69.2	68.6
4962.572	44.1	72.9	48.7	46.2	54.2	63.4	44.9	53.6	59.1	64.2
5054.642	34.6	58.3	29.3	55.9	28.6	36.3	50.1	48.4
5247.049	69.9	85.4	57.4	50.6	67.1	102.6	55.4	72.0	92.0	78.4
5379.574	53.9	78.4	53.8	49.5	61.9	73.9	49.6	58.8	69.9	70.6
5618.631	41.5	66.3	42.9	38.3	49.3	60.6	39.1	47.3	59.1	58.3
5741.846	24.2	48.0	24.4	22.2	34.2	44.0	23.0	28.3	39.8	38.5
5775.081	47.4	55.7	71.9	69.2
5778.453	17.4	34.4	14.5	12.6	21.8	39.7	13.0	19.1	30.9	26.8
5855.076	15.5	36.4	17.6	15.0	23.9	28.2	14.6	19.2	26.5	29.1
5916.247	51.9	...	46.1	39.6	56.5	80.2	44.2	56.1	73.2	57.4
5956.692	53.5	66.8	38.0	29.9	49.2	81.5	38.1	52.3	68.5	57.7
6120.246	18.3	...	5.8	12.4	...
6151.617	46.7	63.8	37.9	33.0	48.9	73.6	38.3	49.4	63.6	57.6
6173.334	65.2	86.5	60.8	54.2	72.9	96.8	57.9	68.5	87.2	78.4
6200.313	69.7	86.9	65.4	58.9	74.6	102.3	61.9	73.9	91.4	84.6
6219.279	87.9	109.7	84.5	78.2	94.7	122.2	80.0	92.0	115.6	101.1
6240.645	45.4	64.7	36.3	36.4	48.6	71.9	37.2	48.4	63.8	58.6
6265.131	84.6	104.1	78.8	73.3	90.2	...	75.1	86.5	108.1	95.0
6380.743	43.8	72.0	45.4	40.8	55.4	54.6	41.5	49.0	59.4	63.7
6593.870	79.8	103.9	91.1	105.8	70.1	85.6	106.1	98.3
6699.141	4.5	...	8.1	...	11.0	10.2	5.3	5.5	9.4	12.0

Table 1—Continued

λ (\AA)	HD20794	HD22104	HD22484	HD25587	HD25680	HD30876	HD31527	HD33473	HD36435	HD36889
6739.520	11.7	...	6.6	...	15.7	28.7	7.7	...	19.3	15.3
6750.150	68.4	90.6	67.5	63.5	76.1	96.0	63.7	72.7	90.6	83.7
6858.145	44.0	71.2	45.1	41.3	54.5	63.3	40.8	46.7	61.5	59.3
4993.358	25.9	51.8	45.9	47.9	40.8	38.6	34.8	46.2	33.2	51.2
5132.669	13.5	46.8	31.0	32.2	29.3	...	23.0	31.5	7.8	42.5
5284.109	40.2	84.5	72.7	73.2	70.6	48.6	61.6	71.3	58.8	82.0
5325.553	23.4	56.3	52.7	54.9	44.3	16.5	39.4	50.9	32.3	55.5
5414.073	13.4	44.6	36.0	34.6	30.8	10.2	24.2	33.3	21.2	42.7
5425.257	24.5	59.2	51.0	52.6	46.3	26.4	39.0	50.1	36.1	59.2
5991.376	15.8	50.3	43.3	42.3	36.6	15.6	29.0	40.7	24.5	49.0
6084.111	10.1	34.3	29.9	28.6	23.3	8.3	18.4	26.7	15.6	33.3
6149.258	19.3	53.2	46.3	48.9	41.3	17.1	34.0	44.2	27.7	50.0
6369.462	9.1	33.2	27.1	26.1	20.8	9.5	17.3	26.5	15.6	32.6
6416.919	23.8	58.7	50.4	47.9	43.7	28.4	36.5	46.5	34.4	55.8
6432.680	23.5	62.5	54.1	52.7	45.8	21.5	38.6	52.7	32.9	62.4

Table 1. Larguras Equivalentes das Linhas de Fe I e Fe II.

λ (Å)	HD38283	HD38382	HD38973	HD39213	HD39587	HD42024	HD43042	HD45701	HD51929	HD52447
4779.439	...	35.1	38.3	67.6	34.1	44.6
4788.751	57.0	61.6	63.1	87.9	62.2	65.3	50.3	75.9	39.4	71.1
4802.875	50.4	56.5	58.4	81.6	55.9	61.2	47.1	67.0	31.9	68.9
4962.572	42.5	51.3	54.4	81.7	60.0	57.9	41.8	65.8	25.2	63.5
5054.642	26.2	32.7	36.2	70.3	31.4	35.8	...	50.7	...	44.4
5247.049	54.2	55.1	61.0	95.9	69.2	57.8	31.7	76.1	38.5	69.3
5379.574	49.1	54.5	58.4	86.6	57.2	60.6	43.6	69.5	30.6	67.2
5618.631	38.1	45.8	48.5	74.8	45.3	50.5	36.6	58.7	22.1	56.2
5741.846	20.6	26.0	28.5	56.0	26.1	30.2	22.0	40.2	9.6	38.9
5775.081	57.0	...	57.9	60.1
5778.453	10.7	14.3	19.3	50.9	16.1	16.6	...	26.4	...	20.7
5855.076	12.8	20.6	20.8	44.1	20.5	21.9	15.7	29.8	7.6	28.4
5916.247	41.7	42.1	49.6	82.1	53.6	50.4	34.6	61.5	23.4	60.0
5956.692	34.5	37.7	42.2	80.2	42.2	37.3	19.6	57.5	...	49.2
6120.246	21.2	7.3
6151.617	33.9	40.9	43.4	76.3	42.9	42.5	27.7	55.3	19.8	50.8
6173.334	55.6	61.1	65.0	98.3	62.3	65.8	45.0	77.3	37.6	73.1
6200.313	60.4	66.7	71.1	97.8	68.9	73.0	51.5	84.5	40.9	80.6
6219.279	79.6	83.5	88.0	131.9	90.9	91.1	72.1	100.3	...	96.8
6240.645	33.1	40.1	43.7	79.2	44.4	41.5	...	58.8	...	51.7
6265.131	74.1	78.4	81.5	124.6	82.4	84.3	64.5	94.5	...	91.2
6380.743	39.6	49.0	50.2	79.9	46.7	54.2	40.4	62.1	22.4	59.9
6593.870	72.3	76.9	84.6	110.3	86.1	84.4	...	94.5	...	92.3
6699.141	...	6.2	9.5	20.4	6.9	9.0	...	11.3	...	9.1

Table 1—Continued

λ (\AA)	HD38283	HD38382	HD38973	HD39213	HD39587	HD42024	HD43042	HD45701	HD51929	HD52447
6739.520	9.2	7.6	10.9	35.0	...	10.0	11.6
6750.150	61.8	65.6	72.1	106.2	70.7	72.7	53.7	83.4	...	77.5
6858.145	39.1	45.7	49.5	76.9	51.6	52.9	36.3	63.7	22.1	56.5
4993.358	40.9	42.6	44.7	46.4	36.1	55.8	50.1	50.3	21.6	51.5
5132.669	25.3	27.8	30.7	25.0	24.5	40.3	32.8	41.4	...	33.4
5284.109	67.4	71.3	72.3	73.8	68.8	83.1	81.2	81.5	43.4	83.0
5325.553	47.3	50.6	48.7	42.2	45.1	63.8	63.6	53.9	25.9	66.3
5414.073	30.6	33.7	35.1	37.0	28.8	45.8	42.8	43.4	12.3	44.8
5425.257	45.5	49.9	50.4	51.3	43.5	64.4	59.2	58.5	24.0	61.6
5991.376	36.4	39.0	38.9	38.7	39.1	54.6	47.4	49.5	16.8	57.3
6084.111	23.7	26.5	27.0	27.7	21.9	37.6	31.6	32.7	10.3	35.9
6149.258	41.3	45.7	43.8	40.5	43.5	59.3	57.8	48.6	20.4	56.4
6369.462	20.7	25.3	23.3	25.4	21.7	36.0	30.4	32.1	8.1	32.7
6416.919	45.4	46.0	47.8	51.0	44.5	63.4	59.1	54.9	21.4	56.2
6432.680	47.7	51.4	50.4	47.9	43.8	63.8	69.7	55.8	23.0	59.7

Table 1. Larguras Equivalentes das Linhas de Fe I e Fe II.

λ (Å)	HD55693	HD64184	HD65907	HD73524	HD76151	HD78429	HD80913	HD84117	HD86819	HD88742
4779.439	...	37.6	23.7
4788.751	76.5	65.1	49.7	68.5	71.8	72.0	30.7	56.1	62.9	61.1
4802.875	70.7	54.8	43.5	63.6	65.3	66.3	26.2	50.1	57.0	56.0
4962.572	70.0	49.9	37.0	59.8	63.0	61.6	19.0	45.7	49.9	51.6
5054.642	51.4	37.3	22.5	39.6	45.3	43.9	...	24.6	32.9	31.3
5247.049	74.9	67.9	44.5	65.8	69.9	75.7	25.2	46.3	59.1	56.9
5379.574	72.5	55.8	42.6	63.1	66.8	66.5	22.3	49.5	55.3	56.1
5618.631	61.9	44.6	32.1	52.5	55.9	55.4	15.9	37.4	43.3	43.7
5741.846	43.3	29.0	20.1	36.1	37.4	37.3	7.5	21.3	26.4	26.7
5775.081	...	53.0	39.4	20.3	...	52.8	...
5778.453	30.5	17.7	8.1	19.6	25.3	26.0	...	9.9	14.5	15.4
5855.076	31.8	17.3	11.5	24.2	25.9	25.8	...	13.3	17.6	18.7
5916.247	...	53.7	38.0	62.4	...	40.0	50.2	49.4
5956.692	...	52.3	27.8	50.2	...	63.0	13.1	...	39.2	...
6120.246	8.4	4.4	6.6	6.5	3.8	...
6151.617	59.5	45.4	28.2	48.6	54.4	55.1	13.1	31.8	39.8	41.3
6173.334	78.9	65.0	47.7	69.4	73.7	74.6	27.8	53.2	61.4	60.3
6200.313	87.3	69.9	52.7	76.0	80.5	80.8	31.6	57.1	67.4	65.6
6219.279	101.4	88.0	70.7	92.2	99.7	96.5	...	77.8	84.3	84.4
6240.645	59.0	44.4	27.3	47.9	54.5	54.9	14.6	30.2	38.4	40.0
6265.131	98.1	84.0	66.7	87.3	93.4	92.6	...	71.5	79.1	78.4
6380.743	65.7	47.2	34.3	56.6	58.3	58.9	17.8	39.8	47.2	47.2
6593.870	95.4	77.9	66.0	79.2	88.7	90.0	40.5	66.1	72.6	73.1
6699.141	13.6	7.6	...	9.6	10.1	9.7	7.4	6.7

Table 1—Continued

λ (\AA)	HD55693	HD64184	HD65907	HD73524	HD76151	HD78429	HD80913	HD84117	HD86819	HD88742
6739.520	17.9	10.5	...	10.5	15.5	16.8	8.0	9.6
6750.150	87.8	71.4	53.2	76.5	82.3	82.4	33.9	62.1	67.1	69.4
6858.145	64.7	44.8	31.2	54.9	55.2	54.5	16.2	39.3	46.2	46.9
4993.358	50.2	30.4	27.3	46.7	40.7	43.1	24.8	43.9	43.6	39.0
5132.669	40.9	23.7	17.3	33.7	31.6	34.4	...	27.7	30.5	25.0
5284.109	82.0	54.6	53.1	75.8	69.2	69.1	46.0	69.6	73.3	67.0
5325.553	55.5	32.5	34.9	53.4	44.7	45.8	30.8	51.6	49.1	44.7
5414.073	42.0	23.1	21.6	39.7	31.0	33.1	16.7	32.3	34.1	29.6
5425.257	54.7	35.0	33.2	51.9	45.2	48.9	29.6	48.9	49.6	43.8
5991.376	46.1	26.6	24.1	42.4	35.8	39.1	18.6	38.0	37.6	33.5
6084.111	32.4	15.9	14.2	28.4	23.3	25.5	11.6	24.7	28.3	23.4
6149.258	50.5	27.8	30.5	48.3	38.9	41.6	24.5	45.0	44.7	39.4
6369.462	29.7	12.8	14.3	27.0	21.2	25.1	10.6	21.9	26.0	19.8
6416.919	53.4	32.5	29.6	49.5	44.2	45.1	23.3	45.9	46.9	40.8
6432.680	54.9	33.9	35.4	54.8	43.1	46.6	28.9	48.2	49.7	42.8

Table 1. Larguras Equivalentes das Linhas de Fe I e Fe II.

λ (Å)	HD92987	HD93385	HD96423	HD102365	HD102438	HD102870	HD105328	HD106453	HD107692	HD108309
4779.439	36.3	39.3	45.8	...
4788.751	68.8	64.3	73.4	59.0	62.1	66.1	72.7	75.8	71.0	74.0
4802.875	62.9	59.1	67.5	51.0	53.4	61.5	65.5	68.4	66.2	67.8
4962.572	57.1	54.8	65.3	45.4	47.6	54.1	61.1	65.6	61.5	64.9
5054.642	41.3	...	47.4	30.9	34.7	36.0	44.3	48.7	43.6	50.0
5247.049	68.9	61.6	78.1	63.2	67.7	58.1	70.1	81.8	70.0	75.2
5379.574	63.7	57.6	68.8	51.2	54.8	60.5	67.0	69.4	67.0	69.2
5618.631	51.8	46.8	57.1	39.2	42.8	49.6	55.2	60.8	55.8	57.1
5741.846	34.5	28.4	39.3	24.2	27.4	34.2	37.9	40.0	37.5	39.6
5775.081	58.1	65.7	...
5778.453	21.0	16.8	28.0	14.3	17.3	16.4	21.8	30.0	25.4	26.8
5855.076	23.3	19.7	27.4	14.3	15.7	21.1	26.2	29.2	28.0	27.9
5916.247	...	52.6	52.6	53.5	...	67.6	62.2	...
5956.692	53.0	44.6	49.0	42.4	52.6	64.7	56.2
6120.246	5.2	4.3	7.8	3.2	4.8	...	5.4	8.6	6.6	8.0
6151.617	49.9	44.7	58.1	40.8	45.9	44.6	51.9	61.2	54.3	56.4
6173.334	69.4	64.6	76.4	60.1	64.5	64.2	73.7	82.2	73.8	77.5
6200.313	75.6	69.2	82.9	63.9	69.2	70.8	78.3	87.9	81.0	83.0
6219.279	92.3	86.0	100.9	83.0	87.6	88.6	96.0	109.3	98.8	93.8
6240.645	49.2	45.1	57.3	39.9	43.9	40.3	50.6	59.6	53.6	57.3
6265.131	85.2	83.0	95.5	78.7	84.3	85.4	91.6	103.6	92.9	95.7
6380.743	54.6	50.2	60.0	41.3	45.9	53.4	59.5	61.6	59.0	62.0
6593.870	87.5	77.1	92.1	74.1	82.0	79.4	82.1	94.1	85.9	93.5
6699.141	9.3	7.2	11.6	5.2	5.5	9.5	9.2	10.9	10.8	10.0

Table 1—Continued

λ (Å)	HD92987	HD93385	HD96423	HD102365	HD102438	HD102870	HD105328	HD106453	HD107692	HD108309
6739.520	...	11.5	17.8	9.1	10.8	...	13.1	...	12.7	...
6750.150	75.9	73.5	84.7	65.3	68.7	71.2	78.2	86.4	78.6	82.9
6858.145	52.0	47.5	57.5	38.2	41.7	50.4	56.1	62.9	60.2	56.9
4993.358	46.9	43.0	42.4	26.0	27.6	52.9	50.2	39.8	44.6	44.9
5132.669	35.4	29.7	32.0	17.4	18.5	38.9	39.0	13.6	23.2	39.4
5284.109	74.7	69.0	71.2	51.6	53.0	86.0	82.5	68.3	74.6	75.7
5325.553	51.2	48.9	46.2	29.4	29.5	62.6	57.8	39.7	48.0	51.1
5414.073	39.6	33.4	33.4	20.1	18.6	47.8	43.9	26.7	34.2	39.9
5425.257	51.9	47.5	46.0	30.4	30.0	61.2	56.9	42.5	50.2	52.7
5991.376	41.1	36.7	37.5	21.4	21.4	49.8	46.9	27.7	34.8	47.5
6084.111	28.3	25.7	25.1	13.0	14.0	37.1	33.6	21.0	26.7	28.0
6149.258	45.3	43.3	40.3	25.1	24.1	58.7	52.7	36.9	44.5	45.7
6369.462	25.8	23.2	21.1	12.0	11.8	33.4	30.9	19.0	22.8	26.7
6416.919	47.0	45.6	44.8	26.9	27.3	56.6	53.2	42.2	47.2	48.0
6432.680	53.2	47.3	45.9	31.7	30.4	64.8	58.1	39.8	48.6	52.0

Table 1. Larguras Equivalentes das Linhas de Fe I e Fe II.

λ (Å)	HD109200	HD110810	HD114613	HD114853	HD115383	HD115617	HD11585	HD117105	HD117939	HD118972
4779.439	51.3	72.9	54.4	63.2
4788.751	74.6	94.0	79.6	59.7	66.6	72.2	85.9	52.8	62.5	84.6
4802.875	61.6	75.1	72.9	53.9	64.0	65.4	78.2	45.8	56.5	73.7
4962.572	53.2	...	68.5	44.2	62.1	57.0	76.6	39.4	49.3	67.1
5054.642	53.4	71.4	54.7	31.5	38.3	45.6	65.9	...	33.7	57.3
5247.049	91.3	...	86.4	62.4	65.7	79.0	93.4	51.7	65.7	...
5379.574	63.4	78.7	75.7	52.8	62.9	66.5	83.4	45.5	54.9	74.9
5618.631	51.0	65.4	61.5	41.7	52.1	56.5	70.7	35.1	44.5	64.0
5741.846	33.8	48.3	43.5	25.4	32.5	37.1	54.3	18.6	26.3	44.2
5775.081	...	75.0	71.4	...	60.8	77.0
5778.453	31.4	46.4	34.1	15.3	19.1	28.4	40.5	10.3	18.0	39.1
5855.076	22.3	33.6	31.6	14.2	23.6	26.4	40.1	12.4	17.6	31.4
5916.247	65.8	88.1	...	47.6	...	63.5	...	37.6	50.8	82.3
5956.692	71.1	93.0	66.1	45.3	46.5	63.9	74.0	35.9	53.3	82.8
6120.246	11.6	23.0	9.8	8.2	13.9	...	4.3	15.0
6151.617	60.8	80.1	63.6	42.2	45.0	58.5	70.1	33.4	45.6	74.2
6173.334	78.9	105.6	84.0	60.4	69.5	76.0	92.4	52.1	64.3	98.4
6200.313	85.8	104.2	85.4	65.1	75.7	82.6	89.6	56.2	68.4	103.7
6219.279	103.9	135.3	106.6	83.6	94.5	96.1	119.2	74.6	87.0	132.9
6240.645	60.4	77.5	62.3	41.2	47.7	57.4	...	32.3	44.3	71.4
6265.131	101.8	137.2	103.0	78.1	86.5	91.8	115.9	71.0	82.8	125.0
6380.743	53.4	60.0	65.9	42.7	54.1	57.7	74.7	35.3	46.4	63.6
6593.870	92.8	134.2	100.1	80.8	82.3	90.5	103.0	67.0	79.9	126.6
6699.141	7.2	13.4	11.8	4.7	7.0	10.0	17.4	5.0	6.2	12.0

Table 1—Continued

λ (Å)	HD109200	HD110810	HD114613	HD114853	HD115383	HD115617	HD11585	HD117105	HD117939	HD118972
6739.520	24.1	33.2	17.8	9.4	9.6	16.6	27.0	5.3	10.6	...
6750.150	83.6	109.6	89.5	66.2	72.1	81.8	97.5	59.2	71.7	100.9
6858.145	48.2	64.7	65.4	40.4	57.3	58.3	70.7	35.1	41.6	64.9
4993.358	33.7	44.3	54.4	31.3	48.2	36.5	51.0	32.5	32.7	34.0
5132.669	46.7	20.4	36.8	11.8	57.5	18.4	22.2	24.7
5284.109	39.4	50.7	83.3	55.5	81.5	62.2	83.5	58.4	57.1	53.7
5325.553	17.1	17.0	56.4	33.8	60.5	35.5	54.4	37.2	34.2	18.6
5414.073	9.4	10.1	43.3	20.2	40.9	24.2	47.0	21.4	22.0	13.9
5425.257	23.4	30.5	57.5	34.0	57.1	39.2	59.3	35.3	34.5	31.5
5991.376	8.4	16.3	51.6	29.1	52.1	23.9	51.5	21.8	25.7	...
6084.111	6.5	11.4	35.3	15.4	31.0	18.4	34.3	...	16.1	12.3
6149.258	14.7	17.9	52.6	27.6	54.1	33.5	50.1	32.4	29.2	24.1
6369.462	...	10.2	33.9	13.9	31.1	17.6	31.1	15.9	16.3	...
6416.919	23.7	33.2	53.1	31.2	54.7	38.4	54.0	33.4	32.3	32.4
6432.680	20.0	19.6	57.3	32.2	57.7	36.2	58.6	35.3	33.6	26.5

Table 1. Larguras Equivalentes das Linhas de Fe I e Fe II.

λ (Å)	HD120237	HD120690	HD120780	HD121384	HD122742	HD122862	HD124584	HD125072	HD126053	HD125881
4779.439	30.8	...	59.6	38.3
4788.751	57.5	70.4	76.5	67.0	73.5	59.5	61.1	101.8	54.8	64.1
4802.875	53.5	62.9	63.1	57.2	66.3	54.1	56.8	81.6	49.1	58.7
4962.572	47.7	58.9	52.6	48.1	63.2	46.0	50.0	72.1	42.5	54.5
5054.642	28.1	44.8	55.8	36.1	48.9	...	34.4	...	28.6	...
5247.049	50.7	77.0	99.6	82.2	81.4	57.3	59.4	116.2	59.3	59.6
5379.574	51.8	63.7	68.2	57.2	68.9	53.2	55.8	92.8	48.7	57.8
5618.631	40.8	51.7	52.4	42.4	56.1	39.8	45.0	71.9	36.6	46.0
5741.846	23.7	36.4	38.1	24.4	38.0	22.8	24.4	59.4	19.9	29.5
5775.081	...	64.0	61.4	50.6	...	49.3	...	86.7
5778.453	11.6	26.6	36.0	22.7	29.7	14.2	16.0	59.9	14.7	16.7
5855.076	16.0	25.2	26.0	16.5	27.1	15.5	18.3	43.3	13.2	19.8
5916.247	43.4	63.7	...	59.1	66.1	...	36.8	98.1	...	51.3
5956.692	36.0	59.0	71.8	63.5	66.1	36.4	42.1	94.3	40.7	44.7
6120.246	...	8.2	13.1	8.0	9.5
6151.617	35.5	55.1	64.4	54.6	59.1	37.9	40.0	84.9	37.5	43.2
6173.334	56.5	75.0	84.6	71.0	78.0	57.8	60.1	121.2	57.0	64.2
6200.313	61.3	82.3	91.6	74.2	84.1	62.1	66.2	105.0	61.1	69.2
6219.279	79.3	98.3	118.3	91.9	102.5	82.5	84.5	137.8	78.4	85.7
6240.645	34.0	55.8	62.2	52.5	59.7	36.9	40.1	88.5	37.5	42.6
6265.131	74.8	96.0	109.8	90.1	99.0	76.9	80.2	147.3	74.1	82.4
6380.743	43.4	55.3	51.3	45.6	58.8	42.1	46.3	75.6	38.6	49.1
6593.870	67.6	87.7	94.7	84.5	91.1	73.5	73.9	122.6	69.1	77.4
6699.141	7.4	9.0	6.4	4.8	10.3	...	6.0	...	3.9	7.2

Table 1—Continued

λ (Å)	HD120237	HD120690	HD120780	HD121384	HD122742	HD122862	HD124584	HD125072	HD126053	HD125881
6739.520	...	14.7	22.3	14.5	17.8	7.6	...	46.3	...	11.0
6750.150	62.4	81.5	90.9	75.4	84.8	64.2	65.7	118.7	61.9	69.8
6858.145	44.4	54.5	57.5	40.5	58.2	43.2	46.1	...	38.1	49.5
4993.358	41.8	38.0	36.2	33.9	35.4	43.0	42.7	55.2	27.1	42.6
5132.669	28.9	13.5	...	21.8	11.6	29.0	29.9	29.3
5284.109	69.7	63.6	45.6	54.9	62.5	70.5	71.3	56.8	52.3	72.2
5325.553	48.1	36.5	17.2	32.4	35.0	48.7	47.5	20.5	28.7	48.4
5414.073	32.6	23.8	8.5	20.4	23.6	32.7	31.9	13.3	16.9	33.7
5425.257	48.6	41.4	22.6	33.8	39.5	48.5	48.1	38.3	29.7	47.8
5991.376	36.0	29.4	15.5	23.6	23.1	45.0	42.0	...	24.5	38.5
6084.111	24.9	20.8	6.2	14.2	18.1	23.0	24.3	15.4	12.6	26.2
6149.258	45.3	35.4	15.8	26.4	33.0	44.2	43.3	20.9	25.2	44.2
6369.462	23.2	19.8	...	14.2	17.3	23.9	24.3	13.0	11.9	23.5
6416.919	...	39.5	22.3	27.9	37.7	44.9	43.1	40.2	27.7	47.9
6432.680	47.4	39.8	20.8	31.6	36.3	48.3	48.1	26.2	28.7	49.5

Table 1. Larguras Equivalentes das Linhas de Fe I e Fe II.

λ (Å)	HD128674	HD130948	HD131511	HD131977	HD131923	HD134060	HD134606	HD136352	HD141004	HD140785
4779.439	...	35.5	60.8	...	51.2	...	59.5	30.6	39.2	...
4788.751	57.5	61.2	85.1	97.1	74.3	69.9	82.4	57.7	65.5	70.1
4802.875	50.3	56.0	74.6	...	67.3	62.7	75.8	49.4	58.8	62.3
4962.572	45.1	52.8	70.7	94.5	64.5	58.9	74.6	42.0	53.4	55.4
5054.642	30.0	32.6	62.0	...	51.4	41.9	62.6	28.5	35.1	39.2
5247.049	63.0	59.5	...	109.4	81.9	67.5	91.7	60.0	65.6	73.4
5379.574	50.4	55.0	77.1	79.0	69.0	63.8	80.3	50.0	59.6	62.1
5618.631	38.5	46.3	66.2	61.2	56.6	51.8	67.9	36.7	47.2	51.4
5741.846	24.1	26.2	46.9	...	41.3	36.2	48.8	21.2	30.4	32.1
5775.081	...	54.3	...	66.9	67.3	...	78.1	45.8	56.4	...
5778.453	14.6	14.8	41.2	51.5	27.9	20.6	40.3	14.1	18.6	22.5
5855.076	13.6	19.4	31.5	32.8	28.9	23.3	39.0	13.3	19.6	22.3
5916.247	48.1	50.6	78.3	91.8	65.4	54.2	78.1	43.3	54.3	...
5956.692	44.7	...	78.7	97.4	62.0	50.8	70.8	46.3	53.7	53.6
6120.246	4.1	...	16.4	...	9.3	4.9	13.0	3.8	4.9	5.2
6151.617	40.9	41.6	72.5	80.6	58.5	49.9	68.4	38.5	45.1	51.9
6173.334	59.8	62.8	97.7	108.2	78.3	70.7	88.5	57.1	65.6	71.0
6200.313	65.0	67.9	104.9	115.8	84.4	76.5	88.4	61.5	71.3	76.9
6219.279	82.2	87.7	121.5	136.3	101.3	92.3	116.9	77.7	88.7	94.3
6240.645	40.1	40.4	71.0	85.3	57.7	48.3	69.3	36.4	44.6	49.4
6265.131	79.4	83.3	124.0	133.2	98.9	88.8	112.0	74.5	84.4	87.5
6380.743	41.7	46.7	64.3	...	59.7	56.5	68.2	39.7	50.6	52.7
6593.870	73.5	134.8	94.8	82.4	114.9	68.0	78.1	83.5
6699.141	4.6	6.7	14.9	13.1	11.1	9.2	17.2	5.2	7.3	8.4

Table 1—Continued

λ (Å)	HD128674	HD130948	HD131511	HD131977	HD131923	HD134060	HD134606	HD136352	HD141004	HD140785
6739.520	9.1	7.4	28.7	39.4	17.2	12.2	23.8	11.7	9.7	...
6750.150	65.0	67.9	100.9	111.2	82.0	74.8	96.3	62.3	70.7	76.0
6858.145	37.7	47.9	69.8	63.1	58.2	53.2	71.5	37.1	47.9	50.1
4993.358	22.5	38.7	36.7	...	40.6	42.6	46.1	29.1	43.5	45.8
5132.669	15.2	26.4	22.6	...	41.8	33.6	53.1	18.9	31.0	33.9
5284.109	47.8	69.6	59.1	38.8	68.1	73.7	76.9	49.8	73.3	72.8
5325.553	25.9	46.7	28.1	8.6	43.2	51.1	45.3	29.6	48.6	49.4
5414.073	16.1	29.2	19.5	5.4	33.2	37.7	37.7	16.9	33.2	34.3
5425.257	26.0	47.4	35.7	...	47.0	50.4	52.7	30.5	50.3	51.7
5991.376	18.2	36.6	28.4	...	37.1	44.1	42.6	20.9	38.2	37.6
6084.111	10.2	...	13.7	5.6	25.1	27.1	28.8	13.4	25.2	27.6
6149.258	20.3	44.2	30.2	11.1	41.0	45.2	44.0	26.1	45.5	44.0
6369.462	10.3	...	18.0	...	23.7	24.9	25.4	12.2	26.1	26.1
6416.919	24.1	44.9	35.3	...	42.3	46.5	48.5	28.3	46.5	44.7
6432.680	26.1	44.3	29.2	...	46.8	50.5	49.1	29.0	47.6	48.5

Table 1. Larguras Equivalentes das Linhas de Fe I e Fe II.

λ (Å)	HD140901	HD143114	HD144009	HD144628	HD145825	HD146481	HD149661	HD150248	HD153075	HD155974
4779.439	51.1	54.2	...	27.5	61.1	40.6	...	21.5
4788.751	75.2	49.5	74.4	69.8	68.1	54.2	82.8	66.9	44.5	45.7
4802.875	67.6	43.4	66.9	58.3	61.0	46.6	72.0	59.8	39.3	42.1
4962.572	61.2	36.6	65.8	48.7	59.5	38.5	68.1	55.7	29.8	36.3
5054.642	52.0	22.2	49.3	52.3	41.3	23.1	58.8	38.9
5247.049	82.1	50.9	82.0	88.5	67.1	58.4	103.2	69.1	45.1	33.3
5379.574	70.9	41.3	71.2	60.5	62.3	45.1	75.5	60.6	35.9	38.6
5618.631	60.5	30.8	57.9	46.5	52.7	32.1	64.4	47.7	25.5	28.9
5741.846	40.6	17.0	40.7	31.8	35.0	20.1	45.8	32.3	...	15.7
5775.081	...	38.7	40.5	...	59.9
5778.453	30.5	9.2	30.6	26.7	22.2	11.2	39.4	20.9
5855.076	29.3	10.3	28.5	18.5	23.7	11.4	30.9	20.1	...	9.4
5916.247	69.0	35.5	...	64.8	57.7	43.7	79.5	55.9	31.0	29.1
5956.692	63.8	31.4	64.2	68.1	52.2	38.5	81.7	52.7	27.0	18.1
6120.246	9.7	...	9.7	10.7	6.4	...	15.8	4.3
6151.617	60.3	30.4	60.9	58.6	51.2	35.6	70.7	49.5	24.9	20.8
6173.334	81.8	49.7	79.8	77.4	70.7	54.3	94.0	68.2	42.6	42.7
6200.313	87.9	53.0	86.6	82.6	76.6	57.3	99.8	72.9	47.5	45.9
6219.279	107.5	71.0	100.0	106.3	94.2	77.3	125.3	89.3	65.5	67.8
6240.645	60.7	28.4	58.2	57.2	50.1	34.1	69.8	47.2	...	24.3
6265.131	102.6	67.1	99.4	102.3	88.6	74.2	119.2	86.1	61.8	62.2
6380.743	63.0	33.0	...	47.8	56.2	34.6	65.9	50.3	27.8	31.1
6593.870	103.5	67.8	96.7	94.0	90.9	70.5	106.8	83.3	58.9	56.7
6699.141	10.9	4.5	10.8	5.6	8.3	4.8	12.5	7.5

Table 1—Continued

λ (Å)	HD140901	HD143114	HD144009	HD14628	HD145825	HD146481	HD149661	HD150248	HD153075	HD155974
6739.520	18.7	6.7	19.6	21.8	13.2	17.0	28.0	15.1
6750.150	85.9	56.4	84.9	82.2	77.1	60.3	99.7	73.1	48.5	47.5
6858.145	61.3	30.6	...	46.5	54.8	31.9	66.5	50.8	...	33.4
4993.358	38.3	26.9	38.7	33.2	38.7	27.8	35.0	35.5	22.9	41.5
5132.669	12.3	15.3	27.5	...	28.0	18.2	24.0	25.7	13.0	26.5
5284.109	66.9	50.2	64.4	33.5	67.9	51.6	55.7	61.8	44.5	68.6
5325.553	39.3	29.6	37.5	14.5	43.2	31.2	26.3	38.9	26.6	54.1
5414.073	29.1	17.8	28.3	7.2	29.3	19.2	18.3	24.8	14.9	32.8
5425.257	43.3	30.8	41.6	19.5	43.8	29.7	33.8	39.5	26.0	50.2
5991.376	34.1	21.3	32.9	11.4	34.9	20.7	24.7	30.2	17.6	40.5
6084.111	21.6	13.8	20.2	7.0	22.9	16.0	15.0	17.8	10.1	24.8
6149.258	35.6	24.9	34.2	11.3	38.0	26.0	24.4	33.2	22.1	44.9
6369.462	20.4	11.6	19.7	5.7	21.1	11.6	14.4	16.3	9.3	23.1
6416.919	41.8	26.5	39.3	19.4	42.5	27.8	34.2	36.7	22.6	47.0
6432.680	39.9	29.8	40.1	17.1	44.6	30.5	29.7	37.4	25.7	48.3

Table 1. Larguras Equivalentes das Linhas de Fe I e Fe II.

λ (Å)	HD156274	HD155918	HD158783	HD161612	HD162255	HD163272	HD166553	HD168060	HD168723	HD168871
4779.439	43.2	...	46.9	53.9	...	48.8	38.4	59.5	71.8	33.3
4788.751	67.0	41.9	71.6	76.8	72.2	72.5	64.1	83.7	90.1	59.0
4802.875	56.0	36.0	65.8	72.6	65.9	69.0	58.6	77.0	78.6	52.6
4962.572	51.2	27.0	62.3	68.8	60.7	65.3	55.7	74.0	70.3	45.8
5054.642	38.4	...	46.6	53.4	46.5	45.6	35.5	64.2	60.0	29.2
5247.049	80.0	42.0	...	84.0	73.0	68.0	63.8	97.2	...	57.7
5379.574	59.4	32.9	66.0	74.7	67.1	69.6	60.9	82.7	82.3	53.1
5618.631	45.9	21.9	55.0	63.6	55.8	58.2	47.3	68.6	64.6	41.7
5741.846	28.9	11.6	37.2	44.1	36.4	40.0	28.8	50.4	48.5	25.5
5775.081	...	29.5	65.5	79.3	76.6	...
5778.453	25.0	...	25.3	34.2	24.7	24.3	17.9	41.5	51.6	14.0
5855.076	17.8	...	25.6	33.2	25.7	28.5	20.6	38.6	34.6	15.9
5916.247	60.0	25.7	61.3	70.4	...	55.8	46.6	80.2	90.5	46.5
5956.692	61.2	24.6	55.2	68.4	55.6	51.1	42.7	75.3	99.3	37.6
6120.246	8.3	...	8.2	11.2	5.8	5.9	...	15.0	30.6	...
6151.617	53.9	23.2	53.9	63.4	53.7	53.7	43.9	71.9	84.8	39.2
6173.334	72.0	40.9	73.6	82.2	74.8	74.3	65.1	91.9	103.5	58.1
6200.313	77.3	42.9	80.4	90.3	79.9	83.0	71.2	91.7	99.3	63.8
6219.279	...	62.9	97.6	108.9	96.0	97.5	81.9	114.1	130.0	80.1
6240.645	53.0	...	53.4	62.2	54.1	52.2	42.1	70.0	83.0	37.6
6265.131	94.5	58.9	82.3	102.8	91.5	91.6	83.1	102.4	126.5	79.6
6380.743	47.9	24.4	59.5	65.5	59.2	62.1	51.1	72.5	68.6	44.2
6593.870	85.3	55.4	84.9	105.3	85.9	88.4	83.1	110.5	113.8	75.9
6699.141	5.8	...	10.4	11.5	9.3	10.2	6.0	17.4	14.2	4.9

Table 1—Continued

λ (Å)	HD156274	HD155918	HD158783	HD161612	HD162255	HD163272	HD166533	HD168060	HD168723	HD168871
6739.520	18.1	...	13.4	20.6	16.3	...	13.5	27.6	43.5	8.0
6750.150	78.2	45.4	79.8	88.7	78.8	79.4	72.7	97.7	108.0	66.0
6858.145	47.0	25.5	58.0	64.1	58.4	62.9	50.1	70.6	63.6	44.2
4993.358	28.4	22.5	46.3	39.4	48.0	52.6	49.8	52.8	46.1	40.3
5132.669	9.3	...	35.6	33.2	35.8	41.7	32.9	49.7	18.2	25.4
5284.109	40.9	40.8	76.1	68.5	75.4	84.5	76.8	78.8	69.5	66.2
5325.553	20.6	24.9	50.0	41.1	52.5	57.6	53.4	51.2	43.9	49.2
5414.073	11.4	11.9	35.4	30.5	38.4	43.4	36.2	43.3	30.5	29.1
5425.257	23.4	22.2	51.8	45.3	52.7	59.0	52.9	56.6	45.4	44.5
5991.376	15.6	14.6	41.5	36.8	43.5	50.0	42.5	47.0	39.7	35.5
6084.111	9.0	9.5	28.3	22.8	29.8	34.8	29.3	33.3	25.9	22.6
6149.258	16.6	19.1	44.8	37.0	45.4	53.0	48.8	48.6	35.6	40.2
6369.462	7.9	9.4	27.3	20.6	26.8	32.1	29.5	30.6	25.9	20.4
6416.919	23.7	21.3	47.2	44.8	47.7	55.2	49.8	51.1	42.3	42.1
6432.680	20.3	20.6	51.6	43.7	51.1	59.1	53.8	55.0	44.7	45.6

Table 1. Larguras Equivalentes das Linhas de Fe I e Fe II.

λ (Å)	HD175345	HD177565	HD179140	HD181428	HD183877	HD184985	HD187691	HD188641	HD190406	HD189567
4779.439	28.8	50.2	...	34.6	38.9	29.5	39.0	...	38.9	...
4788.751	55.5	74.6	70.5	61.7	63.8	55.8	64.0	66.1	58.5	58.5
4802.875	49.9	68.1	65.5	57.4	55.4	51.0	60.7	57.1	59.8	52.9
4962.572	44.2	65.4	58.8	52.2	50.4	45.1	56.0	50.0	54.6	46.3
5054.642	25.0	49.8	41.9	31.5	38.0	25.9	34.4	...	37.0	30.8
5247.049	47.1	79.3	68.6	57.3	67.6	43.2	59.5	65.3	60.6	61.8
5379.574	48.2	69.7	64.4	55.2	57.6	49.9	60.2	56.1	59.6	52.3
5618.631	39.8	60.2	51.7	45.0	43.5	38.9	48.0	42.8	47.6	40.3
5741.846	20.9	40.5	34.5	28.1	26.7	22.8	30.9	26.1	31.2	24.2
5775.081	45.9	53.7	47.8	58.2	52.7	57.9	...
5778.453	10.2	29.9	20.6	13.7	19.6	9.7	16.1	17.8	17.6	15.6
5855.076	14.4	29.7	23.2	17.0	17.8	14.9	21.6	17.8	21.2	15.9
5916.247	38.8	...	58.4	49.0	52.6	39.4	51.5	50.7	52.1	47.9
5956.692	28.5	63.9	49.6	37.8	49.9	26.0	39.9	45.5	43.6	43.2
6120.246	...	8.1	5.6	...	5.2	3.4	5.6	4.1
6151.617	31.2	60.1	50.2	39.8	46.7	30.8	42.6	43.3	44.7	41.8
6173.334	51.1	78.9	71.5	61.7	65.6	52.8	65.3	64.5	65.4	61.3
6200.313	57.0	84.5	75.8	66.6	70.4	58.2	70.3	70.0	69.9	65.6
6219.279	75.2	104.7	96.9	83.3	82.2	78.5	88.2	84.8	85.2	83.3
6240.645	30.6	58.2	49.8	38.2	44.9	30.0	42.5	43.0	43.3	40.3
6265.131	69.8	100.0	90.6	81.0	81.3	73.1	82.1	82.1	83.7	77.4
6380.743	41.8	62.2	56.1	47.6	46.8	42.3	52.6	46.5	51.5	43.2
6593.870	73.1	92.5	90.2	...	75.1	66.0	...	77.9	87.9	74.4
6699.141	5.0	10.6	8.9	5.5	8.4	5.3	7.7	...	7.8	5.9

Table 1—Continued

λ (Å)	HD175345	HD177565	HD179140	HD181428	HD183877	HD184985	HD187691	HD188641	HD190406	HD189567
6739.520	5.6	...	14.4	11.3	12.1	5.9	8.3	10.0	9.8	10.1
6750.150	57.1	85.7	76.2	65.9	73.4	61.4	70.4	72.7	71.0	67.8
6858.145	41.1	60.2	56.6	49.2	47.2	42.1	53.7	42.8	52.2	41.1
4993.358	40.8	39.7	50.0	47.4	30.5	55.6	52.0	44.2	41.6	30.6
5132.669	26.4	39.1	36.9	34.0	24.5	36.6	36.4	30.4	30.4	21.6
5284.109	67.3	65.0	82.2	75.0	54.9	84.2	79.8	72.5	70.6	57.0
5325.553	48.5	41.5	57.3	58.3	30.9	66.4	60.5	49.4	47.6	33.8
5414.073	30.1	28.7	40.2	38.4	21.8	43.6	41.7	34.1	31.9	20.5
5425.257	46.3	44.5	55.5	53.8	33.5	61.8	58.7	49.4	47.2	35.6
5991.376	36.5	35.5	46.6	44.4	25.7	49.6	48.4	40.2	37.8	25.5
6084.111	23.6	22.9	32.0	30.4	15.5	35.5	33.5	27.5	25.2	17.4
6149.258	43.5	36.8	50.9	48.1	27.0	58.6	55.1	44.1	42.3	29.7
6369.462	22.4	19.4	29.5	26.0	14.9	31.8	31.9	24.9	22.8	13.9
6416.919	45.1	40.4	52.8	48.3	29.0	57.9	55.3	45.0	44.8	31.6
6432.680	44.9	41.5	55.6	52.9	31.2	63.1	59.5	48.9	46.5	35.2

Table 1. Larguras Equivalentes das Linhas de Fe I e Fe II.

λ (Å)	HD190248	HD191408	HD192310	HD193193	HD192865	HD193307	HD194640	HD196390	HD196378	HD196800
4779.439	63.6	56.0	66.8	...	36.5	24.5	48.0	42.6
4788.751	84.5	66.1	86.1	60.9	63.8	50.1	72.3	67.3	45.5	70.1
4802.875	78.6	53.0	70.7	56.3	58.6	44.7	62.9	63.3	37.9	64.2
4962.572	77.2	...	68.3	48.3	53.5	36.9	58.8	57.4	31.1	59.9
5054.642	66.1	...	67.0	31.6	31.7	20.3	48.1	40.1	...	42.4
5247.049	95.0	...	99.5	56.7	57.9	46.1	77.9	66.9	40.3	66.4
5379.574	79.5	56.5	78.3	53.2	58.1	42.4	65.7	62.3	37.4	66.8
5618.631	70.7	42.1	63.9	42.7	45.8	31.2	54.3	51.8	25.8	53.6
5741.846	53.2	28.4	47.0	26.9	28.2	17.3	37.9	34.1	12.6	36.1
5775.081	...	48.0	72.8	...	55.8	39.7	33.6	...
5778.453	44.4	25.2	45.4	15.4	...	7.8	27.2	21.6	7.5	24.4
5855.076	42.1	...	31.7	16.9	19.5	10.4	26.4	23.3	9.1	25.8
5916.247	...	60.4	81.2	46.9	49.0	34.0	63.0	57.4	27.4	60.3
5956.692	76.6	66.3	81.0	40.4	36.7	27.1	59.4	49.2	20.4	48.3
6120.246	17.1	...	21.1	8.8	4.7	...	5.9
6151.617	73.2	54.8	74.4	40.7	38.7	28.5	56.2	49.5	22.6	50.9
6173.334	94.2	72.9	94.3	59.9	62.7	47.6	76.2	68.8	41.3	71.6
6200.313	92.8	78.6	94.3	66.3	66.5	51.0	80.6	74.2	46.3	77.8
6219.279	121.8	100.9	126.1	81.9	89.9	72.9	94.5	92.5	67.4	95.0
6240.645	74.2	55.2	75.1	39.3	38.9	27.1	55.0	49.2	23.3	48.6
6265.131	116.0	97.7	120.9	77.1	80.1	68.5	92.3	86.9	61.8	89.7
6380.743	75.8	42.4	61.5	44.8	48.6	33.4	56.6	54.9	27.4	57.0
6593.870	107.3	86.3	105.1	78.3	...	67.8	89.5	80.6	...	84.0
6699.141	19.9	15.4	...	7.0	...	9.0	...	8.9

Table 1—Continued

λ (Å)	HD190248	HD191408	HD192310	HD193193	HD192865	HD193307	HD194640	HD196390	HD196378	HD196800
6739.520	30.3	...	30.2	11.9	7.1	4.9	17.2	12.2
6750.150	103.5	76.2	100.4	65.4	68.8	54.2	81.3	73.9	52.2	77.2
6858.145	75.3	40.1	64.6	47.7	49.9	33.8	57.4	55.4	27.7	56.9
4993.358	50.8	...	40.8	41.0	54.0	36.7	36.4	40.3	37.3	49.5
5132.669	45.4	28.5	38.6	21.1	11.3	28.1	22.1	37.2
5284.109	79.0	33.9	50.1	68.1	81.4	60.5	61.3	70.4	62.2	73.8
5325.553	48.1	...	21.8	46.9	63.7	43.7	33.5	47.4	44.0	54.8
5414.073	41.6	...	13.3	30.9	43.2	26.4	25.3	32.2	26.6	38.9
5425.257	56.9	18.0	31.6	46.4	59.9	40.4	38.2	46.5	42.0	55.0
5991.376	46.5	...	21.4	37.1	50.9	30.6	29.2	38.1	33.2	44.7
6084.111	31.6	...	12.2	24.3	34.1	19.9	19.0	24.6	20.3	31.4
6149.258	45.2	...	20.3	40.8	56.7	35.2	28.6	41.5	38.4	50.9
6369.462	28.3	...	6.0	22.7	32.4	18.0	16.6	22.2	19.6	29.3
6416.919	51.0	...	33.7	40.5	56.9	38.1	36.0	44.1	37.7	50.7
6432.680	53.1	11.3	25.6	44.3	61.9	39.7	36.8	45.1	41.8	56.7

Table 1. Larguras Equivalentes das Linhas de Fe I e Fe II.

λ (Å)	HD196068	HD199288	HD199190	HD199509	HD204385	HD205420	HD205390	HD206395	HD207129	HD207700
4779.439	37.9	...	59.9	41.6	...	48.7
4788.751	72.8	40.3	70.9	55.6	63.7	59.6	80.9	66.9	62.1	73.8
4802.875	66.9	34.0	65.1	49.4	60.2	54.6	67.0	63.7	57.0	66.1
4962.572	61.3	27.2	61.1	40.7	54.9	52.6	63.4	65.9	54.6	62.3
5054.642	43.9	...	44.3	26.4	34.6	...	60.5	37.3	34.2	49.4
5247.049	69.4	40.6	71.7	54.9	60.3	48.5	107.5	60.5	62.6	78.5
5379.574	67.5	31.6	67.8	48.8	58.0	50.3	69.8	64.4	57.4	67.9
5618.631	54.3	22.3	55.4	35.5	48.0	41.8	56.2	51.5	46.6	55.9
5741.846	36.7	10.9	36.2	20.4	30.7	23.4	40.0	33.6	28.6	38.0
5775.081	63.9	28.3	49.9	65.2	62.7	...	65.0
5778.453	22.8	...	24.5	13.2	18.1	11.5	35.7	17.5	17.4	27.4
5855.076	27.0	...	26.1	13.4	20.7	16.0	25.4	24.1	21.2	27.4
5916.247	59.8	25.8	61.2	40.7	51.1	43.6	75.2	55.2	50.7	63.9
5956.692	51.3	21.1	53.8	39.1	43.2	27.8	77.6	37.5	43.7	59.2
6120.246	5.1	...	6.8	15.2	7.4
6151.617	52.2	22.1	53.6	36.4	44.2	32.8	69.1	44.3	44.1	56.1
6173.334	72.8	39.1	73.2	55.1	64.3	57.4	93.1	67.8	63.5	75.4
6200.313	79.0	42.2	80.4	58.8	69.8	61.5	96.0	74.7	69.2	80.5
6219.279	95.0	61.8	96.2	77.4	87.1	83.2	124.3	93.4	87.5	100.8
6240.645	51.8	...	52.5	35.5	42.9	...	67.6	43.5	42.7	54.9
6265.131	91.6	57.8	90.9	74.6	81.5	76.8	...	86.1	81.2	94.2
6380.743	58.7	24.4	58.3	37.3	51.7	42.1	57.5	56.8	49.6	58.7
6593.870	93.8	54.1	85.6	71.5	82.3	...	102.8	...	79.2	100.1
6699.141	11.4	...	9.7	4.7	7.2	...	8.7	8.3	7.9	10.4

Table 1—Continued

λ (Å)	HD196068	HD199288	HD199190	HD199509	HD204385	HD205420	HD205390	HD206395	HD207129	HD207700
6739.520	13.1	6.3	7.9	...	25.6	8.0	10.4	14.4
6750.150	80.1	46.3	81.6	64.1	72.2	65.3	95.1	77.4	70.7	83.5
6858.145	57.0	22.2	54.4	37.0	49.6	44.2	59.6	55.4	50.3	58.0
4993.358	53.0	20.4	49.6	27.5	44.3	58.0	38.8	56.0	39.6	40.9
5132.669	43.2	...	40.3	17.3	30.7	39.4	...	47.3	26.5	34.5
5284.109	85.1	40.7	79.7	50.6	74.6	92.3	43.0	87.2	68.6	66.4
5325.553	59.6	23.1	55.1	30.0	49.5	75.2	13.6	67.3	43.8	42.8
5414.073	45.6	11.2	39.0	16.4	33.8	47.8	9.1	47.7	28.6	31.4
5425.257	60.3	22.2	55.6	29.9	49.1	68.7	24.7	63.4	44.4	46.6
5991.376	49.5	15.3	46.2	16.0	39.5	58.3	15.9	54.5	35.2	35.8
6084.111	36.6	10.3	31.8	13.0	27.4	39.4	8.1	40.0	22.4	23.9
6149.258	55.3	18.6	49.9	26.2	46.3	64.1	14.4	61.5	38.3	36.8
6369.462	33.0	8.1	29.4	11.7	24.6	37.7	8.5	36.0	20.3	22.2
6416.919	57.2	20.8	51.9	29.1	48.5	64.2	27.1	61.0	42.7	41.6
6432.680	61.7	22.6	53.7	30.2	50.6	70.4	19.8	64.2	44.9	44.2

Table 1. Larguras Equivalentes das Linhas de Fe I e Fe II.

λ (Å)	HD208801	HD208998	HD209633	HD212291	HD212330	HD212168	HD212708	HD214759	HD214953	HD215648
4779.439	...	24.0	31.9	41.4	47.8	38.7	...	60.5	36.6	...
4788.751	96.3	48.9	59.6	66.4	72.2	65.8	80.0	82.6	62.9	45.5
4802.875	79.6	42.0	54.0	58.0	65.5	59.5	74.4	75.4	59.7	41.2
4962.572	75.2	34.4	46.0	53.7	58.3	54.2	74.2	73.2	52.7	30.0
5054.642	67.8	21.0	28.7	37.6	46.2	35.4	60.8	58.1	31.8	...
5247.049	118.6	45.9	55.6	71.2	77.3	64.9	88.9	94.0	58.1	36.7
5379.574	87.5	42.4	52.8	58.8	68.1	58.8	78.2	80.0	57.1	37.5
5618.631	67.4	31.3	40.2	48.0	54.6	48.3	66.8	68.1	45.9	27.4
5741.846	53.8	15.1	23.7	30.3	36.3	30.4	48.3	50.0	28.6	15.2
5775.081	...	38.1	63.6	57.1	35.0
5778.453	61.2	10.2	13.5	21.8	24.6	18.1	37.5	42.9	14.9	...
5855.076	41.2	10.2	15.4	19.6	24.8	20.8	36.2	36.5	19.7	...
5916.247	...	33.9	43.1	55.3	58.3	53.5	49.2	29.2
5956.692	102.4	29.1	36.6	52.9	60.3	45.4	71.5	76.7	37.7	19.1
6120.246	5.2	7.6	4.7	11.4	15.4
6151.617	87.0	28.8	37.5	49.7	54.8	44.5	67.8	70.5	41.4	22.5
6173.334	107.6	48.2	58.6	68.2	75.6	65.6	88.9	92.3	62.3	41.7
6200.313	104.4	50.7	62.7	74.2	82.1	70.5	87.3	86.5	67.3	47.1
6219.279	135.2	69.8	80.8	93.2	99.1	88.3	110.7	121.4	86.2	66.9
6240.645	86.2	27.6	36.4	49.2	56.3	43.2	67.7	72.1	40.5	22.8
6265.131	136.6	66.5	77.8	87.0	92.3	83.8	108.3	116.4	80.5	63.6
6380.743	77.6	32.4	42.3	49.4	58.4	50.0	70.0	70.4	49.3	30.0
6593.870	...	64.7	72.4	...	92.2	80.6	99.5	117.2
6699.141	21.4	...	5.2	6.4	7.7	7.4	15.9	17.5	6.5	...

Table 1—Continued

λ (Å)	HD208801	HD208998	HD209653	HD212291	HD212330	HD212168	HD212708	HD214759	HD214953	HD215648
6739.520	52.1	5.9	6.7	12.5	14.2	9.2	23.3	28.3
6750.150	115.8	56.2	64.7	72.8	81.2	71.0	93.0	99.9	68.3	52.6
6858.145	...	30.9	43.0	48.9	55.2	49.9	69.4	70.4	48.5	29.5
4993.358	50.2	28.7	42.6	30.7	46.1	42.0	47.4	38.1	44.1	42.3
5132.669	36.2	18.1	28.9	20.3	34.0	28.9	44.8	28.0	31.4	27.4
5284.109	60.1	54.3	68.5	55.9	75.9	71.0	77.4	67.6	76.1	69.3
5325.553	31.2	34.4	49.5	31.0	50.8	47.3	48.1	36.9	55.9	50.6
5414.073	26.5	20.4	32.1	20.0	36.4	32.8	38.0	29.3	35.6	31.3
5425.257	41.9	33.4	46.9	33.3	51.6	47.3	53.2	44.1	51.5	48.4
5991.376	33.1	26.0	37.7	24.4	41.6	40.2	43.0	33.9	42.3	39.1
6084.111	23.4	14.8	24.7	15.0	28.6	26.0	29.1	21.1	29.5	24.7
6149.258	31.2	30.2	42.6	27.3	45.3	42.5	45.0	35.2	47.8	45.7
6369.462	20.1	13.9	22.0	13.2	27.8	23.3	27.5	20.0	27.9	22.2
6416.919	39.9	30.9	43.1	32.0	49.6	44.8	51.4	44.2	49.8	44.1
6432.680	37.6	31.5	46.3	31.5	52.7	48.2	53.0	40.5	51.8	48.7

Table 1. Larguras Equivalentes das Linhas de Fe I e Fe II.

λ (Å)	HD217958	HD218261	HD219077	HD220507	HD221420	HD222237	HD222335	HD222368	HD222480	HD223171
4779.439	53.4	48.0	58.5	...	52.1	26.3	50.4	45.9
4788.751	77.4	60.8	75.3	72.0	81.9	77.8	74.3	52.4	75.4	73.7
4802.875	72.6	56.5	66.7	63.9	76.8	62.3	63.3	46.5	69.5	67.2
4962.572	68.1	57.1	61.6	59.5	74.8	...	54.8	40.9	65.9	61.3
5054.642	53.3	33.0	46.9	47.0	57.8	...	47.1	20.9	49.0	46.3
5247.049	76.7	54.7	90.9	75.4	...	102.4	88.5	43.0	78.2	...
5379.574	72.6	56.1	68.7	65.0	81.4	65.1	66.2	44.9	71.2	66.7
5618.631	62.4	45.9	53.8	54.0	69.7	53.0	53.9	34.3	57.7	55.6
5741.846	43.0	29.2	36.5	36.0	48.2	...	36.6	18.0	40.1	36.0
5775.081	72.3	...	64.9	62.2	...	57.2	...	42.6	68.4	...
5778.453	29.4	15.1	34.3	24.9	33.9	36.6	31.6	8.2	28.0	24.6
5855.076	33.0	19.1	25.7	25.5	35.8	20.3	24.2	12.5	29.5	26.6
5916.247	...	47.3	69.8	62.3	...	72.8	66.5	35.6	66.2	61.2
5956.692	59.7	33.6	69.8	57.5	70.1	84.2	68.1	23.8	59.5	54.6
6120.246	7.9	...	12.7	7.2	...	16.2	11.1	...	7.2	6.0
6151.617	59.4	37.8	62.9	54.7	67.2	67.7	61.9	27.6	58.0	54.6
6173.334	81.1	60.1	79.9	73.4	89.1	88.0	81.3	48.9	77.8	74.2
6200.313	88.2	66.8	85.2	78.5	87.9	96.2	87.3	53.7	84.9	80.2
6219.279	104.1	83.6	101.5	96.2	113.0	124.6	109.1	73.3	102.4	97.1
6240.645	59.8	39.0	62.4	54.2	67.8	69.8	60.8	27.7	57.2	53.7
6265.131	97.1	78.5	97.8	90.7	107.6	109.8	104.2	68.2	96.3	92.3
6380.743	65.8	49.1	57.4	56.0	70.9	40.7	57.2	37.0	62.0	59.2
6593.870	106.7	88.2	...	108.2	96.3	...	91.7	85.5
6699.141	13.5	7.6	9.3	9.1	...	6.2	9.9	...	11.8	8.7

Table 1—Continued

λ (Å)	HD217958	HD218261	HD219077	HD220507	HD221420	HD222337	HD222335	HD222368	HD222480	HD223171
6739.520	...	8.2	23.0	13.7	...	27.0	21.4	...	14.7	13.1
6750.150	86.9	69.0	87.8	79.4	93.4	91.2	85.3	58.6	83.2	79.7
6858.145	63.9	49.8	54.7	53.8	69.2	50.5	56.2	36.5	61.5	57.0
4993.358	51.7	45.7	38.9	40.5	60.3	...	31.6	46.1	50.7	47.5
5132.669	44.9	39.0	27.6	33.1	49.9	...	13.8	29.3	41.5	39.0
5284.109	77.0	76.1	61.6	66.4	92.3	33.1	50.6	73.5	79.5	76.7
5325.553	56.6	55.6	36.6	43.3	66.5	11.6	22.7	54.5	55.3	52.7
5414.073	43.9	37.8	26.4	31.2	50.0	...	14.5	34.4	41.3	39.0
5425.257	58.7	53.9	40.4	45.9	66.0	...	28.0	51.8	56.2	53.1
5991.376	50.2	43.7	31.2	37.1	57.8	...	18.8	40.4	46.3	45.0
6084.111	34.6	31.1	19.3	23.7	40.6	4.4	10.5	27.3	32.3	30.3
6149.258	51.9	50.8	32.5	37.7	58.8	8.2	19.8	49.7	48.8	47.2
6369.462	32.4	27.0	19.5	21.4	40.6	...	9.3	24.9	30.6	27.4
6416.919	55.0	51.8	36.8	41.7	61.8	...	28.0	48.1	52.7	49.4
6432.680	57.8	53.1	37.4	42.6	67.7	...	23.5	51.7	54.0	53.2

Apêndice C

Tabelas Eletrônicas

Neste apêndice, reproduzimos as tabelas 1, 3 e 4 do Artigo I e a tabela 1 do Artigo III, as quais serão publicadas apenas no formato eletrônico. O formato é o mesmo das amostras incluídas nos artigos.

Table 1. Log of Observations (Paper I).

Star	<i>V</i>	Observation Date	<i>T_{exp}</i>	S/N
			(s)	(~ 6700 Å)
HD142	5.70	2007 Aug 30	200	367
HD1237	6.59	2007 Aug 30	480	466
HD2039	9.00	2007 Aug 28	3000	362
HD2638	9.44	2007 Aug 29	3000	276
HD3651	5.88	2007 Aug 29	200	356
HD4113	7.88	2008 Aug 19	1200	496
HD4208	7.78	2007 Aug 30	1200	362
HD4308	6.55	2007 Aug 30	480	459
HD4203	8.70	2007 Aug 29	3000	339
HD6434	7.72	2007 Aug 30	1200	370
HD10647	5.52	2007 Aug 30	200	423
HD11506	7.51	2007 Aug 28	1200	475
HD12661	7.43	2007 Aug 29	480	245
HD13445	6.12	2007 Aug 30	400	379
HD16141	6.83	2007 Oct 02	480	482
HD16417	5.78	2008 Aug 20	200	410
HD17051	5.40	2007 Aug 28	80	308
HIP14810	8.52	2007 Aug 30	2400	374
HD19994	5.07	2007 Aug 28	80	312
HD20782	7.36	2007 Aug 28	480	399
HD22049	3.72	2007 Aug 28	30	388
HD23079	7.12	2007 Oct 02	720	414
HD27894	9.36	2007 Aug 30	3000	230
HD28185	7.80	2007 Aug 28	1200	357
HD30177	8.41	2007 Oct 02	1200	260
HD37124	7.68	2008 Feb 20	1200	285
HD39091	5.65	2007 Apr 08	200	446
HD37605	8.67	2007 Oct 02	3000	339
HD40307	7.17	2008 Aug 19	500	355
HD41004A	8.65	2007 Oct 02	3000	336
ABPic	9.13	2008 Apr 06	3000	343

Table 1—Continued

Star	<i>V</i>	Observation Date	<i>T_{exp}</i>	S/N
			(s)	($\sim 6700 \text{ \AA}$)
HD45652	8.10	2008 Aug 19	1200	345
HD46375	7.91	2007 Apr 08	1200	300
HD47186	7.63	2008 Aug 19	1200	481
HD50499	7.21	2007 Apr 08	480	332
HD50554	6.84	2008 Feb 20	500	281
HD52265	6.29	2007 Apr 08	200	333
HD63454	9.37	2007 Apr 08	3000	225
HD65216	7.97	2007 Apr 07	1200	429
HD66428	8.25	2007 Apr 06	1200	386
HD69830	5.95	2007 Apr 07	200	454
HD70642	7.17	2007 Apr 07	480	350
HD70753	8.70	2008 Feb 21	3000	376
HD72659	7.46	2007 Apr 07	480	362
HD73256	8.08	2007 Apr 07	1200	394
HD74156	7.61	2007 Apr 07	1200	456
HD75289	6.35	2007 Apr 07	200	410
HD76700	8.16	2007 Apr 06	1200	371
HD81040	7.72	2007 Apr 06	1200	491
HD82943	6.54	2007 Apr 06	480	550
HD83443	8.23	2007 Apr 07	1200	329
HD86081	8.73	2007 Apr 06	3000	521
HD89307	7.02	2007 Apr 07	480	378
HD92788	7.31	2007 Apr 07	480	387
HD93083	8.30	2007 Apr 06	1200	326
BD-10-3166	10.08	2007 Apr 08	3600	228
HD99109	9.10	2007 Apr 07	3000	295
HD100777	8.42	2008 Feb 21	1200	323
HD101930	8.21	2007 Apr 06	1200	359
HD102117	7.47	2007 Apr 06	480	395
HD102195	8.07	2007 Apr 07	1200	430
HD106252	7.41	2007 Apr 06	480	380

Table 1—Continued

Star	<i>V</i>	Observation Date	<i>T_{exp}</i>	S/N
			(s)	(~ 6700 Å)
HD107148	8.01	2007 Apr 07	1200	405
HD108147	6.99	2007 Apr 07	480	380
HD108874	8.76	2007 Apr 07	3000	381
HD109749	8.08	2007 Apr 06	1200	402
HD111232	7.59	2007 Apr 07	1200	521
HD114386	8.73	2007 Apr 07	3000	337
HD114762	7.30	2007 Apr 06	480	400
HD114783	7.56	2007 Apr 07	1200	424
HD114729	6.68	2007 Apr 06	480	586
HD117207	7.26	2007 Apr 06	480	399
HD117618	7.17	2007 Apr 06	480	498
HD120136	4.50	2007 Apr 06	80	352
HD121504	7.54	2007 Apr 06	1200	486
HD125612	8.31	2007 Aug 29	1200	244
HD128311	7.48	2007 Apr 06	1200	341
HD130322	8.04	2007 Apr 07	1200	370
HD134987	6.47	2007 Apr 06	200	388
HD330075	9.36	2007 Apr 06	3000	309
HD141937	7.25	2007 Apr 07	480	392
HD142415	7.33	2007 Apr 07	480	293
HD142022A	7.70	2007 Apr 06	1200	454
HD147513	5.37	2007 Apr 06	80	452
HD149143	7.89	2007 Apr 06	1200	430
HD160691	5.12	2007 Apr 06	80	392
HD162020	9.10	2007 Apr 07	3000	288
HD164922	7.01	2007 Aug 29	480	355
HD168443	6.92	2007 Apr 06	480	512
HD168746	7.95	2007 Apr 06	1200	477
HD169830	5.90	2007 Apr 07	200	509
HD170469	8.21	2007 Aug 28	1200	339
HD179949	6.25	2007 Apr 07	200	426

Table 1—Continued

Star	V	Observation Date	T_{exp}	S/N
			(s)	($\sim 6700 \text{ \AA}$)
HD181433	8.40	2008 Aug 19	1200	192
HD183263	7.86	2007 Apr 08	1200	357
HD231701	8.97	2007 Aug 28	3000	281
HD187085	7.22	2007 Apr 07	480	380
HD189733	7.67	2007 Aug 28	1200	338
HD192263	7.79	2007 Apr 08	1200	341
HD195019	6.87	2007 Apr 08	480	351
WASP2	11.98	2007 Aug 30	10800	215
HD196050	7.50	2007 Apr 08	480	328
HD196885	6.39	2007 Apr 08	200	320
HD202206	8.08	2007 Aug 28	1200	402
HD208487	7.47	2007 Apr 08	480	352
HD209458	7.65	2007 Aug 28	1200	402
HD210277	6.54	2007 Apr 08	200	294
HD212301	7.76	2007 Apr 08	1200	379
HD213240	6.81	2007 Aug 29	480	367
HD216435	6.03	2007 Aug 30	200	394
HD216437	6.04	2008 Apr 07	400	442
HD216770	8.11	2007 Aug 30	1200	308
HD217014	5.45	2007 Aug 30	80	347
HD217107	6.17	2007 Aug 30	200	293
HD219828	8.04	2007 Aug 29	1200	323
HD221287	7.82	2007 Aug 28	1200	411
HD222582	7.68	2007 Aug 30	1200	448
HD1581	4.23	2008 Aug 20	30	216
HD1835	6.39	2007 Oct 02	200	388
HD3823	5.89	2007 Oct 02	200	452
HD4628	5.74	2008 Aug 20	200	375
HD7199	8.06	2008 Aug 19	1200	348
HD7693	7.22	2008 Aug 20	500	254
HD7570	4.97	2008 Aug 20	100	414

Table 1—Continued

Star	V	Observation Date	T_{exp} (s)	S/N ($\sim 6700 \text{ \AA}$)
HD10180	7.33	2008 Aug 20	500	330
HD10476	5.24	2008 Aug 20	100	299
HD10700	3.49	2008 Aug 20	15	341
HD11112	7.13	2008 Aug 19	500	423
HD12387	7.37	2008 Aug 19	500	455
HD16160	5.79	2008 Aug 20	200	233
HD17925	6.05	2008 Aug 20	200	315
HD19632	7.29	2008 Aug 20	500	360
HD20029	7.05	2008 Aug 19	500	456
HD20201	7.27	2008 Aug 20	500	318
HD20630	4.84	2008 Aug 20	100	316
HD20794	4.26	2008 Aug 20	30	284
HD22104	8.32	2008 Aug 20	1200	312
HD22484	4.29	2008 Aug 20	30	271
HD25587	7.40	2008 Aug 19	500	432
HD25680	5.90	2008 Aug 20	200	335
HD30876	7.49	2008 Aug 19	500	346
HD31527	7.49	2008 Aug 19	500	433
HD36435	6.99	2007 Aug 30	480	350
HD36889	7.37	2008 Aug 20	500	288
HD38283	6.69	2008 Aug 20	500	327
HD38382	6.34	2008 Aug 20	200	347
HD38973	6.63	2008 Aug 20	500	341
HD39213	8.96	2008 Aug 20	2400	297
HD39587	4.39	2008 Aug 20	30	282
HD42024	7.24	2008 Aug 20	500	319
HD43042	5.20	2008 Aug 20	100	322
HD45701	6.45	2008 Aug 20	200	273
HD51929	7.39	2008 Apr 07	500	317
HD52447	8.38	2008 Apr 07	1200	274
HD55693	7.17	2008 Apr 07	500	347

Table 1—Continued

Star	<i>V</i>	Observation Date	<i>T_{exp}</i>	S/N
			(s)	(~ 6700 Å)
HD64184	7.49	2008 Apr 07	500	340
HD65907	5.59	2008 Apr 07	200	436
HD73524	6.53	2008 Apr 07	500	493
HD76151	6.01	2008 Apr 07	200	433
HD78429	7.31	2008 Apr 07	500	386
HD80913	7.49	2008 Apr 07	500	298
HD84117	4.93	2008 Apr 07	100	419
HD86819	7.38	2008 Feb 21	500	371
HD88742	6.38	2008 Apr 07	200	400
HD92987	7.03	2008 Apr 07	500	387
HD93385	7.49	2008 Apr 07	500	390
HD96423	7.23	2008 Apr 07	500	449
HD102365	4.89	2008 Apr 07	100	480
HD102438	6.48	2008 Apr 07	200	358
HD102870	3.59	2008 Apr 07	30	244
HD105328	6.72	2008 Apr 07	500	501
HD106453	7.47	2008 Apr 07	500	431
HD107692	6.70	2008 Apr 07	500	494
HD108309	6.25	2008 Apr 07	200	324
HD109200	7.13	2008 Feb 21	500	392
HD110810	7.82	2008 Feb 21	1200	369
HD114853	6.93	2008 Feb 21	500	398
HD115383	5.19	2008 Apr 07	100	390
HD115617	4.74	2008 Apr 07	100	504
HD115585	7.43	2008 Apr 07	500	293
HD117105	7.20	2008 Apr 07	500	406
HD117939	7.29	2008 Apr 07	500	374
HD118972	6.92	2008 Apr 07	500	498
HD120237	6.56	2008 Apr 07	500	489
HD120690	6.43	2008 Apr 07	200	361
HD120780	7.37	2008 Apr 07	500	369

Table 1—Continued

Star	<i>V</i>	Observation Date	<i>T_{exp}</i>	S/N
			(s)	(~ 6700 Å)
HD122742	6.27	2008 Apr 07	200	304
HD122862	6.02	2008 Apr 07	200	368
HD124584	7.29	2008 Apr 07	500	415
HD125072	6.66	2008 Apr 07	500	258
HD126053	6.25	2008 Apr 07	200	459
HD125881	7.26	2008 Apr 07	500	333
HD128674	7.39	2008 Apr 07	1000	478
HD130948	5.86	2008 Apr 07	200	418
HD131511	6.00	2008 Apr 07	200	342
HD131977	5.72	2008 Apr 07	200	235
HD131923	6.34	2008 Apr 07	200	299
HD134060	6.29	2008 Apr 07	200	352
HD134606	6.86	2008 Apr 07	500	391
HD136352	5.65	2008 Apr 07	200	436
HD141004	4.42	2008 Apr 07	30	287
HD140901	6.01	2008 Aug 20	200	466
HD143114	7.34	2008 Aug 20	500	413
HD144009	7.23	2008 Aug 20	500	325
HD144628	7.11	2008 Aug 20	500	317
HD145825	6.55	2008 Aug 20	500	472
HD146481	7.09	2008 Aug 20	500	515
HD149661	5.77	2008 Aug 20	200	401
HD150248	7.03	2008 Aug 20	500	427
HD153075	6.99	2008 Aug 19	500	449
HD155974	6.09	2008 Aug 19	200	366
HD156274	5.47	2008 Aug 20	200	484
HD155918	7.00	2008 Aug 19	500	464
HD158783	7.09	2008 Aug 19	500	448
HD161612	7.20	2008 Aug 20	500	297
HD162255	7.15	2008 Aug 19	500	471
HD163272	7.39	2008 Aug 19	500	368

Table 1—Continued

Star	<i>V</i>	Observation Date	<i>T_{exp}</i>	S/N
			(s)	(~ 6700 Å)
HD166553	7.27	2008 Aug 20	500	310
HD168871	6.45	2008 Aug 20	200	338
HD175345	7.37	2008 Aug 19	500	370
HD177565	6.15	2008 Aug 20	200	332
HD179140	7.23	2008 Aug 19	500	370
HD181428	7.10	2008 Aug 19	500	431
HD183877	7.14	2008 Aug 19	500	418
HD184985	5.46	2008 Aug 19	100	406
HD187691	5.12	2008 Aug 19	100	487
HD190406	5.80	2008 Aug 19	200	502
HD189567	6.07	2008 Aug 20	200	386
HD190248	3.55	2008 Aug 20	30	329
HD191408	5.32	2008 Aug 20	100	363
HD192310	5.73	2008 Aug 20	200	328
HD193193	7.20	2008 Aug 19	500	401
HD192865	6.91	2008 Aug 19	500	390
HD193307	6.26	2008 Aug 19	200	403
HD194640	6.61	2008 Aug 19	500	455
HD196390	7.33	2008 Aug 19	500	366
HD196800	7.21	2008 Aug 20	500	419
HD196068	7.18	2007 Oct 02	480	368
HD199288	6.52	2008 Aug 20	500	451
HD199190	6.86	2008 Aug 20	500	415
HD199509	6.98	2007 Oct 02	480	283
HD204385	7.14	2007 Oct 02	480	277
HD205390	7.14	2008 Aug 19	500	385
HD206395	6.67	2008 Aug 19	500	445
HD207129	5.57	2008 Aug 20	200	430
HD207700	7.43	2008 Aug 19	500	340
HD208998	7.12	2008 Aug 20	500	327
HD209653	6.99	2008 Aug 19	500	404

Table 1—Continued

Star	<i>V</i>	Observation Date	<i>T_{exp}</i>	S/N
			(s)	(\sim 6700 Å)
HD212291	7.91	2008 Aug 19	1200	522
HD212168	6.12	2008 Aug 19	200	385
HD212708	7.48	2008 Aug 20	500	278
HD214759	7.41	2008 Aug 20	500	252
HD214953	5.99	2008 Aug 19	200	418
HD215648	4.20	2008 Aug 19	30	388
HD217958	8.05	2008 Aug 19	1200	432
HD218261	6.44	2008 Aug 19	200	360
HD220507	7.59	2008 Aug 19	1200	514
HD222237	7.09	2008 Aug 20	500	226
HD222335	7.18	2007 Oct 02	480	386
HD222368	4.13	2008 Aug 19	30	440
HD222480	7.11	2007 Oct 02	480	476
HD223171	6.89	2008 Aug 19	500	453

Table 3. Atmospheric Parameters (Paper I).

Star	T_{eff} (K)	log g	ξ (km s $^{-1}$)	A(Fe)	σ (Fe I)	N (Fe I)	σ (Fe I)	N (Fe II)	[Fe/H]
HD142	6338 ± 46	4.34 ± 0.14	2.27 ± 0.08	7.46	0.09	23	0.07	10	0.03 ± 0.04
HD1237	5572 ± 40	4.58 ± 0.09	1.34 ± 0.04	7.55	0.09	27	0.05	9	0.12 ± 0.04
HD2039	5934 ± 36	4.30 ± 0.13	1.26 ± 0.04	7.73	0.08	27	0.05	12	0.30 ± 0.03
HD2638	5236 ± 70	4.38 ± 0.19	0.86 ± 0.04	7.65	0.07	26	0.07	9	0.22 ± 0.05
HD3651	5252 ± 65	4.32 ± 0.18	0.81 ± 0.02	7.62	0.08	27	0.05	10	0.19 ± 0.03
HD4113	5646 ± 70	4.22 ± 0.25	1.06 ± 0.04	7.62	0.07	25	0.05	10	0.19 ± 0.05
HD4208	5638 ± 26	4.39 ± 0.11	1.12 ± 0.04	7.15	0.06	26	0.05	12	-0.28 ± 0.02
HD4308	5768 ± 31	4.52 ± 0.10	1.50 ± 0.06	7.12	0.08	25	0.05	11	-0.31 ± 0.03
HD4203	5644 ± 65	4.11 ± 0.16	1.16 ± 0.04	7.86	0.09	27	0.04	10	0.43 ± 0.05
HD6434	5742 ± 29	4.52 ± 0.06	0.70 ± 0.02	6.85	0.09	19	0.05	12	-0.58 ± 0.03
HD10647	6155 ± 29	4.44 ± 0.16	1.47 ± 0.04	7.37	0.05	21	0.06	11	-0.06 ± 0.02
HD11506	6066 ± 25	4.22 ± 0.08	1.33 ± 0.04	7.72	0.07	24	0.05	12	0.29 ± 0.02
HD12661	5785 ± 50	4.39 ± 0.15	1.20 ± 0.04	7.80	0.06	25	0.05	10	0.37 ± 0.03
HD13445	5189 ± 41	4.47 ± 0.14	0.89 ± 0.04	7.17	0.07	27	0.07	8	-0.26 ± 0.02
HD16141	5730 ± 38	4.05 ± 0.09	1.22 ± 0.04	7.54	0.08	27	0.04	12	0.11 ± 0.03
HD16417	5788 ± 30	4.05 ± 0.06	1.23 ± 0.04	7.57	0.08	27	0.04	12	0.14 ± 0.04
HD17051	6239 ± 45	4.55 ± 0.12	1.54 ± 0.04	7.59	0.07	26	0.06	10	0.16 ± 0.03
HIP14810	5541 ± 63	4.19 ± 0.21	1.02 ± 0.04	7.69	0.07	26	0.05	9	0.26 ± 0.04
HD19994	6081 ± 40	4.07 ± 0.10	1.84 ± 0.04	7.51	0.08	25	0.07	11	0.08 ± 0.04
HD20782	5732 ± 22	4.23 ± 0.09	1.03 ± 0.04	7.37	0.07	26	0.04	12	-0.06 ± 0.02
HD22049	5096 ± 45	4.29 ± 0.17	1.17 ± 0.04	7.25	0.09	27	0.07	8	-0.18 ± 0.03
HD23079	6017 ± 38	4.52 ± 0.08	1.41 ± 0.04	7.31	0.07	26	0.05	12	-0.12 ± 0.03
HD27894	4832 ± 85	4.02 ± 0.16	0.77 ± 0.06	7.64	0.10	24	0.02	3	0.21 ± 0.03
HD28185	5706 ± 40	4.35 ± 0.20	1.02 ± 0.04	7.70	0.07	26	0.06	11	0.27 ± 0.02
HD30177	5595 ± 50	4.15 ± 0.13	1.13 ± 0.04	7.82	0.08	26	0.05	11	0.39 ± 0.05
HD37124	5492 ± 26	4.40 ± 0.13	0.67 ± 0.06	7.03	0.07	27	0.04	11	-0.40 ± 0.02
HD39091	6037 ± 45	4.42 ± 0.13	1.36 ± 0.02	7.51	0.06	25	0.05	12	0.08 ± 0.03
HD37605	5405 ± 55	4.23 ± 0.21	0.98 ± 0.04	7.74	0.08	26	0.06	11	0.31 ± 0.04
HD40307	4956 ± 50	4.21 ± 0.21	1.06 ± 0.04	7.08	0.09	23	0.06	3	-0.35 ± 0.02
HD41004A	5310 ± 65	4.37 ± 0.22	0.85 ± 0.04	7.66	0.08	24	0.06	8	0.23 ± 0.04
ABPic	5378 ± 55	4.44 ± 0.21	2.59 ± 0.06	7.38	0.11	21	0.09	3	-0.05 ± 0.04

Table 3—Continued

Star	T_{eff} (K)	log g	ξ (km s $^{-1}$)	A(Fe)	σ (Fe I)	N (Fe I)	σ (Fe I)	N (Fe II)	[Fe/H]
HD45652	5306 ± 57	4.13 ± 0.17	0.88 ± 0.04	7.70	0.09	27	0.07	10	0.27 ± 0.04
HD46375	5336 ± 70	4.37 ± 0.22	0.87 ± 0.06	7.75	0.09	27	0.06	9	0.32 ± 0.05
HD47186	5640 ± 60	4.21 ± 0.21	1.16 ± 0.04	7.64	0.08	27	0.05	10	0.21 ± 0.05
HD50499	5927 ± 40	4.05 ± 0.08	1.31 ± 0.04	7.69	0.07	24	0.05	12	0.26 ± 0.04
HD50554	5982 ± 26	4.29 ± 0.08	1.37 ± 0.06	7.36	0.07	24	0.06	12	-0.07 ± 0.02
HD52265	6036 ± 35	4.11 ± 0.09	1.50 ± 0.06	7.54	0.08	24	0.05	12	0.11 ± 0.04
HD63454	4907 ± 60	4.11 ± 0.17	1.20 ± 0.06	7.43	0.09	20	0.13	6	0.00 ± 0.03
HD65216	5632 ± 31	4.43 ± 0.13	1.02 ± 0.04	7.27	0.06	25	0.04	12	-0.16 ± 0.02
HD66428	5615 ± 55	4.06 ± 0.10	1.12 ± 0.04	7.66	0.08	26	0.04	10	0.23 ± 0.05
HD69830	5435 ± 31	4.42 ± 0.14	0.89 ± 0.04	7.43	0.07	26	0.06	12	0.00 ± 0.02
HD70642	5711 ± 41	4.42 ± 0.13	1.09 ± 0.04	7.65	0.07	25	0.05	10	0.22 ± 0.02
HD70573	5884 ± 26	4.57 ± 0.08	1.69 ± 0.06	7.39	0.08	19	0.06	6	-0.04 ± 0.03
HD72659	5851 ± 25	4.01 ± 0.04	1.27 ± 0.04	7.36	0.05	24	0.04	12	-0.07 ± 0.02
HD73256	5487 ± 65	4.35 ± 0.23	1.19 ± 0.04	7.65	0.10	27	0.07	10	0.22 ± 0.05
HD74156	6071 ± 36	4.28 ± 0.12	1.67 ± 0.04	7.47	0.08	26	0.06	12	0.04 ± 0.04
HD75289	5974 ± 36	4.06 ± 0.06	1.18 ± 0.04	7.63	0.10	27	0.04	11	0.20 ± 0.03
HD76700	5687 ± 57	4.14 ± 0.15	1.09 ± 0.04	7.84	0.08	27	0.05	9	0.41 ± 0.05
HD81040	5620 ± 38	4.13 ± 0.11	1.21 ± 0.04	7.22	0.06	25	0.05	12	-0.21 ± 0.03
HD82943	6011 ± 36	4.37 ± 0.13	1.21 ± 0.04	7.71	0.06	24	0.06	12	0.28 ± 0.03
HD83443	5527 ± 50	4.35 ± 0.17	0.97 ± 0.04	7.87	0.06	26	0.06	9	0.44 ± 0.04
HD86081	5864 ± 35	3.93 ± 0.13	1.30 ± 0.04	7.56	0.06	24	0.04	12	0.13 ± 0.02
HD89307	5914 ± 25	4.28 ± 0.11	1.29 ± 0.04	7.25	0.05	24	0.05	12	-0.18 ± 0.02
HD92788	5772 ± 57	4.30 ± 0.17	1.08 ± 0.04	7.75	0.08	27	0.05	10	0.32 ± 0.05
HD93083	5059 ± 60	4.28 ± 0.23	0.82 ± 0.06	7.60	0.08	23	0.07	7	0.17 ± 0.03
BD-10-3166	5388 ± 75	4.44 ± 0.20	0.83 ± 0.04	7.85	0.08	27	0.05	9	0.42 ± 0.05
HD99109	5311 ± 79	4.22 ± 0.22	0.95 ± 0.04	7.81	0.09	26	0.06	10	0.38 ± 0.06
HD100777	5542 ± 50	4.27 ± 0.16	1.00 ± 0.02	7.73	0.06	24	0.07	8	0.30 ± 0.04
HD101930	5190 ± 65	4.31 ± 0.23	0.79 ± 0.04	7.70	0.09	27	0.07	6	0.27 ± 0.04
HD102117	5631 ± 50	4.08 ± 0.15	1.09 ± 0.04	7.73	0.08	27	0.05	10	0.30 ± 0.04
HD102195	5339 ± 55	4.37 ± 0.20	1.06 ± 0.04	7.48	0.08	26	0.06	10	0.05 ± 0.04
HD106252	5923 ± 38	4.44 ± 0.11	1.26 ± 0.04	7.38	0.06	24	0.06	12	-0.05 ± 0.03

Table 3—Continued

Star	T_{eff} (K)	log g	ξ (km s $^{-1}$)	A(Fe)	σ (Fe I)	N (Fe I)	σ (Fe I)	N (Fe II)	[Fe/H]
HD107148	5739 ± 65	4.20 ± 0.17	1.13 ± 0.04	7.71	0.06	25	0.07	12	0.28 ± 0.04
HD108147	6179 ± 54	4.26 ± 0.14	1.41 ± 0.06	7.52	0.07	24	0.06	12	0.09 ± 0.03
HD108874	5572 ± 50	4.25 ± 0.15	1.01 ± 0.04	7.67	0.07	26	0.04	9	0.24 ± 0.04
HD109749	5853 ± 38	4.17 ± 0.12	1.25 ± 0.04	7.66	0.08	27	0.06	12	0.23 ± 0.04
HD111232	5406 ± 26	4.31 ± 0.08	0.97 ± 0.04	6.97	0.09	27	0.05	10	-0.46 ± 0.03
HD114386	5040 ± 57	4.19 ± 0.20	1.18 ± 0.06	7.25	0.08	20	0.10	5	-0.18 ± 0.03
HD114762	5837 ± 31	4.42 ± 0.13	0.60 ± 0.02	6.71	0.06	13	0.06	10	-0.72 ± 0.04
HD114783	5089 ± 60	4.27 ± 0.22	0.80 ± 0.04	7.52	0.09	27	0.06	7	0.09 ± 0.03
HD114729	5779 ± 31	4.01 ± 0.09	1.41 ± 0.04	7.10	0.08	25	0.04	11	-0.33 ± 0.03
HD117207	5615 ± 40	4.16 ± 0.15	1.16 ± 0.04	7.62	0.07	26	0.05	10	0.19 ± 0.03
HD117618	5901 ± 35	4.19 ± 0.09	1.14 ± 0.04	7.43	0.06	24	0.04	12	0.00 ± 0.02
HD120136	6460 ± 95	4.37 ± 0.22	1.94 ± 0.10	7.61	0.09	16	0.05	6	0.18 ± 0.07
HD121504	5951 ± 42	4.32 ± 0.13	1.23 ± 0.04	7.52	0.07	25	0.05	12	0.09 ± 0.03
HD125612	5894 ± 41	4.30 ± 0.13	1.12 ± 0.04	7.68	0.08	26	0.04	12	0.25 ± 0.04
HD128311	5120 ± 43	4.49 ± 0.13	1.37 ± 0.06	7.44	0.08	19	0.06	4	0.01 ± 0.03
HD130322	5373 ± 45	4.33 ± 0.13	0.89 ± 0.04	7.48	0.07	26	0.05	9	0.05 ± 0.03
HD134987	5764 ± 43	4.19 ± 0.12	1.10 ± 0.02	7.76	0.05	23	0.06	10	0.33 ± 0.03
HD330075	5140 ± 50	4.38 ± 0.20	0.74 ± 0.04	7.61	0.08	25	0.06	4	0.18 ± 0.03
HD141937	5842 ± 36	4.25 ± 0.13	1.13 ± 0.04	7.53	0.06	25	0.06	12	0.10 ± 0.03
HD142415	5939 ± 41	4.38 ± 0.18	1.02 ± 0.04	7.58	0.07	24	0.06	11	0.15 ± 0.03
HD142022A	5467 ± 55	4.20 ± 0.17	1.00 ± 0.02	7.63	0.07	26	0.05	8	0.20 ± 0.04
HD147513	5888 ± 36	4.54 ± 0.09	1.07 ± 0.04	7.52	0.05	23	0.04	12	0.09 ± 0.03
HD149143	5892 ± 50	4.04 ± 0.11	1.21 ± 0.04	7.75	0.07	25	0.07	12	0.32 ± 0.04
HD160691	5695 ± 45	4.02 ± 0.13	1.26 ± 0.04	7.66	0.07	27	0.06	10	0.23 ± 0.03
HD162020	4891 ± 36	4.09 ± 0.11	1.04 ± 0.04	7.36	0.06	17	0.07	3	-0.07 ± 0.02
HD164922	5378 ± 50	4.30 ± 0.22	0.79 ± 0.02	7.64	0.06	26	0.05	10	0.21 ± 0.03
HD168443	5645 ± 50	4.16 ± 0.15	1.14 ± 0.04	7.55	0.07	27	0.04	10	0.12 ± 0.03
HD168746	5625 ± 25	4.36 ± 0.11	0.97 ± 0.04	7.38	0.06	26	0.04	11	-0.05 ± 0.02
HD169830	6305 ± 38	4.09 ± 0.10	1.85 ± 0.06	7.52	0.07	25	0.06	11	0.09 ± 0.03
HD170469	5736 ± 40	4.08 ± 0.09	1.18 ± 0.04	7.69	0.06	24	0.05	10	0.26 ± 0.04
HD179949	6230 ± 41	4.38 ± 0.11	1.41 ± 0.04	7.58	0.05	23	0.05	12	0.15 ± 0.02

Table 3—Continued

Star	T_{eff} (K)	$\log g$	ξ (km s $^{-1}$)	A(Fe)	σ (Fe I)	N (Fe I)	σ (Fe I)	N (Fe II)	[Fe/H]
HD181433	4915 ± 63	4.28 ± 0.31	0.67 ± 0.12	7.89	0.13	24	0.08	2	0.46 ± 0.05
HD183263	5930 ± 30	4.23 ± 0.14	1.21 ± 0.04	7.73	0.06	24	0.05	12	0.30 ± 0.03
HD231701	6148 ± 44	4.26 ± 0.16	1.77 ± 0.06	7.35	0.08	24	0.06	11	-0.08 ± 0.04
HD187085	6190 ± 45	4.43 ± 0.14	1.54 ± 0.06	7.55	0.08	26	0.07	12	0.12 ± 0.04
HD189733	5201 ± 35	4.64 ± 0.10	1.08 ± 0.06	7.45	0.09	26	0.07	7	0.02 ± 0.03
HD192263	5028 ± 55	4.29 ± 0.23	0.98 ± 0.04	7.41	0.07	23	0.09	5	-0.02 ± 0.04
HD195019	5741 ± 20	4.06 ± 0.04	1.20 ± 0.02	7.46	0.05	24	0.04	11	0.03 ± 0.01
WASP2	5227 ± 46	4.42 ± 0.13	0.82 ± 0.04	7.53	0.08	27	0.03	8	0.10 ± 0.03
HD196050	5912 ± 41	4.19 ± 0.12	1.20 ± 0.04	7.72	0.07	26	0.05	11	0.29 ± 0.03
HD196885	6218 ± 41	4.18 ± 0.13	1.46 ± 0.04	7.62	0.08	26	0.06	11	0.19 ± 0.04
HD202206	5722 ± 60	4.27 ± 0.22	1.09 ± 0.04	7.73	0.06	24	0.07	12	0.30 ± 0.04
HD208487	6105 ± 31	4.42 ± 0.13	1.51 ± 0.04	7.45	0.06	25	0.06	9	0.02 ± 0.02
HD209458	6076 ± 31	4.33 ± 0.08	1.38 ± 0.04	7.41	0.05	23	0.06	12	-0.02 ± 0.02
HD210277	5553 ± 50	4.31 ± 0.17	1.06 ± 0.04	7.65	0.07	27	0.04	7	0.22 ± 0.05
HD212301	6303 ± 31	4.57 ± 0.06	1.59 ± 0.04	7.60	0.08	24	0.06	12	0.17 ± 0.03
HD213240	5924 ± 47	4.12 ± 0.13	1.12 ± 0.04	7.62	0.04	18	0.04	12	0.19 ± 0.02
HD216435	5993 ± 35	4.14 ± 0.07	1.38 ± 0.04	7.67	0.08	27	0.06	12	0.24 ± 0.04
HD216437	5806 ± 50	4.06 ± 0.11	1.23 ± 0.04	7.65	0.08	27	0.06	11	0.22 ± 0.05
HD216770	5463 ± 60	4.38 ± 0.19	0.88 ± 0.04	7.79	0.07	27	0.05	8	0.36 ± 0.04
HD217014	5739 ± 50	4.17 ± 0.13	1.10 ± 0.04	7.62	0.09	27	0.06	12	0.19 ± 0.05
HD217107	5665 ± 60	4.25 ± 0.16	1.05 ± 0.02	7.83	0.07	27	0.05	10	0.40 ± 0.04
HD219828	5827 ± 41	4.06 ± 0.12	1.36 ± 0.04	7.57	0.08	27	0.05	12	0.14 ± 0.04
HD221287	6241 ± 21	4.37 ± 0.10	1.27 ± 0.02	7.41	0.04	20	0.05	12	-0.02 ± 0.01
HD222582	5780 ± 31	4.33 ± 0.11	1.17 ± 0.04	7.42	0.06	26	0.04	12	-0.01 ± 0.02
HD1581	5908 ± 31	4.26 ± 0.13	1.17 ± 0.04	7.23	0.08	25	0.08	12	-0.20 ± 0.03
HD1835	5829 ± 41	4.39 ± 0.16	1.24 ± 0.04	7.65	0.07	22	0.05	10	0.22 ± 0.03
HD3823	6012 ± 31	4.18 ± 0.08	1.92 ± 0.10	7.08	0.07	25	0.05	11	-0.35 ± 0.02
HD4628	5055 ± 40	4.33 ± 0.19	0.88 ± 0.04	7.14	0.08	25	0.06	5	-0.29 ± 0.02
HD7199	5349 ± 65	4.09 ± 0.19	1.04 ± 0.04	7.74	0.09	26	0.05	10	0.31 ± 0.05
HD7693	5093 ± 38	4.54 ± 0.10	1.24 ± 0.08	7.57	0.10	18	0.06	5	0.14 ± 0.03
HD7570	6196 ± 38	4.41 ± 0.12	1.30 ± 0.02	7.67	0.06	24	0.04	12	0.24 ± 0.02

Table 3—Continued

Star	T_{eff} (K)	log g	ξ (km s $^{-1}$)	A(Fe)	σ (Fe I)	N (Fe I)	σ (Fe I)	N (Fe II)	[Fe/H]
HD10180	5933 ± 32	4.32 ± 0.13	1.46 ± 0.04	7.47	0.05	23	0.06	12	0.04 ± 0.02
HD10476	5242 ± 40	4.48 ± 0.12	0.89 ± 0.04	7.40	0.07	26	0.05	9	-0.03 ± 0.02
HD10700	5321 ± 25	4.46 ± 0.10	0.99 ± 0.04	6.87	0.08	25	0.06	9	-0.56 ± 0.03
HD11112	5896 ± 45	4.13 ± 0.09	1.18 ± 0.04	7.67	0.06	23	0.06	12	0.24 ± 0.03
HD12387	5722 ± 33	4.35 ± 0.13	1.14 ± 0.06	7.20	0.08	27	0.05	12	-0.23 ± 0.03
HD16160	4922 ± 50	4.33 ± 0.20	1.01 ± 0.04	7.22	0.08	21	0.02	2	-0.21 ± 0.03
HD17925	5187 ± 50	4.35 ± 0.21	1.24 ± 0.04	7.51	0.10	24	0.06	7	0.08 ± 0.03
HD19632	5737 ± 50	4.36 ± 0.18	1.23 ± 0.04	7.54	0.08	24	0.05	11	0.11 ± 0.05
HD20029	6184 ± 41	4.31 ± 0.10	1.68 ± 0.04	7.50	0.06	24	0.06	10	0.07 ± 0.02
HD20201	6061 ± 41	4.49 ± 0.09	1.18 ± 0.04	7.62	0.07	23	0.05	12	0.19 ± 0.03
HD20630	5723 ± 33	4.36 ± 0.17	1.08 ± 0.04	7.52	0.08	24	0.05	11	0.09 ± 0.03
HD20794	5452 ± 30	4.39 ± 0.19	1.17 ± 0.02	7.01	0.06	25	0.05	11	-0.42 ± 0.02
HD22104	5972 ± 42	4.38 ± 0.19	1.36 ± 0.04	7.82	0.05	21	0.07	11	0.39 ± 0.03
HD22484	6097 ± 40	4.23 ± 0.08	1.48 ± 0.06	7.42	0.07	24	0.07	12	-0.01 ± 0.04
HD25587	6134 ± 26	4.16 ± 0.08	1.59 ± 0.04	7.36	0.05	21	0.06	12	-0.07 ± 0.02
HD25680	5903 ± 36	4.52 ± 0.09	1.05 ± 0.04	7.57	0.07	23	0.04	12	0.14 ± 0.03
HD30876	5076 ± 61	4.33 ± 0.22	1.05 ± 0.04	7.29	0.07	24	0.06	7	-0.14 ± 0.03
HD31527	5866 ± 32	4.29 ± 0.11	1.31 ± 0.04	7.21	0.05	24	0.04	12	-0.22 ± 0.02
HD36435	5387 ± 45	4.34 ± 0.14	1.26 ± 0.04	7.34	0.09	26	0.04	9	-0.09 ± 0.04
HD36889	5968 ± 30	4.26 ± 0.12	1.42 ± 0.04	7.66	0.07	26	0.07	12	0.23 ± 0.02
HD38283	5856 ± 36	3.90 ± 0.11	1.53 ± 0.06	7.14	0.06	23	0.06	12	-0.29 ± 0.03
HD38382	6106 ± 33	4.42 ± 0.11	1.46 ± 0.02	7.45	0.05	25	0.06	12	0.02 ± 0.02
HD38973	6064 ± 38	4.48 ± 0.09	1.18 ± 0.04	7.56	0.07	26	0.04	12	0.13 ± 0.02
HD39213	5452 ± 55	4.15 ± 0.15	1.01 ± 0.04	7.81	0.07	26	0.04	9	0.38 ± 0.04
HD39587	6029 ± 51	4.62 ± 0.12	1.62 ± 0.08	7.42	0.09	25	0.07	11	-0.01 ± 0.04
HD42024	6249 ± 53	4.25 ± 0.13	1.52 ± 0.06	7.64	0.07	25	0.06	12	0.21 ± 0.03
HD43042	6511 ± 35	4.20 ± 0.11	1.34 ± 0.06	7.54	0.06	18	0.06	11	0.11 ± 0.02
HD45701	5871 ± 36	4.12 ± 0.10	1.16 ± 0.04	7.68	0.05	24	0.07	12	0.25 ± 0.02
HD51929	5739 ± 33	4.46 ± 0.07	0.70 ± 0.02	6.76	0.06	14	0.04	11	-0.67 ± 0.03
HD52447	6136 ± 50	4.36 ± 0.18	1.58 ± 0.04	7.66	0.07	25	0.07	10	0.23 ± 0.04
HD55693	5865 ± 52	4.20 ± 0.13	1.11 ± 0.04	7.74	0.06	23	0.05	12	0.31 ± 0.03

Table 3—Continued

Star	T_{eff} (K)	$\log g$	ξ (km s $^{-1}$)	A(Fe)	σ (Fe I)	N (Fe I)	σ (Fe I)	N (Fe II)	[Fe/H]
HD64184	5723 ± 40	4.53 ± 0.07	1.15 ± 0.04	7.28	0.08	26	0.07	12	-0.15 ± 0.03
HD65907	6027 ± 36	4.57 ± 0.10	1.70 ± 0.06	7.12	0.08	24	0.05	10	-0.31 ± 0.04
HD73524	6004 ± 45	4.34 ± 0.13	1.21 ± 0.04	7.59	0.07	24	0.05	12	0.16 ± 0.03
HD76151	5770 ± 25	4.40 ± 0.07	1.06 ± 0.04	7.54	0.06	23	0.05	12	0.11 ± 0.02
HD78429	5738 ± 40	4.22 ± 0.12	1.16 ± 0.02	7.51	0.06	25	0.06	12	0.08 ± 0.02
HD80913	6064 ± 25	4.28 ± 0.03	0.80 ± 0.02	6.80	0.08	17	0.03	11	-0.63 ± 0.02
HD84117	6172 ± 20	4.27 ± 0.09	1.94 ± 0.06	7.28	0.07	21	0.05	11	-0.15 ± 0.02
HD86819	5980 ± 30	4.18 ± 0.11	1.21 ± 0.04	7.42	0.08	26	0.05	12	-0.01 ± 0.03
HD88742	5978 ± 35	4.48 ± 0.07	1.22 ± 0.04	7.41	0.06	23	0.04	12	-0.02 ± 0.02
HD92987	5815 ± 36	4.04 ± 0.11	1.12 ± 0.04	7.49	0.06	23	0.05	12	0.06 ± 0.03
HD93385	5823 ± 35	4.08 ± 0.11	1.16 ± 0.04	7.38	0.06	23	0.03	12	-0.05 ± 0.03
HD96423	5724 ± 35	4.29 ± 0.17	1.06 ± 0.04	7.56	0.06	23	0.05	12	0.13 ± 0.02
HD102365	5665 ± 35	4.42 ± 0.13	1.13 ± 0.04	7.12	0.05	24	0.05	12	-0.31 ± 0.02
HD102438	5554 ± 30	4.32 ± 0.11	1.11 ± 0.04	7.12	0.07	26	0.04	12	-0.31 ± 0.02
HD102870	6222 ± 49	4.23 ± 0.13	1.47 ± 0.06	7.62	0.08	25	0.06	12	0.19 ± 0.04
HD105328	5937 ± 30	4.09 ± 0.10	1.26 ± 0.04	7.59	0.06	24	0.05	12	0.16 ± 0.02
HD106453	5627 ± 45	4.49 ± 0.11	1.06 ± 0.04	7.55	0.06	24	0.06	10	0.12 ± 0.03
HD107692	5853 ± 40	4.39 ± 0.13	1.11 ± 0.04	7.60	0.08	27	0.04	11	0.17 ± 0.03
HD108309	5715 ± 36	4.05 ± 0.07	1.10 ± 0.04	7.55	0.06	23	0.06	11	0.12 ± 0.02
HD109200	5113 ± 36	4.43 ± 0.16	0.76 ± 0.04	7.14	0.07	26	0.06	6	-0.29 ± 0.02
HD110810	5029 ± 50	4.24 ± 0.20	1.29 ± 0.04	7.36	0.09	25	0.06	6	-0.07 ± 0.03
HD114853	5687 ± 29	4.30 ± 0.13	1.36 ± 0.04	7.12	0.06	24	0.05	11	-0.31 ± 0.02
HD115383	6101 ± 40	4.33 ± 0.12	1.69 ± 0.04	7.54	0.06	24	0.06	11	0.11 ± 0.03
HD115617	5618 ± 36	4.52 ± 0.10	0.91 ± 0.04	7.49	0.07	25	0.06	10	0.06 ± 0.02
HD115585	5721 ± 25	4.16 ± 0.11	1.16 ± 0.02	7.83	0.06	24	0.08	11	0.40 ± 0.02
HD117105	5892 ± 21	4.36 ± 0.11	1.37 ± 0.06	7.13	0.06	23	0.05	11	-0.30 ± 0.02
HD117939	5608 ± 31	4.19 ± 0.10	1.17 ± 0.02	7.17	0.06	25	0.05	12	-0.26 ± 0.02
HD118972	5191 ± 35	4.37 ± 0.13	1.26 ± 0.04	7.37	0.09	24	0.07	7	-0.06 ± 0.02
HD120237	6092 ± 29	4.30 ± 0.06	1.30 ± 0.06	7.39	0.08	24	0.04	11	-0.04 ± 0.03
HD120690	5610 ± 35	4.29 ± 0.13	1.10 ± 0.04	7.41	0.08	26	0.06	11	-0.02 ± 0.03
HD120780	5160 ± 45	4.43 ± 0.16	1.11 ± 0.04	7.16	0.09	26	0.04	5	-0.27 ± 0.03

Table 3—Continued

Star	T_{eff} (K)	$\log g$	ξ (km s $^{-1}$)	A(Fe)	σ (Fe I)	N (Fe I)	σ (Fe I)	N (Fe II)	[Fe/H]
HD122742	5550 ± 30	4.48 ± 0.07	0.96 ± 0.04	7.47	0.06	25	0.07	10	0.04 ± 0.02
HD122862	5984 ± 20	4.16 ± 0.08	1.51 ± 0.04	7.29	0.04	21	0.05	11	-0.14 ± 0.02
HD124584	6009 ± 26	4.28 ± 0.11	1.43 ± 0.02	7.37	0.04	23	0.06	12	-0.06 ± 0.02
HD125072	5117 ± 81	4.44 ± 0.23	1.13 ± 0.08	7.65	0.11	22	0.11	6	0.22 ± 0.05
HD126053	5671 ± 21	4.32 ± 0.11	1.21 ± 0.02	7.05	0.04	22	0.06	11	-0.38 ± 0.01
HD125881	5953 ± 25	4.28 ± 0.06	1.28 ± 0.04	7.44	0.05	23	0.05	12	0.01 ± 0.02
HD128674	5548 ± 20	4.43 ± 0.09	1.02 ± 0.04	7.05	0.06	25	0.05	12	-0.38 ± 0.02
HD130948	6075 ± 22	4.59 ± 0.07	1.57 ± 0.06	7.43	0.07	24	0.05	10	0.00 ± 0.02
HD131511	5311 ± 50	4.36 ± 0.17	1.08 ± 0.04	7.51	0.08	24	0.06	8	0.08 ± 0.04
HD131977	4799 ± 72	4.60 ± 0.16	0.77 ± 0.08	7.46	0.10	21	0.01	2	0.03 ± 0.03
HD131923	5691 ± 45	4.28 ± 0.13	1.10 ± 0.04	7.56	0.08	27	0.05	10	0.13 ± 0.04
HD134060	5904 ± 38	4.25 ± 0.13	1.19 ± 0.04	7.53	0.06	25	0.06	12	0.10 ± 0.03
HD134606	5677 ± 65	4.31 ± 0.23	1.15 ± 0.04	7.76	0.08	27	0.05	10	0.33 ± 0.05
HD136352	5551 ± 33	4.15 ± 0.09	0.88 ± 0.04	7.05	0.08	27	0.04	12	-0.38 ± 0.03
HD141004	5777 ± 36	3.99 ± 0.06	1.24 ± 0.04	7.35	0.08	27	0.05	12	-0.08 ± 0.04
HD140901	5637 ± 45	4.45 ± 0.13	1.10 ± 0.04	7.55	0.07	25	0.06	11	0.12 ± 0.03
HD143114	5804 ± 32	4.41 ± 0.12	1.16 ± 0.06	7.04	0.07	25	0.05	12	-0.39 ± 0.02
HD144009	5577 ± 53	4.27 ± 0.16	1.02 ± 0.04	7.49	0.07	23	0.04	11	0.06 ± 0.03
HD144628	5061 ± 35	4.37 ± 0.18	0.92 ± 0.02	7.00	0.07	26	0.05	7	-0.43 ± 0.01
HD145825	5758 ± 47	4.33 ± 0.11	1.08 ± 0.04	7.46	0.07	25	0.04	12	0.03 ± 0.03
HD146481	5690 ± 33	4.24 ± 0.13	1.28 ± 0.04	7.01	0.08	25	0.06	12	-0.42 ± 0.03
HD149661	5280 ± 47	4.35 ± 0.15	1.13 ± 0.04	7.44	0.07	26	0.06	10	0.01 ± 0.03
HD150248	5687 ± 33	4.30 ± 0.13	1.12 ± 0.04	7.32	0.06	26	0.04	12	-0.11 ± 0.02
HD153075	5708 ± 25	4.38 ± 0.15	0.80 ± 0.02	6.88	0.07	16	0.03	12	-0.55 ± 0.03
HD155974	6276 ± 21	4.07 ± 0.07	1.88 ± 0.06	7.20	0.05	21	0.06	11	-0.23 ± 0.02
HD156274	5242 ± 30	4.40 ± 0.14	0.85 ± 0.04	7.06	0.06	25	0.05	9	-0.37 ± 0.02
HD155918	5698 ± 33	4.52 ± 0.12	0.70 ± 0.02	6.82	0.09	19	0.05	11	-0.61 ± 0.04
HD158783	5789 ± 42	4.13 ± 0.10	1.07 ± 0.06	7.56	0.10	26	0.04	12	0.13 ± 0.04
HD161612	5617 ± 55	4.30 ± 0.23	1.12 ± 0.04	7.58	0.07	26	0.06	11	0.15 ± 0.04
HD162255	5823 ± 25	4.14 ± 0.09	1.18 ± 0.04	7.55	0.05	24	0.04	12	0.12 ± 0.02
HD163272	6009 ± 46	4.19 ± 0.11	1.19 ± 0.02	7.71	0.07	25	0.05	12	0.28 ± 0.03

Table 3—Continued

Star	T_{eff} (K)	$\log g$	ξ (km s $^{-1}$)	A(Fe)	σ (Fe I)	N (Fe I)	σ (Fe I)	N (Fe II)	[Fe/H]
HD166553	5920 ± 35	4.03 ± 0.06	1.38 ± 0.04	7.41	0.07	25	0.05	12	-0.02 ± 0.02
HD168871	5934 ± 25	4.20 ± 0.08	1.51 ± 0.04	7.26	0.06	25	0.05	12	-0.17 ± 0.01
HD175345	6199 ± 29	4.44 ± 0.11	1.61 ± 0.06	7.36	0.07	26	0.05	11	-0.07 ± 0.02
HD177565	5671 ± 44	4.43 ± 0.13	1.02 ± 0.04	7.56	0.06	24	0.04	11	0.13 ± 0.02
HD179140	5845 ± 33	3.96 ± 0.09	1.26 ± 0.04	7.51	0.07	25	0.04	12	0.08 ± 0.02
HD181428	5977 ± 35	4.02 ± 0.10	1.47 ± 0.06	7.36	0.08	24	0.05	12	-0.07 ± 0.03
HD183877	5649 ± 38	4.46 ± 0.14	0.81 ± 0.06	7.30	0.08	27	0.06	11	-0.13 ± 0.03
HD184985	6309 ± 25	4.03 ± 0.08	1.70 ± 0.06	7.44	0.07	26	0.05	12	0.01 ± 0.02
HD187691	6225 ± 40	4.39 ± 0.13	1.58 ± 0.04	7.59	0.07	25	0.06	12	0.16 ± 0.03
HD190406	5926 ± 41	4.33 ± 0.13	1.10 ± 0.06	7.49	0.10	27	0.03	12	0.06 ± 0.04
HD189567	5656 ± 35	4.20 ± 0.09	1.02 ± 0.04	7.17	0.06	25	0.04	12	-0.26 ± 0.02
HD190248	5691 ± 21	4.26 ± 0.08	1.18 ± 0.04	7.82	0.06	22	0.05	10	0.39 ± 0.02
HD191408	5075 ± 43	4.48 ± 0.17	1.14 ± 0.08	6.87	0.07	18	0.11	3	-0.56 ± 0.04
HD192310	5134 ± 50	4.38 ± 0.18	0.80 ± 0.04	7.50	0.08	27	0.06	6	0.07 ± 0.04
HD193193	5876 ± 25	4.12 ± 0.07	1.21 ± 0.04	7.32	0.07	23	0.04	12	-0.11 ± 0.02
HD192865	6241 ± 46	4.23 ± 0.13	1.71 ± 0.04	7.53	0.07	24	0.05	11	0.10 ± 0.03
HD193307	6018 ± 22	4.18 ± 0.07	1.95 ± 0.08	7.09	0.07	25	0.06	11	-0.34 ± 0.02
HD194640	5581 ± 33	4.42 ± 0.10	0.89 ± 0.04	7.45	0.07	26	0.07	11	0.02 ± 0.02
HD196390	5858 ± 38	4.33 ± 0.15	1.16 ± 0.02	7.48	0.06	26	0.04	12	0.05 ± 0.03
HD196800	5911 ± 35	4.14 ± 0.07	1.12 ± 0.04	7.60	0.07	24	0.04	12	0.17 ± 0.02
HD196068	5947 ± 30	4.03 ± 0.09	1.25 ± 0.04	7.64	0.07	25	0.05	12	0.21 ± 0.02
HD199288	5724 ± 35	4.55 ± 0.09	0.60 ± 0.02	6.83	0.10	18	0.04	11	-0.60 ± 0.04
HD199190	5826 ± 35	4.01 ± 0.09	1.19 ± 0.04	7.55	0.07	25	0.04	12	0.12 ± 0.03
HD199509	5772 ± 31	4.52 ± 0.09	1.27 ± 0.02	7.10	0.05	24	0.05	11	-0.33 ± 0.02
HD204385	6056 ± 45	4.42 ± 0.14	1.49 ± 0.04	7.47	0.07	25	0.05	12	0.04 ± 0.03
HD205390	5099 ± 38	4.41 ± 0.16	1.13 ± 0.04	7.22	0.08	26	0.06	7	-0.21 ± 0.03
HD206395	6305 ± 41	4.38 ± 0.13	1.82 ± 0.06	7.66	0.08	25	0.08	12	0.23 ± 0.04
HD207129	5965 ± 36	4.52 ± 0.07	1.17 ± 0.02	7.47	0.06	24	0.04	12	0.04 ± 0.03
HD207700	5740 ± 38	4.43 ± 0.14	1.15 ± 0.04	7.53	0.08	27	0.06	11	0.10 ± 0.03
HD208998	5862 ± 36	4.24 ± 0.12	1.42 ± 0.06	7.02	0.07	25	0.06	12	-0.41 ± 0.02
HD209653	5980 ± 29	4.17 ± 0.08	1.57 ± 0.04	7.27	0.05	25	0.06	12	-0.16 ± 0.02

Table 3—Continued

Star	T_{eff} (K)	$\log g$	ξ (km s $^{-1}$)	A(Fe)	σ (Fe I)	N (Fe I)	σ (Fe I)	N (Fe II)	[Fe/H]
HD212291	5597 ± 31	4.40 ± 0.13	1.10 ± 0.04	7.24	0.05	25	0.05	12	-0.19 ± 0.03
HD212168	5912 ± 31	4.28 ± 0.08	1.22 ± 0.04	7.45	0.08	27	0.05	12	0.02 ± 0.03
HD212708	5700 ± 60	4.22 ± 0.20	1.11 ± 0.04	7.74	0.05	24	0.05	10	0.31 ± 0.03
HD214759	5493 ± 61	4.40 ± 0.18	0.97 ± 0.02	7.69	0.07	25	0.05	10	0.26 ± 0.05
HD214953	6101 ± 38	4.33 ± 0.14	1.55 ± 0.06	7.45	0.06	23	0.05	11	0.02 ± 0.02
HD215648	6178 ± 26	3.97 ± 0.07	1.68 ± 0.08	7.16	0.06	19	0.05	11	-0.27 ± 0.03
HD217958	5864 ± 44	4.14 ± 0.12	1.16 ± 0.04	7.74	0.07	23	0.06	12	0.31 ± 0.04
HD218261	6237 ± 40	4.46 ± 0.10	1.37 ± 0.04	7.57	0.06	23	0.06	12	0.14 ± 0.03
HD220507	5700 ± 31	4.24 ± 0.10	1.14 ± 0.04	7.46	0.07	27	0.06	12	0.03 ± 0.02
HD222237	4790 ± 50	4.31 ± 0.26	0.95 ± 0.06	6.99	0.08	23	0.10	4	-0.44 ± 0.03
HD222335	5313 ± 33	4.55 ± 0.10	0.79 ± 0.04	7.32	0.07	26	0.05	9	-0.11 ± 0.02
HD222368	6200 ± 25	4.13 ± 0.08	2.17 ± 0.06	7.23	0.08	23	0.05	10	-0.20 ± 0.03
HD222480	5863 ± 35	4.17 ± 0.12	1.26 ± 0.02	7.65	0.07	27	0.05	12	0.22 ± 0.03
HD223171	5835 ± 35	4.11 ± 0.08	1.29 ± 0.04	7.53	0.06	25	0.05	12	0.10 ± 0.02

Table 4. Evolutionary Parameters (Paper I).

Star	π (mas)	σ_π (mas)	A_V	BC_V	$\log(L/L_\odot)$	$\sigma_{\log(L/L_\odot)}$	R (R_\odot)	σ_R (R_\odot)	M_{spec} (M_\odot)	$\sigma_{M_{spec}}$ (M_\odot)	M_{track} (M_\odot)	$\sigma_{M_{track}}$ (M_\odot)	$\log g$ (Hipp)	$\sigma_{\log g}$ (Hipp)	Age (Gyr)	ΔAge (Gyr)
HD142	38.89	0.37	0.05	0.017	0.462	0.061	1.41	0.11	1.59	0.77	1.25	0.10	4.24	0.08	2.5	2.0-3.5
HD1237	57.15	0.31	0.04	-0.075	-0.196	0.060	0.86	0.07	1.02	0.49	1.00	0.10	4.57	0.08	<1.0	0.0-3.0
HD2039	9.75	0.95	0.11	-0.004	0.376	0.104	1.46	0.18	1.55	0.81	1.25	0.10	4.21	0.11	3.5	3.0-4.5
HD2638	20.03	1.49	0.10	-0.159	-0.368	0.089	0.80	0.09	0.55	0.28	0.90	0.10	4.59	0.11	<1.0	0.0-4.0
HD3651	90.42	0.32	0.02	-0.153	-0.287	0.060	0.87	0.07	0.57	0.28	0.90	0.10	4.51	0.08	5.0	0.0-12.0
HD4113	22.70	0.84	0.08	-0.057	0.099	0.068	1.17	0.10	0.83	0.41	1.05	0.10	4.32	0.09	6.5	5.0-10.0
HD4208	30.89	0.75	0.09	-0.078	-0.116	0.064	0.92	0.07	0.75	0.37	0.85	0.10	4.44	0.09	10.0	6.0-14.0
HD4308	45.34	0.32	0.04	-0.060	0.015	0.060	1.02	0.08	1.25	0.61	0.90	0.10	4.38	0.08	10.0	7.0-14.0
HD4203	12.95	1.03	0.04	-0.047	0.238	0.092	1.38	0.15	0.89	0.45	1.15	0.10	4.22	0.10	5.5	4.5-8.0
HD6434	24.17	0.61	0.06	-0.078	0.109	0.064	1.15	0.09	1.58	0.77	0.80	0.10	4.22	0.09	>13.0	...
HD10647	57.36	0.25	0.03	-0.005	0.197	0.060	1.10	0.08	1.22	0.59	1.10	0.10	4.39	0.08	2.0	0.0-4.0
HD11506	19.34	0.58	0.10	0.013	0.366	0.065	1.38	0.11	1.15	0.56	1.25	0.10	4.26	0.08	3.0	2.0-3.5
HD12661	28.61	0.61	0.00	-0.024	0.033	0.063	1.04	0.08	0.96	0.47	1.10	0.10	4.45	0.08	<1.0	0.0-3.0
HD13445	92.74	0.32	0.02	-0.182	-0.394	0.060	0.79	0.06	0.66	0.32	0.70	0.10	4.49	0.09	>13.0	8.0-14.0
HD16141	25.67	0.66	0.04	-0.042	0.390	0.064	1.59	0.13	1.03	0.50	1.10	0.10	4.08	0.08	7.5	6.5-8.5
HD16417	38.79	0.40	0.08	-0.032	0.463	0.061	1.70	0.13	1.18	0.57	1.15	0.10	4.04	0.08	6.0	5.0-7.0
HD17051	58.25	0.22	0.05	0.017	0.231	0.060	1.12	0.09	1.61	0.78	1.25	0.10	4.44	0.07	<1.0	0.0-1.0
HIP14810	18.71	1.26	0.01	-0.075	-0.010	0.084	1.07	0.11	0.65	0.33	1.00	0.10	4.38	0.10	6.0	3.5-9.5
HD19994	44.29	0.28	0.03	0.003	0.598	0.060	1.80	0.14	1.38	0.67	1.35	0.10	4.06	0.07	3.5	3.0-4.0
HD20782	28.15	0.62	0.08	-0.051	0.1117	0.063	1.16	0.09	0.83	0.41	0.95	0.10	4.29	0.08	10.0	7.0-12.0
HD22049	310.94	0.16	0.00	-0.212	-0.481	0.060	0.74	0.06	0.39	0.19	0.75	0.10	4.58	0.09	9.0	0.0-14.0
HD23079	29.51	0.34	0.09	-0.021	0.164	0.061	1.11	0.09	1.49	0.73	1.05	0.10	4.37	0.08	4.0	2.0-6.0
HD27894	22.79	0.85	0.07	-0.326	-0.393	0.069	0.91	0.08	0.31	0.16	0.75	0.10	4.40	0.10	>13.0	...

Table 4—Continued

Star	π (mas)	σ_π (mas)	A_V	BC_V	$\log(L/L_\odot)$	$\sigma_{\log(L/L_\odot)}$	R (R $_\odot$)	σ_R (R $_\odot$)	M_{spec} (M $_\odot$)	$\sigma_{M_{spec}}$ (M $_\odot$)	M_{track} (M $_\odot$)	$\sigma_{M_{track}}$ (M $_\odot$)	$\log g$	$\sigma_{\log g}$	Age (Gyr)	ΔAge (Gyr)
HD28185	23.62	0.87	0.12	-0.042	0.106	0.068	1.16	0.10	1.09	0.54	1.10	0.10	4.35	0.08	5.0	3.5-6.5
HD30177	18.93	0.63	0.09	-0.059	0.049	0.067	1.13	0.10	0.65	0.32	1.10	0.10	4.38	0.08	5.5	3.0-7.0
HD37124	29.70	0.70	0.06	-0.107	-0.043	0.064	1.05	0.09	1.01	0.49	0.75	0.10	4.27	0.09	>13.0	...
HD39091	54.60	0.21	0.03	-0.005	0.188	0.060	1.14	0.09	1.23	0.60	1.15	0.10	4.39	0.08	2.0	0.0-4.0
HD37605	22.74	1.11	0.03	-0.108	-0.218	0.074	0.89	0.08	0.49	0.24	1.00	0.10	4.54	0.09	<1.0	0.0-5.0
HD40307	76.95	0.37	0.03	-0.264	-0.615	0.060	0.67	0.05	0.26	0.13	0.70	0.10	4.63	0.09	9.0	0.0-14.0
HD41004A	24.53	0.84	0.04	-0.137	-0.261	0.067	0.88	0.08	0.65	0.32	0.95	0.10	4.53	0.09	4.0	0.0-10.0
ABPic	21.71	0.69	0.08	-0.124	-0.336	0.067	0.78	0.07	0.61	0.30	0.90	0.10	4.61	0.09	<1.0	0.0-4.0
HD45652	29.11	0.93	0.04	-0.135	-0.190	0.066	0.95	0.08	0.44	0.22	0.95	0.10	4.46	0.09	ζ_0	2.0-12.0
HD46375	28.72	0.89	0.04	-0.128	-0.105	0.066	1.04	0.09	0.92	0.45	0.95	0.10	4.38	0.09	10.5	7.0-14.0
HD47186	25.26	0.65	0.02	-0.057	0.082	0.064	1.15	0.09	0.78	0.38	1.00	0.10	4.32	0.08	6.5	5.0-10.0
HD50499	21.68	0.49	0.03	-0.005	0.366	0.063	1.45	0.12	0.85	0.42	1.25	0.10	4.22	0.08	3.5	3.0-4.5
HD50554	33.43	0.59	0.03	-0.019	0.143	0.062	1.10	0.09	0.86	0.42	1.05	0.10	4.38	0.08	4.5	2.0-6.5
HD52265	34.53	0.40	0.02	0.000	0.324	0.061	1.33	0.10	0.83	0.40	1.20	0.10	4.27	0.08	3.5	3.0-4.5
HD63454	28.95	0.81	0.05	-0.288	-0.628	0.065	0.67	0.06	0.21	0.10	0.80	0.10	4.69	0.09	<1.0	0.0-7.0
HD65216	28.11	0.59	0.07	-0.074	-0.120	0.063	0.92	0.07	0.82	0.40	0.90	0.10	4.47	0.09	7.5	3.0-12.0
HD66428	18.21	1.07	0.10	-0.060	0.151	0.088	1.26	0.14	0.66	0.34	1.05	0.10	4.26	0.10	9.0	5.5-11.0
HD69830	80.04	0.35	0.01	-0.108	-0.231	0.060	0.87	0.07	0.72	0.35	0.90	0.10	4.52	0.08	4.0	0.0-10.0
HD70642	35.63	0.44	0.02	-0.044	-0.038	0.061	0.98	0.08	0.92	0.45	1.10	0.10	4.50	0.08	1.0	0.0-4.0
HD70573	21.88	0.55	0.09	-0.032	-0.203	0.072	0.76	0.07	0.78	0.39	1.00	0.10	4.68	0.09	<1.0	...
HD72659	20.07	0.75	0.10	-0.034	0.373	0.079	1.50	0.15	0.83	0.42	1.05	0.10	4.11	0.09	8.0	6.5-8.5
HD73256	26.48	0.64	0.05	-0.089	-0.114	0.064	0.97	0.08	0.77	0.38	1.00	0.10	4.46	0.08	5.5	1.0-10.0
HD74156	15.52	0.54	0.12	-0.003	0.531	0.082	1.67	0.17	1.93	0.97	1.20	0.10	4.07	0.09	4.5	3.5-5.5

Table 4—Continued

Star	π (mas)	σ_π (mas)	A_V	BC_V	$\log(L/L_\odot)$	$\sigma_{\log(L/L_\odot)}$	R (R $_\odot$)	σ_R (R $_\odot$)	M_{spec} (M $_\odot$)	$\sigma_{M_{spec}}$ (M $_\odot$)	M_{track} (M $_\odot$)	$\sigma_{M_{track}}$ (M $_\odot$)	$\log g$ (Hipp)	$\sigma_{\log g}$ (Hipp)	Age (Gyr)	ΔAge (Gyr)
HD75289	34.31	0.32	0.02	-0.002	0.306	0.061	1.33	0.10	0.74	0.36	1.20	0.10	4.27	0.08	3.5	3.0-4.5
HD76700	16.59	0.56	0.08	-0.039	0.252	0.067	1.38	0.12	0.95	0.47	1.20	0.10	4.24	0.08	5.0	4.0-7.0
HD81040	30.20	1.03	0.00	-0.077	-0.109	0.067	0.93	0.08	0.43	0.21	0.90	0.10	4.46	0.09	8.5	4.0-14.0
HD82943	36.40	0.47	0.04	0.005	0.184	0.061	1.14	0.09	1.11	0.54	1.20	0.10	4.40	0.08	1.0	0.0-3.0
HD83443	24.29	0.73	0.04	-0.074	-0.109	0.066	0.96	0.08	0.75	0.37	1.05	0.10	4.49	0.08	2.0	0.0-6.0
HD86081	10.49	0.99	0.03	-0.020	0.394	0.102	1.53	0.19	0.72	0.38	1.20	0.10	4.15	0.11	6.0	4.5-7.0
HD89307	30.90	0.68	0.01	-0.035	0.138	0.063	1.12	0.09	0.87	0.42	1.00	0.10	4.34	0.08	7.0	5.0-9.0
HD92788	28.20	0.73	0.01	-0.028	0.099	0.064	1.12	0.09	0.91	0.45	1.10	0.10	4.38	0.08	4.0	1.5-5.5
HD93083	35.90	0.89	0.04	-0.224	-0.417	0.064	0.81	0.07	0.45	0.22	0.90	0.10	4.58	0.09	5.0	0.0-14.0
BD-10-3166	12.50	1.56	0.10	-0.113	-0.233	0.124	0.88	0.13	0.77	0.42	1.00	0.10	4.55	0.14	<1.0	0.0-4.0
HD99109	20.03	1.38	0.02	-0.133	-0.274	0.086	0.86	0.09	0.45	0.23	1.00	0.10	4.57	0.10	<1.0	0.0-5.0
HD100777	20.16	0.95	0.02	-0.074	-0.031	0.073	1.05	0.10	0.74	0.37	1.00	0.10	4.40	0.09	5.5	2.0-9.0
HD101930	34.24	0.81	0.03	-0.175	-0.363	0.064	0.82	0.07	0.49	0.24	0.90	0.10	4.57	0.09	<1.0	0.0-6.0
HD102117	25.19	0.61	0.04	-0.055	0.156	0.064	1.26	0.10	0.69	0.34	1.10	0.10	4.28	0.08	6.0	5.0-9.5
HD102195	33.74	0.83	0.02	-0.132	-0.315	0.064	0.81	0.07	0.56	0.28	0.90	0.10	4.57	0.09	<1.0	0.0-6.0
HD106252	26.52	0.57	0.00	-0.027	0.108	0.063	1.08	0.09	1.16	0.57	1.10	0.10	4.42	0.08	3.5	1.0-6.0
HD107148	19.53	0.75	0.02	-0.034	0.144	0.069	1.20	0.10	0.82	0.41	1.10	0.10	4.33	0.09	5.0	3.0-6.0
HD108147	26.26	0.46	0.06	0.010	0.293	0.062	1.23	0.10	0.99	0.48	1.20	0.10	4.34	0.08	2.0	0.0-3.0
HD108874	15.97	1.07	0.03	-0.070	0.037	0.084	1.12	0.12	0.81	0.41	1.00	0.10	4.34	0.10	8.0	5.0-11.0
HD109749	17.77	1.26	0.10	-0.019	0.224	0.086	1.26	0.13	0.85	0.43	1.15	0.10	4.30	0.10	4.5	3.5-5.5
HD111232	34.08	0.66	0.04	-0.128	-0.126	0.062	0.99	0.08	0.72	0.35	0.70	0.10	4.30	0.09	>13.0	...
HD114386	34.61	1.17	0.05	-0.230	-0.550	0.067	0.70	0.06	0.27	0.13	0.75	0.10	4.63	0.10	5.0	0.0-14.0
HD114762	25.87	0.76	0.02	-0.078	0.202	0.065	1.24	0.10	1.46	0.71	0.80	0.10	4.16	0.09	>13.0	...

Table 4—Continued

Star	π (mas)	σ_π (mas)	A_V	BC_V	$\log(L/L_\odot)$	$\sigma_{\log(L/L_\odot)}$	R (R $_\odot$)	σ_R (R $_\odot$)	M_{spec} (M $_\odot$)	$\sigma_{M_{spec}}$ (M $_\odot$)	M_{track} (M $_\odot$)	$\sigma_{M_{track}}$ (M $_\odot$)	$\log g$ (Hipp)	$\sigma_{\log g}$ (Hipp)	Age (Gyr)	ΔAge (Gyr)
HD114783	48.78	0.59	0.01	-0.213	-0.403	0.061	0.81	0.07	0.44	0.22	0.85	0.10	4.55	0.09	7.0	0.0-14.0
HD114729	27.69	0.54	0.09	-0.058	0.411	0.062	1.60	0.13	0.95	0.47	1.00	0.10	4.03	0.08	9.5	8.0-10.5
HD117207	30.26	0.70	0.06	-0.062	0.091	0.063	1.18	0.10	0.73	0.35	1.00	0.10	4.30	0.08	8.0	5.0-11.0
HD117618	26.34	0.60	0.07	-0.024	0.236	0.063	1.26	0.10	0.89	0.43	1.10	0.10	4.28	0.08	6.0	4.0-8.0
HD120136	64.03	0.19	0.01	0.037	0.484	0.060	1.40	0.11	1.66	0.81	1.40	0.10	4.30	0.07	1.0	0.0-2.0
HD121504	22.17	0.73	0.08	-0.014	0.238	0.067	1.24	0.10	1.17	0.57	1.10	0.10	4.30	0.08	4.0	3.0-6.0
HD125612	18.45	1.09	0.14	-0.013	0.113	0.079	1.09	0.11	0.87	0.43	1.15	0.10	4.42	0.09	1.5	0.0-3.5
HD128311	60.60	0.83	0.02	-0.205	-0.559	0.061	0.67	0.05	0.50	0.25	0.80	0.10	4.69	0.09	<1.0	...
HD130322	31.54	1.18	0.04	-0.123	-0.241	0.069	0.88	0.08	0.60	0.29	0.90	0.10	4.51	0.09	4.0	0.0-10.0
HD134987	38.16	0.60	0.06	-0.028	0.192	0.062	1.25	0.10	0.88	0.43	1.15	0.10	4.31	0.08	4.5	3.0-6.0
HD330075	20.16	1.38	0.06	-0.195	-0.343	0.085	0.85	0.09	0.63	0.32	0.90	0.10	4.53	0.10	7.0	0.0-14.0
HD141937	30.96	0.64	0.16	-0.028	0.102	0.067	1.10	0.09	0.78	0.38	1.10	0.10	4.40	0.08	4.0	2.0-6.0
HD142415	29.21	0.72	0.04	-0.013	0.066	0.064	1.02	0.08	0.91	0.44	1.15	0.10	4.48	0.08	<1.0	0.0-2.0
HD142022A	29.13	0.57	0.07	-0.094	-0.035	0.062	1.07	0.09	0.66	0.32	1.00	0.10	4.38	0.08	9.5	6.0-13.0
HD147513	78.26	0.37	0.04	-0.024	-0.001	0.060	0.96	0.07	1.16	0.56	1.10	0.10	4.52	0.08	<1.0	0.0-2.0
HD149143	16.12	0.83	0.16	-0.007	0.404	0.088	1.53	0.16	0.93	0.47	1.30	0.10	4.18	0.10	4.0	3.0-6.0
HD160691	64.47	0.31	0.02	-0.044	0.267	0.060	1.40	0.11	0.74	0.36	1.10	0.10	4.19	0.08	8.0	5.0-9.0
HD162020	33.98	1.31	0.03	-0.295	-0.664	0.071	0.65	0.06	0.19	0.09	0.75	0.10	4.69	0.10	<1.0	0.0-9.0
HD164922	45.21	0.54	0.03	-0.118	-0.147	0.061	0.97	0.08	0.69	0.33	0.95	0.10	4.44	0.08	8.0	4.0-13.0
HD168443	26.72	0.69	0.16	-0.059	0.374	0.068	1.61	0.14	1.36	0.67	1.10	0.10	4.07	0.08	8.0	7.0-9.0
HD168746	23.40	0.76	0.13	-0.070	0.070	0.070	1.14	0.10	1.09	0.54	0.95	0.10	4.30	0.09	10.0	8.0-13.0
HD169830	27.32	0.41	0.09	0.024	0.701	0.061	1.88	0.15	1.58	0.77	1.40	0.10	4.04	0.07	2.5	2.0-3.0
HD170469	15.94	1.03	0.13	-0.035	0.285	0.082	1.41	0.14	0.87	0.44	1.20	0.10	4.22	0.10	5.0	4.0-8.0

Table 4—Continued

Star	π	σ_π	A_V	BC_V	$\log(L/L_\odot)$	$\sigma_{\log(L/L_\odot)}$	R	σ_R	M_{spec}	$\sigma_{M_{spec}}$	M_{track}	$\sigma_{M_{track}}$	$\log g$	$\sigma_{\log g}$	Age	ΔAge
	(mas)	(mas)					(R $_\odot$)	(R $_\odot$)	(M $_\odot$)	(M $_\odot$)	(M $_\odot$)	(M $_\odot$)	(Hipp)	(Hipp)	(Gyr)	(Gyr)
HD179949	36.30	0.70	0.09	0.018	0.317	0.062	1.24	0.10	1.34	0.65	1.25	0.10	4.35	0.08	1.0	0.0-2.5
HD181433	37.37	1.13	0.04	-0.292	-0.464	0.066	0.81	0.07	0.45	0.22	0.90	0.10	4.58	0.09	7.0	0.0-14.0
HD183263	18.15	0.93	0.12	-0.004	0.296	0.078	1.33	0.13	1.10	0.55	1.20	0.10	4.27	0.09	3.5	2.5-4.5
HD231701	8.44	1.05	0.16	-0.005	0.533	0.126	1.63	0.24	1.76	0.96	1.20	0.10	4.10	0.13	4.5	3.5-5.5
HD187085	22.71	0.79	0.12	0.011	0.351	0.067	1.30	0.11	1.66	0.82	1.20	0.10	4.29	0.08	2.5	1.5-3.5
HD189733	51.41	0.69	0.03	-0.177	-0.499	0.061	0.69	0.06	0.76	0.37	0.85	0.10	4.69	0.09	<1.0	...
HD192263	51.77	0.78	0.01	-0.235	-0.538	0.062	0.71	0.06	0.36	0.17	0.80	0.10	4.64	0.09	<1.0	0.0-9.0
HD195019	25.96	0.99	0.05	-0.044	0.369	0.069	1.55	0.13	1.00	0.49	1.05	0.10	4.08	0.09	8.0	7.0-9.0
WASP2	7.14	0.18	0.09	-0.164	-0.490	0.064	0.70	0.06	0.46	0.23	0.90	0.10	4.71	0.09	<1.0	...
HD196050	20.01	0.66	0.10	-0.007	0.348	0.067	1.43	0.12	1.14	0.56	1.25	0.10	4.23	0.08	4.0	3.0-4.5
HD196885	29.83	0.48	0.02	0.023	0.401	0.062	1.37	0.11	1.03	0.50	1.30	0.10	4.28	0.08	2.0	1.0-3.0
HD202206	22.06	0.82	0.08	-0.037	0.036	0.068	1.06	0.09	0.76	0.37	1.10	0.10	4.43	0.08	3.0	0.0-5.0
HD208487	21.81	0.65	0.11	-0.003	0.288	0.065	1.25	0.10	1.49	0.73	1.15	0.10	4.31	0.08	3.5	2.0-4.5
HD209458	20.15	0.80	0.03	-0.007	0.254	0.069	1.21	0.10	1.14	0.56	1.10	0.10	4.32	0.08	3.5	2.0-5.0
HD210277	46.38	0.48	0.04	-0.074	0.005	0.061	1.09	0.09	0.88	0.43	1.00	0.10	4.37	0.08	7.5	4.5-11.0
HD212301	18.20	0.53	0.11	0.023	0.319	0.065	1.21	0.10	1.98	0.97	1.30	0.10	4.39	0.08	<1.0	0.0-1.5
HD213240	24.61	0.59	0.07	-0.010	0.434	0.064	1.57	0.13	1.18	0.57	1.25	0.10	4.15	0.08	4.0	3.5-6.0
HD216435	30.66	0.39	0.06	0.002	0.546	0.061	1.74	0.14	1.52	0.74	1.35	0.10	4.09	0.07	3.5	3.0-5.0
HD216437	37.39	0.36	0.06	-0.025	0.380	0.061	1.53	0.12	0.98	0.48	1.20	0.10	4.15	0.08	6.0	4.0-7.0
HD216770	28.11	0.79	0.07	-0.092	-0.169	0.065	0.92	0.08	0.74	0.36	1.00	0.10	4.51	0.08	1.0	0.0-5.0
HD217014	64.07	0.38	0.03	-0.038	0.142	0.060	1.19	0.09	0.76	0.37	1.10	0.10	4.33	0.08	5.0	4.0-8.0
HD217107	50.36	0.38	0.03	-0.045	0.066	0.060	1.12	0.09	0.81	0.40	1.10	0.10	4.38	0.08	4.5	2.0-6.0
HD219828	13.83	0.74	0.11	-0.026	0.465	0.076	1.68	0.16	1.17	0.58	1.20	0.10	4.07	0.09	6.0	5.0-7.0

Table 4—Continued

Star	π (mas)	σ_π (mas)	A_V	BC_V	$\log(L/L_\odot)$	$\sigma_{\log(L/L_\odot)}$	R (R $_\odot$)	σ_R (R $_\odot$)	M_{spec} (M $_\odot$)	$\sigma_{M_{spec}}$ (M $_\odot$)	M_{track} (M $_\odot$)	$\sigma_{M_{track}}$ (M $_\odot$)	$\log g$ (Hipp)	$\sigma_{\log g}$ (Hipp)	Age (Gyr)	ΔAge (Gyr)
HD221287	18.09	0.64	0.08	0.006	0.295	0.067	1.20	0.10	1.23	0.60	1.20	0.10	4.36	0.08	2.0	0.0-3.0
HD222582	23.94	0.74	0.10	-0.042	0.135	0.066	1.17	0.10	1.06	0.52	1.00	0.10	4.31	0.09	7.5	5.0-10.0
HD1581	116.46	0.16	0.01	-0.037	0.102	0.060	1.08	0.08	0.76	0.37	1.00	0.10	4.38	0.08	6.5	4.0-9.0
HD1835	47.93	0.53	0.08	-0.025	0.033	0.061	1.02	0.08	0.93	0.45	1.10	0.10	4.47	0.08	1.0	0.0-3.5
HD3823	40.07	0.34	0.04	-0.035	0.376	0.061	1.42	0.11	1.11	0.54	1.00	0.10	4.13	0.08	7.5	6.5-9.0
HD4628	134.14	0.51	0.01	-0.226	-0.549	0.060	0.69	0.06	0.37	0.18	0.70	0.10	4.60	0.09	9.0	0.0-14.0
HD7199	28.33	0.57	0.10	-0.122	-0.132	0.063	1.00	0.08	0.45	0.22	0.95	0.10	4.41	0.08	9.0	5.0-13.0
HD7693	46.20	0.82	0.06	-0.215	-0.199	0.063	1.02	0.08	1.32	0.64	0.80	0.10	4.32	0.09	>13.0	...
HD7570	66.16	0.24	0.02	0.021	0.278	0.060	1.20	0.09	1.34	0.65	1.25	0.10	4.38	0.07	1.0	0.0-2.0
HD10180	25.63	0.38	0.11	-0.019	0.210	0.061	1.21	0.09	1.11	0.54	1.10	0.10	4.32	0.08	5.5	3.5-7.0
HD10476	132.76	0.50	0.00	-0.160	-0.370	0.060	0.79	0.06	0.69	0.34	0.90	0.10	4.59	0.08	3.0	0.0-11.0
HD10700	273.96	0.17	0.03	-0.150	-0.291	0.060	0.84	0.07	0.74	0.36	0.65	0.10	4.40	0.10	>13.0	...
HD11112	22.07	0.57	0.06	-0.012	0.397	0.064	1.52	0.12	1.13	0.55	1.25	0.10	4.18	0.08	4.0	3.5-6.5
HD12387	28.44	0.62	0.05	-0.062	0.097	0.063	1.14	0.09	1.06	0.52	0.90	0.10	4.28	0.09	11.0	9.0-14.0
HD16160	139.27	0.45	0.01	-0.283	-0.579	0.060	0.71	0.06	0.39	0.19	0.70	0.10	4.59	0.09	>13.0	0.0-14.0
HD17925	96.60	0.40	0.01	-0.178	-0.407	0.060	0.78	0.06	0.49	0.24	0.90	0.10	4.61	0.08	<1.0	0.0-6.0
HD19632	33.72	0.65	0.07	-0.043	-0.019	0.062	0.99	0.08	0.82	0.40	1.05	0.10	4.47	0.08	3.0	0.0-6.0
HD20029	22.79	0.48	0.11	0.009	0.413	0.063	1.40	0.11	1.46	0.71	1.25	0.10	4.24	0.08	3.0	2.5-3.5
HD20201	26.06	0.49	0.10	0.003	0.207	0.062	1.15	0.09	1.49	0.73	1.20	0.10	4.40	0.08	1.5	0.0-3.0
HD20630	109.41	0.27	0.00	-0.046	-0.088	0.060	0.92	0.07	0.71	0.34	1.05	0.10	4.53	0.08	<1.0	0.0-3.0
HD20794	165.47	0.19	0.02	-0.116	-0.179	0.060	0.91	0.07	0.74	0.36	0.75	0.10	4.40	0.09	>13.0	...
HD22104	15.94	0.57	0.10	0.006	0.213	0.068	1.20	0.10	1.24	0.61	1.20	0.10	4.36	0.08	2.0	0.0-3.0
HD22484	71.62	0.54	0.00	-0.004	0.484	0.060	1.57	0.12	0.73	1.51	0.73	0.10	4.13	0.08	4.0	3.5-5.5

Table 4—Continued

Star	π (mas)	σ_π (mas)	A_V	BC_V	$\log(L/L_\odot)$	$\sigma_{\log(L/L_\odot)}$	R (R $_\odot$)	σ_R (R $_\odot$)	M_{spec} (M $_\odot$)	$\sigma_{M_{spec}}$ (M $_\odot$)	M_{track} (M $_\odot$)	$\sigma_{M_{track}}$ (M $_\odot$)	$\log g$ (Hipp)	$\sigma_{\log g}$ (Hipp)	Age (Gyr)	ΔAge (Gyr)
HD25587	17.04	0.64	0.12	-0.004	0.535	0.068	1.64	0.14	1.41	0.69	1.20	0.10	4.09	0.08	4.5	4.0-5.5
HD25680	59.04	0.33	0.02	-0.019	0.021	0.060	0.98	0.08	1.16	0.56	1.10	0.10	4.50	0.08	<1.0	0.0-2.5
HD30876	56.35	0.48	0.03	-0.219	-0.490	0.061	0.74	0.06	0.42	0.21	0.80	0.10	4.61	0.09	5.0	0.0-14.0
HD31527	25.93	0.60	0.11	-0.043	0.146	0.063	1.15	0.09	0.93	0.45	0.95	0.10	4.30	0.08	8.5	6.0-10.5
HD36435	52.08	0.45	0.03	-0.123	-0.260	0.061	0.85	0.07	0.58	0.28	0.90	0.10	4.53	0.08	8.0	1.0-13.0
HD36889	16.96	0.44	0.10	-0.003	0.542	0.064	1.75	0.14	2.02	0.99	1.30	0.10	4.07	0.08	4.0	3.0-5.0
HD38283	26.10	0.31	0.07	-0.046	0.445	0.061	1.62	0.13	0.76	0.37	1.00	0.10	4.02	0.08	8.5	7.5-9.5
HD38382	39.15	0.47	0.03	-0.003	0.200	0.061	1.13	0.09	1.21	0.59	1.10	0.10	4.38	0.08	2.0	0.0-4.0
HD38973	35.49	0.32	0.05	0.000	0.176	0.061	1.11	0.09	1.35	0.66	1.15	0.10	4.41	0.08	1.5	0.0-3.0
HD39213	16.30	0.87	0.06	-0.093	-0.039	0.076	1.07	0.10	0.59	0.29	1.00	0.10	4.38	0.09	7.0	4.0-10.0
HD39587	115.43	0.27	0.02	-0.013	0.041	0.060	0.96	0.07	1.40	0.68	1.10	0.10	4.51	0.08	<1.0	0.0-1.0
HD42024	18.21	0.44	0.06	0.026	0.505	0.064	1.53	0.12	1.51	0.74	1.30	0.10	4.19	0.08	2.5	2.0-3.0
HD43042	48.04	0.34	0.02	0.038	0.458	0.060	1.33	0.10	1.02	0.50	1.30	0.10	4.31	0.07	1.0	0.0-2.0
HD45701	31.49	0.33	0.06	-0.015	0.362	0.061	1.47	0.11	1.03	0.50	1.25	0.10	4.20	0.08	4.0	3.0-6.0
HD51929	26.34	0.36	0.07	-0.084	0.172	0.061	1.24	0.10	1.60	0.78	0.80	0.10	4.16	0.09	>13.0	...
HD52447	12.48	0.52	0.14	0.015	0.414	0.070	1.43	0.12	1.69	0.83	1.30	0.10	4.25	0.08	3.0	2.0-3.5
HD55693	27.43	0.54	0.02	-0.013	0.177	0.062	1.19	0.09	0.81	0.40	1.15	0.10	4.35	0.08	3.0	2.0-4.5
HD64184	30.01	0.51	0.06	-0.058	0.005	0.062	1.02	0.08	1.29	0.63	0.95	0.10	4.40	0.08	7.5	4.0-10.5
HD65907	61.71	0.21	0.01	-0.034	0.109	0.060	1.04	0.08	1.46	0.71	1.00	0.10	4.40	0.08	5.5	3.0-8.0
HD73524	36.49	0.37	0.02	-0.003	0.181	0.061	1.14	0.09	1.03	0.50	1.20	0.10	4.40	0.08	2.0	0.0-3.5
HD76151	57.52	0.39	0.04	-0.038	0.016	0.060	1.02	0.08	0.95	0.46	1.05	0.10	4.44	0.08	3.5	0.0-6.0
HD78429	26.83	0.51	0.02	-0.043	0.152	0.062	1.21	0.10	0.88	0.43	1.05	0.10	4.30	0.08	7.0	4.5-9.5
HD80913	15.54	0.40	0.09	-0.054	0.587	0.064	1.78	0.14	2.20	1.07	1.00	0.10	3.94	0.08	7.0	6.0-8.0

Table 4—Continued

Star	π	σ_π	A_V	BC_V	$\log(L/L_\odot)$	$\sigma_{\log(L/L_\odot)}$	R	σ_R	M_{spec}	$\sigma_{M_{spec}}$	M_{track}	$\sigma_{M_{track}}$	$\log g$	$\sigma_{\log g}$	Age	ΔAge
	(mas)	(mas)					(R $_\odot$)	(R $_\odot$)	(M $_\odot$)	(M $_\odot$)	(M $_\odot$)	(M $_\odot$)	(Hipp)	(Hipp)	(Gyr)	(Gyr)
HD84117	66.61	0.21	0.02	-0.009	0.301	0.060	1.24	0.09	1.04	0.50	1.10	0.10	4.29	0.08	3.5	2.5-4.5
HD86819	21.11	0.54	0.07	-0.014	0.341	0.064	1.38	0.11	1.05	0.51	1.10	0.10	4.20	0.08	5.0	4.0-7.0
HD88742	43.77	0.41	0.04	-0.018	0.097	0.061	1.04	0.08	1.20	0.58	1.10	0.10	4.45	0.08	2.0	0.0-4.0
HD92987	23.03	0.57	0.07	-0.032	0.412	0.064	1.59	0.13	1.00	0.49	1.15	0.10	4.10	0.08	6.5	5.0-7.5
HD93385	23.70	0.69	0.06	-0.037	0.201	0.065	1.24	0.10	0.67	0.33	1.05	0.10	4.27	0.08	7.0	5.5-9.0
HD96423	31.87	0.60	0.03	-0.044	0.039	0.062	1.07	0.08	0.80	0.39	1.00	0.10	4.39	0.08	5.0	3.0-8.0
HD102365	108.45	0.22	0.01	-0.075	-0.084	0.060	0.94	0.07	0.85	0.41	0.85	0.10	4.42	0.09	11.0	7.0-14.0
HD102438	57.23	0.41	0.05	-0.093	-0.142	0.060	0.92	0.07	0.64	0.31	0.80	0.10	4.42	0.09	12.5	7.5-14.0
HD102870	91.50	0.22	0.00	0.022	0.540	0.060	1.61	0.12	1.59	0.77	1.35	0.10	4.16	0.07	2.5	2.0-3.0
HD105328	25.51	0.48	0.10	-0.010	0.451	0.062	1.59	0.13	1.13	0.55	1.30	0.10	4.15	0.08	4.0	3.0-6.0
HD106453	34.11	0.63	0.07	-0.064	-0.092	0.062	0.95	0.08	1.01	0.49	1.00	0.10	4.49	0.08	3.0	0.0-7.0
HD107692	39.23	0.43	0.04	-0.024	0.066	0.061	1.05	0.08	0.99	0.48	1.10	0.10	4.44	0.08	2.0	0.0-4.0
HD108309	37.58	0.44	0.03	-0.045	0.288	0.061	1.42	0.11	0.83	0.40	1.05	0.10	4.15	0.08	8.0	7.0-9.5
HD109200	61.82	0.48	0.02	-0.208	-0.435	0.061	0.77	0.06	0.58	0.29	0.70	0.10	4.51	0.09	>13.0	11.0-14.0
HD110810	48.79	0.88	0.03	-0.234	-0.491	0.062	0.75	0.06	0.35	0.17	0.80	0.10	4.59	0.09	11.0	0.0-14.0
HD114853	40.95	0.56	0.05	-0.072	-0.040	0.061	0.99	0.08	0.70	0.34	0.85	0.10	4.38	0.09	11.5	8.0-14.0
HD115383	56.95	0.26	0.01	0.004	0.323	0.060	1.30	0.10	1.31	0.64	1.20	0.10	4.29	0.08	3.0	2.0-4.0
HD115617	116.89	0.22	0.02	-0.068	-0.088	0.060	0.96	0.07	1.10	0.53	1.00	0.10	4.48	0.08	3.0	0.0-7.0
HD115585	22.50	0.48	0.14	-0.033	0.301	0.067	1.44	0.12	1.09	0.53	1.20	0.10	4.20	0.08	4.5	4.0-7.0
HD117105	27.30	0.58	0.09	-0.046	0.210	0.063	1.22	0.10	1.25	0.61	0.95	0.10	4.24	0.08	10.0	8.0-11.5
HD117939	33.27	0.61	0.06	-0.082	0.005	0.062	1.07	0.09	0.64	0.31	0.80	0.10	4.29	0.09	>13.0	12.0-14.0
HD118972	63.88	0.49	0.03	-0.178	-0.388	0.060	0.79	0.06	0.53	0.26	0.80	0.10	4.54	0.09	9.0	0.0-14.0
HD120237	33.93	0.69	0.05	-0.007	0.246	0.063	1.19	0.09	1.03	0.50	1.10	0.10	4.33	0.08	3.0	2.0-4.5

Table 4—Continued

Star	π	σ_π	A_V	BC_V	$\log(L/L_\odot)$	$\sigma_{\log(L/L_\odot)}$	R	σ_R	M_{spec}	$\sigma_{M_{spec}}$	M_{track}	$\sigma_{M_{track}}$	$\log g$	$\sigma_{\log g}$	Age	ΔAge
	(mas)	(mas)					(R $_\odot$)	(R $_\odot$)	(M $_\odot$)	(M $_\odot$)	(M $_\odot$)	(M $_\odot$)	(Hipp)	(Hipp)	(Gyr)	(Gyr)
HD120690	51.35	0.45	0.05	-0.071	-0.037	0.061	1.02	0.08	0.73	0.36	0.95	0.10	4.40	0.08	8.0	5.0-11.0
HD120780	58.55	0.68	0.03	-0.191	-0.487	0.061	0.72	0.06	0.50	0.24	0.75	0.10	4.61	0.09	7.0	0.0-14.0
HD122742	58.88	0.62	0.01	-0.082	-0.103	0.061	0.96	0.08	1.02	0.49	0.90	0.10	4.43	0.08	7.5	3.0-12.0
HD122862	35.09	0.31	0.09	-0.023	0.455	0.061	1.57	0.12	1.30	0.63	1.10	0.10	4.09	0.08	6.0	5.0-7.0
HD124584	22.49	0.63	0.08	-0.015	0.326	0.065	1.35	0.11	1.25	0.61	1.10	0.10	4.22	0.08	6.0	4.0-7.0
HD125072	84.76	0.69	0.02	-0.205	-0.522	0.060	0.70	0.06	0.49	0.24	0.90	0.10	4.71	0.08	<1.0	...
HD126053	58.17	0.53	0.02	-0.077	-0.083	0.061	0.94	0.07	0.68	0.33	0.80	0.10	4.40	0.09	13.0	9.0-14.0
HD125881	27.76	0.70	0.07	-0.017	0.152	0.064	1.12	0.09	0.87	0.42	1.10	0.10	4.38	0.08	4.0	2.0-6.0
HD128674	37.71	0.72	0.05	-0.097	-0.142	0.062	0.92	0.07	0.83	0.40	0.80	0.10	4.41	0.09	>13.0	11.0-14.0
HD130948	55.03	0.34	0.02	-0.008	0.094	0.060	1.01	0.08	1.43	0.70	1.10	0.10	4.48	0.08	<1.0	0.0-2.0
HD131511	86.88	0.46	0.01	-0.139	-0.310	0.060	0.83	0.07	0.57	0.28	0.90	0.10	4.56	0.08	1.0	0.0-8.0
HD131977	171.22	0.94	0.02	-0.353	-0.698	0.060	0.65	0.05	0.61	0.30	0.75	0.10	4.69	0.09	<1.0	0.0-10.0
HD131923	41.93	0.83	0.03	-0.050	0.159	0.062	1.24	0.10	1.06	0.52	1.00	0.10	4.25	0.08	8.5	6.0-10.5
HD134060	41.32	0.45	0.05	-0.019	0.187	0.061	1.19	0.09	0.91	0.44	1.10	0.10	4.33	0.08	4.0	3.0-6.0
HD134606	37.74	0.54	0.05	-0.046	0.049	0.061	1.10	0.09	0.89	0.43	1.10	0.10	4.40	0.08	4.5	2.0-6.5
HD136352	67.51	0.39	0.02	-0.096	0.036	0.060	1.13	0.09	0.65	0.32	0.80	0.10	4.24	0.09	>13.0	...
HD141004	82.48	0.32	0.03	-0.044	0.337	0.060	1.47	0.11	0.77	0.37	1.00	0.10	4.10	0.08	9.0	7.5-10.0
HD140901	65.13	0.40	0.03	-0.062	-0.087	0.060	0.95	0.07	0.92	0.45	1.00	0.10	4.48	0.08	3.0	0.0-7.0
HD143114	27.51	0.68	0.18	-0.061	0.189	0.068	1.23	0.10	1.42	0.70	0.90	0.10	4.21	0.09	13.0	11.0-14.0
HD144009	38.80	0.81	0.05	-0.075	-0.112	0.063	0.94	0.08	0.60	0.29	1.00	0.10	4.49	0.08	4.0	0.0-8.0
HD144628	68.17	0.64	0.02	-0.225	-0.505	0.061	0.73	0.06	0.45	0.22	0.70	0.10	4.56	0.09	>13.0	12.0-14.0
HD145825	46.40	0.62	0.07	-0.043	0.000	0.061	1.01	0.08	0.79	0.38	1.00	0.10	4.43	0.08	5.0	1.0-8.0
HD146481	22.47	0.64	0.08	-0.076	0.431	0.065	1.69	0.14	1.81	0.89	0.95	0.10	3.96	0.09	10.0	8.0-11.5

Table 4—Continued

Star	π (mas)	σ_π (mas)	A_V	BC_V	$\log(L/L_\odot)$	$\sigma_{\log(L/L_\odot)}$	R (R $_\odot$)	σ_R (R $_\odot$)	M_{spec} (M $_\odot$)	$\sigma_{M_{spec}}$ (M $_\odot$)	M_{track} (M $_\odot$)	$\sigma_{M_{track}}$ (M $_\odot$)	$\log g$ (Hipp)	$\sigma_{\log g}$ (Hipp)	Age (Gyr)	ΔAge (Gyr)
HD149661	102.55	0.40	0.06	-0.148	-0.339	0.060	0.81	0.06	0.53	0.26	0.90	0.10	4.58	0.08	4.0	0.0-11.0
HD150248	37.54	0.50	0.05	-0.062	-0.008	0.061	1.02	0.08	0.76	0.37	0.95	0.10	4.40	0.08	8.5	5.0-11.5
HD153075	32.77	0.63	0.06	-0.081	0.137	0.062	1.20	0.10	1.25	0.61	0.80	0.10	4.18	0.09	>13.0	...
HD155974	31.81	0.51	0.06	-0.005	0.493	0.062	1.49	0.12	0.95	0.46	1.20	0.10	4.17	0.08	4.0	3.0-5.0
HD156274	113.61	0.69	0.02	-0.165	-0.317	0.060	0.84	0.07	0.65	0.32	0.70	0.10	4.43	0.09	>13.0	...
HD155918	35.67	0.50	0.05	-0.086	0.058	0.061	1.10	0.09	1.45	0.71	0.75	0.10	4.23	0.09	>13.0	...
HD158783	23.67	0.59	0.08	-0.033	0.369	0.064	1.52	0.12	1.14	0.55	1.10	0.10	4.12	0.08	7.0	5.0-8.0
HD161612	38.23	0.81	0.05	-0.064	-0.091	0.063	0.95	0.08	0.66	0.32	1.05	0.10	4.51	0.08	1.5	0.0-5.0
HD162255	24.94	0.77	0.10	-0.028	0.305	0.069	1.40	0.12	0.98	0.48	1.10	0.10	4.19	0.08	7.0	5.0-8.0
HD163272	22.63	0.64	0.11	0.006	0.284	0.069	1.28	0.11	0.92	0.45	1.20	0.10	4.30	0.08	3.0	1.5-3.5
HD166553	21.82	1.03	0.05	-0.022	0.351	0.073	1.43	0.13	0.79	0.39	1.10	0.10	4.17	0.09	6.5	4.5-7.5
HD168871	35.36	0.41	0.04	-0.031	0.259	0.061	1.28	0.10	0.94	0.46	1.00	0.10	4.23	0.08	8.0	6.5-9.5
HD175345	21.26	1.09	0.15	-0.002	0.366	0.078	1.32	0.13	1.75	0.87	1.15	0.10	4.26	0.09	3.5	3.0-4.0
HD177565	58.98	0.47	0.02	-0.055	-0.063	0.060	0.96	0.08	0.91	0.44	1.00	0.10	4.47	0.08	3.0	0.0-6.0
HD179140	18.92	0.75	0.08	-0.026	0.505	0.069	1.75	0.15	1.01	0.50	1.20	0.10	4.04	0.08	6.0	5.0-7.0
HD181428	21.92	0.63	0.12	-0.017	0.441	0.065	1.55	0.13	0.92	0.45	1.10	0.10	4.10	0.08	6.0	5.0-7.0
HD183877	36.72	0.95	0.07	-0.070	-0.022	0.064	1.02	0.08	1.09	0.53	0.90	0.10	4.38	0.09	9.0	6.0-12.0
HD184985	32.72	0.28	0.11	0.019	0.731	0.064	1.94	0.16	1.47	0.72	1.40	0.10	4.01	0.08	2.5	2.0-3.0
HD187691	52.11	0.29	0.03	0.018	0.431	0.060	1.41	0.11	1.78	0.87	1.30	0.10	4.25	0.07	2.5	1.5-3.0
HD190406	56.28	0.35	0.01	-0.019	0.099	0.060	1.06	0.08	0.88	0.43	1.10	0.10	4.43	0.08	2.0	0.0-4.0
HD189567	56.41	0.44	0.04	-0.074	0.023	0.060	1.07	0.08	0.66	0.32	0.85	0.10	4.31	0.09	>13.0	11.0-14.0
HD190248	163.71	0.17	0.01	-0.040	0.080	0.060	1.13	0.09	0.84	0.41	1.10	0.10	4.37	0.08	4.0	2.0-6.0
HD191408	166.25	0.27	0.02	-0.222	-0.565	0.060	0.68	0.05	0.50	0.24	0.65	0.10	4.59	0.10	>13.0	9.0-14.0

Table 4—Continued

Star	π (mas)	σ_π (mas)	A_V	BC_V	$\log(L/L_\odot)$	$\sigma_{\log(L/L_\odot)}$	R (R $_\odot$)	σ_R (R $_\odot$)	M_{spec} (M $_\odot$)	$\sigma_{M_{spec}}$ (M $_\odot$)	M_{track} (M $_\odot$)	$\sigma_{M_{track}}$ (M $_\odot$)	$\log g$ (Hipp)	$\sigma_{\log g}$ (Hipp)	Age (Gyr)	ΔAge (Gyr)
HD192310	112.22	0.30	0.02	-0.198	-0.397	0.060	0.80	0.06	0.56	0.27	0.90	0.10	4.58	0.08	5.0	0.0-13.0
HD193193	24.85	0.65	0.11	-0.034	0.295	0.064	1.36	0.11	0.88	0.43	1.05	0.10	4.20	0.08	8.0	6.0-9.0
HD192865	19.13	0.58	0.11	0.017	0.618	0.066	1.74	0.14	1.88	0.92	1.40	0.10	4.10	0.08	3.0	2.5-3.5
HD193307	32.24	0.47	0.07	-0.034	0.429	0.061	1.51	0.12	1.25	0.61	1.00	0.10	4.08	0.08	7.5	6.5-8.5
HD194640	51.22	0.54	0.04	-0.076	-0.108	0.061	0.95	0.07	0.85	0.42	0.95	0.10	4.47	0.08	6.0	1.0-10.0
HD196390	28.63	0.65	0.07	-0.028	0.102	0.063	1.09	0.09	0.93	0.45	1.10	0.10	4.40	0.08	3.5	1.0-5.5
HD196800	24.89	0.57	0.07	-0.013	0.265	0.063	1.30	0.10	0.84	0.41	1.20	0.10	4.30	0.08	4.0	3.0-5.0
HD196668	20.60	6.21	0.10	-0.005	0.450	0.269	1.58	0.49	0.98	0.76	1.30	0.10	4.15	0.27	4.0	3.0-6.0
HD199288	45.17	0.46	0.05	-0.081	0.043	0.061	1.07	0.08	1.47	0.72	0.75	0.10	4.26	0.09	>13.0	...
HD199190	25.25	0.54	0.09	-0.027	0.406	0.063	1.57	0.13	0.92	0.45	1.15	0.10	4.11	0.08	6.5	5.0-7.5
HD199509	41.95	0.37	0.05	-0.061	-0.085	0.061	0.91	0.07	0.99	0.48	0.90	0.10	4.48	0.08	6.0	2.0-10.0
HD204385	26.80	0.57	0.08	-0.006	0.230	0.063	1.19	0.09	1.34	0.65	1.10	0.10	4.33	0.08	3.5	2.0-4.0
HD205390	68.40	0.58	0.03	-0.212	-0.521	0.061	0.70	0.06	0.46	0.23	0.80	0.10	4.65	0.09	4.0	0.0-14.0
HD206395	25.29	0.47	0.07	0.030	0.450	0.062	1.41	0.11	1.73	0.84	1.30	0.10	4.26	0.08	2.0	1.0-2.5
HD207129	62.52	0.35	0.03	-0.016	0.106	0.060	1.06	0.08	1.35	0.66	1.10	0.10	4.43	0.08	2.5	0.0-5.0
HD207700	25.28	0.51	0.09	-0.043	0.184	0.063	1.25	0.10	1.53	0.75	1.05	0.10	4.27	0.08	7.5	5.0-9.5
HD208998	27.95	0.55	0.06	-0.055	0.213	0.062	1.24	0.10	0.97	0.47	0.90	0.10	4.21	0.08	12.0	10.0-14.0
HD209653	22.50	0.52	0.09	-0.025	0.454	0.063	1.57	0.13	1.33	0.65	1.10	0.10	4.09	0.08	6.5	5.5-7.5
HD212291	30.07	0.60	0.03	-0.081	-0.168	0.063	0.88	0.07	0.70	0.34	0.90	0.10	4.51	0.09	6.0	0.0-11.0
HD212168	43.39	0.50	0.05	-0.022	0.214	0.061	1.22	0.10	1.03	0.50	1.10	0.10	4.31	0.08	6.0	4.0-7.0
HD212708	28.26	0.66	0.06	-0.041	0.054	0.063	1.09	0.09	0.72	0.35	1.10	0.10	4.40	0.08	4.0	2.0-6.0
HD214759	36.28	0.67	0.06	-0.086	-0.117	0.062	0.97	0.08	0.85	0.42	1.00	0.10	4.47	0.08	3.5	0.0-7.0
HD214953	42.31	0.40	0.04	-0.002	0.276	0.061	1.23	0.09	1.18	0.57	1.15	0.10	4.32	0.08	3.5	2.0-4.5

Table 4—Continued

Star	π	σ_π	A_V	BC_V	$\log(L/L_\odot)$	$\sigma_{\log(L/L_\odot)}$	R	σ_R	M_{spec}	$\sigma_{M_{spec}}$	M_{track}	$\sigma_{M_{track}}$	$\log g$	$\sigma_{\log g}$	Age	ΔAge
	(mas)	(mas)					(R $_\odot$)	(R $_\odot$)	(M $_\odot$)	(M $_\odot$)	(M $_\odot$)	(M $_\odot$)	(Hipp)	(Hipp)	(Gyr)	(Gyr)
HD215648	61.36	0.19	0.01	-0.014	0.662	0.060	1.87	0.14	1.19	0.58	1.15	0.10	3.96	0.08	5.0	4.5-5.5
HD217958	17.62	0.83	0.10	-0.013	0.241	0.076	1.28	0.12	0.82	0.41	1.20	0.10	4.30	0.09	4.0	3.0-5.0
HD218261	35.78	0.63	0.05	0.017	0.238	0.062	1.13	0.09	1.33	0.65	1.20	0.10	4.41	0.08	<1.0	0.0-2.0
HD220507	23.79	0.79	0.06	-0.052	0.164	0.067	1.24	0.10	0.97	0.48	1.00	0.10	4.25	0.09	9.5	7.0-11.5
HD222237	87.56	0.51	0.03	-0.341	-0.664	0.060	0.68	0.05	0.34	0.17	0.60	0.10	4.56	0.10	>13.0	...
HD222335	53.85	0.63	0.04	-0.143	-0.353	0.061	0.79	0.06	0.80	0.39	0.85	0.10	4.58	0.09	4.0	0.0-11.0
HD222368	72.92	0.15	0.02	-0.009	0.542	0.060	1.62	0.12	1.29	0.62	1.15	0.10	4.08	0.08	5.0	4.0-5.5
HD222480	22.49	0.61	0.09	-0.018	0.403	0.065	1.54	0.13	1.28	0.63	1.25	0.10	4.16	0.08	6.0	3.5-6.5
HD223171	24.90	0.59	0.08	-0.027	0.402	0.063	1.56	0.13	1.14	0.55	1.15	0.10	4.12	0.08	6.5	5.0-7.5

Table 1. Rotational Velocities and Lithium Abundances (Paper III).

Star	$\text{FWHM}_{Macro+Inst}$ (Å)	$v \sin i$ (km s $^{-1}$)	A(Li)	$\delta A(\text{Li})$
HD142	0.341	3.70	2.88 ± 0.03	0.11
HD1237	0.208	0.70	2.16 ± 0.02	0.10
HD2039	0.156	1.50	2.30 ± 0.03	0.11
HD2638	0.140	0.20	≤ 0.41	...
HD3651	0.149	0.30	≤ 0.28	...
HD4113	0.147	2.10	≤ 0.45	...
HD4208	0.140	2.40	≤ 0.45	...
HD4308	0.140	0.20	1.04 ± 0.24	0.26
HD4203	0.177	1.10	≤ 0.76	...
HD6434	0.150	0.20	≤ 0.66	...
HD10647	0.228	1.80	2.74 ± 0.02	0.10
HD11506	0.166	4.40	2.76 ± 0.02	0.10
HD12661	0.141	3.30	1.10 ± 0.59	0.60
HD13445	0.140	0.20	≤ 0.37	...
HD16141	0.144	1.30	1.19 ± 0.15	0.18
HD16417	0.176	0.90	1.71 ± 0.06	0.12
HD17051	0.164	5.50	2.52 ± 0.04	0.11
HIP14810	0.148	0.50	0.84 ± 0.33	0.35
HD19994	0.140	8.00	1.77 ± 0.13	0.17
HD20782	0.186	3.10	1.02 ± 0.29	0.31
HD22049	0.140	0.20	≤ 0.07	...
HD23079	0.144	3.00	2.17 ± 0.04	0.11
HD27894	0.141	0.20	< -0.17	...
HD28185	0.147	3.00	≤ 0.58	...
HD30177	0.143	2.10	≤ 0.79	...
HD37124	0.141	0.20	≤ 0.50	...
HD39091	0.141	4.20	2.34 ± 0.03	0.11
HD37605	0.147	1.30	≤ 0.44	...
HD40307	0.141	0.20	≤ 0.22	...
HD41004A	0.148	1.30	≤ 0.37	...
ABPic	0.174	9.40	3.35 ± 0.03	0.11

Table 1—Continued

Star	FWHM _{<i>Macro+Inst</i>} (Å)	v sin i (km s ⁻¹)	A(Li)	δA(Li)
HD45652	0.140	0.80	≤0.36	...
HD46375	0.161	1.50	≤0.39	...
HD47186	0.140	1.10	≤0.42	...
HD50499	0.187	3.30	2.62 ± 0.02	0.10
HD50554	0.141	4.70	2.40 ± 0.03	0.11
HD52265	0.141	4.00	2.65 ± 0.03	0.11
HD63454	0.140	0.20	≤0.15	...
HD65216	0.141	3.30	1.22 ± 0.12	0.16
HD66428	0.143	3.00	≤0.45	...
HD69830	0.147	1.10	0.80 ± 0.20	0.22
HD70642	0.147	2.80	≤0.70	...
HD70573	0.230	11.90	3.12 ± 0.02	0.10
HD72659	0.142	0.50	2.16 ± 0.03	0.11
HD73256	0.140	2.30	≤0.57	...
HD74156	0.140	5.10	2.58 ± 0.02	0.10
HD75289	0.212	0.80	2.64 ± 0.02	0.10
HD76700	0.160	1.70	1.30 ± 0.14	0.17
HD81040	0.143	2.00	1.79 ± 0.04	0.11
HD82943	0.178	0.20	2.47 ± 0.02	0.10
HD83443	0.156	2.50	≤0.54	...
HD86081	0.141	5.20	1.82 ± 0.05	0.11
HD89307	0.191	1.50	2.18 ± 0.04	0.11
HD92788	0.144	3.00	≤0.75	...
HD93083	0.142	1.60	≤0.31	...
BD-10-3166	0.149	1.50	≤0.51	...
HD99109	0.142	2.30	≤0.55	...
HD100777	0.147	1.00	≤0.38	...
HD101930	0.141	1.50	≤0.38	...
HD102117	0.155	1.00	≤0.61	...
HD102195	0.153	1.50	≤0.46	...
HD106252	0.156	0.40	1.69 ± 0.08	0.13

Table 1—Continued

Star	FWHM _{Macro+Inst} (Å)	v sin i (km s ⁻¹)	A(Li)	δA(Li)
HD107148	0.143	2.60	1.32 ± 0.13	0.17
HD108147	0.224	0.70	2.16 ± 0.06	0.12
HD108874	0.144	1.40	≤0.58	...
HD109749	0.141	2.60	2.11 ± 0.03	0.11
HD111232	0.140	0.20	< -0.02	...
HD114386	0.140	0.20	≤0.27	...
HD114762	0.187	2.30	1.94 ± 0.04	0.11
HD114783	0.140	0.20	< -0.30	...
HD114729	0.141	4.20	1.88 ± 0.03	0.11
HD117207	0.153	1.20	≤0.64	...
HD117618	0.184	1.30	2.14 ± 0.03	0.11
HD120136	0.259	14.00	1.70 ± 0.34	0.35
HD121504	0.187	0.40	2.47 ± 0.02	0.10
HD125612	0.184	0.40	2.49 ± 0.04	0.11
HD128311	0.143	1.90	≤0.13	...
HD130322	0.143	2.40	≤0.38	...
HD134987	0.142	3.00	≤0.57	...
HD330075	0.140	3.20	≤0.41	...
HD141937	0.159	0.70	2.26 ± 0.03	0.11
HD142415	0.141	4.60	2.03 ± 0.06	0.12
HD142022A	0.143	0.90	≤0.16	...
HD147513	0.142	2.60	2.00 ± 0.04	0.11
HD149143	0.198	1.80	1.79 ± 0.06	0.12
HD160691	0.153	1.40	≤0.64	...
HD162020	0.149	2.80	≤0.25	...
HD164922	0.141	0.20	≤0.35	...
HD168443	0.156	1.30	≤0.49	...
HD168746	0.141	0.70	≤0.51	...
HD169830	0.232	2.00	≤0.68	...
HD170469	0.143	0.20	1.13 ± 0.27	0.29
HD179949	0.236	5.80	2.53 ± 0.03	0.11

Table 1—Continued

Star	$\text{FWHM}_{Macro+Inst}$	$v \sin i$	A(Li)	$\delta A(\text{Li})$
	(Å)	(km s $^{-1}$)		
HD181433	0.157	1.50	0.76 ± 0.14	0.21
HD183263	0.142	3.50	2.27 ± 0.03	0.11
HD231701	0.171	4.20	2.59 ± 0.03	0.11
HD187085	0.208	0.20	2.62 ± 0.03	0.11
HD189733	0.143	0.80	≤ 0.08	...
HD192263	0.143	1.60	≤ 0.02	...
HD195019	0.150	4.20	1.45 ± 0.12	0.16
WASP2	0.140	0.20	≤ 0.58	...
HD196050	0.189	0.20	2.16 ± 0.04	0.11
HD196885	0.140	7.90	2.64 ± 0.03	0.11
HD202206	0.147	1.10	1.37 ± 0.11	0.15
HD208487	0.141	3.90	2.58 ± 0.03	0.11
HD209458	0.173	2.40	2.65 ± 0.02	0.10
HD210277	0.167	1.40	≤ 0.42	...
HD212301	0.140	6.60	2.75 ± 0.03	0.11
HD213240	0.190	0.80	2.43 ± 0.03	0.11
HD216435	0.220	1.70	2.65 ± 0.02	0.10
HD216437	0.141	4.40	1.93 ± 0.04	0.11
HD216770	0.143	1.70	≤ 0.63	...
HD217014	0.140	2.80	1.24 ± 0.19	0.22
HD217107	0.141	2.60	≤ 0.53	...
HD219828	0.172	1.20	2.27 ± 0.03	0.11
HD221287	0.187	3.80	2.80 ± 0.02	0.10
HD222582	0.144	2.20	1.09 ± 0.22	0.24
HD1581	0.203	1.10	2.25 ± 0.05	0.11
HD1835	0.145	6.60	2.55 ± 0.02	0.10
HD3823	0.147	2.60	2.36 ± 0.02	0.10
HD4628	0.167	0.00	≤ 0.01	...
HD7199	0.140	1.80	≤ 0.35	...
HD7693	0.178	2.60	≤ 0.33	...
HD7570	0.179	3.60	2.86 ± 0.02	0.10

Table 1—Continued

Star	$\text{FWHM}_{Macro+Inst}$	$v \sin i$	A(Li)	$\delta A(\text{Li})$
	(Å)	(km s $^{-1}$)		
HD10180	0.151	1.10	1.79 ± 0.08	0.13
HD10476	0.142	1.20	≤ 0.30	...
HD10700	0.173	0.40	≤ 0.21	...
HD11112	0.140	3.90	2.44 ± 0.02	0.10
HD12387	0.140	0.20	≤ 0.56	...
HD16160	0.146	1.70	≤ 0.16	...
HD17925	0.190	0.20	2.66 ± 0.02	0.10
HD19632	0.145	2.30	1.94 ± 0.04	0.11
HD20029	0.249	1.60	2.69 ± 0.02	0.10
HD20201	0.144	4.70	2.74 ± 0.03	0.11
HD20630	0.224	0.20	2.10 ± 0.04	0.11
HD20794	0.148	2.50	≤ 0.58	...
HD22104	0.173	2.00	1.21 ± 0.50	0.51
HD22484	0.190	3.30	2.54 ± 0.04	0.11
HD25587	0.175	7.00	2.12 ± 0.05	0.11
HD25680	0.140	4.70	2.51 ± 0.02	0.10
HD30876	0.149	1.00	≤ 0.20	...
HD31527	0.152	0.20	1.83 ± 0.05	0.11
HD36435	0.202	1.50	1.49 ± 0.05	0.11
HD36889	0.177	0.50	2.91 ± 0.02	0.10
HD38283	0.159	0.80	2.24 ± 0.03	0.11
HD38382	0.160	2.20	2.64 ± 0.03	0.11
HD38973	0.199	2.50	2.35 ± 0.04	0.11
HD39213	0.157	1.40	≤ 0.58	...
HD39587	0.262	4.80	2.90 ± 0.02	0.10
HD42024	0.212	1.60	2.86 ± 0.03	0.11
HD43042	0.140	6.00	≤ 1.43	...
HD45701	0.141	6.00	≤ 1.02	...
HD51929	0.142	2.30	1.19 ± 0.17	0.20
HD52447	0.170	5.60	2.65 ± 0.03	0.11
HD55693	0.190	0.70	1.36 ± 0.19	0.22

Table 1—Continued

Star	$\text{FWHM}_{Macro+Inst}$	$v \sin i$	A(Li)	$\delta A(\text{Li})$
	(Å)	(km s $^{-1}$)		
HD64184	0.156	1.90	≤ 0.64	...
HD65907	0.140	0.20	≤ 0.73	...
HD73524	0.170	1.80	2.46 ± 0.02	0.10
HD76151	0.141	2.70	1.77 ± 0.05	0.11
HD78429	0.141	4.60	≤ 0.64	...
HD80913	0.140	4.90	2.35 ± 0.04	0.11
HD84117	0.142	5.30	2.52 ± 0.03	0.11
HD86819	0.177	3.50	2.29 ± 0.03	0.11
HD88742	0.140	3.70	2.27 ± 0.03	0.11
HD92987	0.153	1.20	1.95 ± 0.04	0.11
HD93385	0.190	1.20	2.07 ± 0.04	0.11
HD96423	0.160	2.00	1.87 ± 0.04	0.11
HD102365	0.140	0.20	≤ 0.52	...
HD102438	0.140	1.00	≤ 0.62	...
HD102870	0.164	1.20	1.99 ± 0.13	0.17
HD105328	0.197	0.50	2.57 ± 0.02	0.10
HD106453	0.155	1.10	1.34 ± 0.09	0.14
HD107692	0.177	1.40	2.23 ± 0.03	0.11
HD108309	0.141	3.00	1.11 ± 0.28	0.30
HD109200	0.140	0.20	< -0.14	...
HD110810	0.142	1.10	< -0.19	...
HD114853	0.144	0.60	≤ 0.67	...
HD115383	0.232	4.10	2.84 ± 0.02	0.10
HD115617	0.149	1.10	≤ 0.22	...
HD115585	0.151	2.50	≤ 0.85	...
HD117105	0.140	0.20	1.84 ± 0.06	0.12
HD117939	0.142	1.00	≤ 0.54	...
HD118972	0.219	2.10	0.70 ± 0.18	0.21
HD120237	0.140	5.80	≤ 0.84	...
HD120690	0.146	1.80	1.10 ± 0.23	0.25
HD120780	0.143	1.70	≤ 0.27	...

Table 1—Continued

Star	$\text{FWHM}_{Macro+Inst}$	$v \sin i$	A(Li)	$\delta A(\text{Li})$
	(Å)	(km s $^{-1}$)		
HD122742	0.157	0.00	≤ 0.67	...
HD122862	0.172	0.40	2.39 ± 0.03	0.11
HD124584	0.143	3.10	2.18 ± 0.03	0.11
HD125072	0.142	2.20	≤ 0.37	...
HD126053	0.140	0.20	0.95 ± 0.22	0.24
HD125881	0.150	3.70	2.45 ± 0.03	0.11
HD128674	0.140	0.40	0.84 ± 0.23	0.25
HD130948	0.243	0.20	2.94 ± 0.02	0.10
HD131511	0.141	4.00	≤ 0.41	...
HD131977	0.143	0.40	≤ 0.11	...
HD131923	0.142	2.40	≤ 0.65	...
HD134060	0.140	5.20	2.04 ± 0.05	0.11
HD134606	0.155	1.80	≤ 0.71	...
HD136352	0.140	5.30	≤ 0.57	...
HD141004	0.153	1.10	1.76 ± 0.08	0.13
HD140901	0.141	3.30	0.76 ± 0.41	0.42
HD143114	0.140	0.20	≤ 0.55	...
HD144009	0.157	1.20	≤ 0.47	...
HD144628	0.162	0.00	≤ 0.15	...
HD145825	0.143	3.20	1.90 ± 0.04	0.11
HD146481	0.160	3.40	1.91 ± 0.03	0.11
HD149661	0.140	0.20	≤ 0.42	...
HD150248	0.140	1.30	≤ 0.51	...
HD153075	0.266	3.50	0.88 ± 0.32	0.34
HD155974	0.258	3.40	2.60 ± 0.03	0.11
HD156274	0.140	0.20	≤ 0.27	...
HD155918	0.369	2.50	0.90 ± 0.35	0.36
HD158783	0.167	1.30	1.17 ± 0.20	0.22
HD161612	0.151	1.10	≤ 0.47	...
HD162255	0.141	2.40	1.49 ± 0.08	0.13
HD163272	0.190	0.20	2.58 ± 0.02	0.10

Table 1—Continued

Star	$\text{FWHM}_{Macro+Inst}$	$v \sin i$	A(Li)	$\delta A(\text{Li})$
	(Å)	(km s $^{-1}$)		
HD166553	0.190	1.60	2.39 ± 0.03	0.11
HD168871	0.143	3.80	2.14 ± 0.04	0.11
HD175345	0.159	0.20	2.61 ± 0.03	0.11
HD177565	0.153	0.00	≤ 0.52	...
HD179140	0.172	3.50	2.52 ± 0.03	0.11
HD181428	0.224	0.80	2.62 ± 0.02	0.10
HD183877	0.146	1.90	≤ 0.62	...
HD184985	0.189	1.90	≤ 1.15	...
HD187691	0.182	0.20	2.66 ± 0.02	0.10
HD190406	0.168	1.60	2.28 ± 0.03	0.11
HD189567	0.146	2.20	0.80 ± 0.48	0.49
HD190248	0.141	2.50	≤ 0.79	...
HD191408	0.140	0.20	≤ 0.01	...
HD192310	0.140	1.20	≤ 0.24	...
HD193193	0.199	1.40	2.04 ± 0.04	0.11
HD192865	0.198	2.10	≤ 0.92	...
HD193307	0.142	0.00	2.48 ± 0.02	0.10
HD194640	0.141	4.80	≤ 0.49	...
HD196390	0.157	2.80	2.06 ± 0.04	0.11
HD196800	0.140	3.50	2.21 ± 0.03	0.11
HD196068	0.198	0.20	2.30 ± 0.03	0.11
HD199288	0.174	2.30	1.05 ± 0.17	0.20
HD199190	0.142	3.50	2.11 ± 0.03	0.11
HD199509	0.141	5.10	1.88 ± 0.06	0.12
HD204385	0.160	1.70	2.37 ± 0.04	0.11
HD205390	0.143	2.00	≤ 0.25	...
HD206395	0.296	2.90	2.78 ± 0.03	0.11
HD207129	0.178	1.00	2.35 ± 0.03	0.11
HD207700	0.143	3.10	≤ 0.62	...
HD208998	0.160	0.40	0.95 ± 0.46	0.47
HD209653	0.141	4.20	≤ 0.74	...

Table 1—Continued

Star	$\text{FWHM}_{Macro+Inst}$	$v \sin i$	A(Li)	$\delta A(\text{Li})$
	(Å)	(km s $^{-1}$)		
HD212291	0.140	0.50	1.06 ± 0.13	0.17
HD212168	0.186	0.40	≤ 0.63	...
HD212708	0.158	1.90	≤ 0.75	...
HD214759	0.145	0.80	≤ 0.61	...
HD214953	0.176	2.90	2.69 ± 0.02	0.10
HD215648	0.192	6.70	2.27 ± 0.04	0.11
HD217958	0.143	4.60	2.28 ± 0.03	0.11
HD218261	0.147	7.30	≤ 0.80	...
HD220507	0.143	2.60	≤ 0.50	...
HD222237	0.143	1.70	≤ 0.28	...
HD222335	0.147	0.30	≤ 0.13	...
HD222368	0.240	1.40	2.23 ± 0.05	0.11
HD222480	0.158	3.00	2.23 ± 0.03	0.11
HD223171	0.164	0.50	2.03 ± 0.04	0.11

Apêndice D

Espectros Sintéticos para a Região do Li

Este apêndice contém os ajustes dos espectros sintéticos aos espectros observados para as outras 5 estrelas cujas razões isotópicas de ${}^6\text{Li}/{}^7\text{Li}$ foram determinadas. No Artigo IV, apenas o gráfico para HD 82943 foi apresentado.

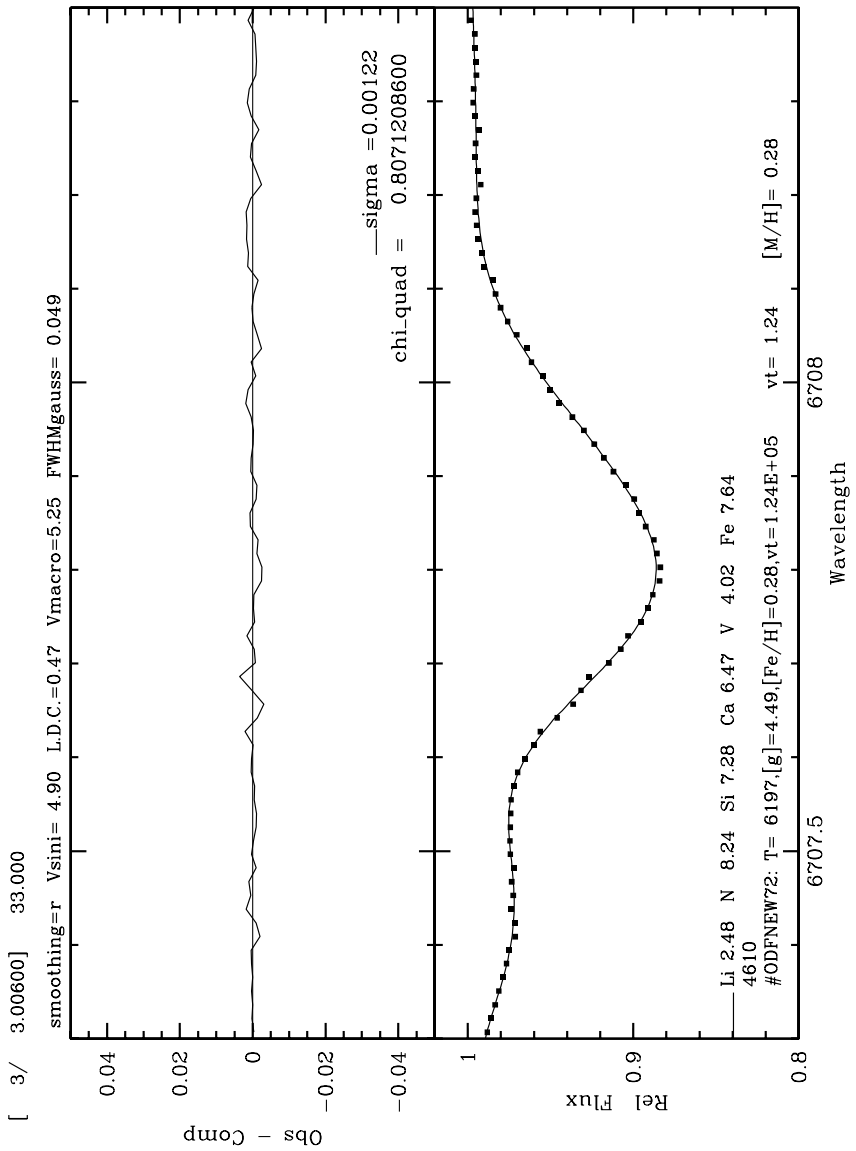


Figura D.1: *Painel superior:* Diferença entre os espectros observado e sintético. *Painel inferior:* Espectros sintético (linha sólida) e observado (quadrados preenchidos) para a estrela com planeta HD 17051. O melhor ajuste ocorre para $A(\text{Li}) = 2,48 \pm 0,01$ e ${}^6\text{Li}/{}^7\text{Li} = 0,03 \pm 0,04$. Este gráfico foi produzido com a versão 2002 do programa MOOG (Sneden 1973).

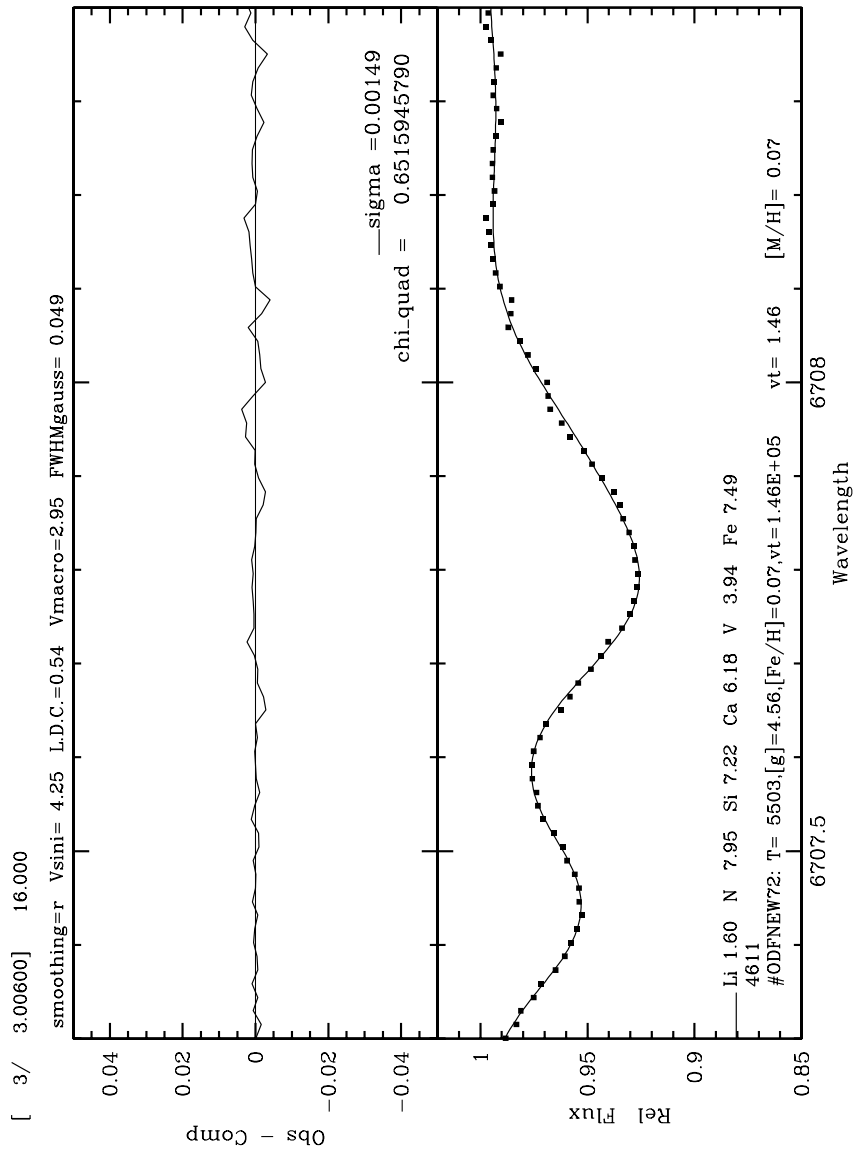


Figura D.2: *Painel superior:* Diferença entre os espectros observado e sintético. *Painel inferior:* Espectros sintético (linha sólida) e observado (quadrados preenchidos) para a estrela sem planeta HD 36435. O melhor ajuste ocorre para $A(\text{Li}) = 1,60 \pm 0,03$ e ${}^6\text{Li}/{}^7\text{Li} = 0,06 \pm 0,08$. Este gráfico foi produzido com a versão 2002 do programa MOOG (Sneden 1973).

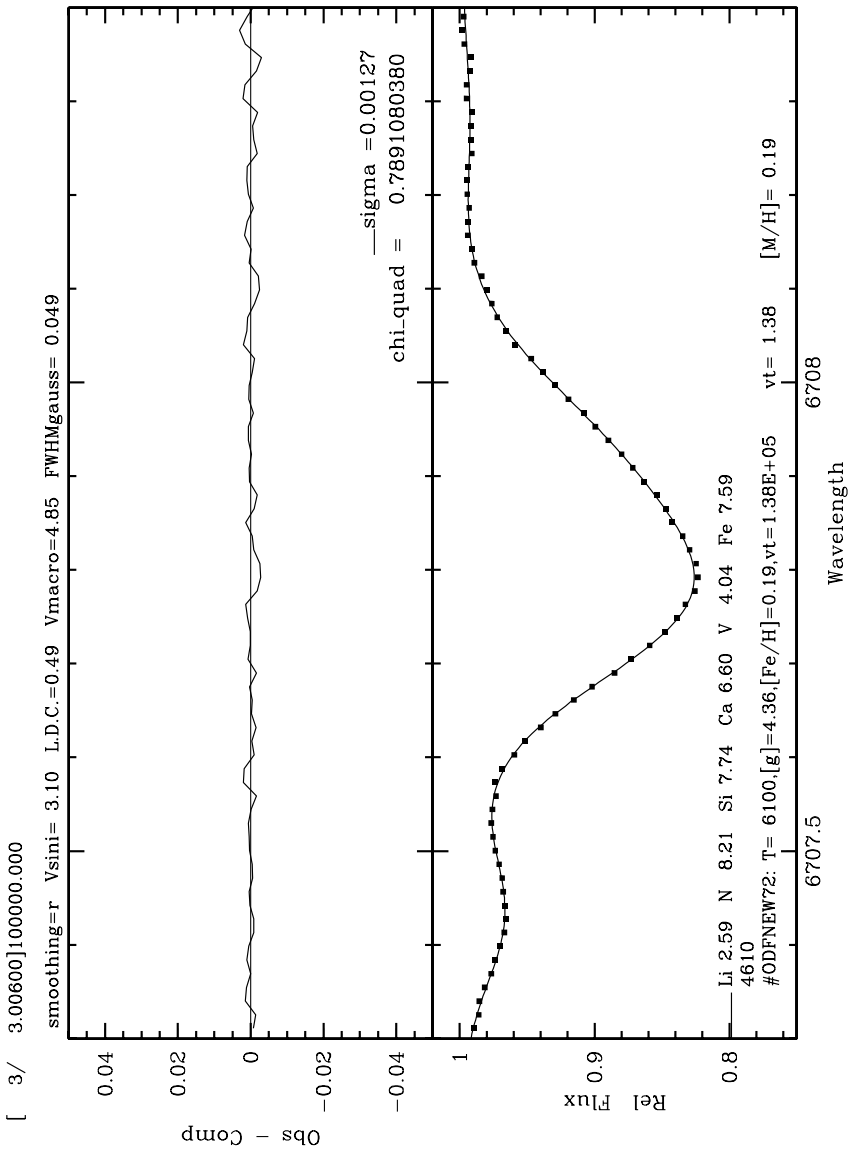


Figura D.3: *Painel superior:* Diferença entre os espectros observado e sintético. *Painel inferior:* Espectros sintético (linha sólida) e observado (quadrados preenchidos) para a estrela com planeta HD 74156. O melhor ajuste ocorre para $A(\text{Li}) = 2,59 \pm 0,01$ e ${}^6\text{Li}/{}^7\text{Li} = 0,00 \pm 0,03$. Este gráfico foi produzido com a versão 2002 do programa MOOG (Sneden 1973).

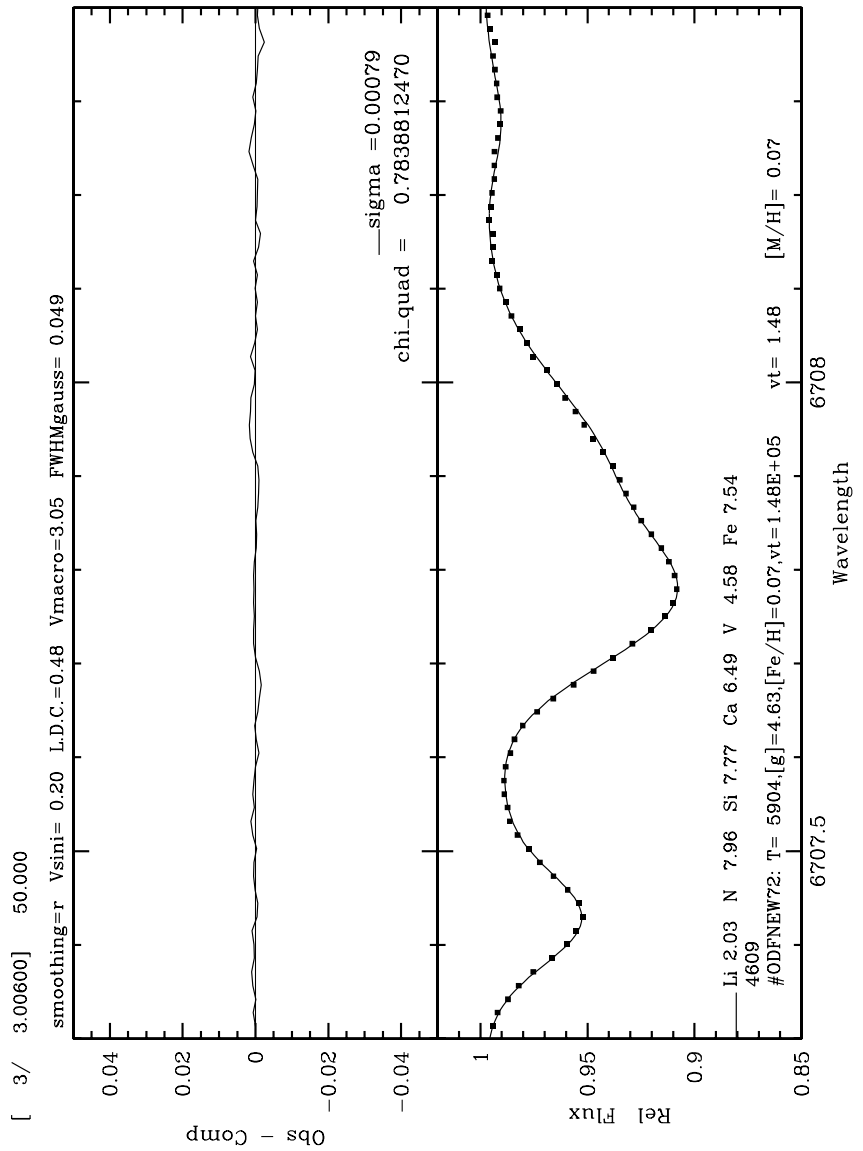


Figura D.4: *Painel superior:* Diferença entre os espectros observado e sintético. *Painel inferior:* Espectros sintético (linha sólida) e observado (quadrados preenchidos) para a estrela com planeta HD 147513. O melhor ajuste ocorre para $A(\text{Li}) = 2,03 \pm 0,01$ e ${}^6\text{Li}/{}^7\text{Li} = 0,02 \pm 0,03$. Este gráfico foi produzido com a versão 2002 do programa MOOG (Sneden 1973).

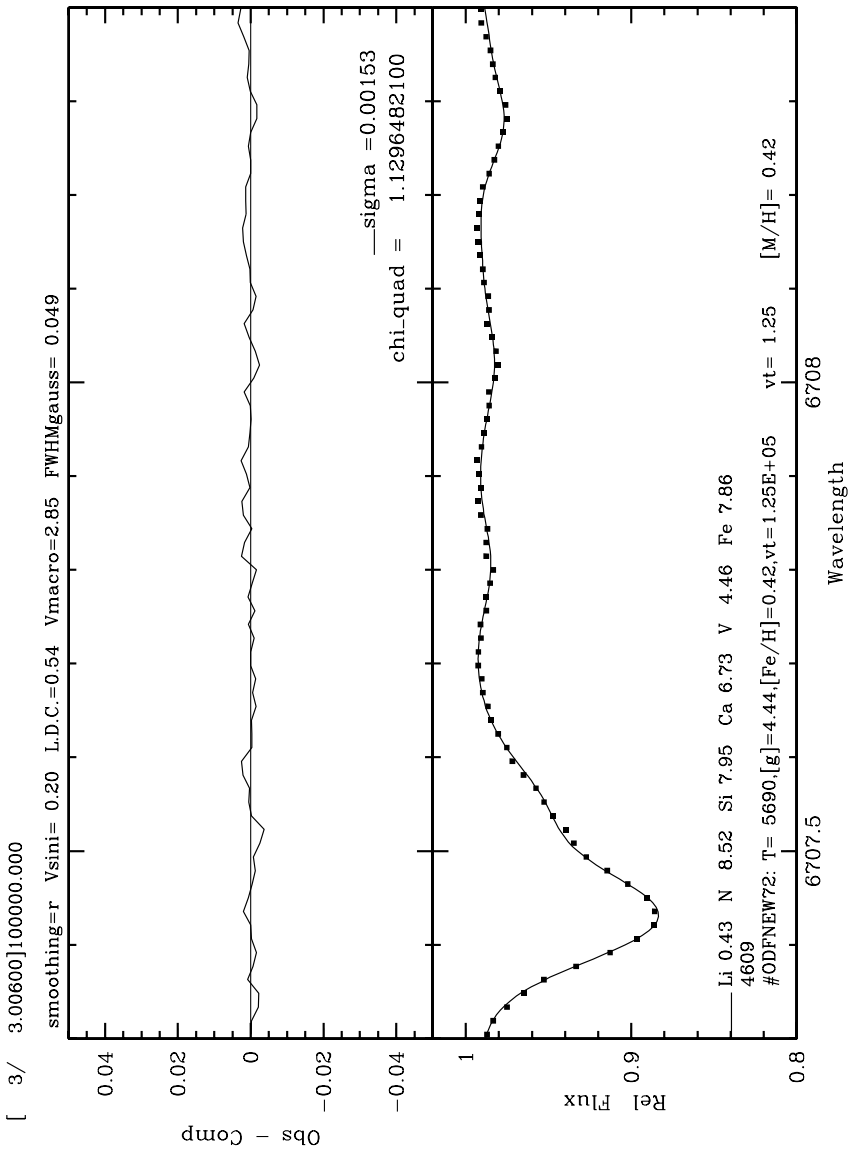


Figura D.5: *Painel superior:* Diferença entre os espectros observado e sintético. *Painel inferior:* Espectros sintético (linha sólida) e observado (quadrados preenchidos) para a estrela com planeta HD 217107. O melhor ajuste ocorre para $A(\text{Li}) \leq 0.36$ e ${}^6\text{Li}/{}^7\text{Li} = 0,00 \pm 0,04$. Este gráfico foi produzido com a versão 2002 do programa MOOG (Sneden 1973).

Referências Bibliográficas

- Bond, J.C., Tinney, C.G., Butler, R.P., Jones, H.R.A., Marcy, G.W., Penny, A.J., & Carter, B.D., 2006, *MNRAS*, 370, 163
- Boss, A.P., 1997, *Science*, 276, 1836
- Boss, A.P., 2010, *IAU Symp. 265, Chemical Abundances in the Universe: Connecting First Stars to Planets*, ed. K. Cunha, M. Spite & B. Barbuy (Cambridge:Cambridge University Press), 391
- Bouvier, J., 2008, *A&A*, 489, L53
- Butler, R.P., & Marcy, G.W., 1996, *ApJ*, 464, L153
- Butler, R.P., Wright, J.T., Marcy, G.W., Fischer, D.A., Vogt, S.S., Tinney, C.G., Jones, H.R.A., Carter, B.D., Johnson, J.A., McCarthy, C., & Penny, A.J., 2006, *ApJ*, 46, 505
- Campbell, B., Walker, G.A.H., & Yang, S., 1988, *ApJ*, 331, 902
- Chen, Y.Q., Nissen, P.E., Benoni, T., & Zhao, G., 2001, *A&A*, 371, 943
- Chen, Y.Q., & Zhao, G., 2006, *AJ*, 131, 1816
- Cochran, W.D., Hatzes, A.P., & Hancock, T.J., 1991, *ApJ*, 380, L35
- Ecuillon, A., Israelian, G., Santos, N.C., Mayor, M., Gilli, G., 2006, *A&A*, 449, 809
- Fischer, D.A., & Valenti, J., 2005, *ApJ*, 622, 1102
- Gonzalez, G., 1997, *MNRAS*, 285, 403
- Gonzalez, G., 2006a, *PASP*, 118, 1494

- Gonzalez, G., 2006b, *MNRAS*, 367, L37
- Gonzalez, G., 2008, *MNRAS*, 386, 928
- Gonzalez, G., Carlson, M.K., & Tobin, R.W., 2010a, *MNRAS*, 403, 1368
- Gonzalez, G., Carlson, M.K., & Tobin, R.W., 2010b, *MNRAS*, aceito para publicação
(arXiv:1004.3313)
- Gonzalez, G., & Laws, C., 2000, *AJ*, 119, 390
- Gonzalez, G., & Laws, C., 2007, *MNRAS*, 378, 1141
- Hale, A., 1995, *PASP*, 107, 22
- Hatzes, A.P., Cochran, W.D., Endl, M., McArthur, B., Paulson, D.B., Walker, G.A.H.,
Campbell, B., & Yang, S., 2003, *ApJ*, 599, 1383
- Hekker, S., & Meléndez, J., 2007, *A&A*, 475, 1003
- Israelian, G., Delgado Mena, E., Santos, N.C., Sousa, S.G., Mayor, M., Udry, S., Domínguez
Cerdeña, C.; Rebolo, R., & Randich, S., 2009, *Nature*, 462, 189
- Israelian, G., Santos, N.C., Mayor, M., & Rebolo, R., 2001, *Nature*, 411, 163
- Israelian, G., Santos, N.C., Mayor, M., & Rebolo, R. 2003, *A&A*, 405, 753
- Israelian, G., Santos, N. C., Mayor, M., & Rebolo, R. 2004, *A&A*, 414, 601
- Konacki, M., & Wolszczan, A., 2003, *ApJ*, 591, L147
- Latham, D.W., Stefanik, R.P., Mazeh, T., Mayor, M., & Burki, G., 1989, *Nature*, 339, 38
- Laws, C., Gonzalez, G., Walker, K.M., Tyagi, S., Dodsworth, J., Snider, K., & Suntzeff,
N.B., 2003, *AJ*, 125, 2664
- Lin, D.N.C., Bodenheimer, P., & Richardson, D.C., 1996, *Nature*, 380, 606
- Luck, R.E., & Heiter, U., 2006, *AJ*, 131, 3069
- Mandell, A.M., Ge, J., & Murray, N., 2004, *AJ*, 127, 1147

- Marcy, G.W., & Butler, R.P., 1996, *ApJ*, 464, L147
- Marcy, G.W., Butler, R.P., Vogt, S.S., Fischer, D., & Liu, M.C., 1999, *ApJ*, 520, 239
- Matsuo, T., Shibai, H., & Ootsubo, T., 2007, *ApJ*, 662, 1282
- Mayor, M., Bonfils, X., Forveille, T., Delfosse, X., Udry, S., Bertaux, J.-L., Beust, H., Bouchy, F., Lovis, C., Pepe, F., Perrier, C., Queloz, D., & Santos, N. C., 2009, *A&A*, 507, 487
- Mayor, M., & Queloz, D., 1995, *Nature*, 378, 355
- Mazeh, T., Latham, D.W., & Stefanik, R.P., 1996, *ApJ*, 466, 415
- Meléndez, J., Asplund, M., Gustafsson, B., & Yong, D., 2009, *ApJ*, 704, L66
- Meléndez, J., Ramírez, I., Casagrande, L., Asplund, M., Gustafsson, B., Yong, D., Do Nascimento, J.D., Castro, M., & Bazot, M., 2010, *Ap&SS*, 328, 193
- Neves, V., Santos, N.C., Sousa, S.G., Correia, A.C.M., & Israelian, G., 2009, *A&A*, 497, 563
- Pasquini, L., Döllinger, M.P., Weiss, A., Girardi, L., Chavero, C., Hatzes, A.P., da Silva, L., & Setiawan, J., 2007, *A&A*, 473, 979
- Pollack, J.B., Hubickyj, O., Bodenheimer, P., Lissauer, J.J., Podolak, M., Greenzweig, Y., 1996, *Icarus*, 124, 62
- Ramírez, I., Meléndez, J., & Asplund, M., 2009, *A&A*, 508, L17
- Rasio, F.A., 1994, *ApJ*, 427, L107
- Reddy, B.E., Lambert, D.L., Laws, C., Gonzalez, G., & Covey, K., 2002, *MNRAS*, 335, 100
- Robinson, S.E., Laughlin, G., Bodenheimer, P., Fischer, D., 2006, *ApJ*, 643, 484
- Ryan, S. G., 2000, *MNRAS*, 316, L35
- Sandquist, E.L., Dokter, J.J., Lin, D.N.C., & Mardling, R.A., 2002, *ApJ*, 572, 1012

- Santos, N.C., Delgado Mena, E., Israelián, G., González-Hernández, J.I., Gálvez-Ortiz, M.C., Mayor, M., Udry, S., Rebolo, R., Sousa, S., & Randich, S., 2010, *IAU Symp. 268, Light Elements in the Universe*, ed. C. Charbonnel, M. Tosi, F. Primas & C. Chiappini (Cambridge:Cambridge University Press), 291
- Santos, N.C., Israelián, G., & Mayor, M., 2001, *A&A*, 373, 1019
- Santos, N.C., Israelián, G., & Mayor, M., 2001, *A&A*, 415, 1153
- Santos, N.C., Israelián, G., Mayor, M., Bento, J.P., Almeida, P.C., Sousa, S.G., & Ecuvillon, A., 2005, *A&A*, 437, 1127
- Santos, N.C., Israelián, G., Mayor, M., Rebolo, R., & Udry, S., 2003, *A&A*, 398, 363
- Schuler, S.C., Kim, J.H., Tinker, M.C., Jr., King, J.R., Hatzes, A.P., & Guenther, E.W., 2005, *ApJ*, 632, L131
- Sigurdsson, S., Richer, H.B., Hansen, B.M., Stairs, I.H., Thorsett, S.E., 2003, *Science*, 301, 193
- Smith, V.V., Cunha, K., & Lazzaro, D., 2001, *AJ*, 121, 3207
- Sneden, C., 1973, *PhD thesis*, Univ. Texas, Austin
- Sousa, S.G., Fernandes, J., Israelián, G., & Santos, N.C., 2010, *A&A*, 512, L5
- Sousa, S.G., Santos, N.C., Mayor, M., Udry, S., Casagrande, L., Israelián, G., Pepe, F., Queloz, D., & Monteiro, M.J.P.F.G., 2008, *A&A*, 487, 373
- Takeda, Y., Honda, S., Kawanomoto, S., Ando, H., & Sakurai, T., 2010, *A&A*, 515, A93
- Takeda, Y., & Kawanomoto, S., 2005, *PASJ*, 57, 45
- Takeda, Y., Sato, B., & Murata, D., 2008, *PASJ*, 60, 781
- Udry, S., Mayor, M., Benz, W., Bertaux, J.-L., Bouchy, F., Lovis, C., Mordasini, C., Pepe, F., Queloz, D., & Sivan, J.-P., 2006, *A&A*, 447, 361
- Udry, S., & Santos, N.C., 2007, *ARA&A*, 45, 397

Valenti, J.A., 2010, *IAU Symp. 265, Chemical Abundances in the Universe: Connecting First Stars to Planets*, ed. K. Cunha, M. Spite & B. Barbuy (Cambridge:Cambridge University Press), 403

Wolszczan, A., 1994, *Science*, 264, 538

Wolszczan, A., & Frail, D.A., 1992, *Nature*, 355, 145

Livros Grátis

(<http://www.livrosgratis.com.br>)

Milhares de Livros para Download:

[Baixar livros de Administração](#)

[Baixar livros de Agronomia](#)

[Baixar livros de Arquitetura](#)

[Baixar livros de Artes](#)

[Baixar livros de Astronomia](#)

[Baixar livros de Biologia Geral](#)

[Baixar livros de Ciência da Computação](#)

[Baixar livros de Ciência da Informação](#)

[Baixar livros de Ciência Política](#)

[Baixar livros de Ciências da Saúde](#)

[Baixar livros de Comunicação](#)

[Baixar livros do Conselho Nacional de Educação - CNE](#)

[Baixar livros de Defesa civil](#)

[Baixar livros de Direito](#)

[Baixar livros de Direitos humanos](#)

[Baixar livros de Economia](#)

[Baixar livros de Economia Doméstica](#)

[Baixar livros de Educação](#)

[Baixar livros de Educação - Trânsito](#)

[Baixar livros de Educação Física](#)

[Baixar livros de Engenharia Aeroespacial](#)

[Baixar livros de Farmácia](#)

[Baixar livros de Filosofia](#)

[Baixar livros de Física](#)

[Baixar livros de Geociências](#)

[Baixar livros de Geografia](#)

[Baixar livros de História](#)

[Baixar livros de Línguas](#)

[Baixar livros de Literatura](#)

[Baixar livros de Literatura de Cordel](#)

[Baixar livros de Literatura Infantil](#)

[Baixar livros de Matemática](#)

[Baixar livros de Medicina](#)

[Baixar livros de Medicina Veterinária](#)

[Baixar livros de Meio Ambiente](#)

[Baixar livros de Meteorologia](#)

[Baixar Monografias e TCC](#)

[Baixar livros Multidisciplinar](#)

[Baixar livros de Música](#)

[Baixar livros de Psicologia](#)

[Baixar livros de Química](#)

[Baixar livros de Saúde Coletiva](#)

[Baixar livros de Serviço Social](#)

[Baixar livros de Sociologia](#)

[Baixar livros de Teologia](#)

[Baixar livros de Trabalho](#)

[Baixar livros de Turismo](#)